GAS PHASE DESULFURIZATION USING REGENERABLE MICROFIBROUS

ENTRAPPED METAL OXIDE BASED SORBENTS FOR LOGISTIC PEM

FUEL CELL APPLICATIONS

Except where reference is made to the work of others, the work described in this dissertation is my own or was done in collaboration with my advisory committee. This dissertation does not include proprietary or classified information.

_____

Hongyun Yang

Certificate of Approval:

_____   _____
Yoon Y. Lee   Bruce J. Tatarchuk, Chair
Professor   Professor
Chemical Engineering   Chemical Engineering

_____   _____
William R. Ashurst   Zhongyang Cheng
Assistant Professor   Assistant Professor
Chemical Engineering   Material Engineering

_____
Joe F. Pittman
Interim Dean
Graduate School

GAS PHASE DESULFURIZATION USING REGENERABLE MICROFIBROUS

ENTRAPPED METAL OXIDE BASED SORBENTS FOR LOGISTIC PEM

FUEL CELL APPLICATIONS

Hongyun Yang

A Dissertation

Submitted to

the Graduate Faculty of

Auburn University

in Partial Fulfillment of the

Requirements for the

Degree of

Doctor of Philosophy

Auburn, Alabama

August 4, 2007

GAS PHASE DESULFURIZATION USING REGENERABLE MICROFIBROUS

ENTRAPPED METAL OXIDE BASED SORBENTS FOR LOGISTIC PEM

FUEL CELL APPLICATIONS

Hongyun Yang

_____

Signature of Author

_____

Date of Graduation

VITA

Hongyun Yang, son of Xuedao Yang and Chaofeng Liu, was born on November 6, 1976. He received his secondary school certificate degree in July 1991 and higher secondary school certificate degree in July 1994. In September 1994, he entered East China University of Science and Technology, Shanghai, China, and graduated with a Bachelor in Chemical Engineering in July 1998. He started the graduate study at the same university and received a Master of Science degree in July 2001. In August 2002, he entered the Graduate School at Auburn University, Auburn, Alabama, for Doctorate of Philosophy. In the same year, he married Yuan Kang, daughter of Le Kang and Yuxin Lü. They have a daughter, Ling-Er (Annie K.) Yang.

DISSERTATION ABSTRACT

GAS PHASE DESULFURIZATION USING REGENERABLE MICROFIBROUS

ENTRAPPED METAL OXIDE BASED SORBENTS FOR LOGISTIC PEM

FUEL CELL APPLICATIONS

Hongyun Yang

Doctor of Philosophy, August 4, 2007
(M.S., East China University of Science and Technology, 2001)
(B.S., East China University of Science and Technology, 1998)

333 Typed Pages

Directed by Bruce J. Tatarchuk

This dissertation presents results of R&D efforts to develop a thin, low pressure drop,

high efficiency zinc oxide based sorbent using glass fibrous media as carrier to remove

gaseous sulfur compounds from reformates for logistic PEM fuel cell power systems.

The glass fibrous entrapped sorbents (GFES) contain 3 vol.% glass fibrous media, 22

vol.% particles (100~200 μm) and 75 vol.% voidage.   Therefore, GFES yielded much

lower pressure drops than packed beds at the same test conditions.   In thin bed tests,

GFES demonstrated exceptional desulfurization and regeneration performance, compared

with the packed beds of ZnO extrudates (1 mm) and particles of similar size (80~100

mesh) at equivalent reactor volume.   Fundamental kinetic studies were conducted to

investigate the improvements observed using GFES. The experimental results at 400 °C indicated that the desulfurization process using ZnO/SiO_2 and GFES sorbents was controlled by the external mass transfer rate at a face velocity less than 11 cm/s, while the process using ZnO extrudates suffered from severe intra-particle mass transfer resistance. A modified Amundson model was applied to describe the relationship between the apparent rate constant (k_a) and the sharpness (lumped K) of a breakthrough curve. Based on this model, the influences of microfibrous media and high voidage were discussed. The sorbent was also evaluated for sulfur removal from realistic reformates. The effects of CO, CO_2 and water on the desulfurization performance were examined for ZnO based sorbents at 400 °C. Water and CO contents determine the H_2S and COS breakthrough respectively, therefore total sulfur breakthrough. The homogenous and heterogeneous COS formation pathways were revealed experimentally. Moreover, the low temperature performance of ZnO/SiO_2 and GFES was also studied. It was found that the addition of copper dopant to ZnO/SiO_2 could significantly improve the sulfur capacity and regenerability for the desulfurization applications at stack temperatures. Due to the high sulfur removal efficiency and low ZnO density, the GFES can be employed as desulfurizer for H_2S removal at extremely low concentrations or as polishing layers in composite beds (packed beds followed by polishing layers downstream) to improve the overall breakthrough capacity.

ACKNOWLEDGEMENTS

Style manual or journal used: *Chemical Engineering Science*

Computer software used: *Microsoft Office*

TABLE OF CONTENTS

LIST OF TABLES

LIST OF FIGURES

xix

xxii

CHAPTER I.

INTRODUCTION AND LITERATURE REVIEW

I.1. Identification of Problem and Significance

Modern societies demand clean fuels.   Clean fuels are compulsory for environment

protections.   Increasingly stringent restrictions have been proposed regarding the quality

of transportation fuels (Song and Ma, 2004).   The concentration of sulfur in the fuels is

an important control factor because the emission of sulfur leads to SOx air pollution.

Governments of numerous countries in the world have implemented new stringent

regulations that aim at drastically reducing sulfur emission using fuels with lower sulfur

content, ca. 50 parts per million (ppm) or less by 2005; 15 ppm or less by 2010 (Song and

Ma, 2004).   However, according to the current refinery technologies, the sulfur content

in liquid fuel is typically around 300-500 parts per million by weight (ppmw) (Song and

Ma, 2004; Vargas-Tah *et al*., 2005).   Novel desulfurization technologies are required.

Besides these environmental issues, desulfurization is also necessary for modern power

technologies.   For example, the integrated gasification combined cycle (IGCC) and

coal-to-electricity in power generation processes need to be operated at low sulfur

concentrations.   With efficient desulfurization, the power generation processes can be

improved significantly (Ben-Slimane and Hepworth, 1994; Lew *et al.*, 1989; Gasper-Galvin *et al.*, 1998).

Desulfurization is also required for fuel cell systems that use hydrocarbon fuels, such as natural gas, liquefied petroleum gas (LPG), gasoline, to protect the precious metal catalysts in fuel processors and the anode material in the fuel cells from sulfur poisoning (Fukunaga *et al.*, 2003; Zheng *et al.*, 2004; Lu *et al.*, 2005). Desulfurization is crucial in logistic fuel cell systems, especially these for military applications, where the sulfur content varies greatly from several hundred to several thousand ppmw due to the different sources of fuels.

In a typical logistic fuel cell power system, water and fuels such as jet fuels, gasoline and diesel are fed to a reformer. In the reformer, liquid hydrocarbons are converted to reformates containing H_2, C_1-C_3 hydrocarbons, CO and CO_2; sulfur compounds are converted to hydrogen sulfide (H_2S), due to the highly reducing environment in the reformer. In following clean up procedures, C_1-C_3 hydrocarbons, CO, CO_2 and H_2S are either converted to H_2 or removed from reformate stream (Lu *et al.*, 2005), as shown in **Figure I-1**. Deep H_2S removal is one of the key steps because of (1) the need to prevent downstream catalysts (mainly made of precious metals) from sulfur poisoning, (2) the requirement to protect the anode materials in fuel cells, especially the proton exchange membrane fuel cells (PEMFCs), and (3) the need to prevent turbines from corrosion (Lu *et al.*, 2005; Song, 2003). For most PEMFCs, an acceptable inlet concentration of H_2S

2

is typically less than one parts per million by volume (ppmv), some even require as low

as 0.1 ppmv. An increasing attention has been focused on developing novel methods

and/or materials for efficient gas phase desulfurization for logistic fuel cell applications.
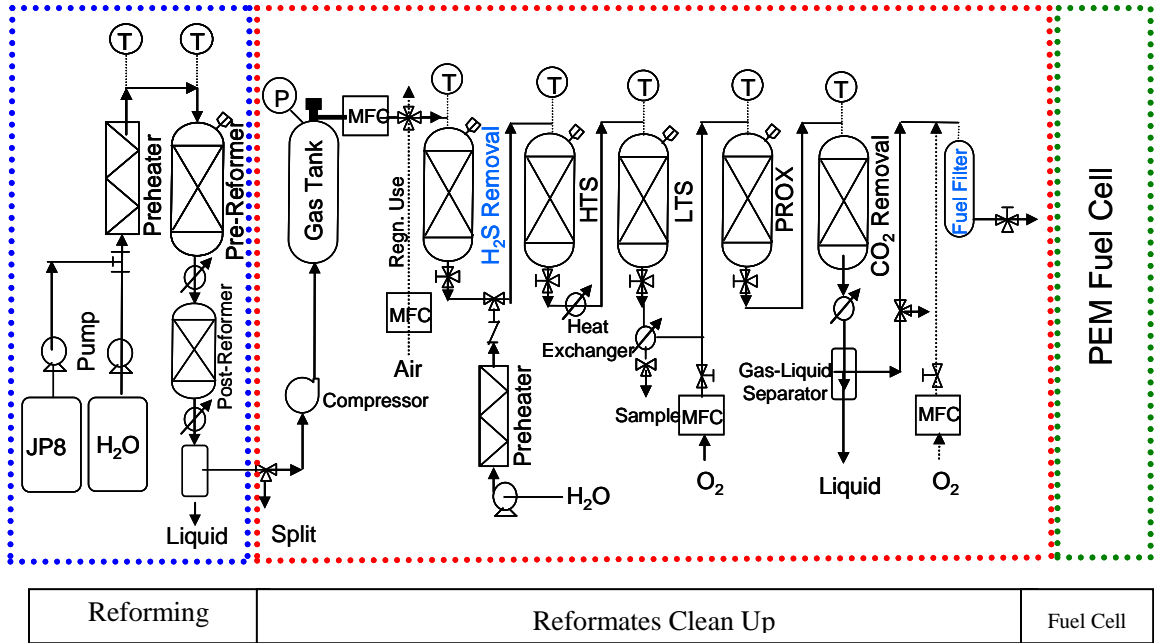
Figure I-1. A typical setup for logistic fuel to H_2 conversion.

No matter which type of approach adopted to remove sulfur, there are common

developmental questions and issues for logistic fuel cell applications, including:

1. Achieving high levels of sulfur removal. The higher level sulfur removal (lower

breakthrough concentration), the larger reactor size in the same flow conditions is. Most

logistic desulfurization units use packed bed reactors. They typically have large reactor

size, due to the channeling, severe intra-particle mass/heat transfer.

2. Minimization in mass, volume and complexity of the desulfurizer and the overall

system to promote rapid system and stack startup.

3

3. High sulfur removal capacity in the whole service life of a catalyst or sorbent (e.g. a disposable sorbent with very high sulfur capacity, or a regenerable sorbent with low capacity);

4. Regenerability of the sorbent: temperature, energy requirements, gas atmosphere needed, disposal/purging of effluent, safety concerns, need for additional valving, pumping and/or other components and utilities;

5. Matching the thermal/energy requirements, temperature limits, and required desulfurization levels of the system (e.g., a low temperature sorbent at ca. 400 ℃ may be a good match to a reformer and cleanup units in a PEMFC system);

6. Manufacturability, cost, and near term availability of the sorbent technology or technologies selected, compatibility with the rest of the system.

I.2. Literature Review

I.2.1. Desulfurization Technologies

In order to obtain clean fuel gases to power fuel cells, two different approaches have been undergoing extensive research and development. The first one is the pre-reformer sulfur removal, which removes sulfur-containing compounds from liquid fuels and yields sulfur-free fuels to feed reformer. In this approach, catalysts in reformers are not necessarily to be sulfur tolerant and H_2S removal units in reformates cleanup process (as

shown in **Figure I-1**) may not be required.   Organic sulfur compounds can be removed

via catalytic reactions.   Catalysts convert organic sulfur compounds to H_2S in the

presence of H_2 and yield ultra-clean liquid fuels.   Hydrodesulfurization (HDS) is such a

kind of process widely used in modern refineries.   Current HDS is able to reduce the

sulfur content to several hundred ppmw as in commercial gasoline and diesels.   With the

most advanced catalysts, sulfur content can be further reduced to several ppmv,

depending on the composition of crude oil (Song and Ma, 2004).   Disadvantages of

HDS, however, are the H_2 requirement, high pressure, and increasing reactor size for

deep desulfurization, as shown in **Figure I-2**.
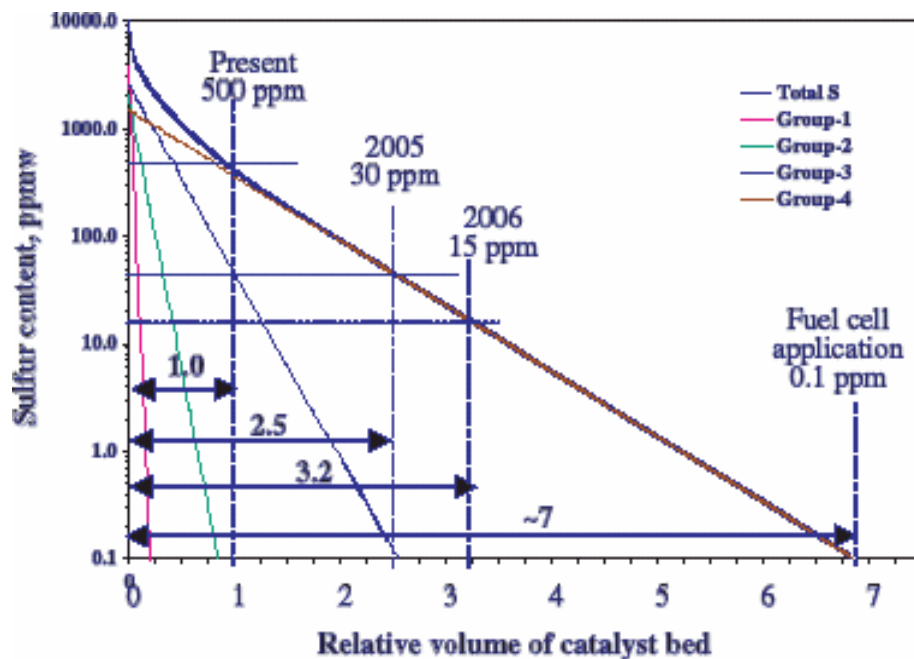
Figure I-2. Simulated HDS for diesel to meet 15 and 0.1 ppm sulfur levels based on a
conventional single-stage reactor, assuming 1.0 wt.% S in feed. Figure adopted from
reference of Song and Ma (2004).

Organic sulfur compounds can also be removed by adsorbents. Several research groups reported that some zeolite based adsorbents successfully reduced the sulfur content in liquid fuels to sub-ppmw levels (Hernandez-Maldonado *et al.*, 2003; Hernandez-Maldonado *et al.*, 2004; Hernandez-Maldonado and Yang, 2004a; Hernandez-Maldonado and Yang, 2004b; Hernandez-Maldonado *et al.* 2005; Yang *et al.*, 2001; Jayaraman *et al.*, 2001; Takahashi *et al.*, 2002; Velu *et al.*, 2003; Velu *et al.*, 2005). Some typical adsorbents are listed in **Table I-1**. However, the adsorbents usually have very low saturation sulfur capacities (<20 mg S/g adsorbent), therefore a large reactor size is required to achieve sub-ppm level sulfur removal. This major drawback of liquid phase desulfurization by adsorbents limits their applications in logistic applications.

The second approach is the post-reformer sulfur removal, which mainly involves with gas phase desulfurization, especially H_2S by sorbents. It applies various sorbents to remove sulfur compounds mainly H_2S from gasified fuels or reformates generated in reformers. The operational temperatures of gas phase desulfurization by sorbents can range from below 400 ℃ to over 900 ℃ depending on: (1) the thermal stability of the active metal or metal oxide phase responsible for sulfur adsorption, and/or (2) the level of sulfur removal desired versus the corresponding equilibrium relationship between H_2S and H_2O over the sorbents in question. Sorbents for gas phase desulfurization usually have high sulfur capacities, compared with their liquid phase counterparts, as shown in **Table I-2**, and therefore require small reactors to remove the same amount of sulfur,

6

which is an advantage for logistic fuel cell applications.   However, the post-reformer

sulfur removal requires the catalysts in reformers or crackers to have good sulfur

tolerance.

Table I-1. Typical adsorbents for liquid phase sulfur removal.

Sorbent	Breakthrough capacity (mg S/g)	Sulfur removal efficiency (ppmw)	Regeneration condition	Disadvantage	Reference
S-Zorb	-	10 at 343-413°C, 7-21atm	H_2 (>70%) at 343-413°C, 7-21atm	High purity H_2 is required continuously	Song, 2003
TReND	-	Mercapton complete removed at 426-535°C	-	H_2 is required to remove thiophenic sulfur	Song, 2003
Cu(I)-Y (π-complex)	12.6(b. at 1ppm) 23.13 (s)	<1 ambient	350°C in air then 450°C in He	Selectivity and Regn. issue	Hernandez-Maldonado et al.,2005
Ni(II)-Y (π-complex)	7.3 (b. at 1ppm) at 200 °C	<1	350°C in air	-	Hernandez-Maldonado et al.,2005
Ag(I)-Y (π-complex)	1.3(b. at 1ppm)	<1	350°C in air	Low capacity	Yang et al., 2001
Ni/SiO$_2$-Al$_2$O$_3$	>10 (b. at 30ppm)	3.5 at 230°C ambient pressure	Oxidation followed reduction at 500°C	-	Velu et al., 2005
Ce(III)-Y (non-π-complex)	>10 (s) at 80°C	<1	-	-	Velu et al., 2003

(b) indicates breakthrough capacity; (s) indicates saturation capacity
Challenge fuel: JP-8 (364.1 ppmw Sulfur)

Table I-2. The capacities and required reactor sizes for liquid phase desulfurization adsorbents and gas phase desulfurization sorbents.

Sorbent	Liquid Phase Desulfurization Adsorbent	Gas Phase Desulfurization Sorbent
Sulfur Content (ppmw)	3000	
Fuel Flow Rate (kg/h)	2.8	
Bench Test Time (h)	500	
Saturation Sulfur Capacity (mg/g)	23 [1]	264 [2]
Adsorbent Density (g/ml)	0.6	1
Reactor Volume (L)	283	16

Data were calculated for a 10KW fuel cell system with an overall efficiency of 30 %
1 best value found in the references;
2. 60 % of ZnO stoichiometric capacity, an experimental data for 3/16" extrudates.

Gas phase desulfurization can be performed using other technologies. The Claus process is the most significant gas desulfurization process (Gary and Handwerk, 1984). In this process, H_2S is oxidized by combustion in oxygen (air) to generate SO_2, which reacts catalytically with H_2S to form elemental sulfur. This process is widely employed to remove H_2S at high concentration ca. 25 vol.% in tail gas generated in HDS in refineries. However, since combustion in the presence of air is employed, this process is not applicable for reformate desulfurization due to the presence of H_2 at high concentrations and sulfur at ppm levels. Hydrogen sulfide (H_2S) was also removed from gas streams by adsorption using sulfur-scrubbing liquid (Stavorinus, 1910; Desgrez, 1926; Gluud and Schonfelder, 1927; Smith and Pryde, 1936). The scrubbing liquids were mainly basic solutions e.g. K_3PO_4 (Rosebaugh, 1938), amines (Gluud and Schonfelder, 1927), or slurries containing transition metal oxides (Desgrez, 1926) or

hydroxides (Stavorinus, 1910). The early dry desulfurization for H_2S by using solid sorbents was conducted by Huff and Logan in 1936. Their sorbent composed of Cu-Cr and Cu-V with magnesite-clay as a binder, was able to remove the H_2S and organic sulfur compounds from gases up to 1100 °C, and the spent sorbents could be regenerated in oxygen containing gases(Huff and Logan, 1936). Compared with wet desulfurization processes, dry desulfurization processes are obviously more convenient (Wood and Storrs, 1938). Therefore, the gas phase desulfurization by using solid reactive sorbents attracted more and more research interests for logistic applications.

I.2.2. Metal Oxide Sorbents

I.2.2.1. Sorbents Screening

Most sorbents used in dry gas phase desulfurization are metal oxides. In 1967, iron oxide was employed to remove sulfur from coal oven gas at 400 ºC (Westmoreland and Harrison, 1976); in 1970, zinc oxide was reported as a sorbent to remove H_2S from hydrocarbon feedstocks for ammonia synthesis (Westmoreland and Harrison, 1976). In 1976, Westmoreland and Harrison conducted the first comparative study on 28 solids, primarily metal oxides. Based on the equilibrium constants and Gibbs free energies, they pointed out that eleven metal oxides of iron (Fe), zinc (Zn), molybdenum (Mo), manganese (Mn), vanadium (V), calcium (Ca), strontium (Sr), barium (Ba) , cobalt (Co), copper (Cu) and tungsten (W) had thermodynamic feasibility for desulfurization for

low-Btu gases.   From this study, the metal oxides can be divided into two groups according to their operational temperatures: (1) the high temperature (T>600 ºC) group including Ba, Ca, Cu, Mn, Mo, Sr, W; (2) the low temperature (300-550ºC) group including Co, Fe, V, and Zn.   In their following study, Westmoreland *et al.* (1977) compared initial reaction rates between H_2S and MnO, CaO, ZnO and V_2O_3 in a thermal-balance reactor with a temperature range from 300 ºC to 800 ºC.   They indicated that the relative magnitude of initial reaction rate dropped in the order of MnO> CaO ≈ ZnO> V_2O_3.

Ayala and Abbasian conducted another evaluation of metal oxide sorbents for low temperature H_2S removal from fuel gases (Slimane and Abbasian, 2000a).   In their study, they added several criteria: (i) favorable thermodynamic equilibria in the temperature range, (ii) minimization of undesired reactions between the sorbents and components in fuel gas during desulfurization, such as oxide reduction, carbonyls and carbides formation and chlorides formation, (iii) feasibility and ease of regeneration and (iv) minimization of undesired reaction in regeneration conditions, such as sulfate formations. Based on these criteria, several oxides, such as BaO, CaO, SrO and V_2O_3 are moved out from Westmoreland's list because of their high sulfidation or regeneration temperatures. Therefore, oxides of Co, Cu, Fe, Mn, Mo, W and Zn remained in the candidates list.

Based on a report of Elseviers and Verelst (1999), both molybdenum (Mo) and tungsten (W) oxides have high desulfurization potential; however, metal carbides

10

formation at moderate temperatures was observed. Cobalt oxide and copper oxide are ready to be reduced to metallic in highly reducing gas atmosphere like reformates; moreover, the performance of cobalt or copper becomes less efficient with increasing temperature (Westmoreland and Harrison, 1976). However, cobalt sulfide requires a higher regeneration temperature than copper sulfide does (Elseviers and Verelst, 1999). Therefore, Co Mo and W are removed from the list above, and the possible candidates for low temperature desulfurization are oxides based on Cu, Fe, Mn and Zn. Sorbents based on these metals oxides, some sorbents widely used in industry such as $CaO/CaCO_3$ and some novel sorbents based on rare earth metal oxides that were not in the initial list of Westmoreland, are discussed alphabetically in this work.

I.2.2.2. Calcium Oxide Based Sorbents

Calcium oxide (CaO), sorbent widely used in both laboratorial and industrial scale, is able to remove most acid gases, e.g. CO_2, H_2S and SO_2, even at low temperatures. In most cases, CaO based sorbents are treated as a disposable sorbents, because of their high regeneration temperatures, which are normally above 1400 ºC. Compared with low cost of CaO, the regeneration is not costly applicable. Because of its high equilibrium constants, as shown in **Table I-3**, high theoretical capacity (0.61 g H_2S/g of CaO), fast reaction kinetics (Westmoreland *et al*. 1977) and low cost , it has attracted lot of research attentions in gas phase desulfurization since 1970s (Biba and Hrncir, 1979; Squires, 1971;

Yang and Chen, 1979; Freund, 1981; Fenouil and Lynn, 1994; Fenouil and Lynn, 1995a, 1995b, 1995c; Yrjas, 1996; Adănez et al., 1998).   In those reports limestones ($CaCO_3$) and dolomites ($CaCO_3$-$MgCO_3$) were pre-mixed with coal and added to gasifiers maintained at a temperature that $MgCO_3$ and $CaCO_3$ are ready to decompose rapidly.

Table I-3. The equilibrium constants of the reactions between CaO and H_2S, CaO and CO_2.   Data were generated using HSC 3 Software.

T	K	
(C°)	CaO-H_2S	CaO-CO_2
0	2.84×10^{11}	6.34×10^{25}
100	2.57×10^{8}	4.65×10^{16}
200	4.56×10^{6}	2.59×10^{11}
300	3.31×10^{5}	1.02×10^{8}
400	5.22×10^{4}	4.30×10^{5}
500	1.32×10^{4}	7.66×10^{3}
600	4.57×10^{3}	3.52×10^{2}
700	1.96×10^{3}	3.11×10^{1}
800	9.76×10^{2}	4.41×10^{0}
900	5.47×10^{2}	8.88×10^{-1}
1000	3.35×10^{2}	2.34×10^{-1}

At a temperature less than 500 ºC, CaO demonstrates more affinity to CO_2 rather than H_2S, see **Table I-3**.   Therefore, CO_2 concentration determines the desulfurization performance of CaO.   Since $CaCO_3$ decomposes at 800 ºC, $CaCO_3$ is considered to be the effective sorbent at temperatures below 800ºC, and CaO, at temperatures above 800ºC (Fenouil and Lynn, 1995b, Adănez et al., 1998), in the environments (e.g., reformates) that CO_2 partial pressure is much larger than that of H_2S, as shown in **Figure I-3**. **Figure I-3** suggests that the H_2S equilibrium concentration is controlled by dashed line at

temperatures below 800 °C; at temperatures above 800 °C, it is controlled by solid line. Data were generated using HSC 3 Software. Therefore, it is clear that CaO/CaCO$_3$ is not a good sorbent to reduce the H$_2$S concentration to sub-ppm levels in the presence of reformates containing 20-30 vol.% CO$_2$. The desulfurization reactions of CaO and CaCO$_3$ are given by reaction 1 and reaction 2 respectively.

$$CaCO_3+H_2S=CaS+CO_2+H_2O \tag{1}$$

$$CaO+H_2S=CaS+H_2O \tag{2}$$

Figure I-3. H$_2$S equilibrium concentrations in the desulfurization for reformates (20 vol.% H$_2$O-20 vol.% CO$_2$-10 vol.% CO-9 vol.% C$_1$-C$_3$-41 vol.% H$_2$) using CaO and CaCO$_3$ sorbents at various temperatures. Data were generated using HSC 3 Software.

Fenouil and Lynn (1995c) discussed the kinetics of H$_2$S adsorption by uncalcined limestones (CaCO$_3$), and pointed out that the reaction between CaCO$_3$ and H$_2$S was a first order reaction with respect to the H$_2$S partial pressure in the temperature range of 560-660 °C, and the adsorption process was controlled by chemical reaction. In the

temperature range of 660 to 710 ºC, the reaction order increased to 1.5 with respect to H_2S partial pressure. In the 710-860 ºC, the adsorption process was under diffusion control in the spent sorbent (CaS) layers. Chauk *et al*. (2000) used CaO powder to remove H_2S from coal gas at high pressures in the temperature range of 650-900 °C, and found the high initial surface area and high pore volume helped the CaO sulfidation. They also pointed out that the kinetics of CaO sulfidation at high pressures was controlled by solid-state diffusion and simulated data by a modified grain model matched the experimental data reasonably well.

Recently, most research efforts focused on the design of new calcium based sorbents with high desulfurization performance. These efforts included preparation of novel calcium sorbents from various precursors, such as calcium acetate (Nimmo, 1999; Adănez, 1999), bio-oil (Sotirchos and Smith, 2004), shell waste (Hamana *et al*., 2004), and mixed oxide sorbent such as calcium ferrite (Kenaga *et al*., 2005). Calcium ferrite is the mixture of Fe_2O_3 and CaO calcined at high temperature and supported on char. This sorbent demonstrated almost 100% of the stoichiometric amount of loaded metal species for the desulfurization at 500 °C.

I.2.2.3. Copper Oxides Based Sorbents

Copper oxide (CuO) has been widely used to remove H_2S and SO_2. Copper oxides including cupric oxide (CuO) and cuprous oxide (Cu_2O), both are excellent sulfur

sorbents. The reactions between H_2S and copper oxides at low temperatures were described by Patrick *et al*. (1989), see reaction 3 and reaction 4. Equilibrium constants are listed in **Table I-4**. They are both able to reduce the H_2S concentration down to less than 0.1 ppm in the presence of 20 vol.% steam, as shown in **Figure I-4**.

$$2CuO+H_2S+H_2=Cu_2S+2H_2O \tag{3}$$

$$Cu_2O+H_2S=Cu_2S+H_2O \tag{4}$$
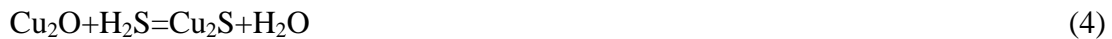
The theoretical capacities are 0.21 g H_2S/ g Sorbent for CuO, and 0.24 g H_2S/g of Sorbent for Cu_2O, which are only one third of CaO sulfur capacity or 50% of ZnO sulfur capacity. Moreover, copper oxides are not the stable in highly reducing gases, such as reformates, they are prone to be reduced to metallic copper even at low temperatures via reactions 5 and 6. They both are rapid reactions and metallic copper becomes the active sorbent for H_2S removal according to reaction 7 (Kamhankar *et al*., 1986).

$$CuO+H_2=Cu+H_2O \tag{5}$$

$$Cu_2O+H_2=2Cu+H_2O \tag{6}$$

$$2Cu+H_2S=Cu_2S+H_2 \tag{7}$$

Although, metallic copper is also a good desulfurization sorbent, its sulfidation equilibrium constant is much inferior to these of copper oxides at the same temperature (Kamhankar *et al*., 1986), as shown in **Table I-4**. Moreover, metallic copper is ready to form metallic agglomeration accompanied with severe surface area loss and poor kinetics. Besides oxide reduction, another shortcoming of copper oxide, according to Kyotani *et al*.

15

(1989) is that the product of sulfidation, Cu_2S, tends to form a dense solid film blocking

the mass transfer.

Table I-4. Equilibrium constants and ΔGs of reactions 3, 4, and 7. Data were generated by HSC 3 Software.

T (°C)	Reaction 3		Reaction 4		Reaction 7	
	ΔG (kJ)	K	ΔG (kJ)	K	ΔG (kJ)	K
0	-252	1.51×10^{48}	-133.7	3.69×10^{25}	-53.8	1.94×10^{10}
100	-259	1.88×10^{36}	-134.5	6.72×10^{18}	-51.5	1.60×10^{7}
200	-267	3.23×10^{29}	-136.8	1.27×10^{15}	-50.9	4.21×10^{5}
300	-276	1.30×10^{25}	-139.7	5.36×10^{12}	-51.2	4.68×10^{4}
400	-284	1.05×10^{22}	142.8	1.22×10^{11}	-52.1	1.10×10^{4}
500	-292	5.28×10^{19}	-146.3	7.63×10^{9}	-53.4	4.05×10^{3}
600	-300	8.76×10^{17}	-149.8	9.19×10^{8}	-55.0	1.95×10^{3}
700	-308	3.28×10^{16}	-153.4	1.71×10^{8}	-56.8	1.12×10^{3}
800	-315	2.21×10^{15}	-156.9	4.35×10^{7}	-58.6	7.16×10^{2}
900	-323	2.32×10^{14}	-160.4	1.39×10^{7}	-60.6	4.99×10^{2}
1000	-330	3.39×10^{13}	163.8	5.26×10^{6}	-62.6	3.69×10^{2}
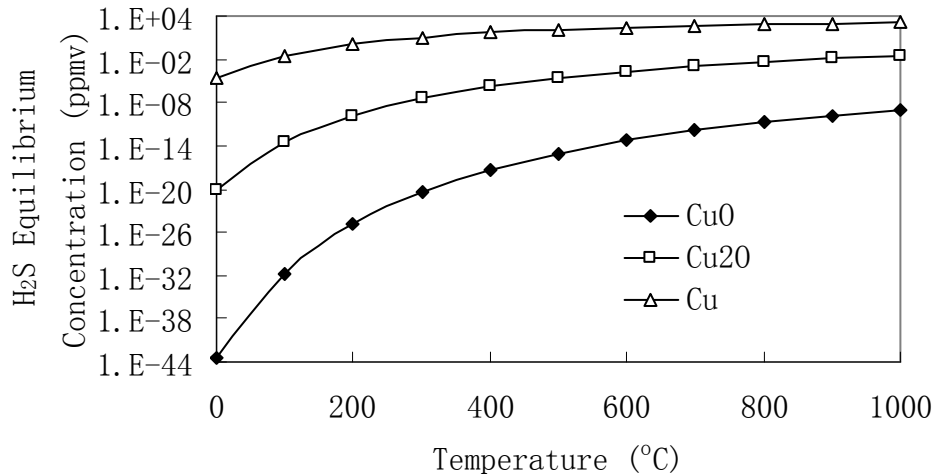
Figure I-4. H_2S equilibrium concentrations in the desulfurization for reformates (20 vol.% H_2O-20 vol.% CO_2-10 vol.% CO-9 vol.% C_1-C_3-41 vol.% H_2) using the sorbents of CuO, Cu_2O and Cu at various temperatures. Data were generated using HSC 3 Software.

16

In order to retain copper at the oxidative states of +2 or +1, copper oxides are commonly supported on or stabilized by inert materials, for instant, zeolite (Kyotani *et al.* 1989; Atimatay *et al.*, 1993; Gasper-Galvin *et al.*, 1998), silica (Kyotani *et al.* 1989) and alumina (Kamhankar *et al.*, 1986; Gasper-Galvin *et al.*, 1998; Wang and Lin, 1998; Ko *et al.*, 2005), or mixed with other metal oxides to form a multi-component sorbent system, such as Cu-Ce-O (Akyurtlu and Akyurtlu, 1999; Li and Flyzani-Stephanopoulos, 1997), Cu-Cr-O (Li and Flyzani-Stephanopoulos, 1997; Alonso *et al.*, 2000; Slimane and Abbasian, 2000b), Cu-Fe-O (Tamhankar *et al.* 1986), Cu-Mn-O (Atimatay *et al.*, 1993; Gasper-Galvin *et al.*, 1998; Alonso *et al.*, 2000; Desai *et al.*, 1990; Slimane and Abbasian, 2000b), Cu-Fe-Al-O (Gangwal *et al.*, 1988; Patrick *et al.*, 1989; Kamhankar *et al.*, 1986), Cu-Mo-Al-O (Gasper-Galvin *et al.*, 1998). Kyotani *et al.* (1989) compared the desulfurization performances of pure copper oxide, supported copper oxide on silica and zeolite, and silica diluted copper oxide. They found that supported copper oxide sorbents exhibited the better desulfurization performance than pure oxide, and physical dilution also improved the desulfurization performance. In 1993, Atimatay *et al.* (1993) discussed performance of zeolite-supported sorbents for regenerable applications in IGCC system. Patrick *et al.* (1989) obtained the detailed mechanism and qualitative kinetic information about sulfidation and regeneration of the binary $CuO-Al_2O_3$ sorbents. They found that $CuAl_2O_4$ formation occurred at 900 °C by X-ray diffraction analysis. The reduction of copper oxide supported on alumina was one order of magnitude slower

17

than the CuO in mixture form, because of the association of CuO with Al_2O_3.   It was recognized that copper was stabilized at oxide state +2 or +1 by alumina supports.   Like pure copper oxide, the supported sorbents were found to be able to achieve sub-ppm H_2S breakthrough levels at a temperature as high as 700 ℃ depending on the reducibility of fuel gases.   However, it was also found the Al_2O_3 supported sorbents exhibited slower sulfidation rate and Al_2O_3 accelerated the formation of sulfate during sorbent regeneration (Patrick *et al*., 1989).

Besides the sorbent of CuO supported on alumina, other supported CuO sorbents and mixed metal oxide sorbents with CuO have also been developed.   As for Cu-Mn-O systems, the NaOH co-precipitated Cu-Mn-O tends to form $CuMnO_2$, which was considered to stabilize Cu in oxide states.   Fresh $CuMnO_2$ demonstrated capability to remove H_2S to sub-ppm level at 500 °C; however, the regenerated $CuMnO_2$ at 650-750 °C demonstrated poor desulfurization performance with a pre-breakthrough H_2S concentration at 30 ppmv. $CuMnO_2$ prepared by calcination of CuO and MnO at 950 °C was tested at 600 °C for H_2S desulfurization and the results suggested MnO did not stabilize CuO and CuO did not prevent the sulfate formation of MnO (Alonso *et al*., 2000).   Similarly, iron oxide in copper ferrite (Cu-Fe-O) was not found to stabilize the Cu at its oxide state (Kamhankar *et al*., 1986).   Tamhankar *et al*. (1986) suggested that a sorbent ($2CuO$-Fe_2O_3-Al_2O_3) had a superior sulfidation performance to CuO-Al_2O_3 and CuO-Fe_2O_3 at temperatures as high as 650 °C.   Li and Flytzani-Stephanopoulos (1998)

18

prepared and tested novel copper oxide sorbents: $CuO-Cr_2O_3$ and $CuO-CeO_2$. They found that the first binary-oxide sorbent, like $Cu-Al_2O_3$, can form copper chromite, which demonstrated the lowest reducibility of all copper oxide-containing compounds reported in literature. They noticed that CeO_2 and CuO were immiscible, and CeO_2 made CuO well dispersed and maintained CuO/Cu as small cluster rather than retaining its oxidative states. Both sorbents demonstrated nice desulfurization performance for hot fuel gases.

I.2.2.4. Iron Oxides Based Sorbents

Iron oxides, one of the best metal oxides candidates for H_2S removal, have been studied extensively in 1970s and 1980s. Compared with ZnO, iron oxides though do not have favorable sulfidation thermodynamics, as shown in **Table I-5**; they excel ZnO from the cost point of view (Sasaoka *et al*., 1992). Fe_2O_3 is not stable in reducing environments; the stable form of iron oxides in fuel gases is either FeO or Fe_3O_4, depending on the reducing power of the fuel gas and the temperatures. The desulfurization performance of FeO is shown in **Figure I-5**. The sulfidation reactions of iron oxides are following:

$$FeO+H_2S=FeS+H_2O \tag{8}$$

$$Fe_3O_4+3H_2S+H_2=3FeS+4H_2O \tag{9}$$

According to reactions 8 and 9, FeO has a capacity of 0.47 g H_2S/g sorbent; Fe_3O_4, 0.44, compared with 0.42 of ZnO. Focht *et al*. (1988) indicated that iron oxides such as

19

Fe_3O_4 were more reactive than Fe metal. Therefore, iron oxides are suitable for fuel gases with low reducibility. Moreover, iron oxides based sorbents require much lower temperatures for both sulfidation and regeneration than most other metal oxides. These properties make iron oxide based sorbents be the best candidate for the desulfurization in the temperature range of 350-550 ºC (Slimane and Abbasian, 2000a).

Table I-5. Equilibrium constants of the sulfidaions of FeO and ZnO at various reaction temperatures. Data were generated using HSC 3 software.

T	FeO	ZnO
(°C)	K	K
0	8.25×10^9	5.32×10^{13}
100	1.17×10^7	1.03×10^{10}
200	3.20×10^5	7.60×10^7
300	3.45×10^4	3.15×10^6
400	7.57×10^3	3.39×10^5
500	2.48×10^3	6.50×10^4
600	1.05×10^3	1.82×10^4
700	5.24×10^2	6.64×10^3
800	2.98×10^2	2.92×10^3
900	1.86×10^2	1.48×10^3
1000	1.24×10^2	8.30×10^2

Iron ores have been practically used as desulfurization sorbents since 1988 (Sasaoka *et al.*, 1992). Sasaoka *et al.* (1993) indicated that the iron ores were suitable for a H_2O-lean and/or H_2-rich coal gases and they optimized the manufacturing methods for iron ore based sorbents in 1993. Pham-Huu *et al.* (1998) developed a supported iron sorbent: iron oxide on high surface area β-SiC. The sorbent showed an excellent desulfurization performance at 400 ºC. They also observed a dramatic loss in sorbent

area during sulfidation.   In the same year, White *et al*. (1998) developed a novel process

to removal H_2S from fuel gas by an iron oxide based sorbent for IGCC applications, with

elemental sulfur production during sorbent regeneration.
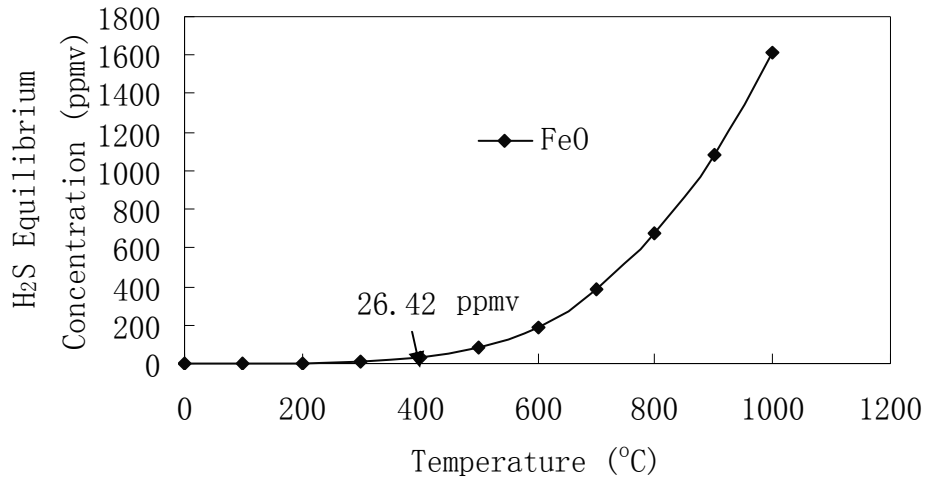
Figure I-5. H_2S equilibrium concentrations in the desulfurization for reformates (20
vol.% H_2O-20 vol.% CO_2-10 vol.% CO-9 vol.% C_1-C_3-41 vol.% H_2) using FeO sorbent
at various temperatures. Data were generated using HSC 3 Software.

However, iron oxide based sorbents have some drawbacks for practical use.   The

sulfur capacity drops severely in the presence of water, and equilibrium H_2S

concentrations are much higher than the threshold of PEMFC applications, as shown in

Figure I-5.   In highly reducing gases containing large fraction of H_2 or CO, such as

reformates and coal gas, iron oxides become unstable and reduced to metallic iron.   For

example, at 700 ºC, Fe_3O_4 was found to be reduced to FeO in presence of coal gas, which

showed detrimental effects on sulfidation reactivity (Focht *et al*., 1988).   At

temperatures above 500 ºC, the excess iron reduction and iron carbide formation lead to

21

severe sorbent decrepitation (Focht *et al.*, 1988; Ayala and Marsh, 1991; Gupta *et al.*, 1992).   Another drawback is high temperatures, ca. 850 °C, are required to regenerate FeS without sulfate formation (Woods *et al.*, 1991).

Besides being used as sulfur sorbent, iron oxides are widely used as a component in mixed oxides to form metal ferrites, such as calcium ferrite (Kenaga *et al.*, 2005), copper ferrite (Kamhankar *et al.*, 1986), zinc ferrite.   Zinc ferrite was study extensively in 1980s and 1990s.   It is discussed in section **I.2.2.8.**

I.2.2.5. Manganese Oxide Based Sorbents

Among all manganese oxides, MnO is the stable oxide phase in reducing atmospheres, including the highly reducing environments and slightly reducing environments.   MnO maintains this feature even at high temperatures (T>750 ºC) (Gasper-Galvin, *et al.*, 1998; Westmoreland and Harrison, 1976; Ben-Slimane and Hepworth, 1994a).   Therefore, manganese based sorbents are exceptionally suitable for desulfurization of highly reducing gases at high temperatures.   The sulfidation of MnO is described by reaction 10.

$MnO+H_2S=MnS+H_2O$ (10)

Another advantage of manganese based sorbent is that the manganese sulfide can be regenerated at temperatures above 750 ºC to void sulfate formation, which means both sulfidation and regeneration of MnO sorbents can be conducted at the same temperature

(Ben-Slimane and Hepworth, 1994b). Such an arrangement in desulfurization and regeneration is quite cost effective and time saving. Compared with copper oxides or zinc oxide based sorbent, MnO has a slightly higher H_2S capacity of 0.48 g H_2S/g Sorbents, however, manganese oxide based desulfurization sorbents including MnO are not thermodynamically favorable for H_2S removal. The equilibrium constant of manganese oxide is much smaller than those of copper oxides or zinc oxide. As a result, the sulfur outlet concentrations therefore are much higher using MnO as sorbents. This drawback becomes significantly remarkable at elevated temperatures, as shown in **Figure I-6**. The performance of MnO may not meet the requirements for PEMFC applications, but it may find applications for solid oxide fuel cell (SOFC) systems, which have higher sulfur tolerance. Another possible disadvantage of MnO is the effect of CO_2 at a temperature below 400 °C due to $MnCO_3$ formation (Westmoreland and Harrison, 1976).
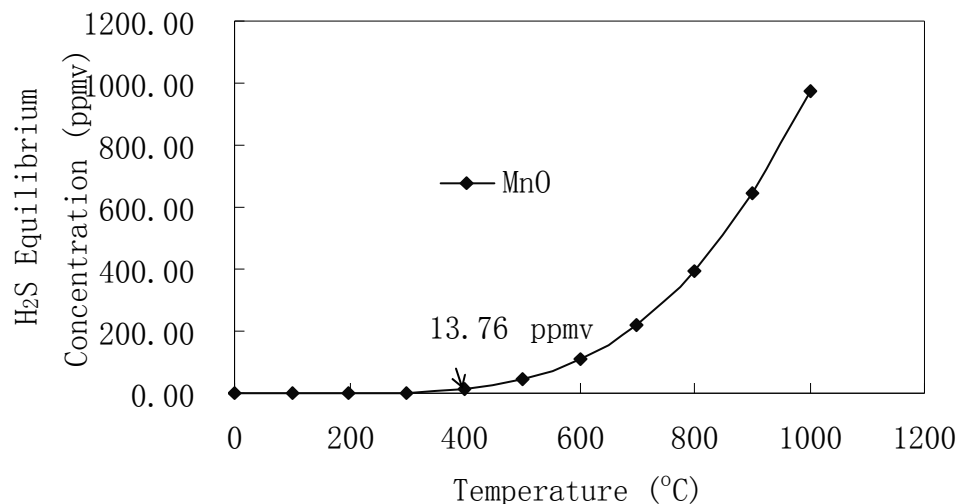
Figure I-6. H_2S equilibrium concentrations in the desulfurization for reformates (20 vol.% H_2O-20 vol.% CO_2-10 vol.% CO-9 vol.% C_1-C_3-41 vol.% H_2) using MnO sorbent at various temperatures. Data were generated Using HSC 3 Software.

23

In 1970s, manganese oxides were investigated for the feasibility to remove the hydrogen sulfide from reducing gases. Turkdogan and Olsson (1978) prepared manganese pellets by mixing manganese ore and alumina with a 3:1 weight ratio. The pellets demonstrated high structural integrity and rapid reaction kinetics at high temperatures. They found the pellets successfully removed the H_2S from H_2-H_2S hot gas at 800 ℃, and the sorbents can be regenerated in air for multicycles applications. In 1994, Ben-Slimance and Hepworth (1994a, 1994b) prepared another kind of manganese oxide based sorbent. The sorbent made of high purity manganese carbonate, alundum and bentonite as binder exhibited highly effective for sulfur removal in a temperature range of 800-1000 ℃. This sorbent was able to be regenerated in air or oxygen-deficient air. An interesting phenomenon they observed is the increasing capacity and improved kinetics after 5 regeneration-adsorption cycles. They believed these were possibly due to the cracks developed in the pellets.

Manganese oxide based sorbents have been studied for desulfurization at moderate temperatures. Wakker $et\ al$. (1993) prepared mixed oxide supported sorbents, such as manganese aluminate, for evaluation in the temperature range of 400-800 ℃. The supported sorbents demonstrated low sulfur capacities, although they successfully reduced the sulfur concentration down to 20 ppmv at 400 ℃, for multi-cycle applications. Among the supported sorbents, Ko $et\ al$. (2005) indicated that manganese oxide supported on γ-Al_2O_3 exhibited the better desulfurization ability than those supported on

silica and titania. Bakker *et al.* (2003) tested manganese oxide supported on γ-Al$_2$O$_3$ monoliths, cordierite monoliths with about 25 wt.% γ-Al$_2$O$_3$ wash-coated layer and particles, by wet impregnation, for high temperature desulfurization. They developed a sorbent with layered structure: the bottom layer was bulk MnAl$_2$O$_4$, the middle layer was amorphous MnAl$_2$O$_4$, and the top was discrete MnO grains. The bulk layer offered high sulfur capacity; the middle, good performance; the top, the efficient hydrogen sulfide removal in presence of H$_2$O. The sorbent was able to reduce the sulfur concentration down to below 100 ppmv from dried coal gas containing 0.4-2.0 vol.% H$_2$O. Moreover, the sorbent was quite stable, at least good for 110 cycles, and the sulfur uptake capacity was 20 wt.% of sulfur as they claimed. The most interesting part of their design is that SO$_2$ instead of air or oxygen in most other cases was used in regeneration with element sulfur production. The sorbent also demonstrated high capacities for HCl and HF in coal gas. Zhang *et al.* (2003) developed a regenerable MnO based sorbent: Mn-Fe-Zn/γ-Al$_2$O$_3$ (Mn/Fe/Zn=2:1:0.2) for multicycle applications. Another successfully developed sorbent was Zn doped MnO by Alonso and Palacios (2002).

I.2.2.6. Rare Earth Metal Oxide Based Sorbents

Rare earth metals have been widely used in catalysts, and they also have found many applications in gas phase desulfurization (Kundakovic and Flytzani-Stephanopoulos, 2002). Rare earth metal oxides such as cerium oxide (Zeng *et al.*, 1999; Zeng *et al.*,

2000; Kobayashi and Flytzani-Stephanopoulos, 2002), lanthanum oxide (Rajagopalan and Amiridis, 1998) have been developed for H_2S removal from hot fuel gases.

Cerium oxide, or ceria (CeO_2), is typically used as a promoter in three-way catalysts (TWC), because it can stabilize the surface area of alumina and interact with noble metals such as Rh, Pt and Pd (Akyurtlu and Akyurtlu, 1999). Ceria is also known for its high oxygen storage capacity (Akyurtlu and Akyurtlu, 1999, Kundakovic and Flytzani-Stephanopoulos, 2002; Zeng $et~al.$, 2000). Ceria is not active to sulfur, while reduced cerium oxide (Ce_2O_3) is an active desulfurizer. In gas desulfurization, cerium was used firstly in fluorite-type oxide, namely La doped CeO_2, as a support for CuO, which was the active chemical for H_2S removal. It was found that CeO_2 can keep Cu well dispersed and the reduced cerium oxide (Ce_2O_3) was found to be a superior H_2S capturer (Zeng $et~al.$, 2000). Zeng $et~al.$ (1999, 2000) designed a process in which bulk cerium oxide was used as regenerable H_2S sorbent to produce elemental sulfur with high yield. Although the equilibrium data from HSC chemistry 3 data station show a magnificent H_2S removal performance at high temperatures in high reducing atmosphere in the presence of water, the performance of reduced CeO_2 was far from the equilibrium data (Zeng $et~al.$, 2000). The possible explanation for this difference is that reduced CeO_2 was oxidized by water at high temperatures. Instability of reduced ceria in reformates with steam is an obvious drawback, which also explains the low sulfur capacity of ceria based sorbent (Zeng $et~al.$, 2000). Flytzani-Stephanopoulos and Wang

26

(2004) evaluated various doped cerium oxide sorbents for high temperature desulfurization, and found that the addition of La maintained the high surface area of ceria at high temperatures while addition of Cu accelerated the sulfidation kinetics. Another possible reason for effect of dopant is that the addition of La^{3+} creates more oxygen vacancies in the CeO_2 lattice and therefore accelerates the reaction between oxygen or sulfur anion and CeO_2.   The sulfidation of reduced ceria is given by

$$Ce_2O_3 + H_2S \rightarrow Ce_2O_2S + H_2O \hspace{4cm} (11)$$

Compared with cerium oxide, lanthanum did not attract much attention in desulfurization.   Actually, lanthanum has a strong affinity to sulfur atoms, and La metal is used as an additive to remove the sulfur from liquid steel by reducing FeS to Fe. Rajagopalan and Amiridis (1999) reported that lanthanum based perovskite-type sorbent such as $LaMnO_3$, $LaCoO_3$, $LaFeO_3$ and La_2CuO_4 demonstrated high initial capacities (0.15-0.34 g of H_2S/g of Sorbent) but poor regenerability due to the significant surface area loss in regeneration.

The rare earth metal oxide based H_2S sorbents normally do not have high capacities, however, their sulfidation is thermodynamically favored.   For example, at 800 ºC, with 20 vol.% of water, reduced cerium oxide is able to reduce the H_2S concentration down to 34 ppmv, compared with 77 ppmv of zinc titanate, as shown in **Figure I-7**.   Because of their high performance at elevated temperatures, the rare earth metal oxides based sorbents are the best desulfurization candidates for SOFC applications.
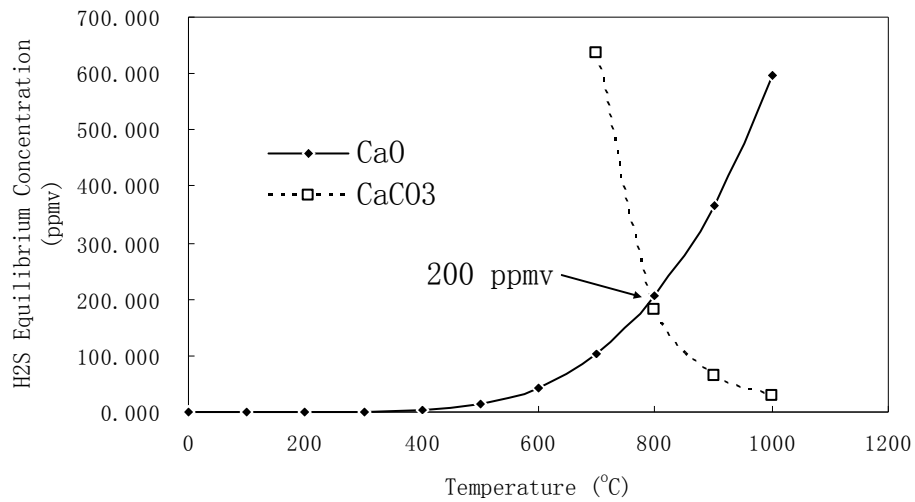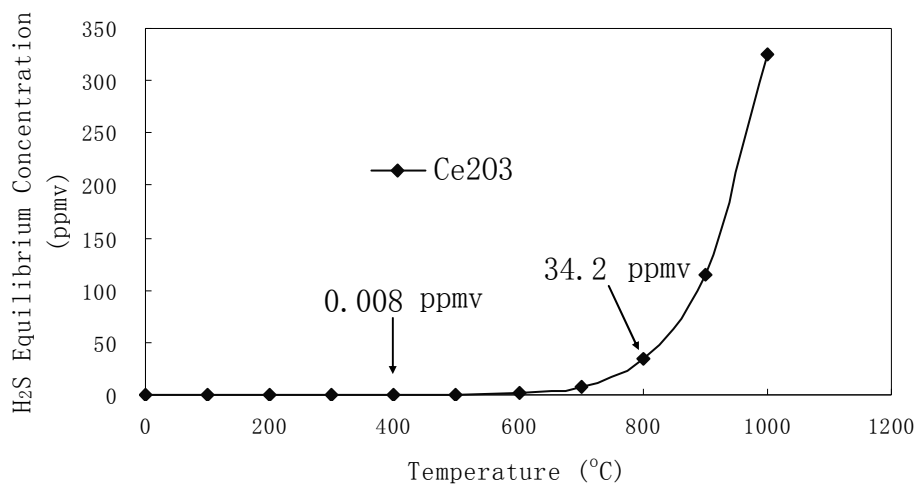
Figure I-7. H_2S equilibrium concentrations in the desulfurization for reformates (20 vol.% H_2O-20 vol.% CO_2-10 vol.% CO-9 vol.% C_1-C_3-41 vol.% H_2) using Ce_2O_3 sorbent at various temperatures. Data were generated using HSC 3 Software.

I.2.2.7. Zinc Oxide Based Sorbents

Zinc oxide has been employed for H_2S removal since 1970s. It was first used as a non-regenerable sorbent in "guard bed" protecting catalyst beds from sulfur poisoning in ammonia synthesis (Westmoreland and Harrison, 1976). The sulfidation reaction of ZnO (reaction 12) is thermodynamically favorable at low temperatures (T<500 °C), as shown in **Table I-5**, yielding outlet H_2S concentration at several ppmv or sub-ppm levels depending on gas composition. The performance of ZnO is shown in **Figure I-8.**

$$ZnO+H_2S=ZnS+H_2O \tag{12}$$
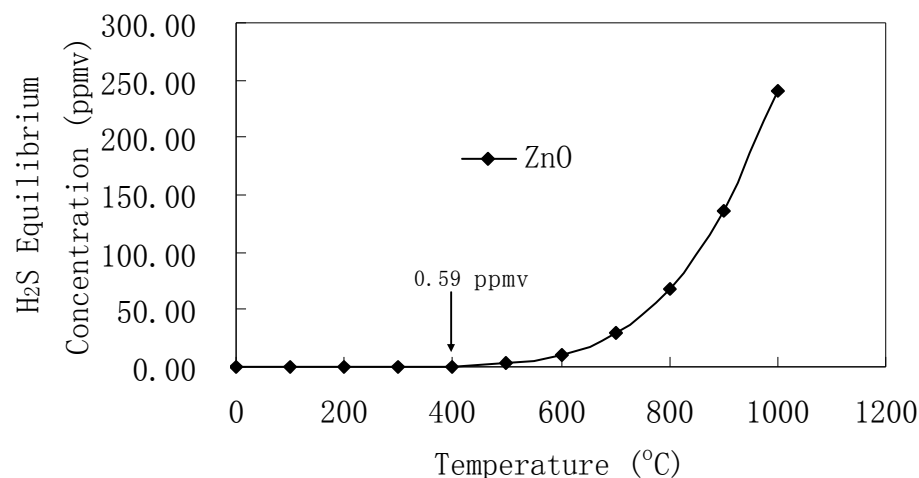
Figure I-8. H$_2$S equilibrium concentrations in the desulfurization for reformates (20 vol.% H$_2$O-20 vol.% CO$_2$-10 vol.% CO-9 vol.% C$_1$-C$_3$-41 vol.% H$_2$) using ZnO sorbent at various temperatures. Data were generated using HSC 3 Software.

Pure ZnO has a high stoichiometric capacity of 0.42 g H$_2$S/g ZnO, in practice the saturation sulfur capacity of commercial ZnO extrudates can reach > 60% of the stoichiometric value depending on the process temperature, flow conditions and sorbent properties. ZnO is an excellent desulfurization sorbent in the low temperature range of 300-550 °C (Newby *et al.*, 2001). At high temperatures (T>550 ℃), zinc loss in reducing fuel gases becomes significant (Westmoreland and Harrison, 1976). In a lower temperature range (from room temperature to 200 ℃), several studies have demonstrated the feasibility of modified zinc oxide based sorbent. Several ZnO based sorbents that were doped with first-row transition metal oxides, such as Co$_3$O$_4$, CuO, Fe$_2$O$_3$ and NiO, were prepared and evaluated by Baird *et al.* (1992) and Davison *et al.* (1995). They found that iron dopant did not significantly affect sulfur uptake at 200 ℃, while copper

and cobalt doped ZnO sorbents resulted in a remarkable enhancement. The main role of transition metals was considered to increase the total surface area available on the sorbents (Baird *et al*., 1992) and reduce the grain size in order of Cd < Co< Pd <Ni < Cu < Ca (Davison *et al*., 1995). Another interesting result in their study is that the reaction between H_2S and metal oxide was confined in a very thin surface layer (0.6 monolayer on average). It means that the ZnO beneath one monolayer was inaccessible to H_2S molecule, due to the limited mass transfer (solid diffusion) at 200 ºC. Baird *et al*. (1995) doped Co-Zn oxide mixture with Al^{3+} and found Al^{3+} did not improve the sulfur capacity at all. Baird *et al*. (1999) studied the Co doped ZnO again and pointed out that $ZnCo_2O_4$ spinel structure was formed in the doped sorbents and sulfur uptake was proportional to surface area of sorbents. They also observed surface structure of Co doped ZnO was reconstructed during the sulfidation due to the Co^{3+} reduction (Baird *et al*., 1999). Xue *et al*. (2003) doped ZnO micro-crystals with Fe, Ni, Co, Mn, Cu, Al, Ti and Zr, and found Cu doped and Ti-Zr doped ZnO had high saturation sulfur capacities. They pointed out that ZnO with hexagonal structure showed high sulfur capacity at room temperature.

I.2.2.7.1. Reaction Schemes

In most cases of heterogeneous reactions between H_2S and sorbents are controlled by pore and/or lattice diffusion. In the pore diffusion, the reaction rate is controlled by diffusion rate of H_2S in the pores to the fresh oxide. On the surface of ZnO sorbent,

according to Baird *et al*. (1999), the H_2S is dissociated into H^+ and HS^-. HS^- reacts with

ZnO at the oxide surface and the sulfide surface is replenished by the migration of oxide

and water to the surface. In the lattice diffusion, the rate is controlled by the diffusion

rate of HS^- into the oxide/sulfide lattice and migration of oxide and water to the surface.

The inert sulfide formed in the reaction will increase the diffusion resistance.

The reactions between ZnO/ZnS and compounds present in most reformates such as

H_2, CO_2, CO, C_1-C_4 hydrocarbons, H_2O, H_2S, are quite complicated. Sasaoka (1994b)

described the detailed reaction scheme, as shown in **Figure I-9**. It was found that H_2S

tended to decompose into elemental sulfur in the absence of other reactive gases. At

high temperatures (T>500 °C), H_2 accelerated the sulfidation reaction while inhibited at

low temperatures (T<400 °C). A possible reason was that ZnO was reduced to Zn vapor

at high temperatures in H_2 rich environment, and Zn vapor has a faster sulfidation rate.

It was observed that water inhibited the sulfidation reaction (Sasaoka, 1994b;

Novochinskii *et al*., 2004), so did CO with a less effect. CO inhibited the sulfidation

reaction and formed COS when H_2 was absent from the system; ZnO was reduced by H_2

and/or CO at 500 °C and followed by zinc vaporization when H_2O and/or CO_2 were

absent. In a later study, they found ZnS catalyzed the conversion of COS to H_2S in the

presence of H_2O and H_2 (Sasaoka *et al*., 1995). They also found that the concentration

of COS was controlled by the equilibrium of reaction 13 given enough residence time.

$$2H_2S+CO+CO_2=2COS+H_2+H_2O \tag{13}$$
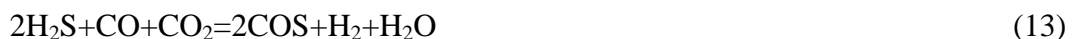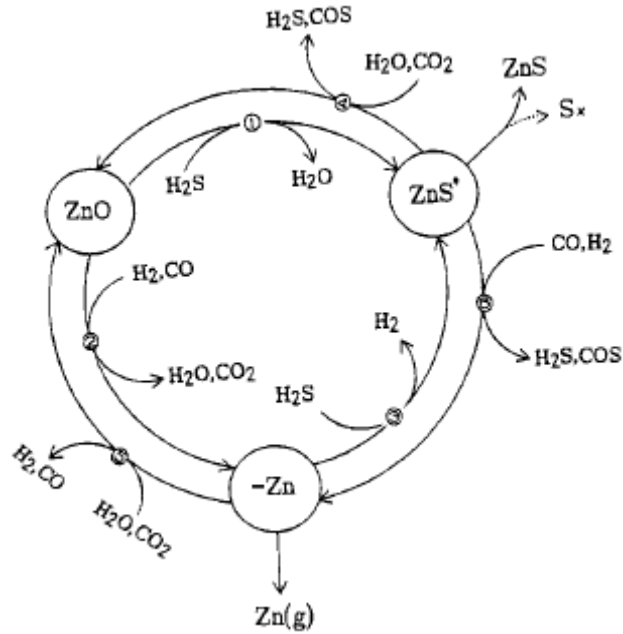
Figure I-9. The reaction scheme of ZnO sulfidation, ZnS regeneration and Zn formation. Adopted from the reference of Sasaoka (1994b).

Sasaoka *et al.* (1995) pointed out that a long ZnS zone in the packed bed reactor will keep reaction 13 under equilibrium control. Moreover, their results hint that the sorbent with high reactivity to H_2S is the most important factor to keep system from COS formation, since the equilibrium of reaction 13 will shift to left side at very low H_2S concentrations.

During regeneration, the spent ZnO sorbents are normally regenerated in oxidative atmospheres, such as air (Focht *et al.*, 1989), oxygen-lean air (for example 2 or 3 vol.% O_2 in N_2) (Lew *et al.*, 1989), and steam (Focht *et al.*, 1989). If regenerations are conducted at a low temperature (around 500 ºC), the oxygen-lean air with high face velocities could be applied to avoid SO_2 absorption and sulfate formation; for

regenerations at high temperatures (T>600 ℃), air and/or steam are applicable since zinc

sulfate is unstable at such high temperatures (Ayala, 1993). The regeneration reactions

can be described as:

$$ZnS+{}^3/_2O_2=ZnO+SO_2 \tag{14}$$

$$ZnS+2H_2O=ZnO+SO_2+H_2 \tag{15}$$

The role of H_2O in oxidative regeneration of ZnO at high temperatures was studied

by Sasaoka *et al.* (2000) using temperature programmed reaction (TPR) technology and

$H_2{}^{18}O$.

I.2.2.7.2. Drawbacks of ZnO Sorbents

ZnO is an excellent sorbent for low temperature desulfurization applications. The

main drawbacks of ZnO are mainly related to the chemical and physical properties of Zn

metallic and ZnO. Zinc loss in highly reducing environment is the critical drawback

that limits its applications at high temperatures. In high temperature fuel gases, ZnO is

partially reduced to elemental zinc. Metal zinc exists as micron-sized or even

nano-sized clusters whose melting points are much less than that of bulk zinc (407 ℃)

(Westmoreland and Harrison, 1976; Lew *et al.*, 1989; Woods *et al.*, 1990; Lew *et al.*,

1992; Sasaoka, 1994a). Therefore, elemental zinc is volatile at elevated temperatures.

Although it is believed that zinc vapor can react with H_2S faster than ZnO, significant

zinc loss was also observed at temperatures above 600 ℃ (Lew *et al.*, 1989; Woods *et al.*,

1990).   The reduction rate of zinc is accelerated by H_2 partial pressure and depressed by

H_2O (Sasaoka, 1994b).   For the gas with tiny amount of H_2O ca. 6 vol.%, the zinc loss

rate was found negligible till 650 °C.   In the absence of H_2O, this temperature dropped

to 550 °C.   CO and CO_2 demonstrated similar but weaker effects to H_2 and H_2O,

respectively.   From the discussion of Sasaoka, H_2 and H_2O, CO and CO_2 had the same

effects on the zinc loss rate.   Zinc loss rate at high temperatures (T>500 °C) was

controlled by equilibria of two reactions (Sasaoka, 1994b):

$$ZnO(s)+H_2(g)=Zn(g)+H_2O(g) \tag{16}$$

$$ZnO(s)+CO(g)=Zn(g)+CO_2(g) \tag{17}$$

Because of the zinc loss, several modified zinc based sorbents, such as zinc ferrite

and zinc titanate, have been developed to meet the high temperature needs.

Another drawback of zinc oxide based sorbents is the high equilibrium H_2S

concentrations at high temperatures, especially in the presence of H_2O.   At 400 °C, the

equilibrium H_2S concentration using ZnO as sorbent is 0.6 ppm in the presence of 20

vol.% water, as shown in **Figures I-8**.   This H_2S concentration is higher than the sulfur

tolerances of some PEMFCs, ca. 0.1 ppm.   At temperatures above 400 °C, the

performance of ZnO in the presence of high water concentrations becomes inapplicable

for PEMFC application.   In these cases, a secondary desulfurization unit is required.

Other metal oxides, such as copper-based sorbents, and low temperature desulfurization

processes may be used as alternatives to reach a low H_2S concentration.

I.2.2.8. Zinc Ferrite

Since both pure zinc oxide and iron oxide have favorable thermodynamics at low temperatures (300-500 °C), and both have limitations at high temperatures due to oxides reduction, Grindley and Steinfield (1981), at Morgantown Energy Technology Center of DOE, combined these two metal oxides and made a novel sorbent, zinc ferrite, trying to overcome the drawbacks of both. Gangwal *et al*. (1989) and Gupta *et al*. (1992) also prepared zinc ferrite. Zinc ferrite was tested at 538 °C for fifty cycles and the result was promising (Ayala and Marsh, 1991). The overall reaction describing the absorption of H_2S from coal gas by $ZnFe_2O_4$ is given by

$$ZnFe_2O_4+3H_2S+H_2=ZnS+2FeS + 4H_2O \tag{18}$$

and the regeneration of sulfides by oxygen is give by

$$ZnS+2FeS+5O_2=ZnFe_2O_4+3SO_2 \tag{19}$$

Zinc ferrite has a slightly higher capacity than zinc oxide and at the same time maintains the good thermodynamic properties as ZnO at moderate high temperatures (550-650 °C). Focht *et al*. (1988) found that zinc ferrite (formulation L-1442) lost its pore volume when reduced at 749 °C and subsequent loss of reactivity during sulfidation. The formulation was further refined to overcome this limitation. Bentonite, as an inorganic binder, was added into zinc ferrite (formulation T-2465) (Woods *et al*., 1991). The capacity of zinc ferrite was maintained at 70% of fresh sorbents capacity, and test results at 550 °C suggested that no Zn loss or metal reduction was observed (Kobayashi

et al., 2002a).   It was found that the maximum operating temperature of zinc ferrite was about 649 °C for multicycle applications, and 550 °C for multicycle applications in fluidized beds due to the severe chemical attrition at higher temperatures (Gupta *et al*. 1992).   The working temperature of zinc ferrite was still not high enough for the targeted hot gas desulfurization at around 850 ℃.   Similar to zinc based sorbents, zinc loss is still an issue that persists for zinc ferrite.   Both components in zinc ferrite, ZnO and Fe_2O_3 are prone to be reduced at high temperatures in highly reducing gases (Lew *et al*., 1992; Gupta *et al*. 1992).   Recently, research efforts on zinc ferrite were focused on the design of novel metal oxide doped (Pineda *et al*., 1997) or supported sorbents (Kobayashi *et al*., 2002b, Ikenaga *et al*., 2004).

I.2.2.9. Zinc Titanate

Besides zinc ferrite, another well-known modified ZnO sorbent is $ZnO-TiO_2$ or zinc titanate (Ahmeda *et al*., 2000; Harrison and Jothimurugesan, 1990). $ZnO-TiO_2$ mixed oxide systems have been of great interest in pigment industry.   Zinc titanates are prepared by mixing zinc oxide and titanium dioxide and calcined at high temperatures. $ZnO-TiO_2$ system contains three commonly found compounds, they are zinc orthotitanate (Zn_2TiO_4), zinc metatitanate ($ZnTiO_3$), and $Zn_2Ti_3O_8$ (Lew *et al*., 1989).   Zinc orthotitanate (Zn_2TiO_4) is the only stable phase at high temperatures (>1000 ℃), and it is also the only stable oxide phase after long time calcination (>12 hour) at temperatures

above 700 °C (Lew *et al*., 1989).   In short time calcination at a temperature less than 800 °C, zinc titanates of three phases may be present (Lew *et al*., 1989).

Zinc titanate (Zn_2TiO_4) was first used in hydrodesulfurization (HDS) in a patent of Farha and Gardner (1982).   In that work, zinc orthotitanate (Zn_2TiO_4) was promoted by different metals, such as ruthenium, rhodium, palladium, silver, tungsten, iridium, platinum, and it functioned as a HDS catalyst in a partial sulfide form.   It was also used as a regenerable sorbent to capture H_2S at low temperatures (205-538 °C).   In 1980s, TiO_2 was used as additives to stabilized ZnO from reduction and subsequent zinc loss at high temperature, by Lew *et al*. (1989, 1992) and Woods *et al*. (1990).   From the available thermodynamic data, zinc orthotitanate (Zn_2TiO_4) has a sulfidation equilibrium constant, which is inferior to those of ZnO and $ZnFe_2O_4$, but superior to those of any other zinc compounds, such as zinc aluminate and zinc silicate (Lew *et al*., 1992).

The addition of TiO_2 to ZnO improves the performance of ZnO sorbent at high temperatures.   According to Lew *et al*., 1992, the reduction of Zn-Ti-O was 3.6 times lower than ZnO in the temperature range of 600-700 °C.   At 800 °C, no evident zinc loss or zinc vapor were observed for Zn-Ti-O; no chemical attrition nor pellet cracking was observer either, though all the phenomena mentioned above were observed for pure zinc based sorbent under the same test conditions.   At 870 °C, Woods *et al*. (1990) observed that approximately 3.5 % weight loss occurred for Zn-Ti-O (Zn/Ti=1.5) during 30 minute reduction period in a model coal gas.   Thus, it was considered that Zn-Ti-O

(Zinc titanate) can work very well in the temperature range of 650-760 °C (Woods *et al*., 1990), which is almost 100 °C higher than that of zinc ferrite.

Although the addition of TiO_2 stabilizes the ZnO at its oxide form, it also brings some side effects on desulfurization performance as well. Since the TiO_2 is inert to H_2S, unlike iron oxide in zinc ferrite, the addition of TiO_2 decreases the capacity of sorbents. The stoichiometric capacity of zinc titanate is 0.210 g H_2S /g of Sorbent (Zn/Ti=1), compared with 0.422 of zinc ferrite and 0.419 of ZnO. Moreover, the addition of TiO_2 to ZnO reduces the equilibrium sulfidation reaction, and yields higher equilibrium H_2S concentrations than ZnO does, as shown in **Figure I-10**. The addition of TiO_2 also affects the intrinsic sulfidation kinetics. Lew *et al*. (1989, 1992) found that Zn-Ti-O sorbent had similar sulfur removal efficiency as ZnO at 650 ºC. At the temperatures between 400-700 ºC, similar activation energies (9-10 kcal / mol) were found for both ZnO and Zn-Ti-O sorbents, but lower frequency factors were measured for $ZnO-TiO_2$ sorbents (The sulfidation reaction rate constant can be expressed by an Arrhenius equation as $k = k_0 \exp(-\dfrac{E_a}{RT})$, where E_a is the activation energy, k_0 is the frequency factor.). Lew *et al*. (1989, 1992) found that the sulfidation of $ZnO-TiO_2$ had the same mechanism as ZnO but with less active sites. The addition of TiO_2 only eliminated certain amount of reaction sites but not all, since increasing in TiO_2 content above 25 mol.% did not lead to any further drop in Zn-Ti-O frequency factors.
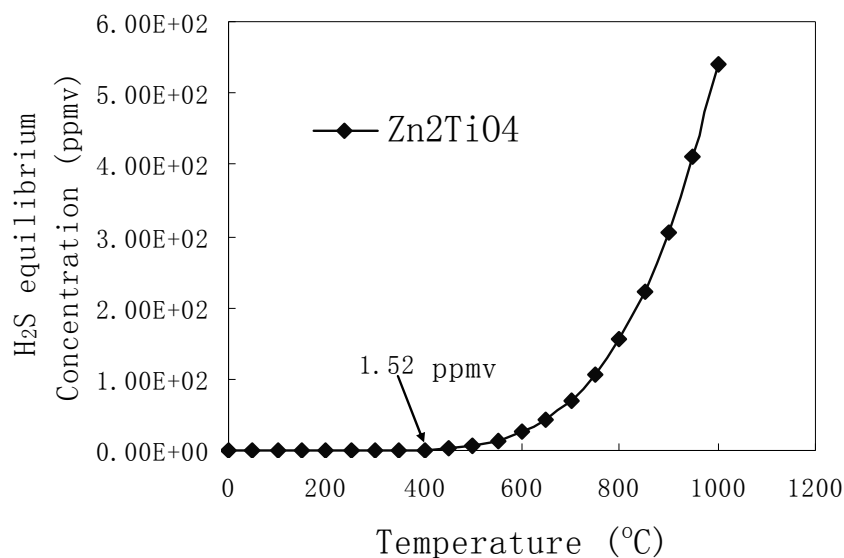
Figure I-10. H_2S equilibrium concentration in the desulfurization for reformates (20 vol.% H_2O-20 vol.% CO_2-10 vol.% CO-9 vol.% C_1-C_3-41 vol.% H_2) using zinc titanate sorbent at various temperatures. Data were generated using HSC 3 Software.

The Ti/Zn atomic ratio affects the physical properties of prepared sorbents. Hatori *et al*. (2001) found that the addition of TiO_2 changed the surface area and pore volume of prepared sorbents. The addition of small amount of TiO_2 demonstrated the greatest effect. With a Zn/Ti=9, both the surface area and pore volume reached the maximum values, compared with pure ZnO, surface area increased 6 times; pore volume 2.5 times. Possible explanation is that TiO_2 disperses ZnO particles and prevents them from growth. However, a further addition of TiO_2 decreased both surface area and pore volume slowly (Jothimurugesan and Gangwal, 1998).

According to Woods *et al*. (1990) and Lew *et al*. (1992), the spent ZnO-TiO_2 sorbents can be regenerated in N_2 diluted air with 2-10 vol.% O_2 at temperatures from

675-760 ºC. Under these conditions, no zinc sulfate ($ZnSO_4$) formation was observed, because the regeneration temperature of 675 ºC exceeded zinc sulfate decomposition temperature. Woods *et al*. (1990) found that the regeneration time was reduced by increasing the regeneration temperature. At 760 ºC, only 170 min was required to achieve complete regeneration; at 720 ºC, 200 min; at 675 ºC, 200 min was not long enough (Woods *et al*., 1990). A high oxygen concentration also accelerates the regeneration process too. For example, they found that the regeneration was approximately 8 times faster in 8 vol.% of O_2 than that in 1 vol.% O_2. However, the pellet temperature was found to increase dramatically at high O_2 concentrations during regeneration because of the exothermic nature of sulfide oxidation (Woods *et al*., 1990). Hatori *et al*. (2001) discussed the role of TiO_2 on sorbent regeneration and they suggested that TiO_2 was able to accelerate the ZnS regeneration in the presence of water and/or O_2.

Recent researches related to zinc titanates focused on modifying ZnO-TiO_2 system by addition various transition metals to improve the reactivity, regenerability and stability. In 1998, Research Triangle Institute in North Carolina modified the zinc titanate sorbents by adding 5 wt.% Ni and 5 wt.% Co in co-precipitation, which effectively reduced the regeneration temperature by at least 100 ºC (Jothimurugesan and Gangwal, 1998). The addition of 5 wt.% Cu demonstrated the same effect on fresh sorbent as 5 wt.% Ni and 5 wt.% Co, however the performance of Cu-added sorbent dropped after several sulfidation-regeneration cycles. Sasaoka *et al*. (1999) studied ZrO_2 as a stabilizer in

ZnO based sorbents, and they reported that ZrO_2 had similar effect as TiO_2 on stabilization of ZnO, and the addition of ZrO_2 5-10 mol.% to $ZnO-TiO_2$ greatly improved the reactivity and regenerability. Pineda *et al.* (2000) reported that Cu doped zinc titanate improved reactivity and yielded lower H_2S outlet concentrations. Jun *et al.* (2002) suggested the addition of iron to zinc titanate helped to separate ZnO in a spinel structure and improved the regenerability of ZnS.

I.2.3. Common Issues for Metal Oxide Sorbents

I.2.3.1. Oxide Reduction

Metal oxides have been used as sorbents in sulfur removal for about 70 years, and they share some common issues, including the issues related to their intrinsic properties and the issues related to their properties of their existence. The first issue is oxide reduction in fuel gases containing H_2 and/or CO, which could be described as:

$$MO_x + yH_2 = MO_{x-y} + yH_2O \quad (y \leq x) \tag{20}$$

and/or

$$MO_x + yCO = MO_{x-y} + yCO_2 \quad (y \leq x) \tag{21}$$

It is very possible for the metal ion (M^{2x+}) in MO_x to be reduced to any low oxide states or metallic, depending on the reducibility of fuel gases. Reduced metal oxides or metallic normally have lower sulfur capacity than these in high oxidative states. For

example, pure Fe_2O_3 has a stoichiometric capacity of 0.6 g S/ g Sorbent, while FeO, 0.444 g S/ g Sorbent.   Another worse effect is that the reduction makes the sorbent structure collapse in some cases.   Moreover, sulfidation kinetics decreased slightly after the reduction of metal oxides.   Sometime, the reduction of metal oxides to metallics may cause detrimental effects on sulfidation, because metallics have much lower equilibrium constants than metal oxides, and they cannot remove H_2S to very low levels, e.g. copper oxides, iron oxide.   The third drawback for metallics is the formation and growth of metal clusters.   Metallics tend to grow into large clusters thus decrease the surface area or block the pores, making active sorbent inaccessible.   For example, Co and Cu are ready to reduce by coal gas (Gasper-Galvin *et al*., 1998; Westmoreland and Harrison, 1976).   Moreover, for some volatile metals, i.e., zinc and lead, the formation of metallic is a disaster for sorbents.   It causes metal vaporization and subsequent metal loss.

I.2.3.2. Equilibrium Constant at High Temperatures

Another intrinsic phenomenon of metal oxides is their degrading equilibria at high temperatures.   For most metal oxides, the equilibrium constants of sulfidation decrease with temperature increases as shown in **Figure I-5**.   The decrease in equilibrium constant means the increase in equilibrium H_2S concentration.   For example, although MnO sorbent can remove H_2S to 1 ppmv at 300 ℃, it becomes impossible at 600 ℃. Therefore, metal oxides with low equilibrium constants are not favorable for deep

desulfurization at high temperatures. Sorbent based on rare earth metals, such as Lanthanum oxide (La_2O_3) and cerium oxide (CeO_2) demonstrated potential to remove sulfur to extremely low concentration even at high temperatures (>800 ℃), though their sulfur capacities need further improvements for practical applications.

I.2.3.3. Surface Area Loss

It is critical to maintain high surface area and pore structure of the sorbents especially for multi-cycle applications. At low temperatures, e.g. room temperature, only the active chemicals in the first monolayer can be accessed by H_2S. The more active chemicals in this monolayer (Baird *et al*., 1992), the larger capacity the sorbent has. It means that a sorbent with high surface area will certainly have a high capacity and breakthrough capacity (or dynamic capacity) for low temperature applications. The sorbents of active chemical supported on inert particles with high surface area will performance at least as well as the sorbent made of pure active chemical in the respect of sulfur capacity at low temperatures. The high surface area is not as important for desulfurization at a high temperature as it is at low temperatures, because more active chemical can be accessed due to the faster mass transfer at high temperatures. However, the high specific surface area is still a helpful to enhance the breakthrough capacities. The more specific surface area the sorbents have, the faster the intrinsic reaction rate can be reached.

However, it is almost impossible to maintain the high specific surface area of regenerable sorbents during multi-cycles. Actually, surface area loss is a very common phenomenon during spent sorbent regeneration due to the growth of grains (Slimane and Abbasian, 2000a; Patrick *et al*., 1989; Kamhankar *et al*., 1986; Jun *et al*., 2002). Companying with the surface area loss, the loss in pore volume is another widely observed phenomenon during high temperature desulfurization or regeneration (Slimane and Abbasian, 2000a; Pineda *et al*., 2000; Mojtahedi, 1995; Jun *et al*., 2002; Ross *et al*., 2003). The reduction in porosity significantly increases the pore diffusion resistance and severely decelerates the reaction rate. Therefore, to maintain the high surface area and high porosity become critical for successful sorbent and/or catalyst designs.

In order to maintain the surface area and porosity of sorbents, the active sorbent substances are mixed with other oxides. The first mixed oxide scheme is to support active chemicals on a secondary oxide support. These secondary compounds are mainly inert to sulfur, such as Al_2O_3 (Gasper-Galvin *et al*., 1998; Wang, and Lin, 1998; Ko *et al*., 2005; Wakker *et al*., 1993; Zhang *et al*., 2003; Flytani-Stephanopoulos *et al*., 1998), monolith (Bakker *et al*., 2003), SiO_2 (Kyotani *et al*., 1989; Ko *et al*., 2005), TiO_2 (Ko *et al*., 2005), zeolite (Kyotani *et al*. 1989; Atimatay *et al*., 1993; Gasper-Galvin *et al*., 1998), and the functions of supports are: (1) to provide a good structure stability for the sorbent (Atimatay *et al*., 1993; Wang and Lin, 1998); (2) to hold the sorbent grains in the micropores and prevent increase in grain size and agglomeration (Li and

44

Flyzani-Stephanopoulos, 1997; Goyette and Keenan, 1997), therefore maintain the high surface area, high porosity and high sorbent capacity (Klabunde et $al.$, 2004; Wang and Lin, 1998); (3) to stabilize the active metal oxide sorbent from reduction and vaporization (Flytani-Stephanopoulos et $al.$, 1998). The supported sorbent design may also facilitate the incorporation of sorbent into systems, such as the monolith supported metal oxide sorbents designed by Engelhard (Ruettinger et $al.$, 2002). Due to the advantages of using supports, the sorbents provides stable performance with extended service life (Kyotani et $al.$, 1989).

Another mixed oxide scheme is to diluted active sorbent compounds by secondary metal oxides, such as Al_2O_3 (Kamhankar et $al.$, 1986; Flytani-Stephanopoulos et $al.$, 1998; Schubert, 1993), CeO_2 (Akyurtlu and Akyurtlu, 1999; Li and Flyzani-Stephanopoulos, 1997), Cr_2O_3 (Li and Flyzani-Stephanopoulos, 1997), Fe_2O_3 (Kamhankar et $al.$, 1986; Woods et $al.$, 1991; Grindley et $al.$, 1981; Gangwal et $al.$, 1989; Gupta et $al.$, 1992), SiO_2 (Kyotani et $al.$, 1989; Schubert, 1991; Khare et $al.$, 2002), SnO_2 (Babich and Moulijn, 2003), TiO_2 (Lew et $al.$ 1989, 1992; Ko et $al.$, 2005; Woods et $al.$, 1990; Harrison and Jothimurugesan, 1990; Faha and Gardner, 1982; Hatori et $al.$, 2001; Jothimurugesan and Gangwal, 1998; Sasaoka et $al.$, 1999; Pineda et $al.$, 2000; Mojtahedi, 1995; Jun et $al.$, 2002), in which Al_2O_3, Ce and Cr_2O_3 are usually used to stabilize CuO from reduction, to disperse and reduce CuO grain size; Fe_2O_3 and TiO_2 are widely employed to stabilize ZnO from reductions.

I.2.3.4. Attrition

For industrial applications, metal oxide sorbents are typically prepared in form of pellets, widely used in fixed- and moving beds. Sorbent pellets mainly consist of primary active metal oxides, secondary metal oxides (promoter), stabilizers and binders. For example, in zinc titanate sorbent, zinc oxide is the primary activate metal oxide; Mo, Ni based oxides are secondary oxides used to improve the performance in sulfidation and/or regeneration; TiO_2 is the main stabilizer used to keep Zn at oxidative state; beninate is a inorganic binder used to enhance the strength of pellets. The issues discussed here are mostly related to pellets.

One consideration for industrial application is attrition in fluidized bed. Gupta *et al*. (1992) at Morgantown found that the sorbents for fluidized beds with acceptable sulfur capacity prepared by crushing the zinc ferrite pellets and screening underwent excessive attrition during multiple-cycle of adsorption and regeneration. They applied several different techniques, such as spray drying, impregnation, crushing and screening of pellets, granulation, to build sorbents with robust attrition-resistant structure for fluidized bed reactors. The results indicated that significant sorbent weakening due to chemical attrition occurred at 625 °C, and sorbents prepared using granulation technique showed good attrition resistance and maintained acceptable sulfur capacities (Harrison and Jothimurugesan, 1990).

Attrition is also related to sorbents pellets in packed beds. After several sulfidation-regeneration cycles, sorbent pellets in fixed bed reactor are cracked and even broken into small pieces. Several factors account for this common phenomenon. The first one is thermal attrition. Because of the non-uniform temperature profile in pellets, the different thermal extension rate will gradually introduce cracks. Another reason is chemical attrition. In the sulfidation, sulfur atoms diffuse into the lattice and substitute oxygen atoms, which are smaller than sulfur atoms, therefore, the lattice structure expands; in regeneration, sulfur atoms are moved out from the lattice and substituted by oxygen atoms, and the lattice structure shrinks. The cracks develop when sulfur atoms move into and out from the lattice. Because of these reasons, active sorbents are commonly diluted by stabilizers and strengthened by binders, which are usually Al_2O_3 and SiO_2, to reduce chemical attrition and enhance the pellet integrity (Babich and Moulijn, 2003).

I.2.4. Mathematical Models

The adsorption of H_2S by sorbents in fixed beds is a complicated unsteady state problem. Most desulfurization processes are operated at low face velocities, ca. 2~10 cm/s (Newby et al., 2001). Therefore, the external mass transfer, internal mass transfer (including pore diffusion and solid oxide diffusion), and intrinsic heterogeneous reactions are all possibly involved in these processes. Many mathematical models have been

47

proposed to characterize these dynamic processes. These models can be classified into two groups: single pellets models and service life models.

I.2.4.1. Single Pellet Models

Several mathematical models, such as the shrinking core model (SCM), the uniform conversion model (UCM), the grain pellet model (GPM), the cracking model (CCM), the changing voidage model (CVM), the thermal decomposition model (TDM), and the phase change model (PCM) (Levenspiel, 2002) have been established to describe the changes of solid particles during heterogeneous reactions. Most kinetic studies on ZnO based sorbents, especially zinc ferrites (Kobayashi *et al*., 2002) and zinc titanate (Ozdemir and Bardakci, 1999; Konttinen *et al*., 1997a, 1997b), took a singlet pellet as the research subject. In these kinetic studies, external mass transfer resistance was minimized and neglected at high face velocities, and the intra-particle mass transfer characteristics and intrinsic reaction rate constants were of the research interests. Conversion curves of sorbent pellets (*X-t* plot) were typically obtained via thermal gravity analysis (TGA), and used to determine the reaction and diffusion parameters. Unreacted shrinking core model (USC) (Levenspiel, 1972, 2002; Fogler, 1999) was widely applied for the kinetic study of single pellet. For the systems with more than one rate controlling mechanism, Sohn (1978) proposed the modified τ called "additive reaction times".

USC was developed by Levenspiel (1972) and became a classic part in reaction engineering textbooks. USC is always applied as the first approximation to investigate the reaction mechanism in heterogeneous reaction systems. A rate determining mechanism can be distinguished by extrapolating the conversion (X)-time (t) plot of the solid reactant. For example, if a reaction such as

$$A_{(g)}+bB_{(s)}=R_{(g)}+S_{(s)} \tag{22}$$

is controlled by the film diffusion. The conversion of the solid reactant B (X_B) is

$$\frac{t}{\tau} = X_B \tag{I-1}$$

where t is the time to reach conversion X_B, and τ is the time for 100% conversion under a single control mechanism, it can be estimated by

$$\tau = \frac{\rho_b R}{3bk_g C_{Ag}} \tag{I-2}$$

where ρ_b is the molar density of B in sorbent particles, R is radius of the sphere of B, k_g is the gas film coefficient for mass transfer. For example, for high Re and Sc systems,

$$\frac{k_g d_p}{D} = Sh = 2 + 0.6 Re^{\frac{1}{2}} Sc^{\frac{1}{3}} \tag{I-3}$$

X_B is always a function of radius of core (r_c), since

$$X_B = 1 - \left(\frac{r_c}{R}\right)^3 \tag{I-4}$$

If the reaction is controlled by the diffusion through the ash layer, then

49

$$\frac{t}{\tau} = 1 - 3(1 - X_B)^{2/3} + 2(1 - X_B) \qquad \qquad \text{(I-5)}$$

in which

$$\tau = \frac{\rho_b R^2}{6 b D_e C_{Ag}} \qquad \qquad \text{(I-6)}$$

where D_e is the effective diffusion coefficient of A through the ash layer. Similarly, in a

reaction controlling system

$$\frac{t}{\tau} = 1 - (1 - X_B)^{1/3} \qquad \qquad \text{(I-7)}$$

where

$$\tau = \frac{\rho_b R}{b k_s C_{Ag}} \qquad \qquad \text{(I-8)}$$

in which k_s is the intrinsic surface area based reaction rate. For other non-spherical

particles, the equations listed above are written in slightly different forms, as shown in

Table I-6 (Levenspiel, 2002).

D_e is an important diffusion parameter especially when the ash layer diffusion is the

controlling step. However, it is a variable determined by the properties the challenge

gas components and the ash layer, and it cannot be simply predicted using mathematical

equations. It has to be extrapolated by matching the USC and experimental

conversion-time curves. In a word, single pellet models are good at analyzing the

control mechanism of reaction processes; it is difficulty to be applied to describe the

unsteady state processes of adsorption in a packed bed.

Table I-6. The conversion-time expressions for various shapes of solids (Levenspiel, 2002).

Shape	Film Diffusion Control	Ash Layer Diffusion Control	Reaction Control
Flat plate $X_B = 1 - \dfrac{l}{L}$	$\dfrac{t}{\tau} = X_B$ $\tau = \dfrac{\rho_b L}{b k_g C_{Ag}}$	$\dfrac{t}{\tau} = X_B^2$ $\tau = \dfrac{\rho_b L^2}{2 b D_e C_{Ag}}$	$\dfrac{t}{\tau} = X_B$ $\tau = \dfrac{\rho_b L}{b k_s C_{Ag}}$
Cylinder $X_B = 1 - \left(\dfrac{r_c}{R}\right)^2$	$\dfrac{t}{\tau} = X_B$ $\tau = \dfrac{\rho_b R}{2 b k_g C_{Ag}}$	$\dfrac{t}{\tau} = X_B + (1 - X_B)\ln(1 - X_B)$ $\tau = \dfrac{\rho_b R^2}{4 b D_e C_{Ag}}$	$\dfrac{t}{\tau} = 1 - (1 - X_B)^{\frac{1}{2}}$ $\tau = \dfrac{\rho_b R}{b k_s C_{Ag}}$
Sphere $X_B = 1 - \left(\dfrac{r_c}{R}\right)^3$	$\dfrac{t}{\tau} = X_B$ $\tau = \dfrac{\rho_b R}{3 b k_g C_{Ag}}$	$\dfrac{t}{\tau} = 1 - 3(1 - X_B)^{\frac{2}{3}} + 2(1 - X_B)$ $\tau = \dfrac{\rho_b R^2}{6 b D_e C_{Ag}}$	$\dfrac{t}{\tau} = 1 - (1 - X_B)^{\frac{1}{3}}$ $\tau = \dfrac{\rho_b R}{b k_s C_{Ag}}$

I.2.4.2. Service Life Models

Most of service life models were originally created to predict service times or breakthrough curves of charcoal respirator cartridges. These models treat an entire packed bed as the research subject. The flow conditions for respirator applications are quite different from the classical mass transfer studies for fluidized bed. In most cases, the external mass transfer played an important role than internal mass transfer, which can be found in most of the explicit expressions of these models. Among all the models, three models are widely used; they are Mecklenburg Model, Yoon Model, Wheeler Model. These three models and Amundson's Model will be introduced in this section.

Mecklenburg Model

The Mecklenburg Model can be found in an important early work "Adsorption Wave" of Irving M. Klotz (1946). In this work, Klotz derived a general breakthrough time equation based on the Mecklenburg equation and the concept of critical bed depth.

Using Mecklenburg equation, the mass balance of the species captured by the packed bed can be expressed as

$$t_b V C_{A0} = N_0 A (z_t - z_c) \qquad\qquad\qquad (\text{I-9})$$

where t_b is the breakthrough time of packed bed, L is the flow rate of challenge gas; C_{A0} is the challenge gas concentration. The group of $t_b L C_{A0}$ is the amount of challenge species captured in the packed bed, if the portion of the challenge gas species that has penetrated the bed before breakthrough is neglected. N_0 is the capacity of the packed bed sorbent per unit volume, A is the cross section area of the bed, z is the bed depth and z_c is the minimum bed depth required to yield the breakthrough concentration C_b and is called critical bed depth of the bed at the flow condition.

For fast reactions, the critical bed depth under external mass transfer control, according to Gamson *et al.* (Klotz, 1946) can be expressed as

$$z_c = \frac{1}{a}\left(\frac{D_p G}{\mu}\right)^{0.41}\left(\frac{\mu}{\rho D_v}\right)^{0.67}\ln\left(\frac{C_{A0}}{C_b}\right) \qquad\qquad (\text{I-10})$$

and breakthrough time (t_b) can be written as

$$t_b = \frac{N_0 A}{LC_{A0}} \left[z - \frac{1}{a} \left(\frac{D_p G}{\mu} \right)^{0.41} \left(\frac{\mu}{\rho D_v} \right)^{0.67} \ln \left(\frac{C_{A0}}{C_b} \right) \right] \tag{I-11}$$

Equation I-10 is the well-known Mecklenburg model. Mecklenburg Model can predict the shape of breakthrough curves by directly inserting the flow parameters. Its application is not limited for physical adsorption in cartridges alone; it is applicable to most unsteady state reactions taking place in fixed bed reactors under external mass transfer rate control. Moreover, the assumption used in Equation I-9 that the portion of the challenge gas species has penetrated the bed before breakthrough is negligible makes the Mecklenburg model good only for low breakthrough concentration analysis.

Amundson's Model

Similarly, Amundson derived another equation for the adsorption in packed bed (Amundson, 1948). If the reaction between gas components like H_2S (A) and solid particle likes ZnO (B) is considered to be second order reaction, the reaction rate based on volume of a packed bed can be written as follows:

$$-r = k_2 C_A C_B \tag{I-12}$$

where C_A is H_2S concentration and C_B is amount of accessible B remaining in the packed bed in moles per unit volume of bed. For fresh sorbents C_B is equal to the saturation capacity density ρ_c ($C_B \rightarrow \rho_c$ at $t \rightarrow 0$, $\rho_c = \frac{xy\rho_b}{M_z}$) of the sorbents in the packed bed under the

experimental conditions. Then, the outlet H_2S concentration exiting at the end of the packed bed can be predicted using Amundson's equation as shown in equation I-13.

$$\frac{C_{A0}}{C_A} = 1 + [\exp(-\phi k_2 t C_{A0})] \cdot \left[\exp\left(\frac{\phi k_2 \rho_c z_t}{U}\right) - 1 \right] \qquad \text{(I-13)}$$

Wheeler Model

Wheeler model could be simply expressed as (Yoon and Helson, 1984):

$$t_b = \frac{W_s}{C_{A0}F}\left[W_e - \frac{\rho_c F}{k_v}\ln\left(\frac{C_{A0}}{C_b}\right) \right] \qquad \text{(I-14)}$$

where

$$k_v \approx 14.4 \times 10^{-3} \times V_1^{1/2} d^{-3/2} \qquad \text{(I-15)}$$

In equations I-15 and 15, k_v is the adsorption rate constant (min^{-1}), V_1 is the superficial velocity across the particle (cm/min) and W_e is the weight of active carbon. Wheeler Model is specified for adsorption in charcoal carbon only.

Yoon's Model

Yoon and Helson (1984) derived new model for the adsorption in packed beds using the concept of possibility of breakthrough. This model can be expressed as:

$$t_b = \tau + \frac{1}{K}\ln\left(\frac{C_b}{C_{A0} - C_b}\right) \qquad \text{(I-16)}$$

or

$$\ln\left(\frac{C_{A0}}{C_A} - 1\right) = K(\tau - t) \tag{I-17}$$

where K is the pseudo-reaction rate constant and τ is usually defined as

$$\tau = \frac{W_e}{C_{A0}F} \tag{I-18}$$

Comments on Service Life Models

Yoon and Helson (1984) compared the Yoon's Model, Mecklenburg Model and Wheeler Model and found that all the simulated breakthrough curves using these three models matched well with the experimental data in the low C_A/C_{A0} region. However, only Yoon's model matched the experimental data in the high C_A/C_{A0} region. They also compared the expressions of Yoon's Model, Mecklenburg Model and Wheeler Model; they suggested that these three models could be written in one general form as:

$$t = A' + B'C' \tag{I-19}$$

The detailed comparison is shown in **Table I-6**. The main difference between these three models is the term C'. In Yoon's model, it is $\ln\left(\dfrac{C_b}{C_{A0} - C_b}\right)$ rather than $\ln\left(\dfrac{C_b}{C_{A0}}\right)$. This difference makes simulated breakthrough curve of Yoon's model and experimental data match very well even at high C_A/C_{A0}. However, the pseudo reaction

55

rate constant in Yoon's model, K, has not been correlated with reaction constant at experimental conditions. Yoon and Helson (1984) tried to employ the expression in Mecklenburg Model to correlate the K using the similarity of these three models.

Table I-7. Comparison between service life models (Yoon and Helson, 1984).

Term	Yoon's Model	Wheeler Model	Mecklenburg Model
A'	$\dfrac{W_e}{CF}$	$\dfrac{W_s W_c}{CF}$	$\dfrac{W_s A Z n' \rho_c}{CF}$
B'	$\dfrac{W_e}{kCF}$	$\dfrac{W_s \rho_c}{k_v C}$	$\dfrac{An'}{a_c}(\dfrac{dG}{\eta})^{0.41}(\dfrac{\eta}{\rho_a D})^{0.67}\dfrac{W_s}{CF}$
C'	$\ln\left(\dfrac{C_b}{C_{A0}-C_b}\right)$	$\ln\left(\dfrac{C_b}{C_{A0}}\right)$	$\ln\left(\dfrac{C_b}{C_{A0}}\right)$

Amundson's model can be written in the form of Yoon's model. For most cases, $\exp\left(\dfrac{\phi \cdot k_2 \rho_c z_t}{U}\right) >> 1$, so Amundson's model can be reduced and rearranged as:

$$\ln\left(\frac{C_0}{C_A}-1\right)=\phi \cdot k_2 C_{A0}(\tau-t) \tag{I-20}$$

where

$$\tau = \frac{\rho_c z_t}{U C_{A0}} \tag{I-21}$$

Equation I-20 suggests that Amundson model has the similar expression as Yoon's model, and includes the reaction rate constant. Moreover, Amundson model is tailorable

for different systems. Amundson model can be employed to predicate the service life for all heterogeneous reaction systems given the expression of reaction rate, not matter what is the controlling step. For instance, if external mass transfer controls the desulfurization process, the reaction rate (apparent) can be expressed explicitly using mass transfer correlations, as did in Mecklenburg model. However, Amundson's model is based on the second order reaction. The heterogeneous reactions like the one between ZnO and H_2S are considered to be zero order with respect to solid reactants. Therefore, further modifications to Amundson's equation are required before it can be applied to these reactions.

I.2.5. Microfibrous Entrapped Catalysts and Sorbents

Microfibrous technology developed at the Center of Microfibrous Materials Manufacturing (CM^3) at Auburn University (Tatarchuk, 1992a, 1992b; Tatarchuk *et al*., 1992, 1994; Overbeek *et al*., 2001; Cahela and Tatarchuk, 2001; Cahela *et al*., 2004; Marrion *et al*., 1994; Kohler *et al*., 1990; Ahn and Tatarchuk, 1997; Meffert, 1998; Lu and Tatarchuk, 2003; Chang and Tatarchuk, 2003; Lu *et al*., 2005) provides a novel approach for a versatile design of small, efficient, and lightweight fuel processors. Microfibrous media carrier can be used, with large surface to volume ratios, to entrap micro-sized sorbent and/or catalyst particulates while withstanding considerable vibration and avoiding bypassing. This generic approach can also enhance heat/mass transfer,

improve contacting efficiency, and promote regenerability (Cahela and Tatarchuk, 2001; Meffert, 1998). The fabrication of the microfibrous media is based on reliable, proven, high-speed, roll-to-roll, papermaking and sintering processes, which substantially reduces the production costs and improves the product quality. Microfibrous entrapped 16% Ni/Al_2O_3 catalysts for toluene hydrogenation in a trickle bed reactor have demonstrated 2-6 times higher specific activities than the conventional packed bed catalysts on a gravimetric basis, while volumetric activities of 40 vol.% composite catalysts were 80% higher than conventional extrudates (Meffert, 1998). Microfibrous entrapped 1% $Pt-M/Al_2O_3$ for PrOx CO provided 3-fold higher or more bed utilization than the packed beds of 2-3 mm (dia.) pellets (Chang and Tatarchuk, 2003) at the same CO conversion.

Microfibrous matrix can be manufactured by wet layer paper-making/sintering process. The void volume in these media can be adjusted from 35 vol.% of typical packed beds up to 98 vol.% of the microfibrous media alone (Cahela and Tatarchuk, 2001). The size of the fibers employed in the media ranges 2 to 20 μm, and the size of particles that can be entrapped varies from 10 to 300 μm. Several types of microfibers were chosen to make the matrix and the typical structures of these media are shown in **Figures I-11** and **I-12**. These materials can be employed as carriers for catalyst or sorbent (Chang and Tatarchuk, 2003; Karanjikar *et al.*, 2004; Lu *et al*., 2005), applied in electrochemical cells (Ahn and Tatarchuk, 1997), and also used as HEPA filters (Karanjikar, 2005).

Figure I-11. γ-Al$_2$O$_3$ particles entrapped in the matrix of 8 μm Ni fibers. SEM was provided by CM^3.
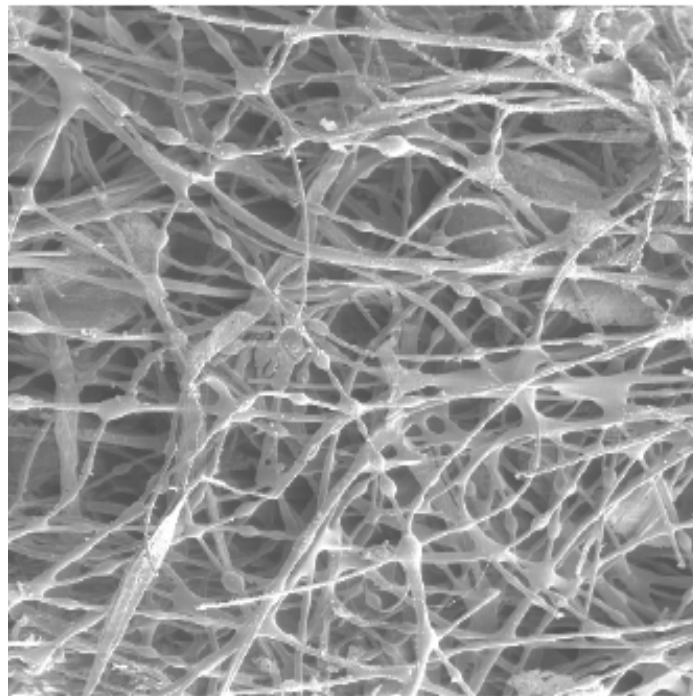
Figure I-12. Activated carbon particles in the matrix of 8 μm polymer fibers. SEM was provided by CM^3.

CM^3 has also developed microfibrous entrapped sorbents (MES) for desulfurization applications. They are Ni fibers entrapped ZnO/SiO$_2$ (150-250 μm) and ZnO/ACP (150-250 μm) sorbents. The first one was designed and employed for the regenerable use to scavenge bulk H$_2$S from reformate streams in a continuous batch mode at ca. 400 °C. It is used in the primary desulfurization unit. ZnO/ACP was designed to remove the trace amount of H$_2$S (< 1 ppmv) to below the threshold of some PEMFCs, ca. 0.1 ppmv, it is a last protection at stack temperatures. It also protects fuel cells during unsteady state operations of fuel cleanup processes, e.g. startup. Composite beds consisting of packed beds of 1-2 mm (dia.) commercial extrudates followed by high contacting efficiency microfibrous entrapped polishing sorbents were also demonstrated. The detail performances of these sorbents were described by Lu et al. (2005) and are demonstrated in the following sections.

I.2.5.1. Characteristics of Microfibrous Entrapped ZnO/SiO$_2$ and ZnO/Carbon

The composition and physical properties of Ni MES are shown in **Table I-8**.

Table I-8. Composition, physic properties of Ni microfibrous entrapped sorbents.

Microfibrous Entrapped Sorbent	ZnO wt.%	Support wt.%	Support vol.%	Ni fiber wt.%	Ni fiber vol.%	Voidage (%)
ZnO/SiO$_2$	18[a]/17.3[b]	43	25	39	2	73
ZnO/Carbon	19[a]/18.6[b]	44	28	37	2	70
ZnO/γ-Al$_2$O$_3$	18[a]	43	24	39	2	74

[a] calculated by mass balance; [b] ICP-AES analysis results, carried out on a Thermo Jarrell Ash ICAP 61 Simultaneous Spectrometer.

SEM images in **Figure I-13** show the microstructures of the thin microfibrous entrapped ZnO/SiO_2 and ZnO/Carbon sorbents for H_2S absorption, respectively. ZnO/support particulates of 150-250 µm were uniformly entrapped into a well sinter-locked network of 8 and 4 µm nickel fibers. The use of small particulate can significantly enhance the external mass transfer rate and reduce intra-particle diffusion resistance. The porosities of ZnO/SiO_2 and Sud-Chemie G-72E are 64 % (as shown in Appendix F) and 53 % (Newby *et al*., 2001) respectively. The high porosity of the ZnO/SiO_2 sorbent particles will further reduce the pore diffusion resistance. XRD patterns of the ZnO/Support sorbents, the supports and the mixture of ZnO (Sud-Chemie) and supports with comparable composition of the corresponding ZnO/support sorbents are shown in **Figure I-14.** It is clear that the mixtures of ZnO and supports demonstrated the strong and narrow peaks assigned to large ZnO grains. The calculated size of ZnO grains in Sud-Chemie extrudates using Debye-Scherrer equation is 17 nm. Both ZnO/Carbon and ZnO/SiO_2 entrapped materials yielded very broad XRD peaks of ZnO. Zinc oxide grain sizes for both SiO_2 and Carbon-supported sorbents were determined to be <5 nm, only 1/3 of that for Sud-Chemie extrudates. This reduction in ZnO crystal size can enhance the lattice diffusion rate.
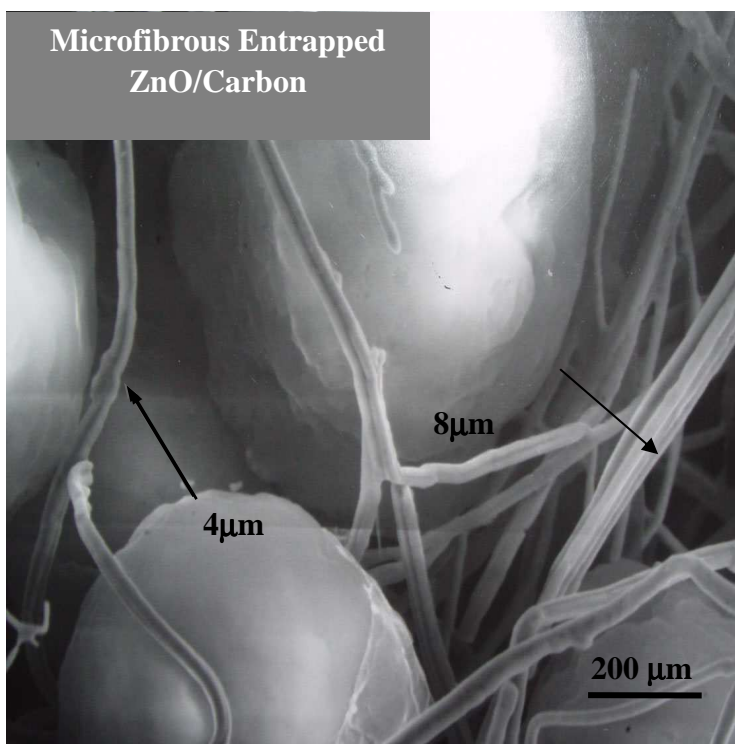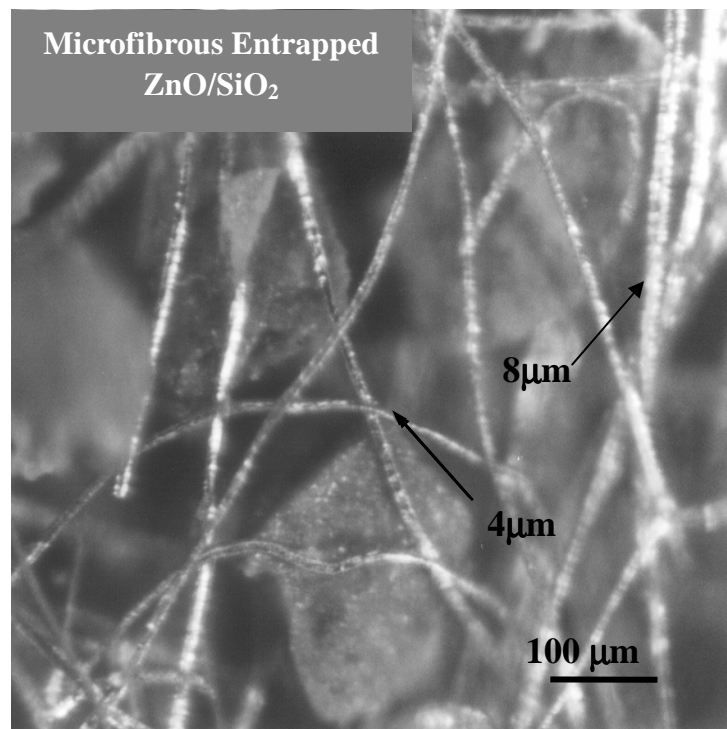
Figure I-13. SEM images of microfibrous entrapped ZnO/support sorbents.
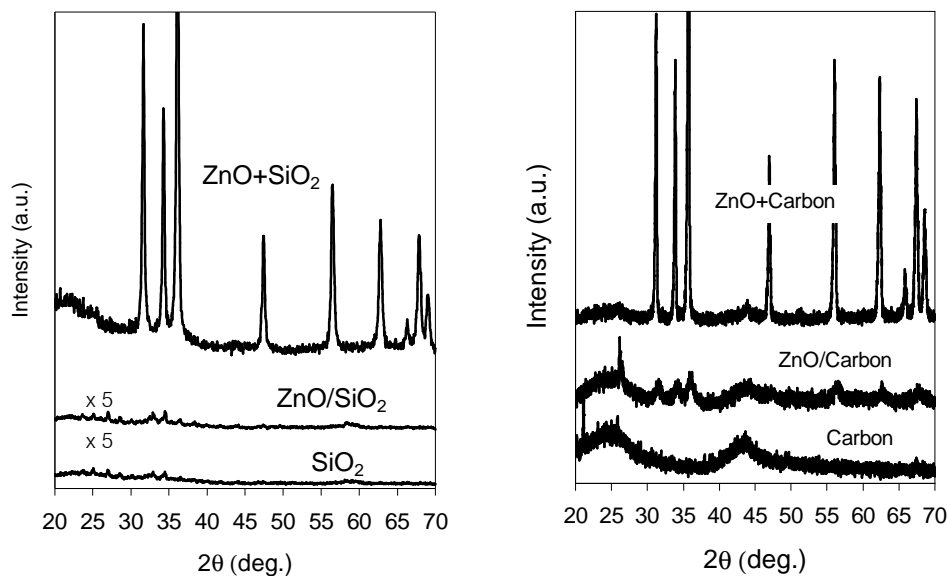
Figure I-14. XRD patterns of microfibrous entrapped ZnO/SiO_2 and $ZnO/Carbon$.

I.2.5.2. Desulfurization Performance at 400 °C

The Ni Microfibrous entrapped sorbent demonstrated excellent desulfurization performance. The desulfurization performance comparison between Ni fiber entrapped ZnO/SiO_2 and Sud-Chemie ZnO sorbent particles of various sizes tested with 2 vol.% H_2S-H_2 at 400 °C is shown in **Figure I-15**. At equivalent ZnO loading (0.02 g), the small Sud-Chemie ZnO particles (60-80 mesh) yielded 2.5 times longer breakthrough time, sharper breakthrough curves and 2.5 times higher ZnO utilization than the one with larger particle size (~1mm), due to the enhancement in external mass transfer rate and intra-particle diffusion rate. Compared with 150-250μm Sud-Chemie ZnO particles, microfibrous entrapped 150-250μm ZnO/SiO_2 sorbents demonstrated longer

63

breakthrough time and higher ZnO utilization.   Possible reasons provided by Lu *et al.*

(2005) are the improved mass transfer rate and the use of Ni microfibrous media.
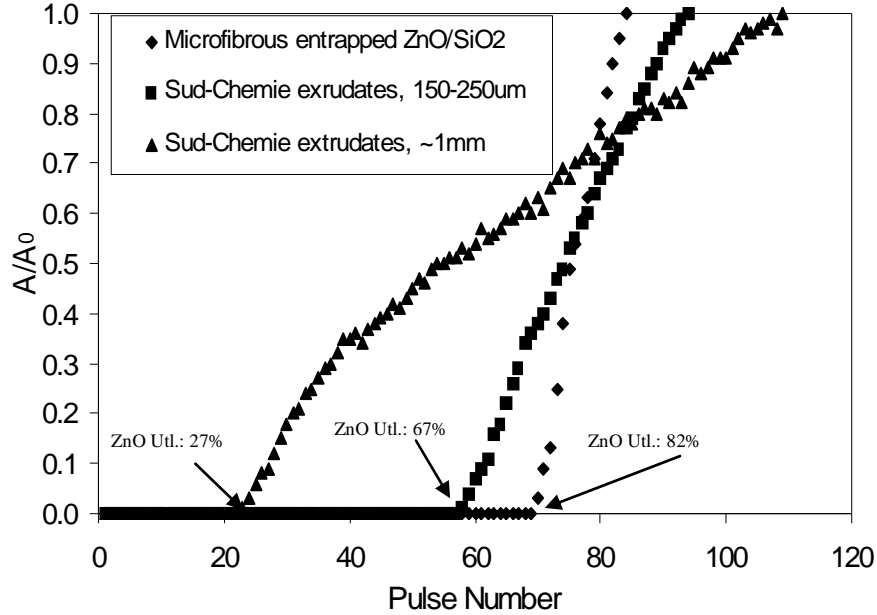
Figure I-15. H_2S pulse reaction results of microfibrous entrapped ZnO/SiO_2 and Sud-Chemie ZnO extrudates at 400°C.

The difference between the performance of Ni microfibrous entrapped sorbent and

Sud-Chemie was more significant at low H_2S challenge concentration in the presence of

water.   The desulfurization performance of Ni microfibrous entrapped ZnO/SiO_2 and

1-2mm Sud-Chemie ZnO extrudates for H_2S removal from model reformates was

compared   with equivalent bed volume (0.29mL, 11mm dia. ⅹ 3mm thick),at 400°C

and face velocity of 3.9 cm/s in 30% H_2O.   The Ni fiber entrapped ZnO/SiO_2

demonstrated 2 times longer breakthrough time than Sud-Chemie extrudates.   The

weight (including microfibrous media) of sorbent loaded in the reactor of Ni microfibrous

entrapped ZnO/SiO_2 sorbent was only 40 % of that in Sud-Chemie test.   The ZnO

utilization of Ni MFES is 13 higher than that in Sud-Chemie test.   These results are just

as expected from earlier discussion.

Table I-9. Comparison between microfibrous entrapped ZnO/SiO_2 and Sud-Chemie ZnO
extrudates for H_2S removal from model reformates at 400 °C in the presence of 30 vol.%
H_2O.*

Sorbent	Microfibrous entrapped ZnO/SiO_2	Sud-Chemie extrudates (1-2mm)
Weight (g)	0.12	0.30
Volume (cm^3)	0.29	0.29
Bed thickness (mm)	3	3
Breakthrough time @1ppmv (h)	12	4.5
ZnO Utilization (%)	57	4

* Face velocity:3.9 cm/s@50 ppmv H_2S in model reformates (40% H_2, 10% CO, 20%
CO_2, 30% N_2); dry gas flow rate: 100 mL(STP)/min.

I.2.5.3. Regenerability of Ni Microfibrous Entrapped ZnO/SiO_2 Sorbents

ZnO usually can be regenerated at a temperature above 600 °C (Ayala, 1993).   The

nano-dispersed nature of the ZnO combined with the use of small SiO_2 particulates in

MFES should also facilitate the regeneration in air.   Experimental data in **Table I-10**

confirmed this.   Compared with ZnO extrudates, microfibrous entrapped sorbents could

be recovered with considerable capacity.   However, the Sud-Chemie extrudates can only

recover 1/3 capacity of fresh sorbent at high temperatures.

Table I-10. Comparison between regenerability of microfibrous entrapped ZnO/SiO$_2$ and Sud-Chemie ZnO extrudates. [a]

Sorbent	ZnO Utilization, %	
	Microfibrous entrapped ZnO/SiO$_2$[*]	Sud-Chemie extrudates (1-2 mm)
Fresh	67	31
3h@600°C in air[**]	60	21
1h@600°C in air[**]	57	13
3h@550°C in air[**]	44	4

a   Bed configuration: 0.9mL, 7mm(dia.)×15mm(thick). H$_2$S absorption was carried out at face velocity of 1.2cm/s@2%H$_2$S/98%H$_2$ (dry gas flow rate: 30mL(STP)/min) at 400°C; * particle size 150-250 μm;   ** Regeneration conditions
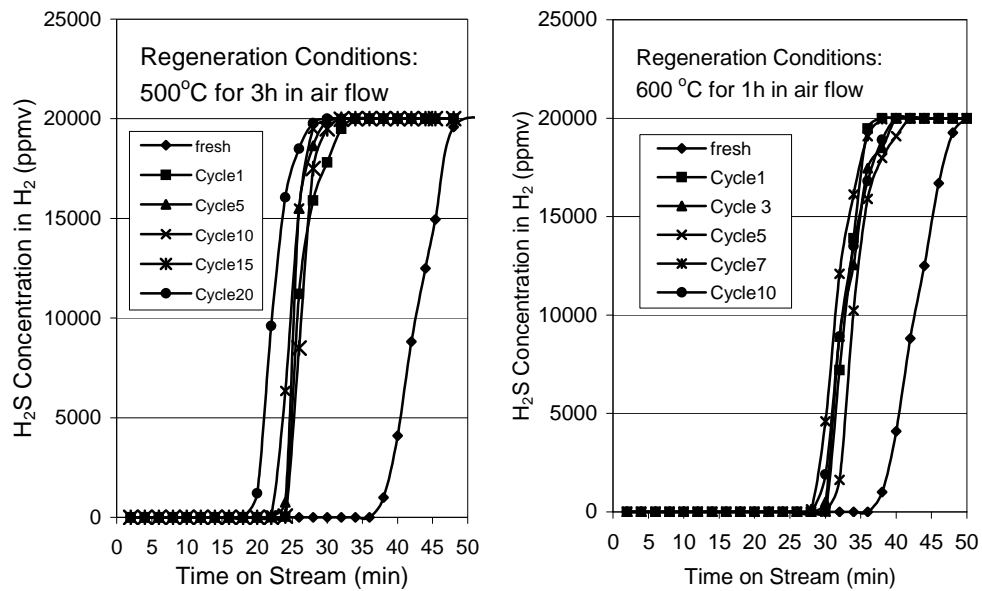
Figure I-16. Absorption/regeneration cycle test results using microfibrous entrapped ZnO/SiO$_2$ sorbent. Adsorption with H$_2$S was carried out at 400°C at a face velocity of 1.2cm/s of 2 vol.% H$_2$S-H$_2$.

Ni microfibrous entrapped ZnO/SiO$_2$ sorbent is also regenerable. **Figure I-16**

shows the cyclic test results over microfibrous entrapped ZnO/SiO$_2$ at 400 °C and at a

face velocity of 1.2 cm/s.   The sorbents maintained good performance for 10 cycles at regeneration temperature of 600 °C, and in 20 cycles at 500 °C.   However, it was found that oxidation of nickel fibrous networks in air at higher temperatures is a problem for regenerable use.

I.2.5.4. Microfibrous Entrapped ZnO/Carbon at Stack Temperatures

Ni microfibrous entrapped ZnO/Carbon sorbent was developed for H_2S removal at stack temperatures (R.T. to 100°C).   **Table I-11** shows the performance of microfibrous entrapped ZnO/Carbon for trace H_2S absorption from model reformates at stack temperatures and face velocity of 1.7 cm/s in the presence of different H_2O content. Considering the poor intra-particle mass transfer resistance, the ZnO utilization achieved by these sorbent is significant.

Table I-11. Performance of microfibrous entrapped ZnO/Carbon for H_2S absorption from model reformates at R.T. to 100°C in the presence of H_2O.*

Sorbent	Breakthrough Time (h)	ZnO Utilization (%)
Ni fiber entrapped ZnO/Carbon (11mm dia. × 3mm thick)	9.5@100°C in 5%H_2O	39
	8.7@70°C in 5%H_2O	36
	7.8@25°C in 5%H_2O	30
	8.0@70°C in 30%H_2O	32

* Face velocity:1.7cm/s@50ppmv H_2S in model reformates (40%H_2, 10%CO, 20%CO_2, 30%N_2); dry gas flow rate: 100mL(STP)/min. Tested with constant bed volume of 0.29mL (11mm(dia.)×3mm(thick) disc sorbent).
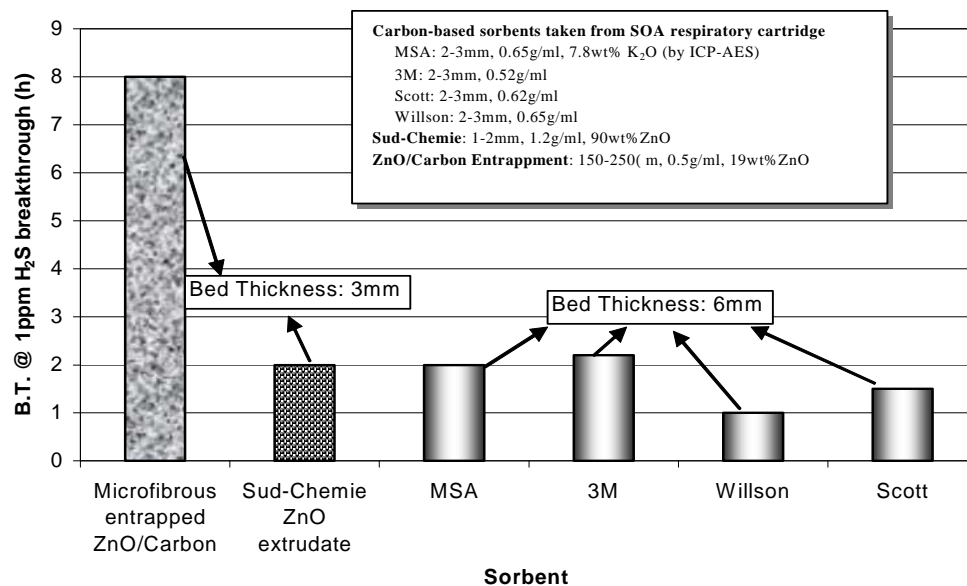
Figure I-17. Comparison of microfibrous entrapped ZnO/Carbon with several commercially available sorbent particulates for absorption with 50ppmv H_2S challenge in a model reformates in 30% at 70 °C and face velocity of 1.7cm/s (100mL(STP)/min).. Sorbent tested at equivalent bed volume of 0.29mL, 11mm(dia.)×3mm(thick).

Figure I-17 compares microfibrous entrapped ZnO/Carbon with several commercial sorbents. Ni microfibrous entrapped ZnO/Carbon (150-250μm) sorbent provided 3 times longer breakthrough times than Sud-Chemie extrudates (1-2mm), the high-temperature sorbent, with a 67% reduction of sorbent loading. Four carbon-based sorbents (2-3mm) for respiratory cartridges taken from different manufacturers were also evaluated versus the low-temperature sorbent, because they made low temperature H_2S absorption. In those cases, ZnO/Carbon entrapped materials provided about 3-fold longer breakthrough times for H_2S compared with the packed beds of those four carbon-based 2-3 mm sorbents, even though their bed thickness was doubled.

I.2.5.5. Comments on Ni Fiber Entrapped Sorbents

The Ni microfibrous entrapped ZnO based sorbents demonstrated excellent H_2S capacity for targeted applications. Ni microfibrous media are flexible and can be cut or folded in any shape to match the reactors. However, they were not successfully developed for multiple regenerable applications. The Ni microfibrous network cannot stand up the highly oxidative environment (in the presence of air) during regenerations at a temperatures ca. 550 °C. Ni fiber itself can react with H_2S to form NiS. This side reaction offers extra H_2S capacity, however it make the sintered network lose its structural integrity. Moreover, Ni also may react with CO to form complex in the presence of reformates. Therefore, Ni may not be the best choice for desulfurization at moderate temperature range (300-500 °C). Novel microfibrous media, inert in air and reformates in the temperature range, are highly favored.

Ni microfibrous entrapped ZnO/Carbon is a good sorbent at stack temperatures. Carbon also offers significant H_2S capacity. Therefore ZnO and carbon should be a good combination. However, the carbon supported ZnO is a non-regenerable sorbent due to the use of carbon. Other combinations are under extensive investigation for multiple applications. A combination of sorbent and support that have high sulfur capacity, low regeneration temperature (<200 °C) will be preferred, because it can be entrapped in Ni or other metal based microfibrous media to achieve regenerable applications.

I.2.6. Summary

Based on the discussion above, the metal oxide based sorbents and their performance are summarized in **Table I-12**.

Table I-12. Metal oxide sorbents (reactive) and mixed oxide sorbents for high temperature H_2S removal.

sorbent	Saturation Capacity (mg H_2S/g)	Equilibrium H_2S Conc. (ppmv)		Regeneration condition	Advantage	Disadvantage
		400 °C	800 °C			
CaO/CaCO$_3$	600/320	3.29×10^5	181	air T>1000 °C	Low Cost High capacity	poor low-T performance very high reg. T.
FeO	472	26.4	382	air 850 °C	Low Cost High capacity	high equil. conc. reduction at high T
MnO	478	13.7	394	air, 800-1000°C	no oxide reduction Desul. T= Regn. T	poor performance with water present
ZnO	419	0.59	68.5	diluted air or water 500-750°C	good low-T performance	zinc loss at T>550 °C
ZnO*Fe$_2$O$_3$	423	0.59	68.5	air T >750 °C	improved moderate T performance	Zn loss at T>650 °C Fe$_2$O$_3$ reduction
Zn$_2$TiO$_4$	264	1.52	165	Diluted air T>475°C	improved high T performance	low capacity Zn loss at T>800 °C
CuO	214	0	0	Diluted air T>650 °C	extremely high equilibrium conc.	low capacity CuO reduction
Cu$_2$O	238	0	0.005	Diluted air T>650 °C	extremely high equilibrium Conc.	low capacity Cu$_2$O reduction
CuO*Al$_2$O$_3$	93.7	0	0	Diluted air T>750 °C	extremely high equilibrium conc.	low capacity CuO reduction
CuO*Cr$_2$O$_3$	73.4	0	0	diluted air 650-850 °C	high equilibrium constant.	low capacity CuO reduction
CuO*CeO$_2$	67.6	0	0	diluted air 650-850 °C	extremely high equilibrium conc.	low capacity sulfate formation
Ce$_2$O$_3$	104	0	0	SO$_2$ at 600 °C	extremely high equilibrium conc	very low capacity unstable with steam

Among the oxides of Ca, Cu, Fe, rare earth metals, and Zn, zinc oxide is the best candidate for gas desulfurization at a temperature less than 500 °C. Zinc oxide based sorbents have been investigated extensively. It has a high desulfurization equilibrium constant, a high capacity, and good regenerability. The issue of zinc loss in this temperature range is not significant, especially in the presence of water. Moreover, it can be mitigated by addition of stabilizers, such as iron oxide and titania. The zinc oxide based sorbents are versatile because their performance can be tailored for specified applications by adding dopants. The low temperature performance of ZnO can also be promoted by adding other transition metal compounds, such as copper, silver and cobalt. At high temperatures, external mass transfer or intra-particle mass transfer resistance may control the process. In these cases, the overall performance of ZnO based sorbents can be further improved using microfibrous entrapped small ZnO grains. For low temperature applications, the design approach used in Ni microfibrous entrapped ZnO/Carbon sorbents gave an important hint to achieve high sulfur capacity, though it was not designed for regenerable use. At low temperatures, sorbent particles with high surface area, larger porosity, small particle and small grain size will be essential to achieve high capacity because lattice diffusion may be the controlling step. The microfibrous media are good candidates to employ these small particles without generating penalties.

71

I.3. Objectives of Research

Based on the literature review, ZnO based sorbents were chosen for the gas phase desulfurization from room temperature to 400 ℃.   The objectives of this research are:

(1) To design novel sorbents to achieve multi-log removal of H_2S with thin layers at 400 ℃;

(2) To design novel sorbents to achieve multi-log removal of H_2S at room temperature;

(3) To withstand multiple adsorption/regeneration without losing activity and contacting efficiency;

(4) To build mathematic model to predict breakthrough curves;

(5) To miniaturize the H_2S removal unit.

Notations

a	particle external surface area per unit bed volume	cm^2/cm^3
A	cross section area of the bed	cm^2
b	reaction equation constant	
C_A	gas specie density	mol/cm^3
C_{Ag}	bulk gas concentration	mol/cm^3
C_{A0}	challenge gas concentration	mol/cm^3

C_b	breakthrough concentration	mol/cm^3
C_B	molar concentration of solid specie B	mol/cm^3
D_p	particle size	cm
D_e	effective diffusivity	cm^2/s
F	flow rate	cm^3/min
G	mass flow rate of gas	g/cm^3
k	the integration constant used in Yoon's model	
k_1	first order reaction rate	s^{-1}
k_2	second order reaction rate	cm^3/mol s
k_g	external mass transfer rate	s^{-1}
k_v	adsorption rate	min^{-1}
K	lumped K or pseudo reaction rate constant (Yoon' Model)	min^{-1}
k_s	surface reaction rate	s^{-1}
l	the distance from the plate surface	cm
L	plate thickness	cm
M_z	molecular weight	g/mol
n'	number of cartridge	
N_0	capacity of the packed bed sorbent per unit volume	mol/cm^3
r_c	core diameter	cm
R	diameter	cm

t_b	breakthrough time	min
U	face velocity	cm/min
V	volume flow rate of challenge gas	cm^3/min
W_c	mass of the sorbent in the bed	g
W_e	saturation capacity of the bed	g
W_s	sorbent saturation capacity	mol/g
x	ZnO utilization	
X_B	conversion specie B	
y	ZnO weight per gram of sorbent	g/g
z	bed depth	cm
z_c	the critical bed depth to yield C_b	cm
z$_t$	bed length	cm

Greek letters

ϕ	void fraction of packed bed	
μ	viscosity	
ρ	gas density	g/cm^3
ρ_c	capacity density	mol/cm^3
ρ_b	bulk density of sorbent in the packed bed	g/cm^3
τ	characteristic time to achieve 100% conversion	min

CHAPTER II.

EXPERIMENTAL

II.1. Sorbent Evaluation

Sorbent design in this study focuses on improving the sorbent utilization, sulfur capacity and structural reliability, and reducing the regeneration temperature and the preparation cost. The prepared sorbents were evaluated for gas phase desulfurization. Two evaluations, integral reactor evaluation and differential reactor evaluation, were conducted using difference challenge gases, such as H_2S-H_2 of various H_2S concentrations and model reformates with CO, CO_2, at difference test conditions.

II.1.1. Integral Reactor Evaluation

Integral reactor evaluation was employed to investigate the reactivity and capacity of the sorbents prepared. The simplest integral reactor evaluation was carried out using 2 vol.% H_2S-H_2 or 321 ppmv H_2S-H_2 mixtures as challenge gases under various reaction conditions. The outlet H_2S concentrations were calculated from gas chromatography data, and the breakthrough curves (C/C_0~time plot) were then established. The breakthrough time (t_b) and the saturation time (τ) were then read from breakthrough

curves and were used to calculate the corresponding sulfur capacities. The equation to calculate the breakthrough capacities (W_b) is

$$W_b = \frac{M_z V C_{A0} t_b}{m}$$ (II-1)

Equation II-1 is only applicable to estimate capacity at low breakthrough concentration, ca, $C_b < 0.01\ C_0$. For high breakthrough concentration applications, manual integration is required. This method will be described in Chapter IV. Similarly, the saturation capacity should be estimated based on the manual integration. However, due to the symmetry of gas phase breakthrough curves, τ is very close to the time to reach the 50% inlet H_2S concentration ($t_{1/2}$), which can be read from a breakthrough curve, as shown in Chapter V. The saturation capacity (W_s) can be estimated using equation II-2.

$$W_s = \frac{M_z V C_{A0} t_{1/2}}{m}$$ (II-2)

The integral reactor evaluation was used to investigate the breakthrough behaviors of the packed beds, such as kinetics, breakthrough Zn utilization, for further reactor and process design. The sharpness of a breakthrough curve, characterized using lumped K in Yoon's model, was used as an index for the apparent reaction rate. For the sorbents tested in the same conditions, the sharper breakthrough curves indicate the fast reaction kinetics. The further interpretation on lumped K is discussed in Chapter V.

II.1.2. Differential Reactor Evaluation

In this study, differential reactor evaluation was employed to estimate the kinetic parameters in the desulfurization process. The plot of outlet H_2S concentration *vs.* onsite time (C~t plot) was established in the evaluation. This plot is similar to breakthrough curves mentioned in integral reaction evaluation. However, due to tiny amount of sorbent loaded in the differential reactor, the initial H_2S outlet concentration is high enough to be detected by GC accurately. There is not breakthrough concentration defined in this type of evaluation. The outlet concentration at time approaching zero is extrapolated by extending the C~t plot. Therefore, the apparent reaction rate constant (void volume based) can be evaluated using equation II-3.

$$k_{av} = \frac{\ln\left(\frac{C_0}{C}\right)\Big|_{t\to0}}{t_r} \tag{II-3}$$

where residence time t_r can be calculated as

$$t_r = \frac{\phi \cdot z_t}{U} \tag{II-4}$$

Besides the apparent reaction rate constant, differential reactor study can also be employed to establish ZnO conversion *vs.* time (*x-t* plot). Then kinetic parameters, such as effective diffusivity, effectiveness factor, can be estimated using the mathematic models described in Chapter I. The detailed procedure is shown in Chapter IV.

II.2. Experimental Setup and Analytic Methods

II.2.1. Desulfurization Setup

The experimental setup is shown in **Figure II-1**. It consisted of a gas supply system, a reaction system and an analyzing unit. If not otherwise addressed, all the gases were purchased from Airgas South Inc. In gas supply system, H_2S-H_2 cylinders with 2 vol.% and 321 ppmv H_2S supplied H_2S for the reaction. H_2 of ultra-high purity (UHP) was employed to dilute the H_2S challenge gas to lower concentration and to stabilize the temperature profile in the reactor before challenge gas passed through. Househood air was used to regenerate the spend sorbents. Helium (UHP) was applied to eliminate the oxygen from the reactor before H_2 or H_2S pass through the reactor. CO (Sigma-Aldrich, >99.5 vol.%) and/or CO_2 (UHP) may be added to the challenging gases to investigate the carbonyl sulfide formation. A vaporizer provided the gas stream saturated steams at various controlled temperatures to investigate the water effects.

The reaction system mainly consisted of a quartz tube reactor in a tube furnace. The detailed dimension of the tube reactor is shown **Figure II-2**. The reactor diameter varied, but the length of the reactor was fixed at 50 cm. The sorbents were loaded at 18 cm from the bottom. Two flat layers of glass wool of 8 μm were put on the top and at the bottom of the packed sorbents. These layers distributed the gas follow and kept the sorbent particles from moving. Ceramic rings, which were inert to H_2S, H_2, and O_2 to a temperature above 600 °C, supported the bed and these two wool layers.
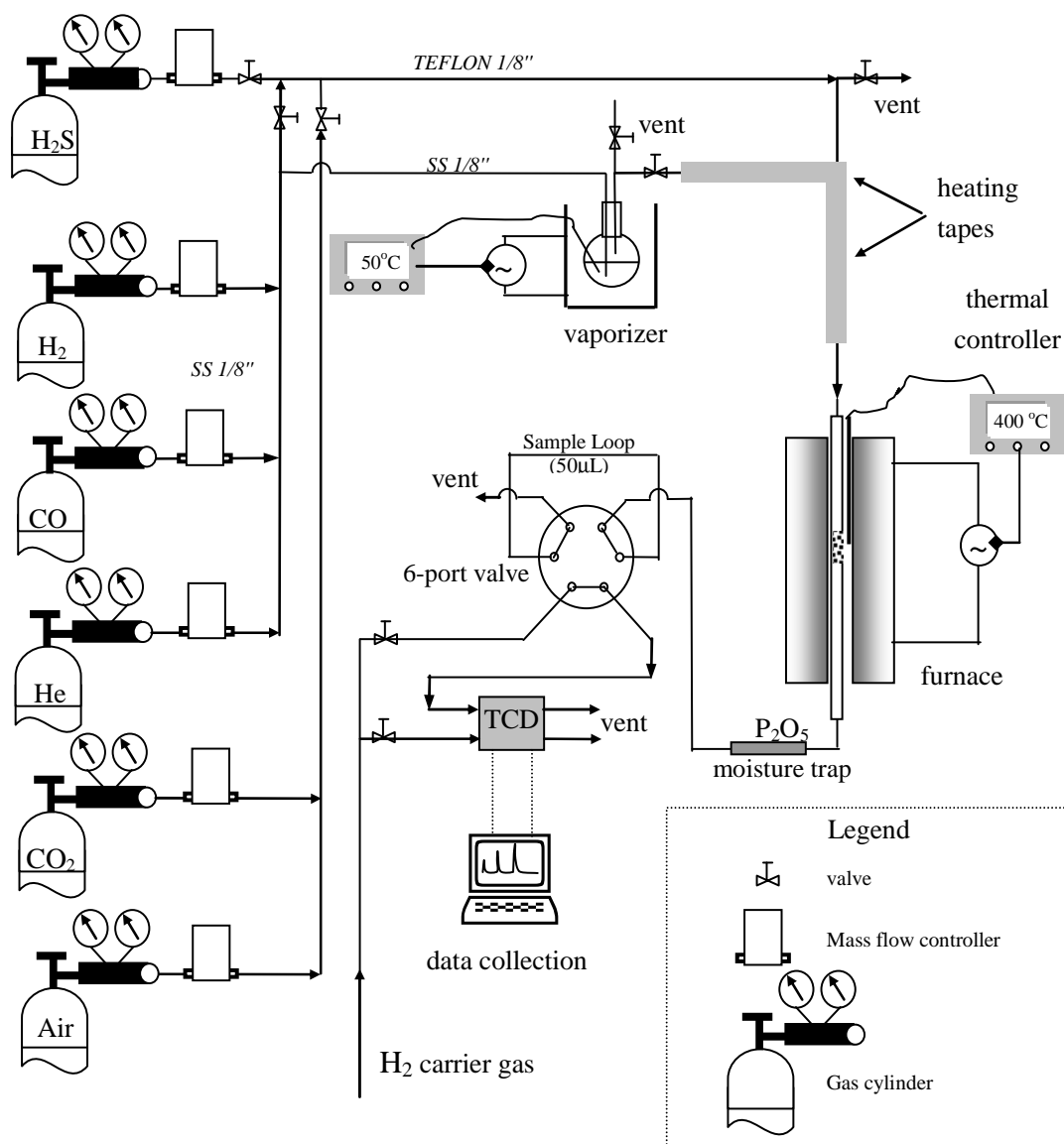
Figure II-1. Experimental setup for gas phase desulfurization.

In the setup, a gas chromatography (GC) was employed to analyze the gas concentrations. After the gas stream left the reactor, it passed through a tiny moisture trap made of phosphorous pentaoxide (P_2O_5) powder. Gas sample was injected to a thermal conductivity detector (TCD) by a 6-port valve every minute after experiment

started. All the tubing connecting the reactor and the valves was 1/8" TEFLON or Stainless Steel tubing. At this tubing size and flow conditions, the pressure drop over the setup was negligible. A packed column (HayeSep Q, 80/100 8'×1/8" SS) was employed with TCD and the column oven temperature was set at 80 °C. The TCD used H_2 (UHP) as the carrier gas. The filament temperature was set at 350 °C. At these configurations, the GC can detect CO (>40 ppm), CO_2 (>20 ppm), COS (>20 ppm) and H_2S (>200 ppm). The detailed method is shown in Appendix G1.
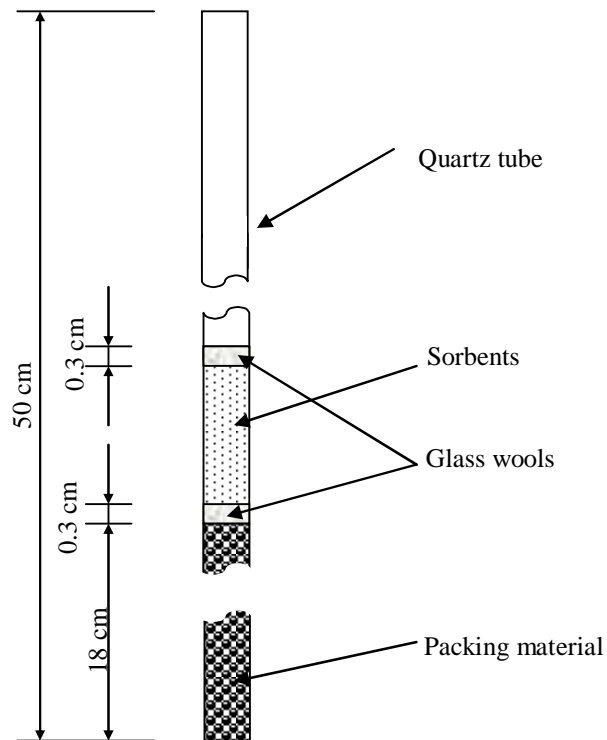
Figure II-2. Reactor employed in desulfurization.

All the low H_2S desulfurization (<300 ppmv) were analyzed by a Varian GC 3800 equipped with a pulse flame photometric detector (PFPD) working at sulfur mode.

Every sample of 250 μL was collected right after the reactor, and injected manually to the PFPD.   The detailed PFPD method is shown in Appendix G2.   With this method, the sulfur concentrations above 20 ppb can be detected.

II.2.2. Setup for Pressure Drop Test

The pressure drops over various fixed beds were tested with the setup shown in **Figure II-3**.   It is simplified from the desulfurization setup, and consisted of a H_2 cylinder, a mass controller, the same tube reactor in **Figure II-1** and a pressure gauge which was able to detect the pressure drop from 0~2 inches of water.
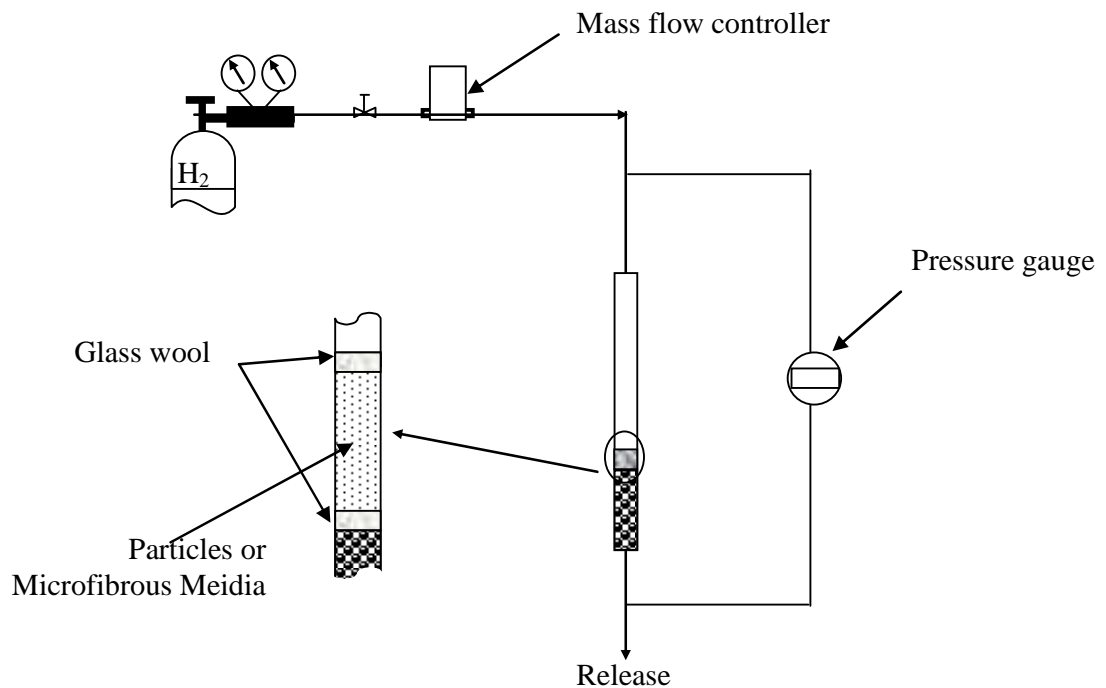
Figure II-3. Experimental setup for pressure drop test at room temperature.

II.2.3. Flow Rate Control

Mass flow controllers (Omega FMA 2400 series) were used to control the gas flow rates.   All of them were calibrated carefully before experiments, especially the mass flow controller for H_2, H_2S, CO and CO_2.   The calibrations for pure gases as well as air were carried out by a digital flow check (Alltech Digital Flow Check 1108), which had been calibrated by the manufacturer, see the appendix for detail.   However, the calibration for mixture such as H_2S-H_2 cannot be calibrated by the digital flow check because of the significant difference in the molecular weights of H_2 and H_2S.   Therefore, the flow rate of H_2S-H_2 mixture was calibrated specially with a soap bubble meter. Although the H_2S may be adsorbed by the soap solution, the experimental error introduced by this calibration method should be less than 2% since only 2 vol.% was occupied by H_2S.   All the calibration curves are shown in Appendix B.

II.2.4. GC Calibration

The TCD and PFPD detectors were also calibrated for the H_2S response.   The TCD response peak area should be proportional to the gas concentration, as shown in **Figure II-4**.   The low H_2S concentrations (<321 ppmv) were calibrated for PFPD, and the square root of PFPD response area should be linear to the H_2S concentration.   The calibration curve of PFPF is shown in **Figure II-5**.
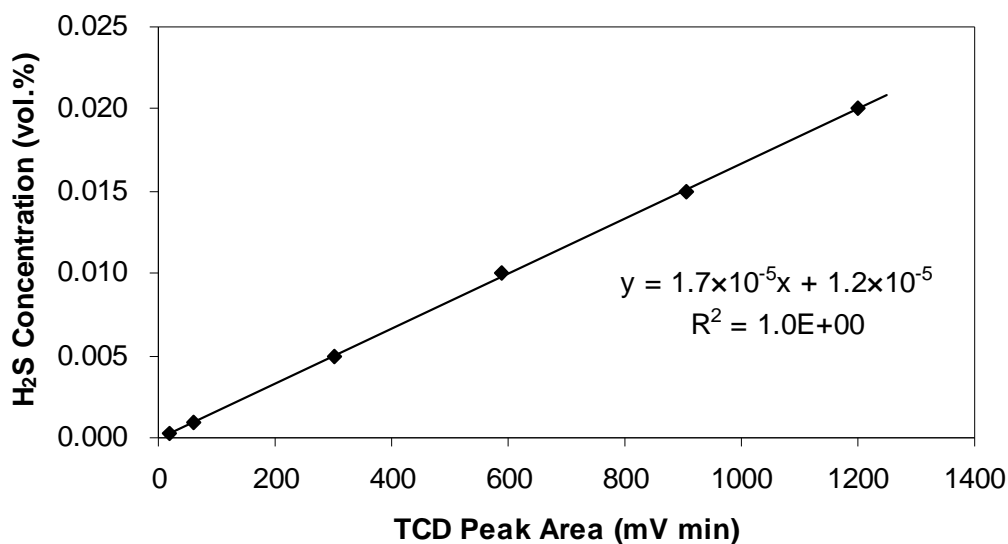
Figure II-4. Relationship between the TCD peak area and H_2S concentration. Samples were injected by an automatic 6-port valve with sampling loop of 50 μL.
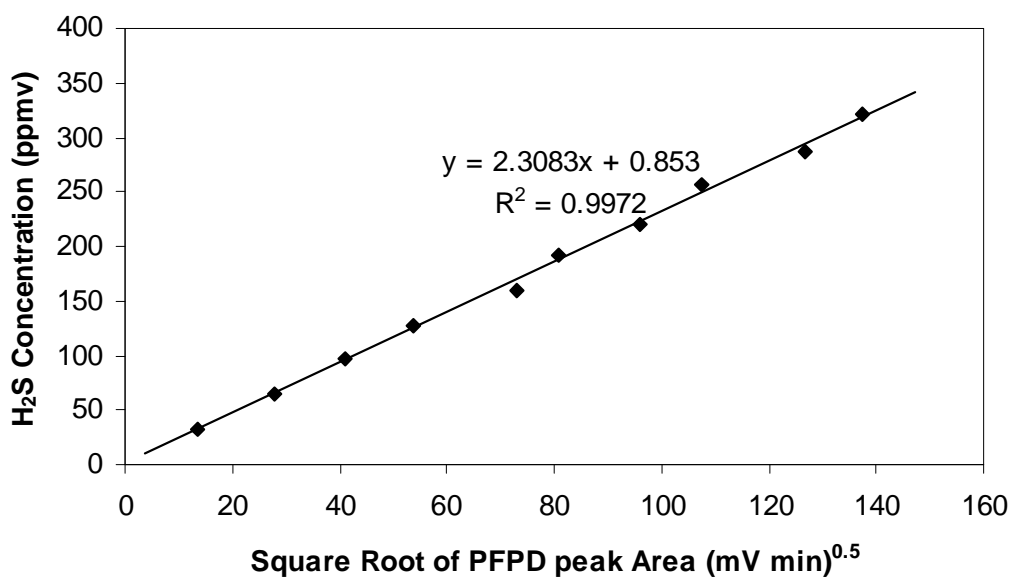
Figure II-5. Relationship between the square root of PFPD peak area and H_2S concentration. Samples were injected manually with a 250 μL syringe. Split ratio was set to be 200.

II.2.5. Steam Table

In this study, the water was introduced to reaction system in form of steam.   As shown in **Figure II-1**, the gases with extremely low solubility in water such as CO, He and H_2 passed through the vaporizer and carried the saturated steam into reactor.   In order to keep the water in vapor phase, the tubing from the vaporizer was wrapped in heating tapes.   The amount of water in gas was controlled by changing the temperature of vaporizer.   Using the steam table shown in **Figure A9** in the Appendix C, an appropriate temperature was set to achieve the desired water content.

II.3. Sorbent Preparation

II.3.1. Sorbents for Packed Beds

Sorbents in the research were prepared by incipient wetness impregnation.   For example, a zinc nitrate aqueous solution (2 mol/l) was slowly added to 20 g dried SiO_2 particles, which were kept well stirred, till the particles became wet.   The products were subsequently dried naturally overnight.   Then it was dried at 100 °C for 1 hour, and then calcined for 1 hour at the appointed temperature ca. 450 °C to form supported-ZnO sorbents.

Supported-ZnO sorbents were also prepared by a 2-step impregnation method, i.e., a sorbent collected from the above prepared samples as 1st-step product with ZnO loading

of 15-30 wt.% was added again into appointed amount of a ZnO sol-gel. As-prepared

sorbent was dried at 80 °C, and calcined for 3h at 180 °C to form a final sample with

ZnO loading of 30-45 wt.%. ZnO sol-gel was prepared by adding 52 ml $NH_3 \cdot H_2O$, 43 g

$(NH_4)_2CO_3$, and 20-40 g $ZnCO_3$ in series into 56ml water under vigorously stirring.

II.3.2. Sorbents Entrapped in Microfibrous Media

Sintered glass fiber entrapped 150-250 μm (dia.) SiO_2 (300m^2/g, Grace Davison)

support particulates were fabricated by regular wet layer paper-making/sintering

procedure. For example, 6 g of S-2 glass fiber chops (8μm dia.×6mm length, Advanced

Glassfiber Yarns LLC), and 0.7 g of 30-60 μm (dia.) cellulose (100-1000 μm in length)

were added into 2.5 L water and stirred vigorously at 50 Hz for 2 min. The produced

suspension and 18 g SiO_2 (can be increased up to 36 g) were added into a headbox of the

six-inch (dia.) circular sheet former and stirred to a uniform suspension. The 6-inch

circular preform was then formed by draining, pressing at ~ 400kNm^{-1}, and drying in air

at ~110 °C. The as-prepared preform was directly sintered in air for 30 min at 925 °C

while burning off the celluloses.

To place the ZnO onto the support, the as-prepared microfibrous entrapped SiO_2

sheet was immersed into the sol-gel (or the zinc nitrate solution) for 10 min. The paper

was subsequently removed from the ZnO sol-gel, drained under vacuum, and calcined in

air for 20 min at selected temperatures (80, 100, 120, 140, 160, and 180 °C). If zinc

nitrate was used in the impregnation, then drying and calcinations procedure can simply follow the procedure for packed bed sorbents.   The final composite sorbent has a ZnO loading of 13~17 wt.% (including the mass of the glass fibers).

II.4. Characterization Technology

XRD

Powder X-ray Diffraction (XRD) patterns were recorded on Rigaku instrument using a scanning speed of 4 °/min and an accelerating voltage of 40kV, unless stated otherwise.

SEM

Scanning Electron Microscopy (SEM) of the sorbent were obtained using a Zeiss DSM 940 instrument.

ICP

The ZnO loading (wt.%) was calculated by mass balance, and was characterized by Inductively Coupled Plasma (ICP) carried out on a Thermo Jarrell Ash ICAP 61 Simultaneous Spectrometer.

BET

The surface areas of sorbents were measured by N_2-BET.   BET stands for Brunauer, Emmett, and Teller, who published the theory in 1938.

Notation

C_0	initial H$_2$S concentration	ppmv
C_b	H$_2$S breakthrough concentration	ppmv
C_{A0}	initial H$_2$S concentration	mol/cm^3
k_{av}	apparent reaction rate (void based)	1/s
M_s	molecular weight of H$_2$S	34 g/mol
m	mass of sorbents	g
t	onsite time	min
$t_{1/2}$	time to reach 0.5 C$_0$	min
t_r	residence time	s
U	face velocity	cm/s
V	flow rate	cm^3/min
z_t	bed thickness	cm
W_b	breakthrough capacity	g H$_2$S/g sorbent
W_s	saturation capacity	g H$_2$S/g sorbent

Greek symbols

ϕ	void fraction of packed bed	

87

CHAPTER III.

GLASS FIBER ENTRAPPED SORBENT FOR GAS PHASE

DESULFURIZATION IN LOGISTIC PEM FUEL CELL SYSTEMS

Abstract:

Glass fiber entrapped ZnO/SiO_2 sorbent (GFES) was designed and optimized for gas phase desulfurization for logistic PEM fuel cell systems. Due to the use of microfibrous media and supported sorbent design, GFES demonstrated superior desulfurization performance. In the thin bed test, at equivalent ZnO loading, the GFES yielded two times longer breakthrough time than the ZnO/SiO_2 sorbent; at equivalent bed volumes, GFES provided 2-fold longer breakthrough time (with a 67% reduction in ZnO loading) than packed beds of 1-2 mm commercial extrudates. Five-log reduction in H_2S concentration with up to 75% ZnO utilization at breakthrough was achieved. H_2S concentrations from 60 to 20,000 ppmv were reduced to less than 1 ppmv at 400 °C in the presence of 30 vol.% H_2O at face velocities of 3.9 cm/s for layers as thin as 1.0 mm. GFES demonstrated significant improvement in regenerability compared with the commercial extrudates. During 50 regeneration/desulfurization cycles, GFES maintained its structural integrity. Furthermore, a composite bed consisting of a packed

bed of large extrudates followed by a polishing layer of GFES demonstrated a great extension in gas life and overall bed utilization. This approach synergistically combines the high volume loading of packed beds and the overall contacting efficiency of small particulates.

Key Words: Glass Fiber, ZnO, H_2S removal, Sorbent, Fuel Cell

III.1. Introduction

High efficiency desulfurization is critical to keep the activities of fuel processing catalysts and high-value membrane electrode assemblies in logistic PEM fuel cell systems (O'Hayre *et al*., 2005; Song, 2002; Lu *et al*., 2005; Heinzel *et al*., 2006). Metal oxides can be used to remove sulfur species from gas streams (Westmoreland and Harrison, 1976; Sasaoka *et al*., 1992; Ben-Slimane and Hepworth, 1994; Baid *et al*.,, 1992; Gupta *et al*., 1992; Lew *et al*., 1989; Slimane and Abbasian, 2000a; Alonso *et al*., 2000; Kundakovic *et al*., 1998). Among them, zinc oxide (ZnO) based sorbents are widely applied in gas phase desulfurization to remove sulfur species such as H_2S from fuel gases because of its high sulfur capacity and favorable sulfidation thermodynamics at moderate temperatures (Sasaoka, 1994b). Traditional packed bed reactors can successfully remove sulfur compounds from several thousand ppm to sub-ppm levels using metal oxide based sorbents given enough reactor volume (Song, 2002). In packed beds, catalysts and/or sorbents of big particles sizes ca. 1-5 mm are widely used and

normally demonstrate low sorbent utilization and poor regenerability because of low contacting efficiency and intra-particle and lattice diffusion limits (Twigg, 1989). As a result, packed beds with huge reactor sizes are usually required to achieve low H_2S concentrations. In order to improve sulfur removal efficiency, different approaches have been proposed. Rare metals and catalysts washcoats have been used to avoid one or more of these problems (McCreedy, 2000; Srinivasan *et al*., 1997; Watanabe *et al*., 2001; Wu *et al*., 2001), but surface areas per unit reactor volume still need further improvements. However, in logistical fuel cell systems, the overall system weights and volumes are critical concerns. Therefore, the novel sorbent and/or reactor designs with high sorbent utilization, high capacity and miniaturized reactors are definitely favored.

Microfibrous media developed at Center for Microfibrous Materials Manufacturing (CM^3) at Auburn University have demonstrated significant improvements in heat/mass transfer, contacting efficiency and regenerability (Overbeek *et al*., 2001; Tatarchuk, 1992a, 1992b; Cahela and Tatarchuk, 2001; Marrion *et al*., 1994; Kohler *et al*., 1990; Ahn and Tatarchuk, 1997; Meffert, 1998; Harris, 2001). This generic approach utilizes micro-sized fibers to entrap sorbent and/or catalyst particulates into sinter-locked microfibrous structures with a high voidage. With improved contacting efficiency, these materials can reduce both the reactor weight and volume. As for H_2S removal, Ni microfibrous entrapped sorbents were prepared and demonstrated 3 times longer breakthrough time than a commercial ZnO extrudate (Lu *et al*., 2005). However, Ni

fiber cannot stand up to the high oxidizing atmosphere during sorbent regeneration. Therefore, new microfibrous entrapped sorbents with microfibrous structures that are able to work in both reducing and oxidizing environments were demanded. In this study, glass fiber entrapped micro-sized supported-ZnO sorbent particulates were prepared and optimized for regenerable desulfurization applications in fuel processing for logistic PEM fuel cell power systems.

III.2. Experimental

III.2.1. Sorbents Preparation and Characterization

A series of supported-ZnO sorbents were prepared by incipient-wetness impregnation methods, using SiO_2 ($300m^2/g$, mean pore size of 15nm, Grace Davision), γ-Al_2O_3 ($150m^2/g$, mean pore size of 7 nm, Alpha) as supports. Activated carbon is not regenerable during ZnO sorbent regeneration, therefore it was not employed in this study.

Detailed procedure for glass fiber entrapped sorbents is described in a sample preparation: 6 g of S2 glass fiber (8 μm dia. $\times$ 6 mm length), 2 g of cellulose were added into water and stirred vigorously to produce a uniform suspension. The suspension and 18 g SiO_2 particles (150-250 μm) were added into the headbox of the 1.0 ft^2 M/K sheet former under aeration. The preform (1 ft^2) was then formed by vacuum filtration followed by drying on a heated drum. The glass fiber sheet was pre-oxidized in airflow for 30 min at 500 °C followed by sintering for 1h at a high temperature, ca. 900 °C. The

prepared microfibrous entrapped SiO_2 was immersed into the zinc nitrate solution (2 mol/L) for 10min, and subsequently vacuum drained and natural dried overnight.   Then it was calcined in air for 1 hour at 450 °C.

Powder XRD patterns were recorded on Rigaku instrument using a scanning speed of 4°/min and an accelerating voltage of 40kV, unless stated otherwise.   SEM micrographs of the GFE ZnO/SiO_2 sorbent were obtained by a Zeiss DSM 940 instrument.   The ZnO loading on support was analyzed by ICP-AES, carried out on a Thermo Jarrell Ash ICAP 61 Simultaneous Spectrometer.   The surface areas of sorbents were measured by N_2-BET.

III.2.2. Gas and Sample Analysis

All gases in this work were purchased from Airgas Inc.   Two challenge gases were employed in this paper: 2 vol.% H_2S-H_2, and 60 ppm H_2S in a model reformate stream (40%CO_2, 10%CO, 9%C1-C3 hydrocarbon, balance H_2).   The outlet H_2S concentrations were analyzed by a Gow-Mac 550 GC equipped with a TCD detector (H_2 as carrier gas) which was able to measure the H_2S concentration down to 200 ppmv.   Gas samples were injected to the GC every one minute by a 6-port-valve with a sampling loop of 50 μL. The whole sampling system was connected by 1/8" tubing, and the pressure drop of this sampling system was negligible at the experimental conditions.   The concentration below 200 ppmv was measured by a Varian 3800GC equipped with a pulse flame

photometric detector (PFPD) which was able to analyze H_2S concentration to sub-ppmv levels. Gas samples (250 μL) in low concentration tests were collected at the outlet of the reactor and injected manually.

III.3. Result and Discussion

III.3.1. Commercial Sorbent Evaluation and Supported Sorbents Design

In a preliminary experiment, a packed bed of commercial extrudates (3/16" or 4.7 mm, 16.50 g) containing 90 wt.% ZnO was tested with 5050 ppmv H_2S in H_2 at a face velocity of 20.3 cm/s at 400 ° C. The packed bed size was 2.14 cm diameter × 3.4 cm thickness. The test result, as shown in **Figure III-1,** suggests that 70% ZnO in extrudates was accessible at 400 ºC. Under the test conditions in **Figure III-1**, the packed bed failed to yield a H_2S concentration below 1 ppmv. For a higher breakthrough concentration at 50 ppmv (1% of inlet H_2S concentration), the breakthrough time read from the breakthrough curve was 40 minutes, which suggests only 8 % ZnO reacted with H_2S at the breakthrough under the test conditions. A further analysis showed that only the ZnO in a layer of 50 μm (average) from the outer surface was accessed prior the breakthrough. Therefore, ZnO particles with a size less than 100 μm should be fully utilized under the test conditions and the breakthrough concentration. In a similar experiment done by Song *et al*. (2002), only 3 ‰ ZnO was utilized at 0.1 ppmv breakthrough in the presence of 20 % water, and the layer thickness was calculated to be

93

0.2 µm. In this case, only the ZnO particles than 0.4 µm could be fully utilized at the specified desulfurization application.
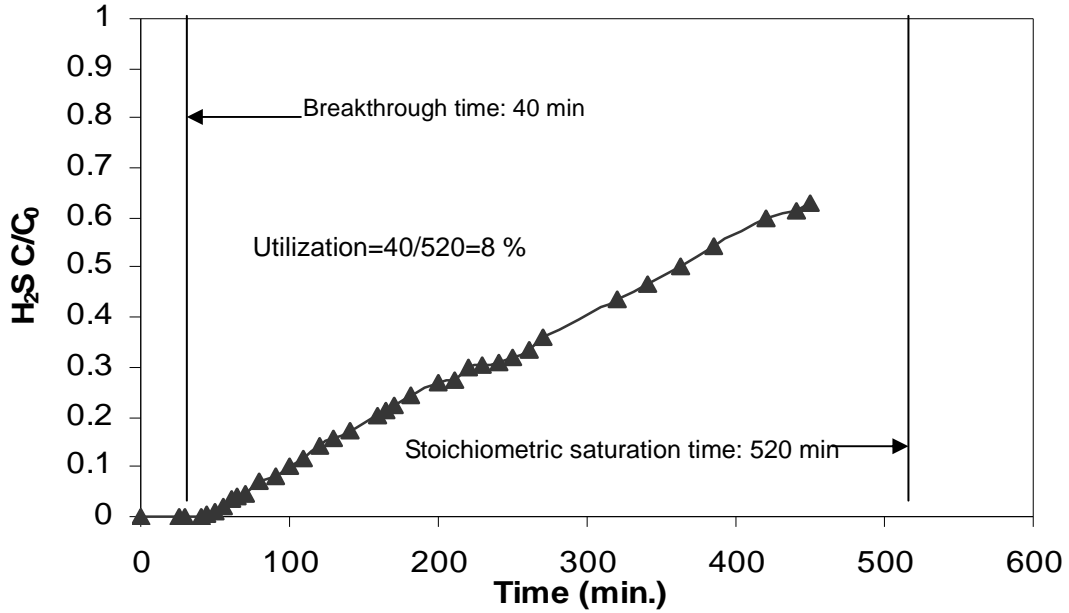
Figure III-1. Desulfurization performance of a commercial ZnO sorbent.

It is well known that small particle size can reduce the intra-particle mass transfer resistance and enhance the external mass transfer rate. Further tests for the commercial sorbent of various particle sizes were performed at 400 °C at a low face velocity, and the result is shown in **Figure III-2**. The saturation capacity of the commercial sorbent increased with the decrease in particle size, and breakthrough capacity followed the same trend but not significantly.
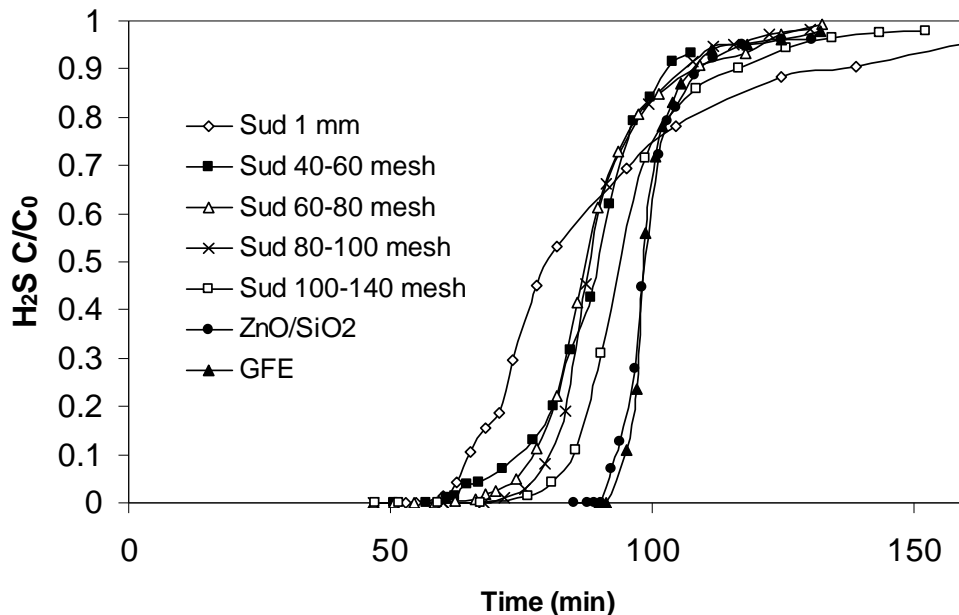
Figure III-2. Breakthrough curves of commercial ZnO sorbents of different sizes, and breakthrough curve of ZnO/SiO$_2$ sorbent.

Based on the results from **Figures III**-**1** and **2**, the nanosized particles would achieve complete utilization during desulfurization. Although the use of small particles promotes the mass transfer, it also introduces high pressure drop and channeling in packed beds, and sorbent particles with size less than 100 µm are practically not applicable in packed beds, let alone nanosized sorbents. As a compromised design, nanosized ZnO particles or grains could be loaded on different inert support particles, which can be used in packed beds or entrapped in microfibrous media. The supports with high porosity and high surface area will be favored due to the reduced pore diffusion resistance and high intrinsic reaction rate. Supported sorbent also have several other functions. The supports can stabilize the ZnO, keep ZnO highly dispersed, retard the grain growth, and thus yield stable performance and extended the service life.

95

III.3.2. Supported ZnO Sorbents

III.3.2.1. Support Screening

The supports with high pore volume and surface area are preferred due to the possible enhancement in mass transfer rate and intrinsic reaction rate. Three typical supports, SiO_2, Al_2O_3 and activated carbon particle (ACP), are widely employed in industry. Among them, ACP will react with oxygen during the regeneration of ZnO based sorbent. Therefore, only SiO_2 (40-60 mesh) and γ-Al_2O_3 (40-60 mesh) were chosen as supports for supported-ZnO sorbents. H_2S adsorption performance was found to be strongly dependent on the types of support, and calcination temperatures (see **Figure III-3**). An earlier experiment suggested that H_2S adsorption capacities of these two neat supports at 400 °C were negligible.

Figure III-3 suggests SiO_2 and Al_2O_3 supported ZnO sorbents demonstrated comparable sulfur capacities at a calcination temperature of 300 °C. However, the results at the calcination temperature of 500 °C are quite different. After calcination at 500°C for 60 minutes, H_2S saturation capacity of SiO_2-supported ZnO sorbent almost remained unchanged, but that of γ-Al_2O_3-supported ZnO demonstrated a dramatic reduction. It is well known that the surface of γ-Al_2O_3 is quite reactive, but that of SiO_2, very inert. As a result, strong interaction even solid reaction between ZnO and γ-Al_2O_3 took place at a temperature above 500°C, while SiO_2 remained inert to ZnO. Meanwhile, the formation of inactive "$ZnAl_2O_4$-like" compound via the solid reaction was mostly

accelerated with increase in calcination temperature. This is the possible reason for the deactivation of γ-Al$_2$O$_3$-supported ZnO sorbent at high calcination temperatures. Because ZnO based sorbents are usually regenerated at a temperature above 500 °C, **Figure III-3** hints that the Al$_2$O$_3$ supported ZnO sorbent will not maintain its performance after regeneration. Therefore, SiO$_2$ was chosen as the appropriate support.
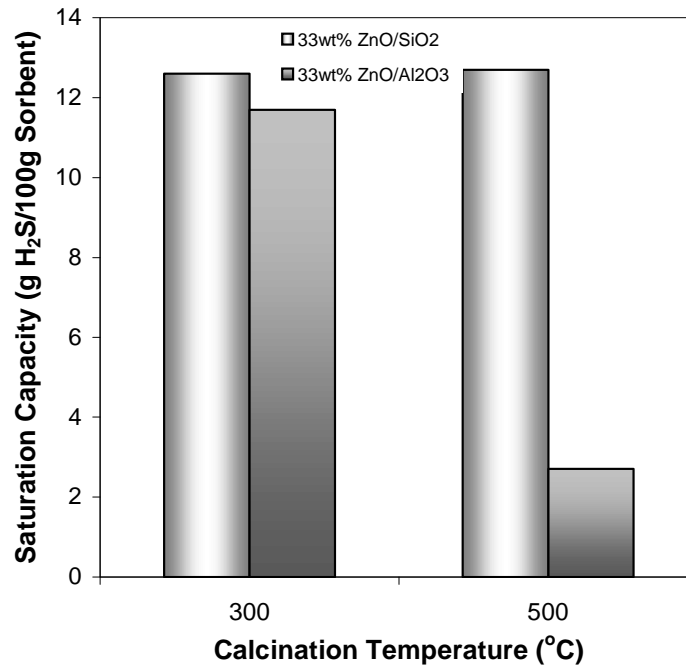
Figure III-3. Support screening.

The calcination temperature should also affect the performance of SiO$_2$ supported ZnO sorbent (ZnO/SiO$_2$), because ZnO grains grows with the calcination temperature and regeneration temperature, as shown in **Table III-1**. Therefore, it concludes that the calcination temperature determines the performance of the sorbent. Therefore, low calcination and regeneration temperatures are always preferred to retard the grain growth.

Table III-1. Calculated grain sizes at different calcination temperatures using Debye-Scherrer Equation. Calcination time was 1 hour.

Calcination T (^oC)	Grain Size (nm)
350	1.25
450	2.90
600	2.98
752	3.60

III.3.2.2. ZnO Loading Effects

ZnO/SiO$_2$ sorbents with different ZnO loading were prepared using zinc nitrate as precursor. The H$_2$S adsorption performances were displayed in **Figure III-4**. It shows that H$_2$S adsorption capacity increased obviously with ZnO loading up to 33 wt.% and then dropped dramatically with ZnO loading up to 50 wt.%. ZnO utilization decreased sharply from 93% to 24% with the increase in ZnO loading from 25 to 50 wt.%. The above results indicate that optimal ZnO loading of ZnO/SiO$_2$ for high H$_2$S adsorption capacity is ~33 wt.% when zinc nitrate is used as precursor. The sorbents with high capacity and the sorbents with high ZnO utilization can be employed for different applications. For the stoichiometric adsorption reaction between H$_2$S and ZnO, however, high ZnO content in the sorbent inventory with high ZnO utilization was pursued to achieve a long breakthrough time over per unit weight (or volume) of sorbent (i.e. high breakthrough H$_2$S capacity).
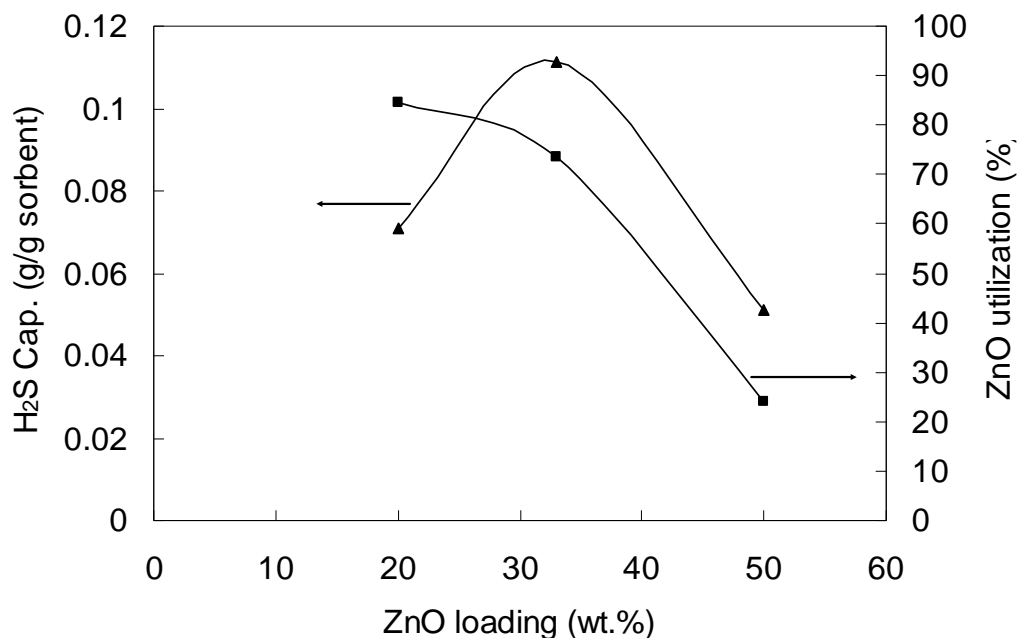
Figure III-4. ZnO loading ratio effects**.**

III.3.2.3. Glass Fiber Screening

As stated earlier, Ni fiber entrapped sorbents demonstrated 2- to 3- fold longer breakthrough time for H_2S removal with a 67 % reduction in sorbent loading, compared with 1-2 mm commercial extrudates. However, Ni fiber was oxidized in regeneration conditions in the presence of oxygen, and sinter-locked networking collapsed after 10 adsorption/regeneration cycles (Lu *et al*., 2005). Therefore, other microfibrous materials that can stand the highly reducing and oxidizing environment and the high temperatures (T>600 °C) will be considered as alternatives for Ni fibers. Glass fibers may be the right choices. Here are several types of glass/ceramic fibers, and their properties and chemical compositions are listed in **Table III-2**.

Table III-2. Properties of several glass fibers. Courtesy of Owens Corning (Hartman *et al.*, 1994).

	A-type	C-type	D-type	E-type	ECR-type	S-type	AR-type	R-type
Density (g/cc)	2.44	2.52	2.11	2.58	2.72	2.46	2.7	2.54
Softening Point (°C)	705	750	771	846	882	1056	773	952
Annealing Point (°C)		588	521	657		810		
Strain Point (°C)		552	477	615		760		

Based on the thermal properties and availability, E- and S-type glass fibers were chosen as the materials to prepare microfibrous media. Preliminary test result suggested that, S2 fiber, one S type of glass fiber (8μm dia.× 6mm length, Advanced Glassfiber Yarns Inc.) was able to be sintered above 900 °C. The sinter-locked structure is shown in **Figure III-5**. E glass fiber (10 μm dia.× 6mm length, Owens Corning) was able to sintered around 800 °C.

III.3.2.4. Properties of Sorbents

Sorbents were characterized by x-ray diffraction (XRD) and scanning electron microscopy (SEM). The SEM images of S2-glass fiber entrapped ZnO/SiO_2 shown in **Figure III-5** suggest that the glass fibers partially melted during sintering and formed a sinter-locked fiber network, which was like cages entrapping SiO_2 particulates. This network held the particles and kept them from being carried away by the gas flow. The

XRD patterns of glass fiber entrapped sorbents and ZnO/SiO$_2$ sorbents and ZnO extrudates are shown in **Figure III-6** for comparison. The XRD pattern of ZnO extrudate (pattern c in **Figure III-6**) demonstrates strong ZnO peaks at 2θ values of 31.2°, 34° and 35.8°, which means that crystal ZnO grains with large grain size existed in the sorbents. While those of glass fiber entrapped sorbent and ZnO/SiO$_2$ sorbents only show three humps at corresponded 2θ positions, which suggests the ZnO in these two sorbents may not have good crystallinity, provided the ZnO grains are in very small size. The grain sizes of ZnO extrudates and glass fiber entrapped ZnO/SiO$_2$ sorbent calculated by Debye-Scherrer equation were estimated to be 17 nm and 5 nm, respectively.

Table III-3. Properties of glass fiber entrapped ZnO/SiO$_2$ sorbent.

Component	Wt.%	Vol.%
ZnO	12	N.A.*
SiO$_2$	66	22*
Fiber	22	3
Void	N.A.	75

* ZnO was supported in the pore of SiO$_2$, it did not change the size of SiO$_2$.

Other physical properties of glass fiber entrapped ZnO/SiO$_2$ sorbents were calculated and are shown in **Table III-3**. It clearly suggests that the glass fibers occupied only 3 vol.%. While glass fiber entrapped ZnO/SiO$_2$ sorbents had a high void fraction at 75 vol.%, which is about 2-2.5 times higher than that of a typical packed bed. As a result, the ZnO loading in the sorbents was 12 wt.% which is much lower than that of ZnO extrudate at 90-95 wt.%.
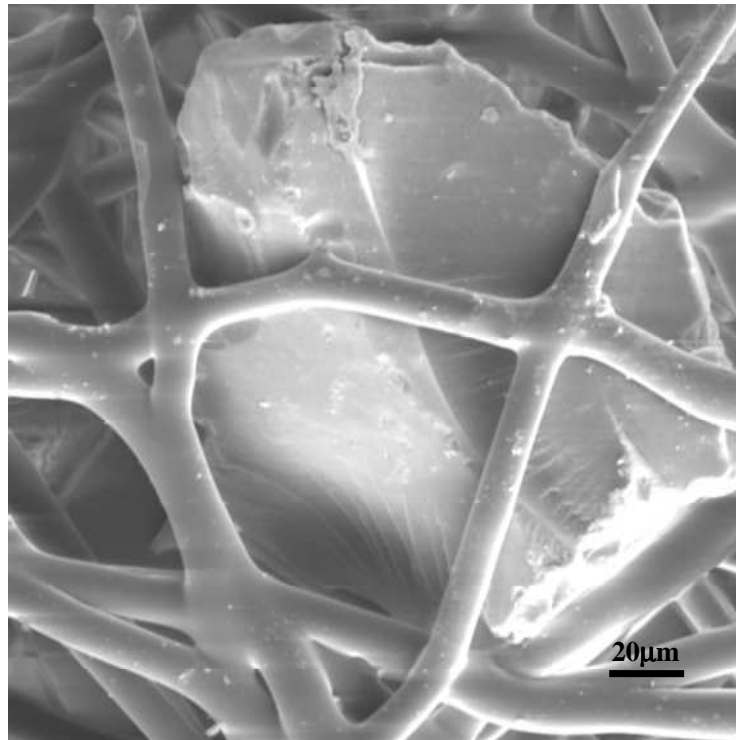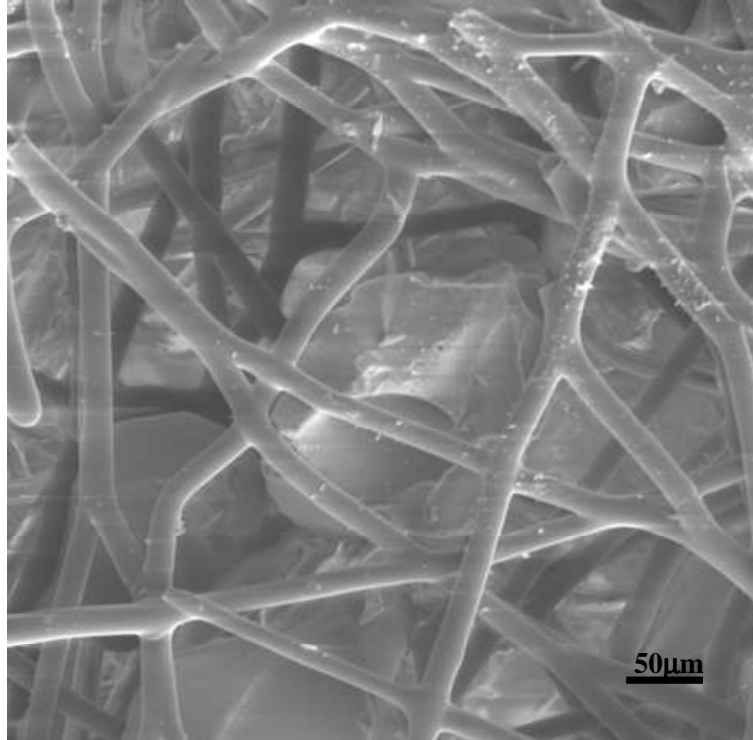
Figure III-5. Morphologies of S2 glass fiber entrapped ZnO/SiO$_2$.
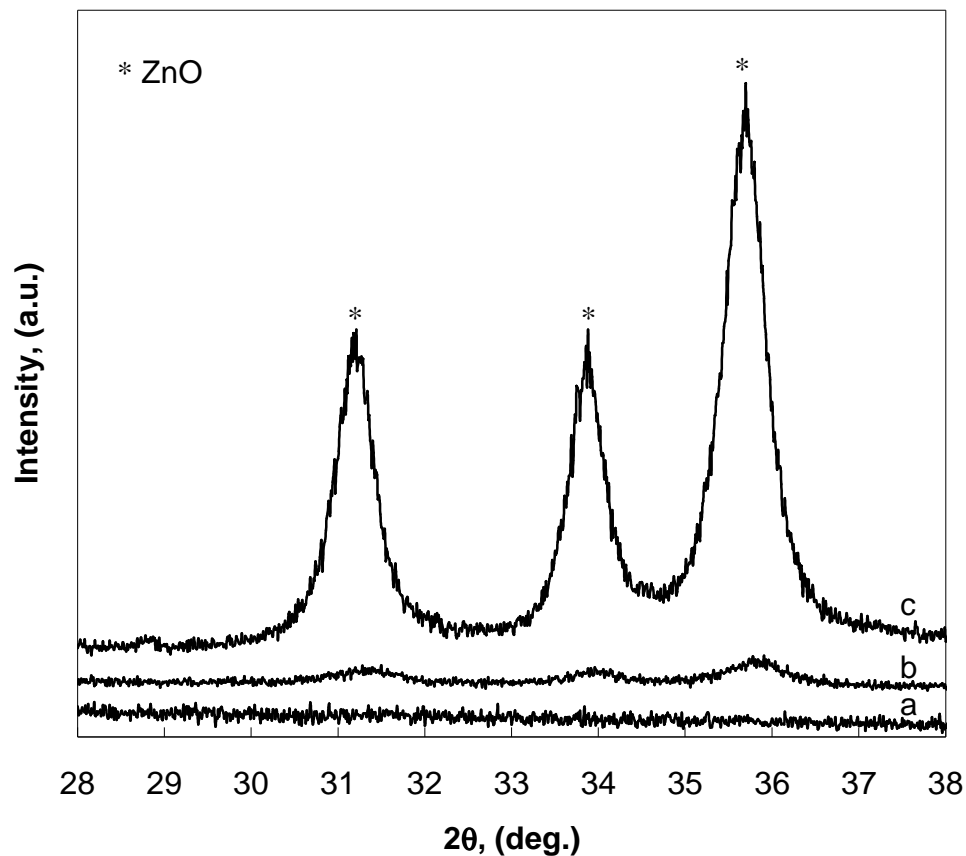
Figure III-6. XRD patterns of (a) GFE SiO_2, (b) GFE ZnO/SiO_2, and (c) commercial extrudates.

III.3.3. Pressure Drop Test

Zinc oxide extrudates were crushed and sifted into desired sizes. The ZnO particles of each size range were loaded in a quartz reactor (10 mm dia.) and made a packed bed with bed thickness (L) of 5 cm. Then the pure H_2 passed through the packed bed, and the total pressure drops (ΔP_t) at various face velocities were measured. The pressure drops introduced by the setup including the packing materials (ΔP_s) were also measured

103

at the same velocities.   The pressure drops introduced by the packed bed (ΔP) were ΔP_t minus ΔP_s.   The pressure drop per unit bed thickness ($\Delta P/L$) of packed bed at various face velocities were then calculated as plotted in **Figure III-7**.   The glass fiber entrapped sorbent (GFES) was tested at the same conditions and the data are also shown for comparison.
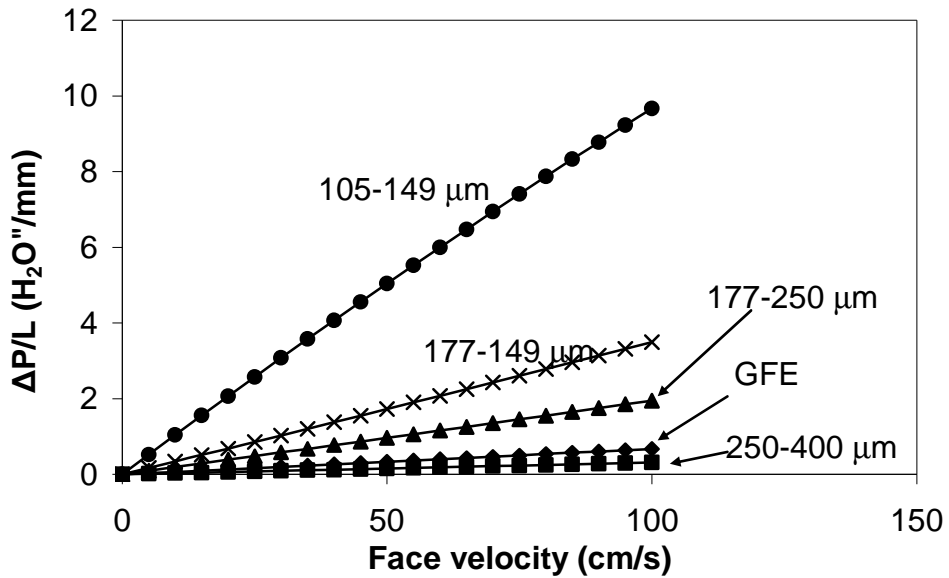
Figure III-7. Pressure drop per unit bed thickness at different face velocities for several desulfurization sorbents. Tested at room temperature using H_2 as challenge gas.

As shown in **Figure III-7**, the pressure drop increased with the increase of face velocity for every packed bed and the packed bed of smaller particles yielded a higher pressure drop.   For example, the pressure drop per unit bed length over 100-140 mesh (105-149 µm) particles was over 30 times larger than that of the particles of 40-60 mesh (250-400 µm).   The pressure drop of GFES (100-200 µm SiO_2 particles in 8 µm matrix)

was two times larger than 40-60 mesh (250-400 μm) particles.   It is only 1/3 of that of

60-80 mesh (177-250 μm) particles at the same face velocity, though the sizes of both

SiO_2 particle and fiber were smaller than the particle size in the packed bed of 60-80

mesh particles.   It is a natural result since 70 vol.% of the GFES was occupied by void.

III.3.4. Desulfurization Test

III.3.4.1. High Sulfur Concentration Test

In this study, all the ZnO/SiO_2 sorbents were tested at 400 °C with the challenge gas

of 2 vol.% H_2S-H_2.   In the experiment "m:v", 0.1 g of prepared ZnO/SiO_2 sorbent was

loaded in the reactor with a bed thickness of 2 mm, at a gas face velocity of 1.2 cm/s.   In

the flowing experiments, the amount of sorbent loaded and face velocity were doubled at

the same time till the sorbent loading reached 0.8 g and face velocity reached 9.9 cm/s.

All the packed beds in this set of tests had the same theoretical saturation time τ (or $t_{1/2}$)

of 12 minutes, and the same residence time of 0.075 s (GHSV=8100 h^{-1}).   The

breakthrough curves are shown in **Figure III-8**.   GFES containing 0.1 g of ZnO/SiO_2

sorbent particles was also tested at the face velocity of 1.2 cm/s.   The breakthrough

sulfur capacities at 1 % C_0 breakthrough for all experiments are shown in **Figure III-9**.
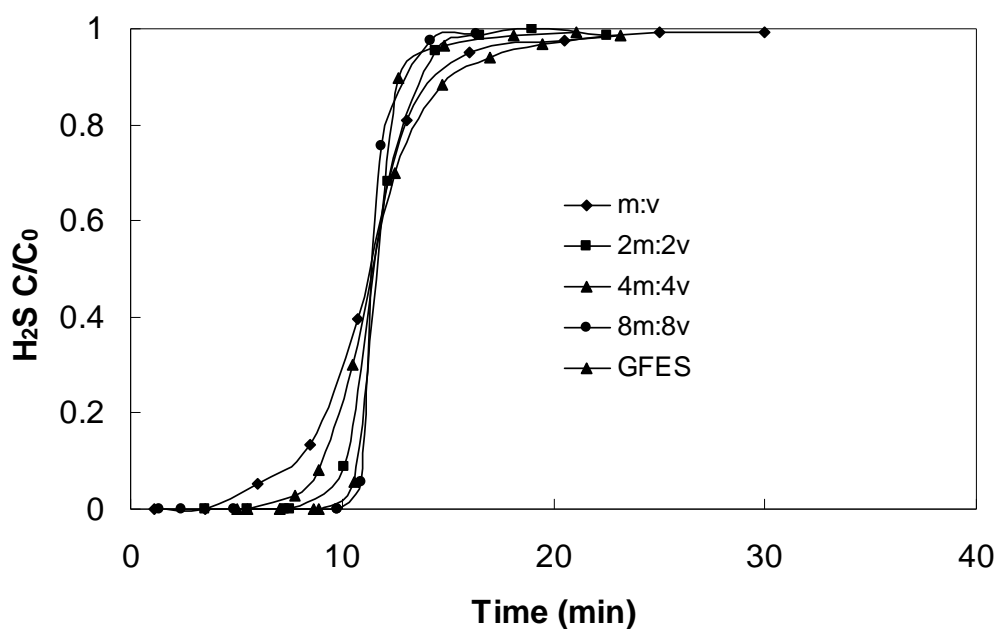
Figure III-8. Breakthrough curves of ZnO/SiO_2 sorbent tested with 2 vol.% H_2S-H_2 challenge gas at various face velocities at 400 °C (effects of glass fibrous media).
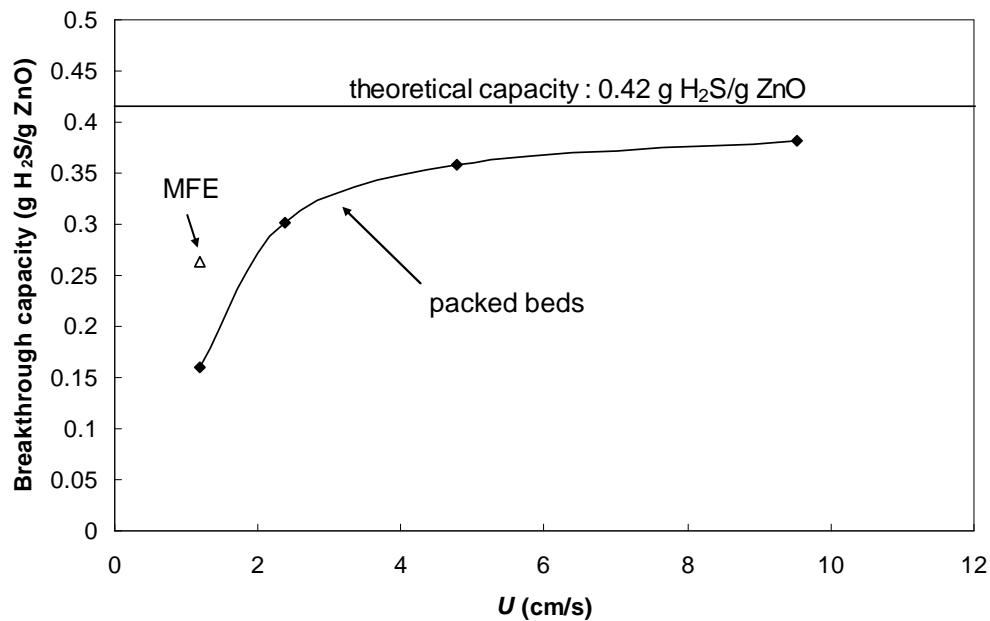
Figure III-9. Breakthrough capacity of ZnO/SiO_2 sorbent tested at different face velocities at 400 °C.

As shown in **Figure III-9**, all the breakthrough curves pass around the same point, which indicates the consistency of the theoretical capacity. It is a clear trend that the breakthrough curves become sharper with the increase in face velocity of challenge gas. The breakthrough capacity of sorbents in each experiment was calculated and is shown in **Figure III-9**. The capacity at breakthrough increased significantly in the low face velocity range. While, after the face velocity reached 5 cm/s, the capacity slowly approached 0.37 g H_2S/g ZnO, about 90% of the theoretical capacity, which suggests that the unutilized ZnO was less than 10% at breakthrough and a further increase in challenge gas face velocity was not necessary at this GHSV. The breakthrough capacity of GFES was about 50% higher than that of ZnO/SiO_2 packed bed in the experiment "m:v", where the same type of sorbent (ZnO/SiO_2) with the same amount of ZnO had been loaded. The only explanations for this improvement could be the enhancement due to the use of glass fiber media.

III.3.4.2. Low Sulfur Concentration Test

Similar test was performed at a low H_2S challenge concentration. The absorption with a H_2S challenge of 60 ppmv in the model reformates (60 ppm H_2S-10 vol.% CO-40 vol.% CO_2-9 vol.% C_1-C_3 and H_2 balance) with 30 vol.% steam added at 400 °C, was studied over GFES, 1-2 mm commercial extrudates, and ZnO sorbent particles (80-100

mesh) prepared by crushing the commercial extrudates.   The face velocity was 3.9 cm/s

(GHSV= 27500 h^{-1} based on dry gas).   The results are summarized in **Table III-4.**   At

equivalent bed volume, GFES provided 3 times longer breakthrough time with a 67%

reduction of the sorbent loading, compared to packed bed of the commercial extrudates;

1.5 times, compared with ZnO particles at a similar size to the SiO_2 particles in GFES.

ZnO utilization was 75% for ZnO/SiO_2 entrapped materials, 14-fold higher than that of

1-2 mm commercial extrudates.

Table III-4. Comparison between GFE and commercial ZnO sorbents. [a]

Sorbent	GFE ZnO/SiO_2	80-100 mesh ZnO	1-2mm ZnO
Total Weight, g	0.2	0.55	0.55
ZnO Content, mg	34	495	495
Breakthrough time[b], min	540	350	180
ZnO Utilization at BT[c], %	74.1	3.3	1.7

a. tested at equivalent bed volume of 0.53 cm^3; b. Breakthrough Time at 1ppmv H_2S
breakthrough; c. BT: breakthrough.

XRD patterns of GFES and the commercial extrudates are presented in **Figure III-6**

(fresh sorbents) and **Figure III-10** (spent sorbents).   **Figure III-10** suggests no ZnO

crystal existed in the spent sorbent of GFES and it was completely converted to ZnS.   In

extrudates, ZnO grains had an average size of 17 nm, which is 3 times larger than those

in GFES.   In addition, commercial extrudate sample had a N_2-BET surface area of

~25m^2/g, 1/10 of that of GFES.   This suggests that most ZnO crystals were buried inside

the bulk, and ZnO in GFES was highly dispersed on the surface of SiO_2.   The size of the

extrudates was around 1 mm, 6 times larger than the ZnO/SiO_2 particle in GFES.   These

differences suggest the mass transfer resistance in extrudates due to lattice diffusion and pore diffusion was much higher than that in GFES was. As a result, ZnO grains in ZnO extrudates were not completely accessible to H_2S, and ZnO still existed and demonstrated strong ZnO peaks in **Figure III-10**. In addition, the glass fibrous media enhanced external mass transfer for GFES. These beneficial properties of GFES therefore create high ZnO utilization and high bed utilization efficiency as shown in **Table III-4**.

III.3.5. Regeneration Test

III.3.5.1. Single Cycle Test

Nano-dispersed nature of the ZnO and the use of small support particulates significantly improved the desulfurization performance; they should also improve the regenerability of GFES as well. Good regenerability always means high capacity that can be recovered after regeneration, and short regeneration time. **Table III-5** compares the regenerability of the GFES with the 1-2mm commercial ZnO extrudates. From the breakthrough time (capacity) recovery percentage of GFE ZnO/SiO_2 at different regeneration conditions, it is safe to draw the conclusion that higher regeneration temperature and longer regeneration time yields higher recovery percentage. It is also true for the commercial ZnO extrudates. Under the same regeneration conditions (in air at 500 °C for 1 hour), GFES, as expected, provided 10 times higher reactivity recovery percentage compared to the packed bed of 1-2mm commercial extrudates. Under these

conditions, ZnO particles (80-100 mesh) also demonstrated a good performance, with ~60% capacity recovered. However, the breakthrough times of these particles were only 50% of these of GFES tested under the same conditions.

Regeneration time is an important concern for process design, especially for a system consisting of several reactors: one in desulfurization and the rests in regeneration. The shorter regeneration time, the fewer reactors are required. For example, if the breakthrough time of a fixed bed desulfurization reactor is 1 hour, then 4 identical reactors are required given the regeneration time for each reactor is 3 hour. If the regeneration can be reduced to 1 hour, then only 2 reactors are required if the transient time is negligible. From the regeneration experiments of GFES, the best regeneration condition for the ZnO/SiO_2 sorbents was regenerated at 600 °C for 1 hour. It yielded a good balance between regeneration time and recovery rate. Therefore, GFES were regenerated at this condition for multicycle test.

Table III-5. Capacity recovered percentage of sorbents after regeneration in air.[a]

Sorbent	GFE ZnO/SiO$_2$		80-100 mesh ZnO		1-2mm ZnO	
	B.T.[b]	C.R.[c]	B.T.[b]	C.R.[c]	B.T.[b]	CR.[c]
	Min	%[c]	min	%[c]	min	%
Fresh	540	--	350	--	180	--
1h Regn.@600°C	400	74	220	63	100	56
3h Regn.@500°C	410	76	210	60	80	44
1h Regn.@500°C	300	56	60	17	10	5.5

a. Absorption experiment was carried out at 400 °C and 3.9 cm/s face velocity in the present of 30% steam, using 60ppmv H_2S challenge in a model reformates; b. Breakthrough Time at 1ppmv H_2S; c percentage of capacity recovered, defined as: (breakthrough time of regenerated sample/Breakthrough time of fresh sample)×100%.
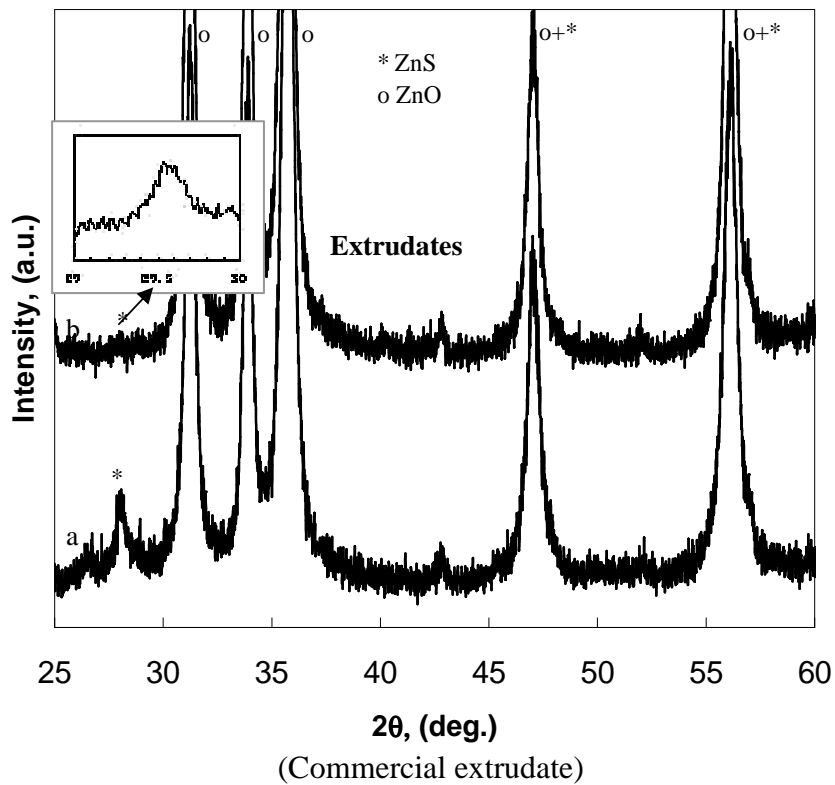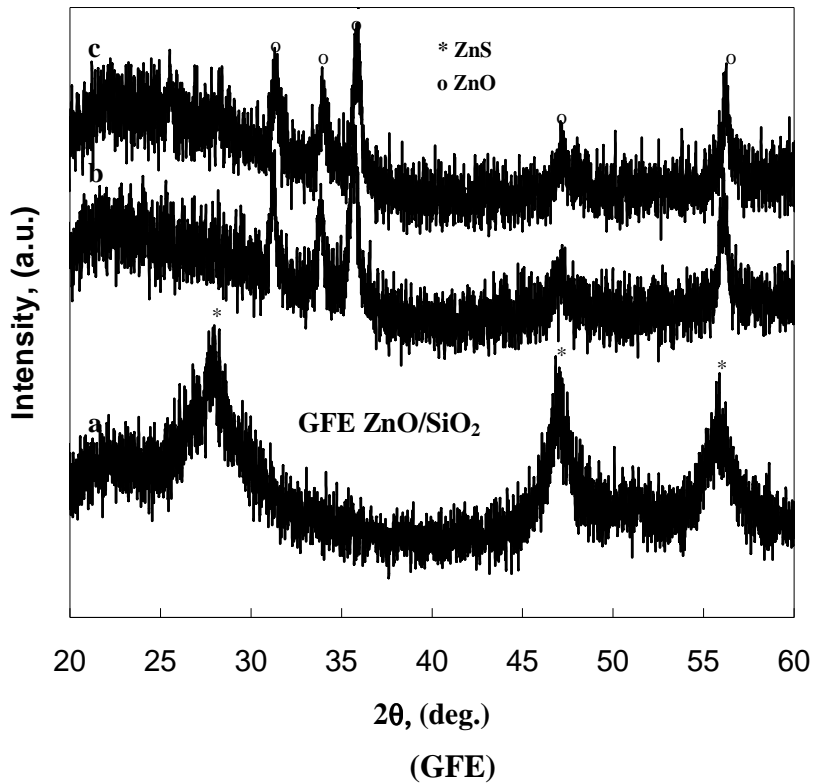
Figure III-10. XRD patterns of GFE ZnO/SiO$_2$ and commercial extrudates. (a) spent, after regeneration in air at (b) 600°C for 1h and (c) 500°C for 3h.

111

To reveal the nature of this significant difference in regenerability, XRD analyses were carried out on spent samples before and after regeneration at 500-600 °C in air. The spent samples were collected when the outlet H_2S concentration reached 60 ppmv (the same as inlet concentration). As shown in **Figure III-10**, cubic ZnS was the only detectable phase on the spent GFES. After regeneration at 600^oC for 1h and at 500^oC for 3h in air, the ZnS phase completely disappeared while the ZnO phase appeared again. While in the case of ZnO extrudate, ZnO was the predominant phase for the spent 1-2mm commercial extrudates, and the ZnS phase was still detectable after 1h regeneration at 600^oC in air (confirmed by XRD using a scanning speed of $0.1^o/min$ and a sampling interval of 0.01 min). The above results strongly supported the conclusion drawn earlier. In **Figure III-10**, the regenerated GFES demonstrated a sharp ZnO peak with a corresponding grain size of 12 nm. Compared with grain size (5nm) in fresh sorbent, it is a significant increase.

III.3.5.2. Multiple Cycle Test

Figure III-11 shows the desulfurization/regeneration cyclic test results over the GFES. All the desulfurization tests were conducted at 400 °C using the same experimental condition as described in **Table III-6**; all regenerations were carried out at 600 °C for 1h in air. **Figure III-11** suggests that a significant breakthrough time

112

(capacity) drop occurred after the first regeneration, and then breakthrough times (capacity) remained almost unchanged through 50 absorption/regeneration cycles. Grain sizes of ZnO were calculated from XRD patterns and are shown in **Figure III-12**. The grain size increased drastically from 5 nm to 12 nm after the first regeneration, and then increase slowly to 15 nm during the rest 49 cycles. It is not a significant change compared with 12 nm after first cycle. This phenomenon is quite common for most sorbents that regenerated at high temperatures. It is also well known that the grain size increase significantly after the first regeneration. The ZnO grains did not grow above 15 nm possibly due to the small pores in the SiO_2 support confined ZnO grains from growing and made them highly dispersed. This may be the main reason accounting for the stabilized breakthrough time of GFE ZnO/SiO_2 during these multiple-cycle tests. Moreover, SEM image in **Figure III-13** shows that the sinter-locked micro-glass structure of the microfibrous sorbent remained robust without any rupture after 50 regeneration cycles. This suggests that the glass fiber media yielded good thermal and structural stability during regeneration at 600 °C in air. Undoubtedly, the significant increase in ZnO grain size after first regeneration cycle resulted more lattice diffusion resistance, which in turn decreased the ZnO utilization, as observed in the reduction in breakthrough time of GFE ZnO/SiO_2 even though ZnS phase was mot detected after regeneration at 600 °C for 1h as well as 500°C for 3h.
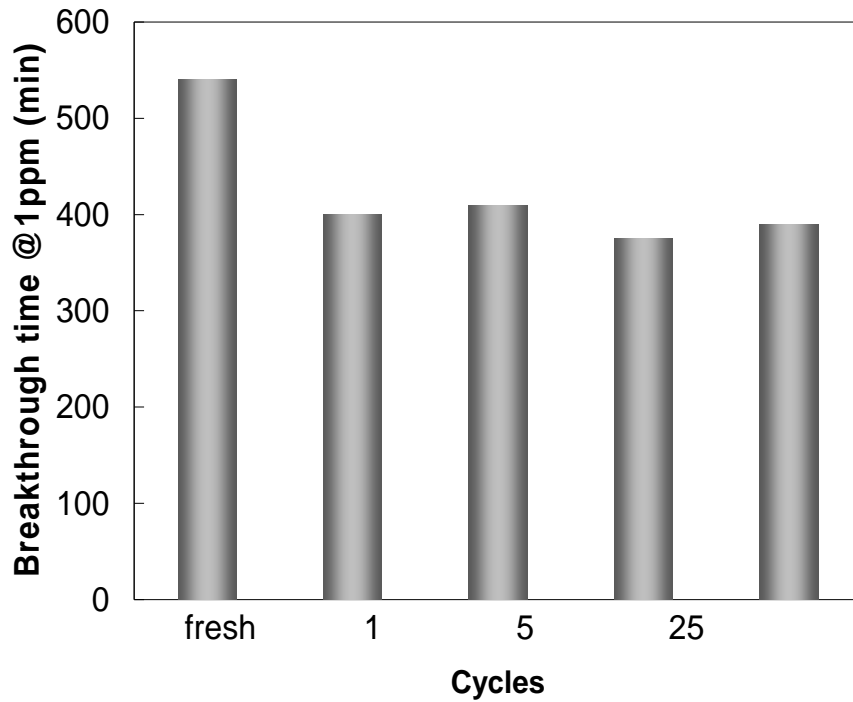
Figure III-11. Breakthrough time *vs.* regeneration cycle numbers

Case	ZnO Crystal Size, nm
b	5
c	12
d	15
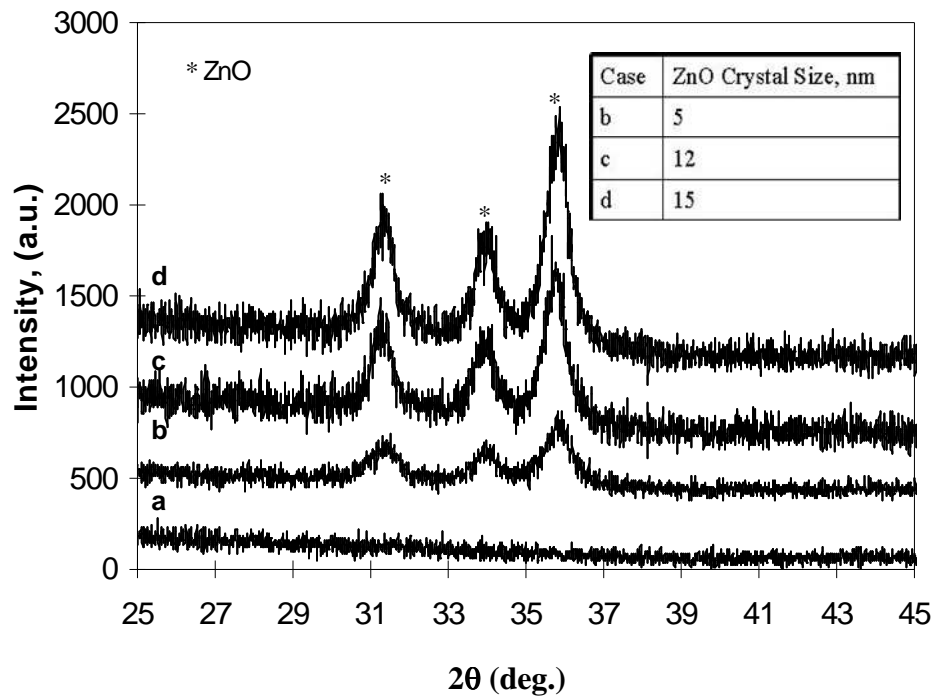
Figure III-12. XRD patterns of (a) GFE SiO$_2$ carriers and GFE ZnO/SiO$_2$ sorbents: (b) fresh, and after (c) 1st regeneration cycle and (d) 50th regeneration cycle. Regeneration was carried out in air at 600°C for 1h in each cycle.
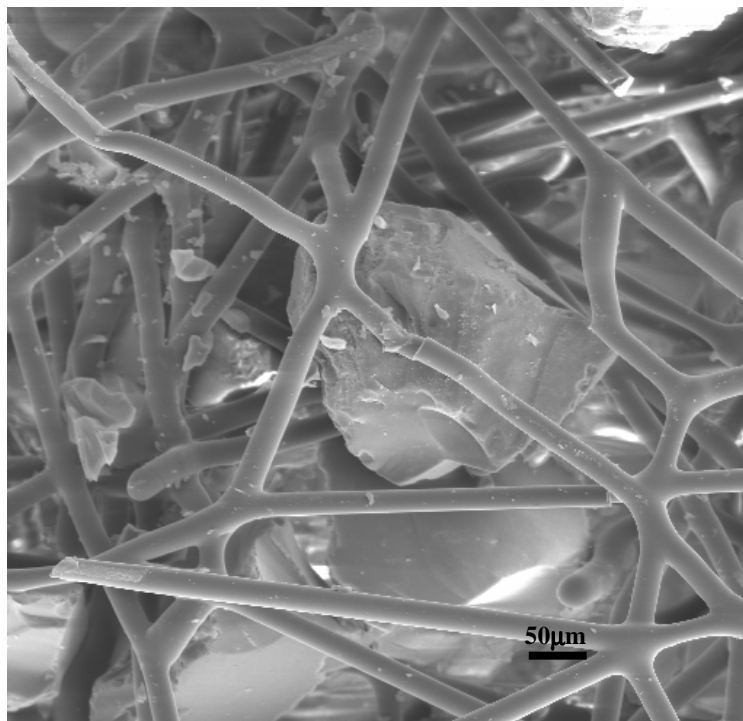
Figure III-13. Structure integrity after 50 cycles (SEM image).

III.3.6. Composite Bed and Reactor Design

Although microfibrous entrapped sorbents, as mentioned earlier, demonstrate higher ZnO utilization and improve contact efficiency, they do not have high ZnO loading. As a result, their sulfur capacity is low and they may not be directly applicable for high concentration H_2S removal, but their high contact efficiency allows them to be applied in low concentration H_2S removals, as shown in the section of low sulfur concentration test. Moreover, they can be applied as polishers to remove trace H_2S from gas streams off packed beds. This unique approach offers opportunities for higher absorption capacity

design by incorporating microfibrous entrapped sorbent as a polishing sorbent layer to back up a packed bed that is called a composite bed, as shown in **Figure III-14**.
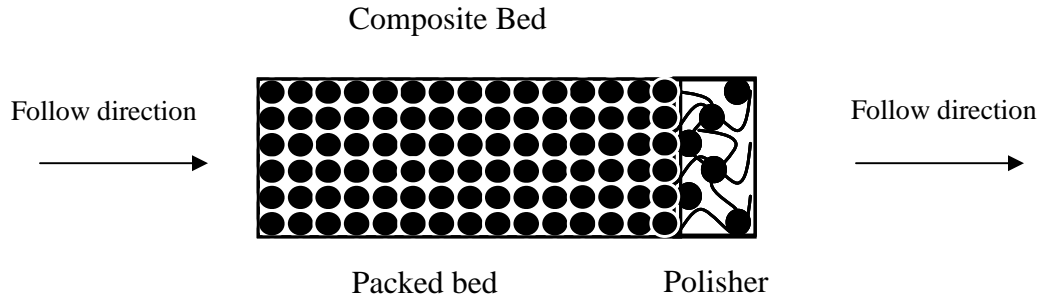
Composite Bed

Figure III-14. A composite bed.

The desulfurization performance of a packed bed and a corresponding composite bed is shown in **Figure III-15**.
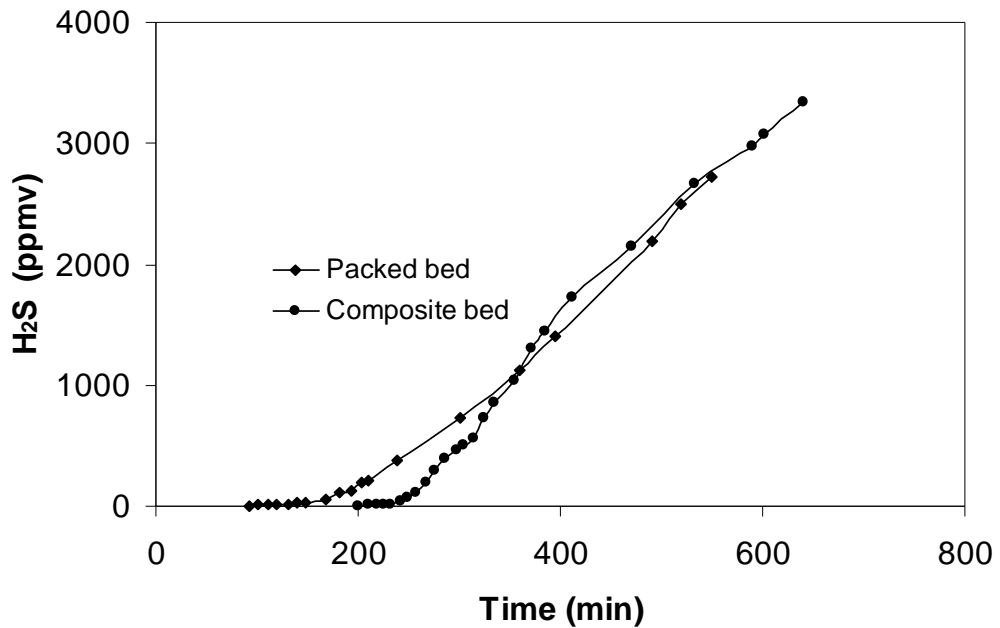
Figure III-15. Breakthrough curves of a 2" thick packed bed of ZnO extrudates and a composite bed (the packed bed followed by a 5 mm polishing layer).

116

The tests were conducted in a quartz tube reactor (dia. 2.14 cm) with 5000 ppmv H_2S-H_2 as challenge gas at face velocity of 10 cm/s at 400 °C.   The polishing layer was made of glass fiber entrapped ZnO/SiO_2 (0.9 g) at a thickness of 5 mm with ZnO loading at 13 wt.%.   The packed bed made of 3/16" commercial extrudates (11 g) with a bed thickness of 2.2 cm.   Therefore, the composite bed had an overall thickness of 2.7 cm.

As shown in **Figure III-15**, the ZnO extrudate yielded broad breakthrough curves and a breakthrough time about 33 minutes at 1 ppmv breakthrough as indicated in **Figure III-16**.   After adding the polishing layer at the end of the packed bed, the composite bed yielded a breakthrough time around 185 minutes at 1 ppmv breakthrough, which means that the breakthrough time increased 6 times by adding the thin polishing layer at 25 vol.% of the packed bed.   Another interesting phenomenon is the shape of breakthrough curves.   The breakthrough curves of the packed bed and composite bed had similar shape at high outlet H_2S concentrations, while at low H_2S concentrations, the breakthrough curve of the composite bed is much sharper than that of the packed bed.   It is obvious that microfibrous entrapped sorbents cannot add 6 times higher saturation capacity to the packed bed due to their low ZnO weight loading.   However, they can further reduce the H_2S concentration in the gas flow from the packed bed, which was much less than 5000 ppmv, to lower concentrations (less than 1 ppmv).   The polishing layer did not capture more sulfur than the packed bed, but it was able to capture the H_2S at low concentration more efficiently than extrudates.   Adding another layer of

117

extrudates can also increase the breakthrough time.   However, because of the poor

contact efficiency of big extrudates, a large amount of extrudates (big volume) is required,

which is a penalty in logistic power systems.   In this case, the thin polishing layer with

high contact efficiency is the best choice to increase the breakthrough time (capacity)

without significant increase in the reactor volume.   This design synergistically takes the

advantages of both the packed bed and polishing layer: high saturation capacity of the

packed bed and high contacting efficiency of the polisher.
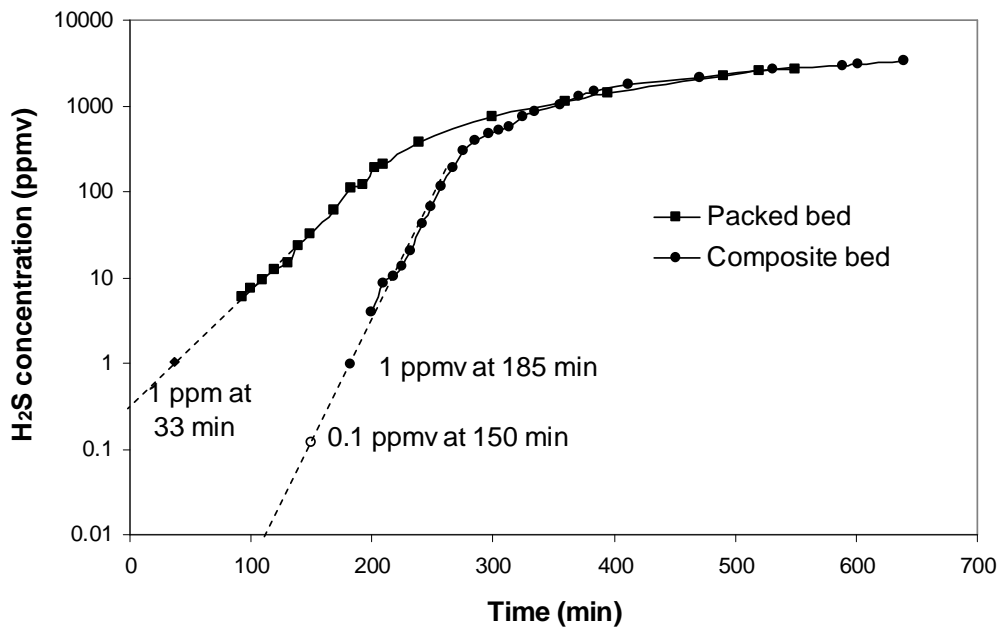
Figure III-16. Breakthrough curves of the packed bed and the composite bed in logarithmic scale.

The polishing layer can improve more significantly in breakthrough time (capacity)

if the breakthrough curve of the packed bed is broader or the breakthrough concentration

is lower, e.g., the desulfurization for reformates, in which CO, CO_2 and water yield broad breakthrough curves. As shown in **Figure III-16**, if the breakthrough is defined as 1% of challenge H_2S concentration (50 ppm), the breakthrough time for the packed bed and composite bed are 150 min and 220 min, respectively. This is not a significant improvement in breakthrough time, compared with the 6 times improvement at 1 ppm breakthrough. This phenomenon can be explained by service time equation (Yoon and Helson, 1984).

$$\ln\left(\frac{C_0}{C}-1\right) = K(\tau - t) \tag{III-1}$$

According to service time equation, at very low H_2S concentration, $\left(\dfrac{C_0}{C}-1\right) \approx \left(\dfrac{C_0}{C}\right)$, and the C_0 can be expressed as

$$\ln(C) = \ln(C_0) - K(\tau - t) \tag{III-2}$$

Equation III-2 suggests the plot of $\ln(C_0)$ *vs.* t in low H_2S concentration region should have good linearity. Extending the line of $\ln(C_0)$-t plot to lower concentrations (ca. 0.1 ppmv), yields a breakthrough time at a new breakthrough concentration, as shown in **Figure III-16**. **Figure III-16** predicts the improvements by adding a polishing layer (5 mm thickness) at the end of a packed bed of ZnO extrudate (2.2 cm thickness) are 200 minutes, 152 minutes and 70 minutes for 0.1 ppmv, 1 ppmv and 50 ppmv breakthrough, respectively.

III.4. Conclusion

Glass microfibrous entrapped ZnO/SiO_2 sorbents were successfully prepared and optimized to substitute Ni microfibrous entrapped sorbents. It consists of 3 vol.% glass fibers, 22 vol.% entrapped 150-250 μm ZnO/SiO_2 sorbent particulates and 75 vol.% void. The microfibrous media made it possible to employ small sorbent particulates in the desulfurization without high pressure drop and channeling. ZnO was nano-dispersed on the high surface area SiO_2 support. This combination made the ZnO easy to be accessed during the desulfurization process and it also facilitated the regeneration of spent sorbent (ZnS/SiO_2) at 500~600 °C. Glass fiber solved the regeneration issues of Ni fiber entrapped ZnO/SiO_2. The glass fiber matrix was inert to most reducing and oxidizing environments and demonstrated nice structural integrity after 50 cycles of desulfurization/regeneration.

Due to the low ZnO loading in microfibrous entrapped ZnO/SiO_2, it can work independently for low concentration H_2S removal. It also can be applied as a polisher used in composite bed design approach. The combination of high sulfur capacity of extrudates in packed bed and high contacting efficiency of microfibrous entrapped sorbents demonstrated significant improvements in the overall bed capacity and efficiency, compared with the packed beds alone. This approach provided a solution to minimize the volume of reactors in logistic fuel cell applications.

Acknowledgement:

CHAPTER IV.

KINETIC STUDY AND MASS TRANSFER CONTROL MECHANISM FOR THE

DESULFURIZATION PROCESS USING ZnO/SILICA AND GFES

Abstract

In this paper, breakthrough curves were utilized to analyze the kinetic behavior of the desulfurization process using ZnO/SiO_2 sorbent by converting the breakthrough curves to ZnO conversion curves. The effective diffusivity of H_2S in ZnO grain, and the intrinsic reaction rate constant for the reaction between ZnO/SiO_2 and H_2S at various temperatures were estimated using differential reactor studies, and then corresponding Arrhenius equations were established. The different controlling mechanism involved in heterogeneous solid-gas reactions were characterized using the unreacted shrinking core model. It was found that the ZnO/SiO_2 sorbent had a high intrinsic rate constant of 3039 s^{-1} at 400 °C. The nano-sized grains in this sorbent minimized the diffusion resistance in grains, while the high porosity and small particle size of the SiO_2 supports demonstrated negligible pore diffusion resistance. A comparative study suggests that desulfurization process using ZnO/SiO_2 at a face velocity less than 11 cm/s was mainly controlled by external mass transfer rate, while that using Sud-Chemie extrudate suffered

from severe pore and lattice diffusion.   The conclusions on ZnO/SiO_2 sorbent are also applicable to glass fiber entrapped ZnO/SiO_2 sorbent.

Key word: Sorbent, Kinetics, Mass Transfer, Differential Reactor

IV.1.Introduction

Efficiency in hydrogen sulfide removal is critical to protect the catalysts and electrolytes made of precious metals in logistic fuel cell systems.   Some fuel cells have low sulfur tolerance, i.e. 0.1 ppmv sulfur for PEMFCs and 10 ppmv for SOFCs. However, the sulfur concentration in reformates varies from several parts per million by volume (ppmv) to 100 ppmv.   ZnO is widely used to remove H_2S from gas flow at low temperatures (T<500 °C) because of its high equilibrium constant and high sulfur capacity (Sasaoka, 1994b; Lu *et al*., 2005; Slimane and Abbasian, 2000a; Tamhankar *et al*., 1986; Westmoreland and Harrison, 1976; Baird *et al*., 1992; Novochinskii *et al*., 2004).   Commercial ZnO extrudates such as G-72E that have high porosity and high surface area demonstrated good desulfurization performance (Newby *et al*, 2001). However, the performance is influenced by severe intra-particle mass transfer resistances due to the use of large particle/grain size.   Novel ZnO based sorbents such as ZnO/SiO_2 and microfibrous entrapped ZnO/SiO_2 have been designed and prepared at Center for Microfibrous Materials Manufacturing.   A thin layer of these sorbents can remove H_2S from reformates containing CO, CO_2, H_2 and H_2O to sub-ppmv level at 400 °C.   The

123

high H_2S removal efficiency of these sorbents makes them good candidates for logistic fuel cell systems. Gas phase desulfurization is usually operated a low face velocities ranging from few centimeters per second (Newby *et al*., 2001) to around 20 cm/s (Novochinskii *et al*. 2004). Under these conditions, external mass transfer resistance and/or intra-particle diffusion resistance may control the desulfurization process. In this paper, the rate limiting step that determines the breakthrough in the desulfurization process using ZnO/SiO_2 (100~200 μm) was investigated by differential reactor analysis.

IV.2. Theory

IV.2.1. Grain Pellet Model (Levenspiel, 2002)

Several kinetic models have been established for solid-gas heterogeneous reactions. They are the unreacted shrinking core model, the uniform conversion model, the grain pellet model, the cracking model, the changing voidage model and the thermal decomposition model. Among them, the grain pellet model is the best match for the ZnO/SiO_2 sorbents that containing ZnO grains in pores of SiO_2 fine particles. This model assumes that every grain has the same grain size and reacts with gas according to the unreacted shrinking core model. There are two possible intra-particle mass transfer control steps in grain pellet model: pore diffusion control and grain (lattice) diffusion control. Both steps can be described by using unreacted shrinking core model. For the reaction between ZnO and H_2S, according to the shrinking core model and grain model,

124

as shown in **Figure IV-1**, there are four possible rate-limiting steps in series in the desulfurization process using ZnO/SiO_2 sorbent:

(1) diffusion of H_2S through the gas film surrounding the sorbent particle;

(2) diffusion of H_2S in pores;

(3) diffusion of H_2S through the ash layer of ZnS of solid grain;

(4) reaction at the unreacted core of solid grains.
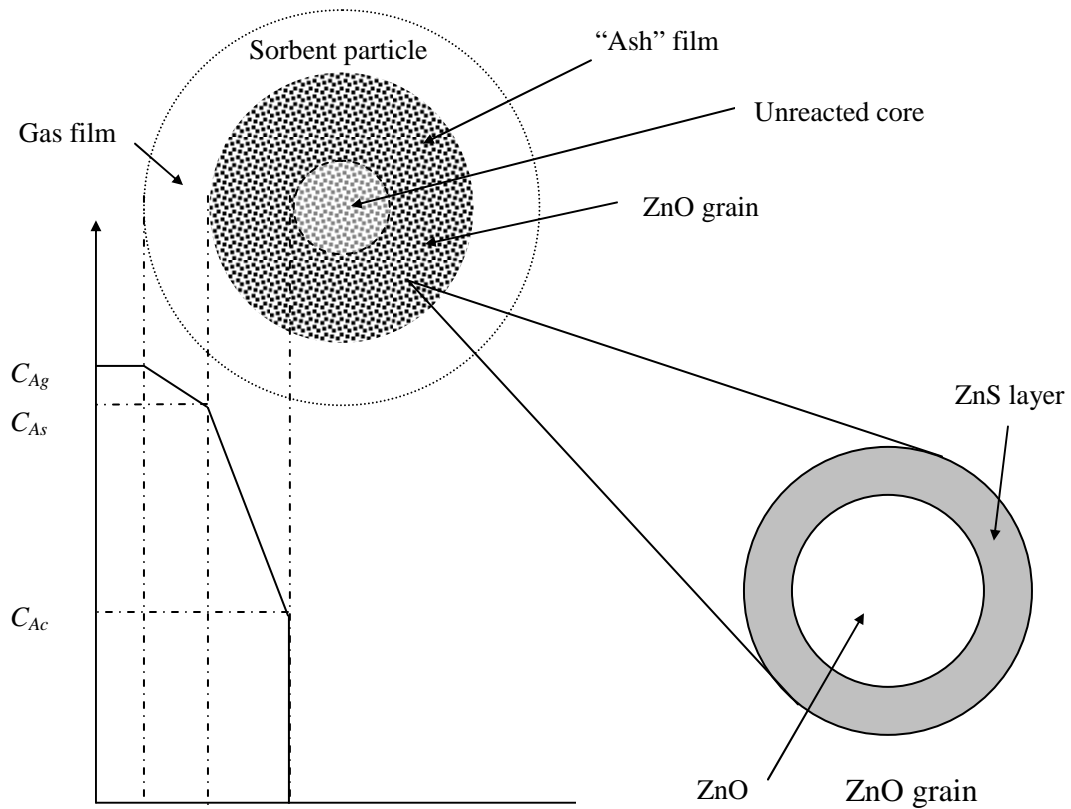
Figure IV-1. The grains model and H_2S concentration profile in the sorbent particle.

Under the film diffusion control, the time (t) required to reach a conversion x can be expressed as a function of x as described by equation IV-1.

$$\frac{t}{\tau} = G(x) = x \tag{IV-1}$$

where τ is the time for complete conversion, and τ can be calculated by

$$\tau = \frac{\rho_m R}{3k_g C_{Ag}} \tag{IV-2}$$

Similarly for ash diffusion control or lattice diffusion control,

$$\frac{t}{\tau} = P(x) = 1 - 3(1-x)^{2/3} + 2(1-x) \tag{IV-3}$$

and

$$\tau = \frac{\rho_m R^2}{6D_e C_{Ag}} \tag{IV-4}$$

for reaction controlled systems

$$\frac{t}{\tau} = R(x) = 1 - (1-x)^{1/3} \tag{IV-5}$$

and

$$\tau = \frac{\rho_m R}{k_s C_{Ag}} \tag{IV-6}$$

D_e is an essential parameter to evaluate the rate-limiting step.   In the $P(x)\sim t$ plot, the slope is $1/\tau$, and D_e is calculated using equation IV-4.   TGA is widely employed to establish the conversion *vs.* time plot (*x-t* plot) and *P(x)-t* plot.   As all kinetic variables are known, the effectiveness factor η can be calculated using Thiele modulus for first order reaction ,ϕ_1 (Fogler, 1992).

$$\phi_1 = R\sqrt{\frac{k'''}{D_{ep}}} \tag{IV-7}$$

$$\eta = \frac{3}{\phi_1^2}(\phi_1 \coth \phi_1 - 1) \qquad\qquad\text{(IV-8)}$$

where k''' is intrinsic reaction rate per unit volume of sorbent/catalyst particle. It has

the relationship with other intrinsic reaction rate constants as described in equation IV-9

$$k = k'\rho_b = k''S_a\rho_b = k'''\phi = k''''(1-\phi) \qquad\qquad\text{(IV-9)}$$

in which k is the reaction rate per unit reactor (bed) volume; k' is the reaction rate per unit

catalyst weight; k'' is the reaction rate per unit sorbent/catalyst surface area; k''' is the

reaction rate per unit void volume; k'''' is the reaction rate per unit particle volume.

Rearrangement of equation IV-4 yields

$$D_e = \frac{\rho_m R^2}{6\tau C_{Ag}} \qquad\qquad\text{(IV-10)}$$

Insertion of equation IV-10 into equation IV-7 yields

$$\phi_1 = \sqrt{\frac{6\tau C_{Ag} k''''}{\rho_m}} \qquad\qquad\text{(IV-11)}$$

Equations IV-10 and IV-11 suggest D_e value is dependent on the characteristic size R;

ϕ_1 is independent to R because τ is estimated from $P(x)$-t plot. Different R values will

yield different D_e values, but will reach the same ϕ_1. Therefore, ϕ_1 can be calculated

directly from experimental data without R value. This result is very useful especially

when the characteristic size is not available. For the same sorbent and at the same

temperature, ϕ_1 values for two different grain sizes can be calculated by equation IV-12.

$$\frac{\phi_{11}}{\phi_{12}} = \frac{R_1}{R_2} \tag{IV-12}$$

It should be noted that ϕ_1 is independent to C_{Ag} as described by equation IV-7. In equation IV-11, τ is reversely proportional to the C_{Ag} for the first order reaction, according to the definition of τ.

The above noted method has been widely used in catalytic heterogeneous reactions. In packed bed for the unsteady state heterogeneous reaction with sorbent consumption, the intra-particle diffusion will eventually be the rate-limiting step. This work focuses on a moving active layer in a packed bed, which is well represented by a thin bed with $z=z_c$, because this layer determines the shape of the breakthrough curve.

IV.2.2. Establishing *x-t* Plot using Breakthrough Curves

Instead of using TGA, breakthrough curves can also be applied to establish *x-t* plots using a simple mass balance. The challenge uptake of sorbents can be calculated from the numeric integration over the area above the breakthrough curves, as shown in **Figure IV-2**. The product of the integrated area and molar flow rate is the moles of H_2S captured by ZnO, which is also the moles of ZnO that was converted; therefore the *x-t* plot could be established. Several *x~t* plots are shown in **Figure IV-3**. Given the *x-t* plot, most reaction kinetic analysis can be conducted using the well-established methods. However, it is should be noted that the *x-t* plot established using this methods is actually the conversion for the whole packed bed. In order to extrapolate the x-t plot correctly

using grain pellet model, a very thin bed is required.   In the thin bed, all the particles

could be considered to experience the same changes, i.e. conversion rate.

IV.2.3. Kinetic Constant Measurement

In order to analyze the intrinsic kinetic behaviors, a high face velocity is preferred to

remove the external mass transfer resistance.   For the sorbents that may suffer from

intra-particle mass transfer resistance, the reaction rate at t→0 is essential for the kinetic

analysis since the sorbent is fresh and the latticediffusion is negligible.
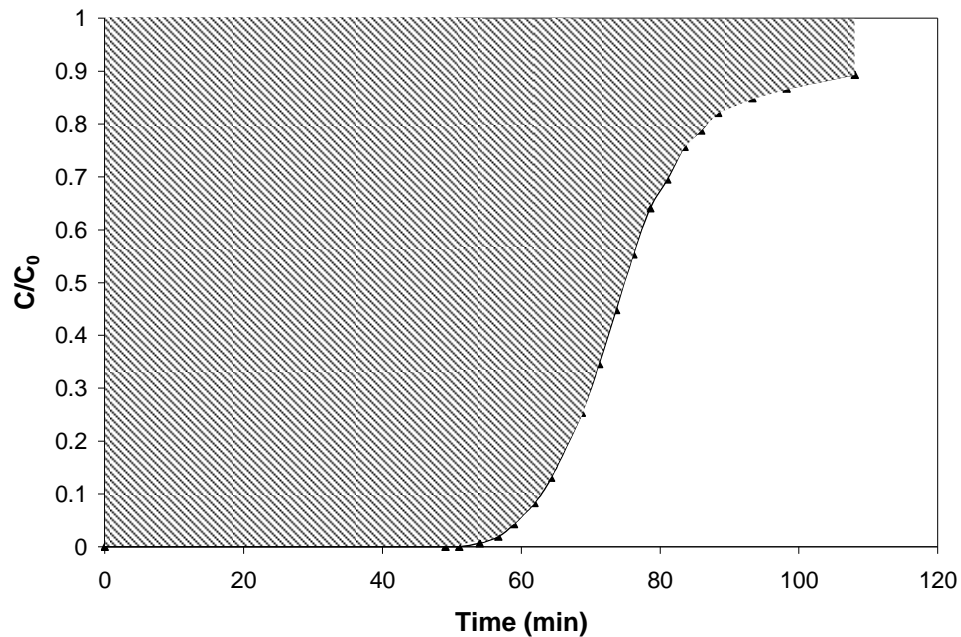
Figure IV-2. Calculation of H_2S uptake using breakthrough curve.

At t→0, all of the sorbent in a packed bed can be considered fresh, and the reaction

between ZnO and H_2S can be treated as a catalytic reaction.   The outlet H_2S

concentration is determined only by the apparent reaction rate by equation IV-13.

129

$$\ln\left(\frac{C_0}{C}\right)\bigg|_{t \to 0} = k_a''' t_r \qquad\qquad\qquad \text{(IV-13)}$$

where k_a''', volumetric (void) apparent reaction rate constant, is equal to $\dfrac{k_a}{\phi}$ in which k_a

is volumetric (reactor volume based) apparent reaction rate constant, and t_r is the resident

time of gas flow in the packed bed. The apparent rate constant k_a is expressed as:

$$k_a = \frac{\phi \ln\left(\dfrac{C_0}{C}\right)\bigg|_{t \to 0}}{t_r} \qquad\qquad\qquad \text{(IV-14)}$$

Apparent rate constant k_a can be expressed in terms of intrinsic rate constant (k) and

external mass transfer rate (k_c) as shown in Equation IV-15. When the external mass

transfer rate is extremely large, e.g., at a very high face velocity, then k_a is approaching to

k (Fogler, 1992).

$$\frac{1}{k_a} = \frac{1}{k_c \alpha} + \frac{1}{k} \qquad\qquad\qquad \text{(IV-15)}$$

Rearrangement of V-15 yields

$$k = k'' S_a \rho_b = \frac{k_a k_c \alpha}{k_c \alpha - k_a} \qquad\qquad\qquad \text{(IV-16)}$$

k can be estimated experimentally using equation IV-16, and can be employed to

calculate k'' if S_a is available. Without S_a, the value of k can also be used to calculate

the value of k''' to estimate Thiele modulus ϕ_1. The values of k at various

temperatures also can be used to establish the Arrhenius plot.

IV.3. Experimental

ZnO/SiO₂ sorbent preparation: ZnO/SiO_2 is the sorbent employed in this study, it contains 17 wt.% of ZnO supported on SiO_2 (100-200 μm fine particles). It was prepared by incipient wet impregnation at room temperature, using $Zn(NO_3)_2$ (2 mol/L solution) as precursor, followed by natural drying and calcination at 450 °C. The ZnO loading was quantified by both mass balance and ICP analysis. Detailed sorbent preparation procedure was described elsewhere (Lu *et al.*, 2005).

Experimental setup and procedure: The experiment setup is shown **Figure II-1**. All gas flows were controlled by mass flow controllers. H_2S source gas (ca. 321 ppmv H_2S-H_2 or 2 vol.% H_2S-H_2, Airgas Inc.) was introduced to reactor by 1/8" Teflon tubing. Other gases were introduced to reactor in stainless steel tubing. The reactor employed was a quartz tube (0.99 cm I.D.). After loading the sorbents, air (100 ml/min) was passed through the reactor before the temperature reached the set point of 400 °C, i.e.. Then helium (100 ml/min) flowed through the reactor for 10 minutes to eliminate oxygen in the reactor, which may introduce side reactions such as sulfide oxidation. Then H_2 passed through the reactor for another 10 minutes to stabilize the temperature profile along the reactor. Finally, the challenge gas passed through the reactor at the same flow rate as H_2, and the experimental record commenced.

The outlet H_2S concentrations (>200 ppmv) were analyzed by a Varian GC-3800 with a TCD detector (H_2 as carrier gas) which was able to detect the H_2S concentration

down to 200 ppmv. Gas samples were injected to the GC every 1 minute by a programmed 6-port-valve with a sampling loop of 50 µL after commencing the experiment. Pulse flame photometric detector (PFPD) was employed to analyze the H_2S at low concentrations (<300 ppmv). A gas sample was collected using a sampling syringe (250 µL) and injected manually to PFPD. The detailed analytic methods are shown in Appendix G.

IV.4. Results and Discussion

IV.4.1. Gas Diffusivity Calculation

The diffusivity of H_2S-H_2 system was calculated using Fuller equation (Nain and Ferron, 1972), which can be expressed as

$$D_{12} = \frac{0.00143T^{1.75}(1/M_1+1/M_2)^{1/2}}{P\left((\sum v_{1i})^{1/3} + (\sum v_{2i})^{1/3}\right)} \tag{IV-16}$$

where D_{12} is the binary diffusion coefficient (cm^2/s), T is temperature (K), P is pressure (atm), M_i is the molecular weight of specie i. v_{ij} is the empirical diffusion volume of atom j in specie i. The diffusivity of H_2S-H_2 is calculated as

$$D_{12} = \frac{0.00143 \cdot (273.15 + 400)^{1.75} \cdot (1/2.01 + 1/34.08)^{1/2}}{1 \cdot \left((6.12)^{1/3} + (27.52)^{1/3}\right)} = 2.8 \ cm^2/s$$

IV.4.2. Viscosity Calculation

The viscosity of single gas component and gas mixtures can be calculated using equations IV-17, 18 and 19 (Bird, 2002).

$$\mu = 2.6693 \times 10^{-5} \left(\frac{\sqrt{MT}}{\sigma^2 \Omega_\mu} \right) \qquad \text{(IV-17)}$$

where μ is in unit of g cm^{-1} s^{-1}, M is molecular weight, σ is the Lennard-Jones characteristic diameter of molecule, and Ω_μ is the parameter for viscosity. The viscosity of H_2S-H_2 mixture can be calculated using the semi-empirical formula of Wilke.

$$\mu_{mix} = \sum_{i=1}^{n} \frac{x_i \mu_i}{\sum_{j=1}^{n} x_j \Phi_{ij}} \qquad \text{(IV-18)}$$

in which

$$\Phi_{ij} = \frac{1}{\sqrt{8}} \left(1 + \frac{M_i}{M_j} \right)^{-1/2} \left(1 + \sqrt{\frac{\mu_i}{\mu_j}} \left(\frac{M_i}{M_i} \right)^{1/4} \right)^2 \qquad \text{(V-20)}$$

The calculated value of H_2 and H_2S are 0.000153 and 0.000272 g/cm s. The viscosity of 2 vol.% H_2S-H_2 mixture is 0.000168 g/cm s.

IV.4.3. Density Calculation

The density of gas mixture was calculated using ideal gas law

$$PV = nR_0 T \qquad \text{(IV-19)}$$

$$\rho_a = \frac{m}{V} = \frac{m}{\dfrac{R_g T}{P}} \qquad \text{(IV-20)}$$

The density of 2 vol.% H_2S-H_2 at 400 °C was calculated to be 4.81×10^{-5} g/cm^3, and the density of 321 ppmv H_2S-H_2 at 400 °C, 3.64×10^{-5} g/cm^3.

IV.4.4. Packed Bed Performance

One gram of Sud-Chemie sorbent (40-60 mesh, 90 wt.% ZnO) was tested at various temperatures. The breakthrough curves are shown in **Figure IV-3**, and the extrapolated x-t plots in Figure **IV-4**. In **Figure IV-3**, breakthrough curves shifted to the right side with the increase in temperature. This indicated the more ZnO became accessible because of the improved mass transfer rate. This was revealed in **Figure IV-4** too. At beginning, all the x-t plots overlapped with each other on a straight line. This straight line, or the ideal x-t plot of gas film controlled process, passes through the origin and (119, 1) point in the x-t plane, where 119 min is the saturation time (τ) of the sorbent loaded in packed beds. As the reaction took place, the x-t plots were separated from this straight line. The x-t plot at a low temperature separated from the ideal x-t plot earlier than that at a high temperature, and reached a lower conversion plateau, due to the high intra-particle resistance at low temperatures.

However, these x-t plots demonstrated an averaged ZnO conversion and they cannot be used to estimate the kinetic parameters. The H_2S concentration and ZnO conversion were not uniform for the particles in the pack beds. Moreover, the H_2S concentrations at t→0 were too low to be practically measurable because of the use of integral reactors. Very thin beds (differential reactors), where the conversion of ZnO can be considered uniform, are required to investigate the reaction control mechanisms, using the single pellet models, i.e., unreacted shrinking core model.
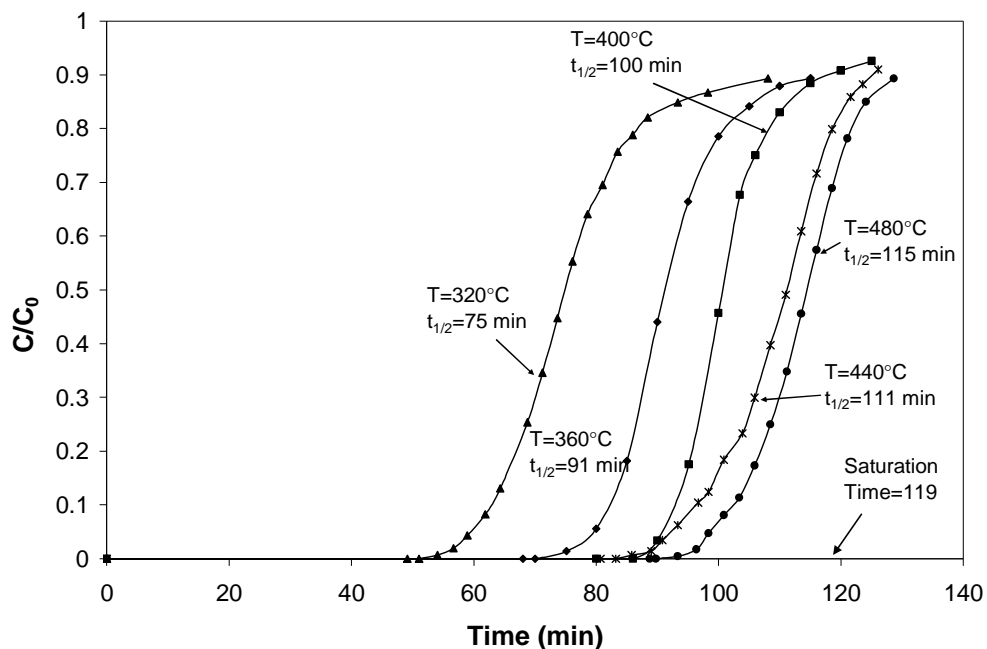
Figure IV-3. Breakthrough curves of packed beds made of Sud-Chemie sorbent particles (40-60 mesh, containing 0.9 g ZnO) at various temperatures. Tested with 2 vol.% H_2S-H_2 at 110 ml/min in a quartz reactor (0.99 cm dia.).
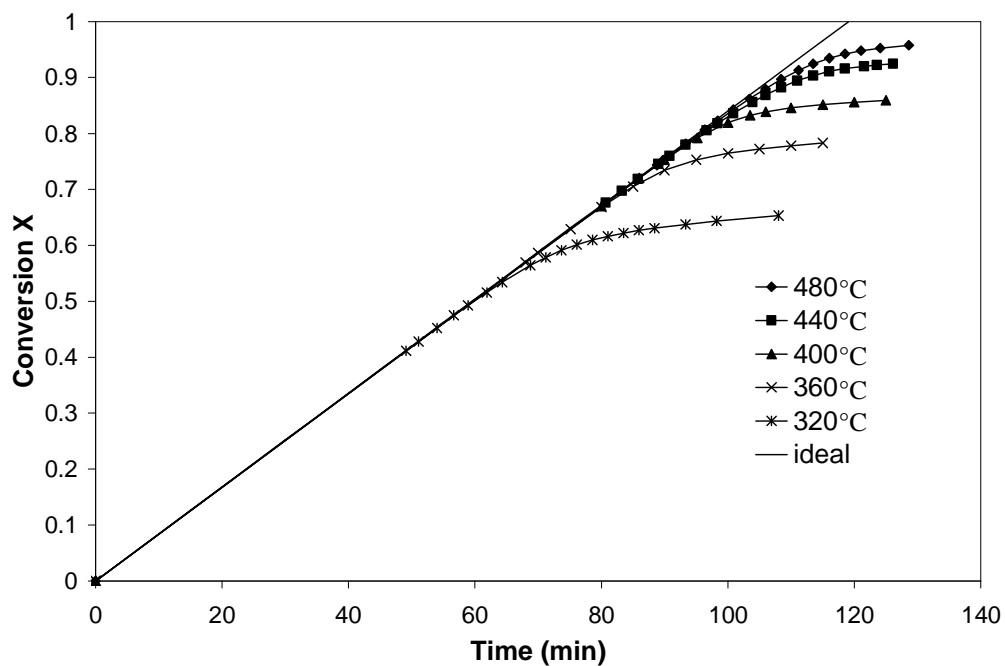
Figure IV-4. Conversion of ZnO in the packed beds of sorbent particles (40-60 mesh, containing 0.9 g ZnO) at various temperatures.

IV.4.5. Control Mechanism Discussion

IV.4.5.1. Intrinsic Reaction Rate

The reaction between ZnO and H_2S was considered as a first order reaction with respect to H_2S (Westmoreland and Harrison, 1976; Lew *et al*., 1992; Turton *et al*., 2004). However, there were different opinions on the reaction order of ZnO. Lew *et al*. (1992), Konttinen *et al*. (1997), and Turton *et al*. (2004) assumed it was a zero-order reaction with respect to ZnO while Westmoreland and Harrison (1976) and Garcia *et al*. (1997) considered it was first order. This paper treats it as a zero order reaction with respect to ZnO. The rate constants available in the literatures are shown in **Table IV-1**.

Table IV-1. Intrinsic reaction rate constants of the reaction between ZnO and H_2S.

Reference:	Sorbent & challenge gas	Activation Energy (Ea) (kJ/mol)	Frequency Factor (k_0) cm/s	k" at 400 °C cm/s
Turton *et al*. (2004)	ZnO, H_2S-N_2	31.4	0.333	0.00122
Lew *et al*. (1992)	ZnO, H_2S-H_2-N_2	43.1	1.31	0.000593
Lew *et al*. (1992)	$Zn_xTi_yO_{x+2y}$, H_2S-H_2-N_2	38.9	0.40	0.000383
Westmoreland (1976)	ZnO, H_2S-H_2	30.3	0.110*	0.004912

* Converted from the second order frequency factor by multiplying with the molar density of ZnO in the packed bed.

It is interesting to notice that the Arrhenius constants vary significantly in the cited works. The possible reason described by Lew *et al*., (1992) is the different crystallinity in the ZnO samples prepared by different researchers. Therefore, it is necessary to calibrate the intrinsic reaction rate for the sorbent of ZnO/SiO_2 prepared in this study.

In a series of differential reactor studies, 0.05 g of ZnO/SiO$_2$ sorbent (ZnO 17 wt.%) was tested with 321 ppmv H$_2$S-H$_2$ at various temperatures at a flow rate of 2000 cm^3/min STP. The outlet H$_2$S concentrations were analyzed by PFPD, and initial H$_2$S concentrations were extrapolated from the "breakthrough curves". The apparent reaction rate constants were then calculated using equation IV-14. The test results after modification using equation IV-16, in which the k_c was calculated using J_d correlation (Levenspiel, 2002) are shown in **Figure IV-5**.

$$\ln(K'') = -4374.9/T + 0.3315$$
$$R^2 = 0.998$$

$$\ln(K) = -4374.9/T + 14.519$$
$$R^2 = 0.998$$
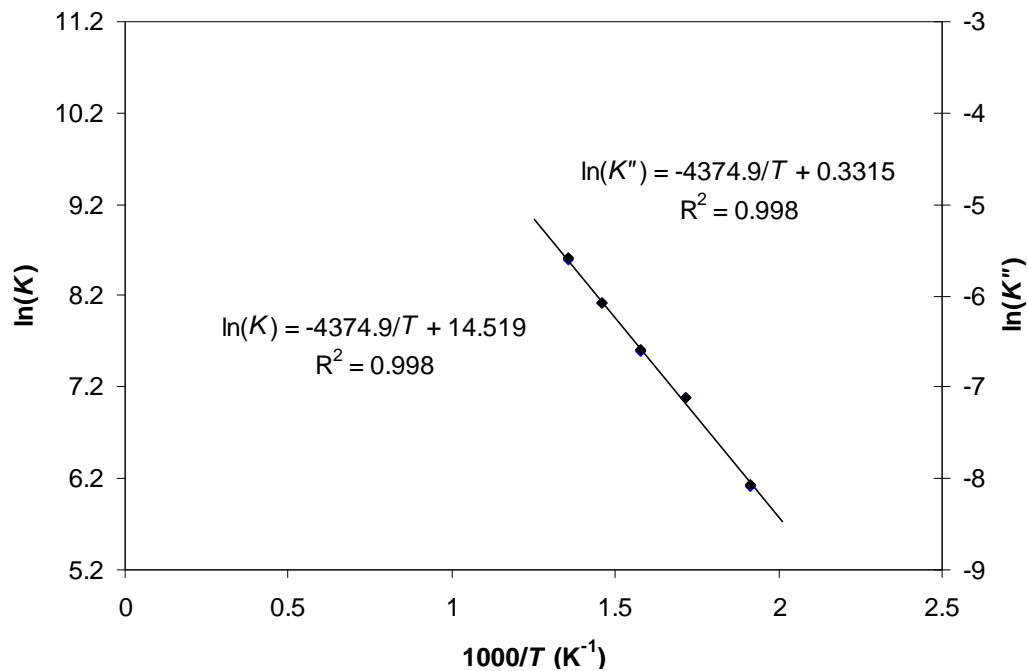
Figure IV-5. Arrhenius plot for intrinsic rate constant.

The calculated reaction rate constant (surface area based) can be expressed as:

$$k'' = 1.39 \exp\left(-36373/R_g T\right) \tag{IV-21}$$

where k'' has the unit of cm/s. The activation energy is close to those from Turton and

Westmoreland.   The intrinsic rate constant at 400 °C was estimated to be 0.0021 cm/s.

This value is in the range covered by the intrinsic rate constants listed in **Table IV-1**.   It

should be noted that the effective surface area S_a of ZnO/SiO$_2$ should be smaller than the

value used to calculate k'', therefore, the effective k'' is higher than the estimated.

The intrinsic rate constant (bed volume based) k calculated from **Figure IV-5** is 3039

s^{-1}; the particle volume based rate constant k'''' is 5065 s^{-1}.   As stated earlier, k_a and

k'''' is independent to S_a.

IV.4.5.2. Diffusion through the Pores

The diffusivity of H$_2$S in the pores (D_{ep}) can be estimated using equation IV-22

(Fogler, 1992).

$$D_{ep} = \frac{D_{12} \Phi_p \sigma}{\tilde{\tau}} \tag{IV-22}$$

where D_{12} is the H$_2$S diffusivity in H$_2$; Φ_{12} is the pellets porosity, which is 0.64 for the

ZnO/SiO$_2$ sorbent particles; σ is the constriction factor, which is around 0.8; $\tilde{\tau}$ is the

tortuosity of the pores, which is around 3.0 as shown in the reference.   The calculated

D_{ep} is 0.46 cm^2/s for ZnO/SiO$_2$.

The Thiele modulus for the first order reaction (ϕ_1) for ZnO/SiO$_2$ particles was

calculated by inserting characteristic radius, R (R=0.0075 cm or 75 μm), and D_{ep} and

k'''' into equation IV-7.   The calculated ϕ_1 is 0.84 for ZnO/SiO$_2$ and the effectiveness

factor η is calculated to be 0.95 using equation IV-8. Therefore, the pore diffusion is negligible for ZnO/SiO$_2$ sorbent at test conditions, and the H$_2$S concentration at the center of the sorbent particle is very close to the concentration on the particle surface. The mass transfer resistance could be lattice diffusion and/or external mass transfer resistance. This result also confirms that intrinsic rate constant by the method in this work is valid.

A similar calculation was performed for Sud-Chemie ZnO extrudates based on the properties shown in Appendix E. The estimated D_{ep} is 0.38 cm^2/s. The k''' of ZnO extrudates was estimated to be 1700 s^{-1}. The calculated effectiveness factor η is 0.32 for 2 mm extrudates, and 0.90 for 390 μm ZnO particles. These results suggest that the pore diffusion resistance in Sud-Chemie ZnO extrudates (2 mm) is severe, and it is negligible for particles with size less than 390 μm.

IV.4.5.3. Diffusion in Grains

In this section, the effective diffusivity of H$_2$S in sorbent grain is measured. In experiments, a high challenge flow rate (219 cm^3/min at room temperature, the face velocity is 11.3 cm/s at 400 °C) was applied to reduce the external mass transfer resistance, and 321 ppmv H$_2$S-H$_2$ was used as challenge gas to capture the breakthrough curves at in the differential reactor tested. The test results are shown in **Figure IV-6**. In **Figure IV-6**, the breakthrough curves at low temperatures are sharper than those at high temperatures. The ZnO in 0.04 g ZnO/SiO$_2$ (0.9 mm bed thickness) loaded are

exact the amount to yield detectible sulfur peaks at $t \rightarrow 0$. Using the integration method

described earlier, the ZnO conversion curves were established and are shown in **Figure**

IV-7. This figure suggests that the ZnO/SiO$_2$ sorbents tested at higher temperatures

required less time to achieve the same conversion than those tested at low temperatures.

In these tests, the external mass transfer resistance was minimized and the diffusion in the

pores was negligible. The process was under the control of diffusion in ZnO grains.

According to the shrinking core model, the conversion and time can be related using

equation IV-3 and IV-4 for the systems controlled by lattice diffusion. The *P(x)~t* plots

were established, the one tested at 300 °C is shown in **Figure IV-8** as an example.
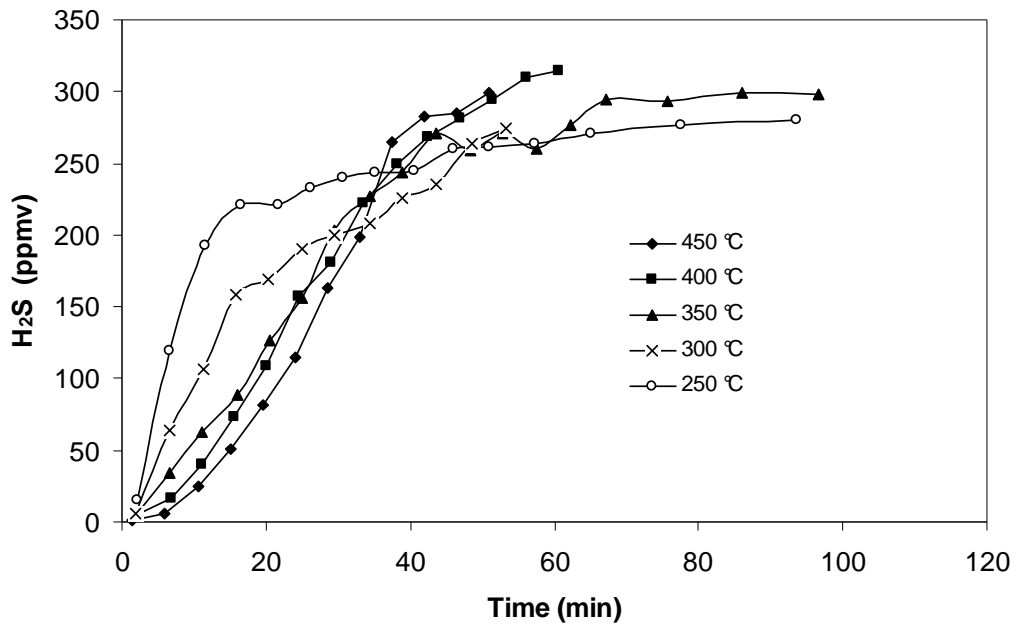
Figure IV-6. Breakthrough curves of differential reactors (0.99 cm ID) containing 0.04 g ZnO/SiO$_2$ sorbents tested with 321 ppmv H$_2$S-H$_2$ (219 ml/min STP) at various reaction temperatures.
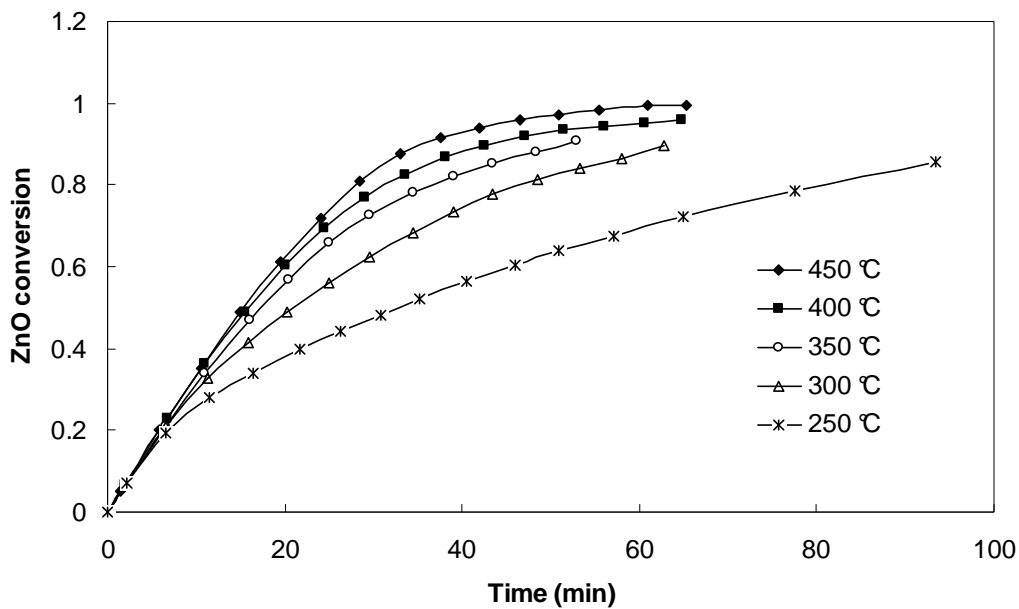
Figure IV-7. ZnO conversion curves of ZnO/SiO$_2$ sorbent tested with 321 ppmv H$_2$S-H$_2$ (219 ml/min, STP) at various reaction temperatures.
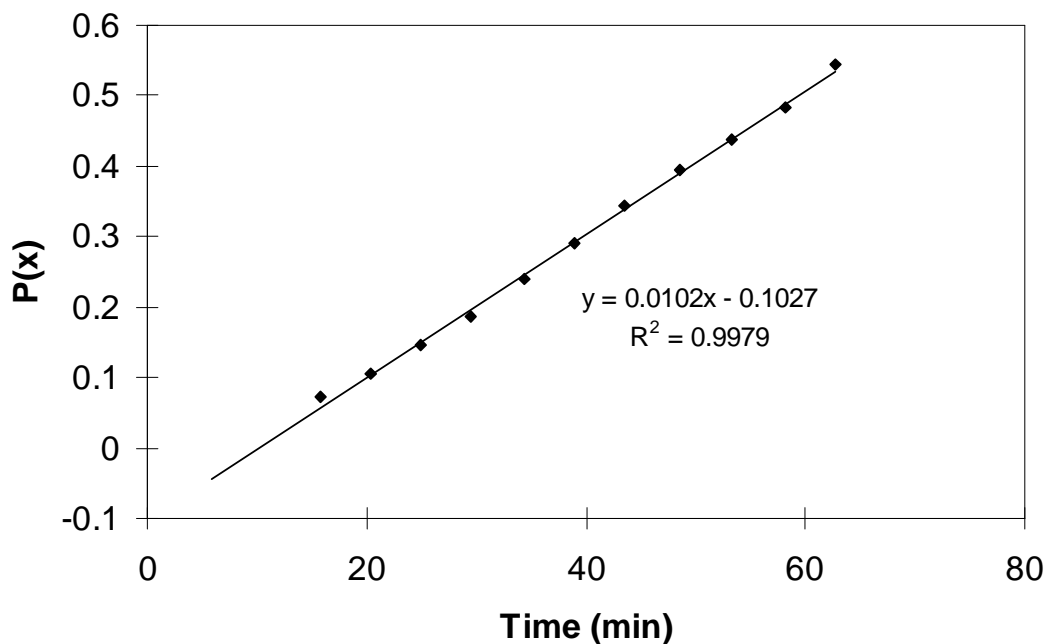
Figure IV-8. P(x)~t plot of ZnO/SiO$_2$ sorbent loaded in a tube reactor (0.99 cm dia.) and tested at 300 °C with 321 ppmv H$_2$S-H$_2$ (219 ml/min, STP).

In equation IV-4, ρ_g, the ZnO molar density in grains, is 0.069 mol/cm^3; R, the ZnO grain radius, is 2.5×10^{-7} cm (2.5 nm) calculated using XRD. D_{eg} is H_2S diffusivity in ZnO grain. C_{Ab} here is close to the H_2S concentration in bulk flow C_{A0}.

The slope of P(x)~t plot is τ^1 (see **Figure IV-7**) and D_{eg} can be calculated easily from equation IV-10. The calculated D_{eg} values at various temperatures are shown in **Table IV-2**. The calculated values of D_{eg} have an order of -11, which is pretty close to the values in literatures (Ozdemir and Bardakci, 1999; Konttinen, *et al.*, 1997). The Arrhenius plot of D_{eg} is shown in **Figure V-8**. The activation energy of D_{eg} is 25 kJ/mol, and the D_{eg} at different temperatures can be calculated using the Arrhenius equation:

$$D_{eg} = 3.34 \times 10^{-9} \exp(-25146 / R_g T) \qquad \text{(IV-23)}$$

Recall the equation IV-7 and calculate the Thiele modulus ϕ_1 for the H_2S diffusion in grains using the intrinsic rate constant (5065 s^{-1}) at 400 °C, the values of R (2.5×10^{-7} cm) and D_{eg} (3.55×10^{-11} cm^2/s). The calculated ϕ_1 is 2.9, and η_g is 0.68. Further calculation suggests that the outside layer within a thickness of 1.1 nm is free from lattice diffusion ($\eta_g{}' > 0.9$). This layer contains 84% ZnO. At ZnO utilization of 84%, the corresponding H_2S concentration in breakthrough curve at 400 °C is 223 ppmw, or 0.70 C_0. These results indicate that the lattice diffusion in the ZnO grain in ZnO/SiO$_2$ sorbent particles is virtually negligible at $C/C_0 < 0.70$, which is the range widely used to extrapolate lumped K from breakthrough curves. Therefore, the external transfer determines the breakthrough characteristics of ZnO/SiO$_2$ beds at low face velocities.

Table IV-2. The calculation table for the effective diffusivities (D_{eg}) of H_2S through the ZnS layer at various temperatures.

T (K)	1000/T (K^{-1})	τ (min)	$1/\tau$ (min^{-1})	C_{Ag} (mol/cm^3)	D_{eg} (cm^2/s)	$Ln(D_{eg})$
523.15	1.91	159	0.0065	7.38×10^{-9}	1.04×10^{-11}	-25.3
572.15	1.75	98	0.0110	6.75×10^{-9}	1.93×10^{-11}	-24.7
621.15	1.61	77	0.0138	6.21×10^{-9}	2.63×10^{-11}	-24.4
672.15	1.49	58	0.0178	5.74×10^{-9}	3.67×10^{-11}	-24.0
720.15	1.39	43	0.0235	5.36×10^{-9}	5.20×10^{-11}	-23.7
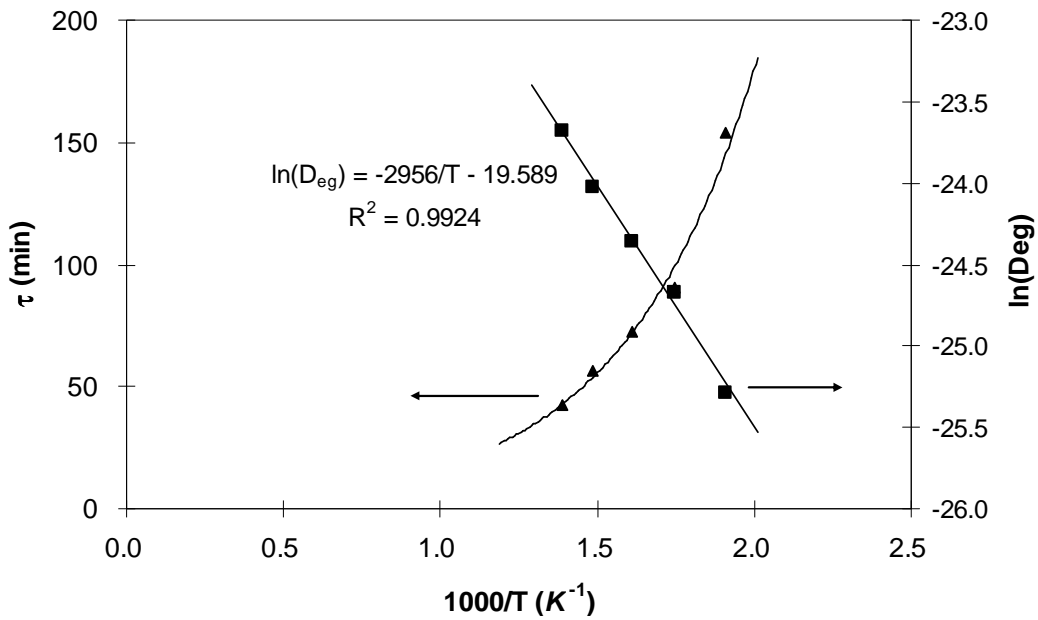
Figure IV-9. Arrhenius plot of D_{eg}.

Similarly, the ϕ_l and η_g for 17 nm gains (a value estimated from XRD pattern) of Sud-Chemie extrudates 19.8 are 0.14 respectively.   A further calculation suggested that Sud-Chemie grains can reach 18% conversion, when the thickness of ZnS layer is 1.1 nm, without suffering from significant penalty in lattice diffusion resistance.   However, the actual effectiveness factor for Sud-Chemie sorbent may be much lower than 0.14,

because ZnO grain in extrudates, unlike ZnO/SiO$_2$, are not well dispersed by supporters and they usually form agglomerates larger than the size obtained from XRD analysis. Therefore, the intra-particle mass transfer determines the breakthrough characteristics using Sud-Chemie extrudates.

IV.5.Conclusions

In this paper, breakthrough curves have been employed to analyze kinetic parameters, such as intrinsic reaction rate constants and effective diffusivities. The Arrhenius plot for intrinsic reaction constant for H$_2$S removal using packed beds of ZnO/SiO$_2$ sorbent particles (100-200 μm) was established by differential reactor analysis. The calculated activation energy Ea for the reaction between ZnO and H$_2$S was close to the values cited in literatures. The conversion-time (x-t) plots of ZnO/SiO$_2$ sorbent bed were established using mass balance, and kinetics parameters were extrapolated from x-t plots. The effective diffusivities for H$_2$S in grains were calculated and plotted in Arrhenius form. Based on the kinetic parameters, the η_g for the pore diffusion and that for lattice diffusion at C/C_0 <70%, using ZnO/SiO$_2$ sorbent, are above 0.9, under typical desulfurization conditions, i.e. at 400 °C and a face velocity less than 11 cm/s. Therefore, the intra-particle mass transfer resistance for ZnO/SiO$_2$ was negligible, and external mass transfer resistance controlled the desulfurization reaction rate and breakthrough characteristics at experimental conditions, before the outlet concentration reaches 70% of

C_{A0}. Since the ZnO/SiO$_2$ particles are the same as the particles in microfibrous entrapped ZnO/SiO$_2$ sorbents, the intra-particle mass transfer resistance can also be ignored for microfibrous entrapped sorbents at the experimental conditions.

Acknowledgement

Notations

C_i	inlet H$_2$S concentration	ppmv
C_o	outlet H$_2$S concentration	ppmv
C_{Ag}	bulk H$_2$S concentration in gas flow	mol/cm^3
C_{As}	H$_2$S concentration on the surface of the particle	mol/cm^3
C_{Ac}	H$_2$S concentration at the core of the particle	mol/cm^3
d	characteristic size	cm
D_{12}	gas diffusion of binary gas mixture	cm^2/s
D_e	effective diffusivity	cm^2/s
k	intrinsic reaction rate constant (reactor or bed volume based)	s^{-1}
k'	intrinsic reaction rate constant (particle weight based)	cm^3/g s

k''	intrinsic reaction rate constant (surface area based)	cm/s
k'''	intrinsic reaction rate constant (void volume based)	s^{-1}
k''''	intrinsic reaction rate constant (particle volume based)	s^{-1}
k_a	apparent reaction rate (reactor or bed volume based)	s^{-1}
k_c	mass transfer coefficient	cm/s
m	mass	g
M	molecular weight	g/mol
P	pressure	atm
R	characteristic radius	cm
R_g	ideal gas constant, 8.314	J/mol K
S_a	surface area per unit mass of particles	cm^2/g
t_r	residence time	s
T	temperature	K
U_i	interstitial velocity	cm/s
v	empirical diffusion volume	
x	molar fraction of gas component	
z	bed depth	cm
z_c	critical bed depth	cm

Greek letters

α	external particle surface area per unit bed volume	cm^2/cm^3
ϕ	void fraction of packed beds	
ϕ_1	Thiele modulus for the first order reaction	
Φ_p	pore fraction the sorbent particles	
η	effectiveness factor	
μ	viscosity	g/ cm s
ρ_a	gas density	g/cm^3
ρ_m	molar density of solid	mol/cm^3
σ	Lennard-Jones characteristic diameter of molecule	
σ_c	constrict factor	
τ	time required to achieve complete conversion	min
$\tilde{\tau}$	tortuosity	
Ω_μ	the parameter for viscosity	

Subscriptions

g	grain
p	particle volume based
v	void volume based

CHAPTER V.

A STUDY OF KINETIC EFFECTS DUE TO USING MICROFIBROUS ENTRAPPED ZINC OXIDE SORBENTS FOR HYDROGEN SULFIDE REMOVAL FROM MODEL REFORMATES

Abstract

A modified Amundson model has been proposed to characterize breakthrough curves of fixed bed reactors during gas phase desulfurization using two variables: saturation time (τ) and shape factor (lumped K). The lumped K depends on the inlet H$_2$S concentration, capacity density of the packed bed and the apparent reaction rate constant. This model has been verified experimentally at 400 °C. The influences of high void volume and microfibrous entrapment of ZnO sorbents (MFES) are also discussed. Utilization of nano-crystallite ZnO sorbent supported on SiO$_2$ (100-200 μm) minimizes intra-particle diffusion resistance resulting in a saturation capacity near the theoretical value. Entrapment in microfibers enhances the external mass transfer rate of the entrapped particles. High void volume increases the residence time and reduces the capacity density resulting in increased overall lumped rate constant. The microfibrous entrapped sorbent demonstrated longer sulfur breakthrough time than ZnO extrudates with a sharper

breakthrough curve and higher ZnO utilization.   The lumped K value of MFES was 34

times larger than that of commercial ZnO extrudates and 1.3 times larger than that of

ZnO/SiO$_2$ sorbent.   MFES is optimally used as a polishing layer at the downstream end of

a packed bed to maximize the overall desulfurization performance.

Keywords: Kinetics; Desulfurization; Breakthrough curve; Sorbent; Mathematical

Modeling; Zinc oxide

V.1. Introduction

Logistic power systems based on on-board Proton Exchange Membrane Fuel Cells

(PEMFCs) have been studied extensively.   PEMFCs require high purity hydrogen as

fuel to generate electricity.   Hydrocarbon reforming is considered the best means to

supply hydrogen for logistic PEMFC.   A challenge in these applications is to remove

sulfur compounds, especially hydrogen sulfide (H$_2$S), from reformates in a reactor with

minimized size.   In order to protect the precious metal catalysts used in fuel processing

and the high-value membrane electrode assemblies, it is critical to reduce the H$_2$S

concentration to less than 0.1 parts per million by volume (ppmv) (Novochinskii *et al*.,

2004).   Most gas phase desulfurization units apply metal oxides, such as zinc oxide

(ZnO) and copper oxide (CuO), as active sorbents (Westmoreland and Harrison,1976;

Tamhankar *et al*., 1986; Slimane and Abbasian,2000a).   Among them, ZnO is a

well-known sorbent used to capture H$_2$S from fuel gas stream in moderate temperature

ranges (300-500 ºC) (Novochinskii *et al.*, 2004; Tamhankar *et al.*, 1986; Baird *et al.*, 1992; Sasaoka,1994b).   The sulfidation reaction between ZnO and H_2S is thermodynamically favorable in moderate temperature ranges, so the outlet H_2S concentration can be reduced to several ppmv or even lower depending on gas composition.

Normally, packed beds of large ZnO sorbent extrudates with high sorbent inventory are widely used to scavenge H_2S from reformates streams for fuel cell applications. However, because of low contacting efficiency, channeling, and intra-particle and lattice diffusion limitations, ZnO utilization and regenerability are usually very poor (Lu *et al.*, 2005)   Reactors based on conventional technology typically require large amounts of sorbent with correspondingly large reactor size to achieve multi-log sulfur removal, which may not be applicable for logistical applications.   Microfibrous entrapped catalysts and sorbents (MFES) developed at the Center for Microfibrous Materials Manufacturing (CM³) at Auburn University provide a novel approach for more effective design of small, efficient, and lightweight fuel processors (Cahela *et al.*, 2004). Microfibrous entrapped sorbents demonstrate excellent performance in heterogeneous reactions such as H_2S removal (Lu *et al.*, 2005) and CO oxidation (Chang *et al.*, 2006). For H_2S removal, microfibrous entrapped sorbents demonstrated lower pressure drop, reduced critical bed depth, improved ZnO utilization, ease of regeneration and high dynamic capacity compared with packed bed counterparts (Lu *et al.*, 2003).   Since the

active component is ZnO in both MFES and extrudates, the difference is due to the apparent kinetic behavior of the materials.   In this work, the basic relationships between breakthrough curves and the kinetic behaviors of fixed bed reactors have been revealed, and the function of microfibrous media is discussed.

V.2. Theory

V.2.1. Mathematic Model

Several mathematical models such as Mecklenburg model (Klotz, 1946), Amundson model (Amundson, 1948), Wheeler model (Wheeler and Robell, 1969; Jonas and Rehrmann, 1973) and Yoon model (Yoon and Nelson, 1984) have been developed to predict the breakthrough time of charcoal cartridges.   In this paper, Amundson's model is adapted and modified to understand the kinetic behavior of ZnO/SiO_2 sorbent and microfibrous entrapped ZnO/SiO_2 sorbent.

In this model, the reaction between H_2S (A) and ZnO (B) is considered as a second order reaction and the reaction rate can be written as follows:

$$-r = k_2 C_A C_B \qquad\qquad\qquad\qquad (V\text{-}1)$$

where C_A is H_2S concentration and C_B is amount of accessible ZnO remaining in the packed bed in moles per unit volume of bed.   For fresh sorbents C_B is equal to the saturation capacity density (ρ_c, $\rho_c = \dfrac{xy\rho_b}{M_z}$) of the sorbents in the packed bed under the experimental

151

condition. Then, the outlet H_2S concentration exiting at the end of the packed bed can be predicted using Amundson's equation as shown in equation V-2.

$$\frac{C_{A0}}{C_A} = 1 + \left[\exp(-\phi k_2 t C_{A0})\right] \cdot \left[\exp\left(\frac{\phi k_2 \rho_c z_t}{U}\right) - 1\right]$$ (V-2)

The time to saturate the bed (τ) is as follows:

$$\tau = \frac{\rho_c z_t}{U C_{A0}}$$ (V-3)

Then equation V-2 can be written as:

$$\frac{C_{A0}}{C_A} = 1 + \exp(-\phi k_2 t C_{A0}) \cdot \left[\exp(\phi k_2 C_{A0} \tau) - 1\right]$$ (V-4)

For most cases, $\exp(\phi k_2 C_{A0} \tau) \gg 1$, so equation V-2 can be reduced and rearranged as:

$$\ln\left(\frac{C_{A0}}{C_A} - 1\right) = \phi k_2 C_{A0}(\tau - t)$$ (V-5)

In the low face velocity ranges, like the case in this paper, the reaction is controlled by external mass transfer rate, and the reaction rate can be expressed in terms of apparent rate constant k_a as shown in equation V-6.

$$-r = k_a C_A$$ (V-6)

Comparison between equation V-1 and equation V-6 yields

$$k_2 C_A C_B = -r = k_a C_A$$ (V-7)

$$C_B \to \rho_c \qquad at\ t \to 0$$ (V-8)

152

Rearrangement of equation V-7 yields

$$k_2 = \frac{k_a}{\rho_c}$$ (V-9)

Insertion of equation V-9 into equation V-5 yields

$$\ln\left(\frac{C_{A0}}{C_A} - 1\right) = \phi \frac{k_a}{\rho_c} C_{A0}(\tau - t)$$ (V-10)

Equation V-10 suggests that $\ln(\frac{C_{A0}}{C_A} - 1)$ should have a linear relationship with onsite

time t. If the absolute value of the slope of $\ln(\frac{C_{A0}}{C_A} - 1)$ *vs. t* curve is defined as the shape

factor, lumped K, then equation V-10 can be reduced to

$$\ln(\frac{C_{A0}}{C_A} - 1) = K(\tau - t)$$ (V-11)

Equation V-11 is the well-known bed depth service time equation proposed by Yoon

(Yoon and Nelson, 1984). Based on the derivation above, lumped K should be expressed as

$$K = k_a \phi \frac{C_{A0}}{\rho_c}$$ (V-12)

Lumped K is an important parameter to characterize breakthrough curves, it can also

be employed to calculate the ZnO utilization and critical bed depth, the minimum bed

thickness to reduce the H_2S concentration below a breakthrough concentration (C_b), as

seen in equation V-13

$$z_c = \ln(\frac{C_{A0}}{C_b} - 1)\frac{UC_{A0}}{K\rho_c} \qquad\qquad\text{(V-13)}$$

Equation V-13 shows that z_c is independent of the bed thickness and it decreases with the increase in the lumped K value.　　It can also be applied to calculate ZnO utilization of sorbents in a fixed bed reactor.　　A simple mass balance yields that

$$X = 1 - \frac{z_c}{z_t} \qquad\qquad\text{(V-14)}$$

where X is the ZnO utilization of all the accessible part at the breakthrough concentration C_b.　　Equation V-14 indicates that for packed beds that have the same critical bed depth, e.g. two packed beds made of the same sorbent and tested at the same temperature, pressure and face velocity, the one has larger bed thickness yields higher ZnO utilization. Equations V-13 and 14 suggest that a fixed bed with a larger K value will have higher ZnO utilization and smaller critical bed depth than the one with lower K value at the same test conditions such as U, C_{A0} and C_b.

V.2.2. Mass Transfer Correlation

Apparent rate constant k_a can be calculated using classic mass transfer correlations. In low face velocity region, the reaction falls into the external mass transfer control region and

$$k_a = \frac{1}{\phi} k_c \alpha \qquad\qquad\qquad (V\text{-}15)$$

where α is the external surface area of sorbent particles per unit bed volume

$$\alpha = \frac{6(1-\phi)}{d_p} \qquad\qquad\qquad (V\text{-}16)$$

and k_c is external mass transfer coefficient, which can be calculated using following equation:

$$k_c = Sh \frac{D_{AB}}{d_p} \qquad\qquad\qquad (V\text{-}17)$$

where Sh is Sherwood number.   It can be calculated by equation V-18

$$Sh = J_d \, \mathrm{Re} \, Sc^{\frac{1}{3}} \qquad\qquad\qquad (V\text{-}18)$$

J_d is the well-known mass transfer factor.   It can be calculated using different mass transfer correlations, as seen in a comprehensive review on mass transfer correlations for different systems conducted by Upadhyay and Tripathi (1975).   In that review, mass transfer correlations for the gas-particle systems at low Reynolds (Re) numbers and low Schmidt (Sc) numbers can be expressed in terms of Re", the surface area based Reynolds number, as shown in equation V-19.

$$J_d = C_1 \, \mathrm{Re}''^{-C_2} \qquad\qquad\qquad (V\text{-}19)$$

where C_1 and C_2 are dimensionless constants. C_1 varies from 0.6 to 2.25 and C_2 from 0.3 to 0.5.   In this paper, the C_1 and C_2 are arbitrarily chosen to be 1.24 and 0.39

respectively from the Colquhoum-Lee's expression (Upadhyay and Tripathi, 1975) to estimate the external mass transfer coefficient.

Inserting equations V-16, 17, 18 and 19 into equation V-15 yields

$$k_a = 7.44 \cdot \frac{(1-\phi)^{1.39}}{\phi} \left(\frac{d_p \rho U}{\mu} \right)^{0.61} Sc^{\frac{1}{3}} \frac{D_{AB}}{d_p^2} \qquad (V-20)$$

Insertion of equation V-20 into equation V-12 yields

$$K = 7.44 \cdot (1-\phi)^{1.39} \left(\frac{d_p \rho U}{\mu} \right)^{0.61} Sc^{\frac{1}{3}} \frac{D_{AB}}{d_p^2} \frac{C_{A0}}{\rho_c} \qquad (V-21)$$

Insertion of equation V-21 into equation V-13 yields

$$z_c \propto \ln(\frac{C_{A0}}{C_b})(1-\phi)^{-1.39} \left(\frac{d_p \rho U}{\mu} \right)^{-0.61} Sc^{-\frac{1}{3}} \frac{d_p^2}{D_{AB}} U \qquad (V-22)$$

In the case of microfibrous entrapped sorbents, the larger external surface area introduced by the microfibers dominates the flow field. The effect of fibers on mass transfer should be taken into account. A new parameter, $\overline{d_s}$, a surface area average diameter should be applied to substitute for d_p in the expression of Reynolds number for sorbents entrapped in microfibrous media. Similarly, for the calculation of k_c using equation V-17, the external surface area determines the diffusional film thickness at the low Re number region, therefore, $\overline{d_s}$ should be used again in the expression of Sh. Expressions for the apparent reaction rate constant, lumped K and critical bed depth for MFES are as follows:

156

$$k_a = 7.44 \cdot \frac{(1-\phi)^{1.39}}{\phi} \left(\frac{\overline{d_s}\rho U}{\mu} \right)^{0.61} Sc^{\frac{1}{3}} \frac{D_{AB}}{\overline{d_s}d_p} \tag{V-23}$$

$$K = 7.44 \cdot (1-\phi)^{1.39} \left(\frac{\overline{d_s}\rho U}{\mu} \right)^{0.61} Sc^{\frac{1}{3}} \frac{D_{AB}}{\overline{d_s}d_p} \frac{C_{A0}}{\rho_c} \tag{V-24}$$

$$z_c \propto \ln(\frac{C_{A0}}{C_b})(1-\phi)^{-1.39} \left(\frac{\overline{d_s}\rho U}{\mu} \right)^{-0.61} Sc^{-\frac{1}{3}} \frac{\overline{d_s}d_p}{D_{AB}} U \tag{V-25}$$

In equations V-23, 24 and 25, $\overline{d_s}$ is can be estimated by the following equation (Harris *et al*., 2001):

$$\frac{1}{\overline{d_s}} = \frac{a_f}{\varphi_f d_f} + \frac{a_p}{\varphi_p d_p} \tag{V-26}$$

where φ_f and φ_p in equation V-26 are 1.5 and 1 respectively.

Ratio of mass transfer coefficient for MFES versus packed bed is obtained by comparing equation V-20 and equation V-23 as follows:

$$\frac{k_{am}}{k_{ap}} = \left(\frac{d_p}{\overline{d_s}} \right)^{0.39} \left(\frac{1-\phi_m}{1-\phi_p} \right)^{1.39} \frac{\phi_p}{\phi_m} \tag{V-27}$$

and similarly for lumped *K*:

$$\frac{K_m}{K_p} = \left(\frac{d_p}{\overline{d_s}} \right)^{0.39} \left(\frac{1-\phi_m}{1-\phi_p} \right)^{1.39} \left(\frac{\rho_{cp}}{\rho_{cm}} \right) \tag{V-28}$$

In this study, the validity of equations V-11 and 12 will be verified and applied to explain the performance of packed beds and MFES.

V.3. Experimental

All gases in this work were purchased from Airgas South Inc.   The sources of H_2S were 2 vol.% (20000 ppmv) H_2S in H_2, and 321 ppmv H_2S in H_2.   Other H_2S challenge gas concentrations, (i.e. 1 vol.% and 5000 ppmv) employed in this study were produced by diluting 2 vol.% H_2S with ultra-high purity hydrogen.   The outlet H_2S concentrations were analyzed by a Gow-Mac 550 GC equipped with a TCD detector (H_2 carrier gas) which detects H_2S concentrations down to 200 ppmv.   Gas samples were injected into the GC every minute using a 6-port-valve with a sampling loop of 50 µL.   The sampling system was connected by 1/8" tubing, and the pressure drop of this system was negligible at all experimental conditions.   Concentrations below 200 ppmv were measured by a Varian 3800GC equipped with a pulse flame photometric detector (PFPD) which measures H_2S concentrations to sub-ppmv levels.   Gas samples (250 µL) in low concentration tests were collected and injected manually.

Three sorbents were investigated in this study.   They were a commercial ZnO sorbent (90 wt.% of ZnO, 3/16" extrudate), ZnO supported on SiO_2 (ZnO/SiO_2 ,17 wt.% of ZnO, 100-200 µm fine particles) and glass fiber entrapped ZnO/SiO_2 (GFES, 12 wt.% of ZnO, 100-200 µm fine particles entrapped in glass fiber media with a fiber diameter of 8 µm).   The last two sorbents were prepared by pseudo-incipient wetness impregnation at room temperature, using zinc nitrate ($Zn(NO_3)_2$) solutions of various concentrations, followed by drying and calcination.   ZnO loading was quantified by both mass balance

158

and ICP analysis. In GFES, ZnO loading is 17 wt.% as in ZnO/SiO_2 if the weight of glass fibrous media is neglected. Detailed preparation procedures were described elsewhere (Lu *et al*., 2005). The microfibrous entrapped sorbents were characterized by scanning electron microscopy (SEM) using a Zeiss DSM 940 instrument.
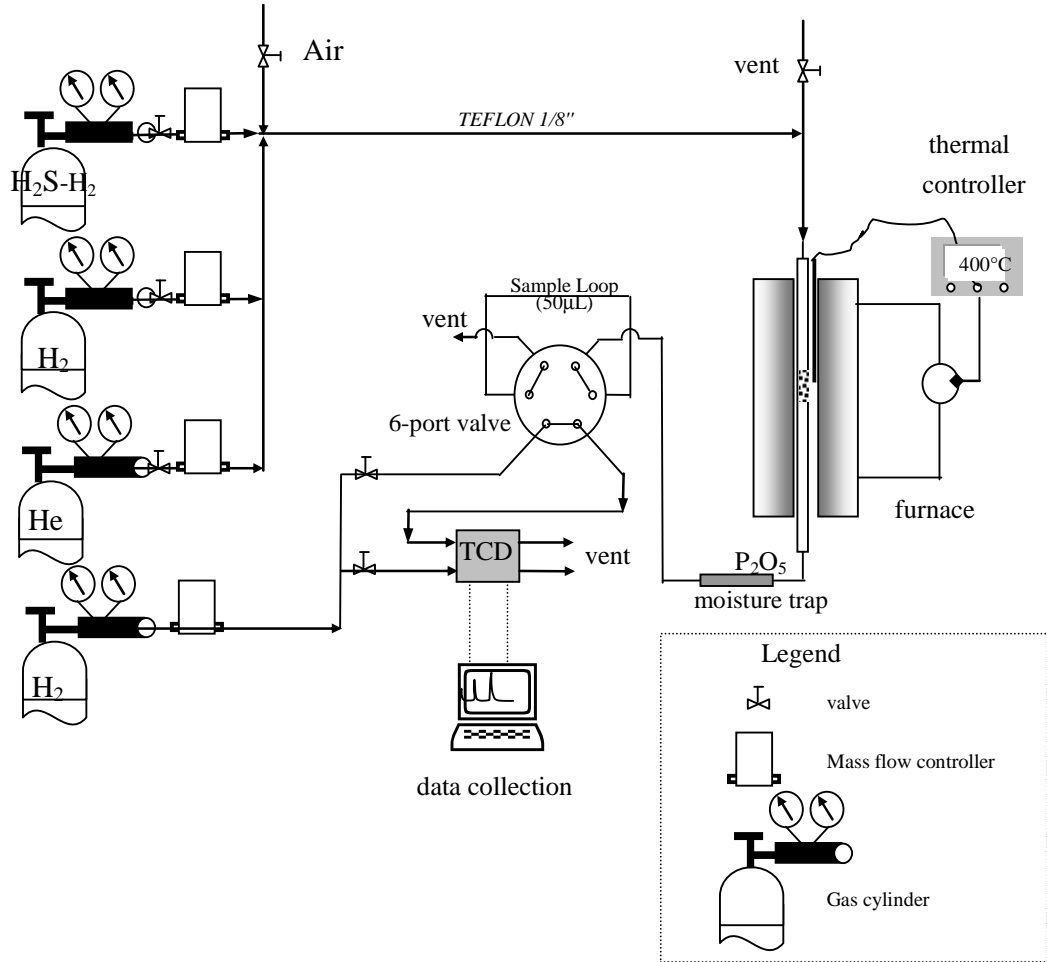
Figure V-1. Experimental setup for H_2S removal.

The reactor employed was a quartz tube (0.99 cm I.D.), if not otherwise noted. After loading the sorbents, air (100 ml/min) was passed through the reactor until the temperature reached the set point of 400 °C. Then, helium (100 ml/min) was passed

159

through the reactor for ten minutes to eliminate oxygen from the reactor, which may introduce side reactions such as sulfide oxidation. Then H_2 was passed through the reactor for another 10 minutes to stabilize the temperature profile along the reactor. Finally, the challenge gas of various H_2S concentrations was passed through the reactor at the same flow rate as H_2. The 6-port-valve, as shown in **Figure V-1**, was switched every minute starting at 1 minute after commencing the experiment to inject samples into the GC.

V.4. Results and Discussion

V.4.1. Microfibrous Entrapped Catalysts/Sorbents

Three different types of microfibrous media (MFM) have been developed at CM^3 at Auburn University. They are metal fiber media, glass fiber media and polymer fiber media. All of these media utilize micron-sized fibers to interlock catalyst or sorbent particles (30~300 μm) into sintered networks, as shown in **Figure V-2**.

Only 2-3 % of total volume is occupied by microfibers, and the MFM is 70~98 vol.% void, which is a unique feature of microfibrous entrapped sorbents. A comparison between microfibrous entrapped sorbents and two packed beds is shown in **Table V-1**. The glass fiber entrapped ZnO/SiO_2 sorbent has a high void fraction of about 75 vol.%, about twice that of a typical packed bed. Therefore, microfibrous entrapped catalyst or sorbents could be treated as highly diluted packed beds, diluted by void rather than inert

160

particles, and the amount of active catalyst or sorbent is only one-third of that in the

packed bed of ZnO/SiO_2 sorbents.

(a)   (b)
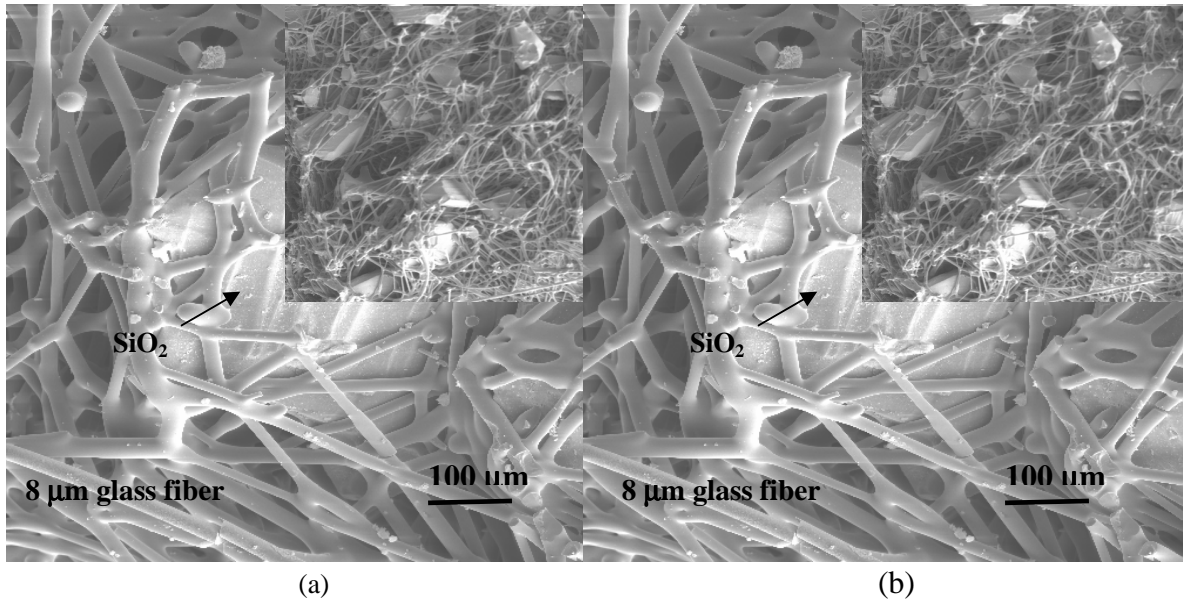
Figure V-2. Morphologies of several microfibrous entrapped sorbents. (a) Al_2O_3 particles in Ni fiber media; (b) SiO_2 particles in glass fiber media.

Table V-1. Comparison between microfibrous entrapped ZnO/SiO_2 sorbent (MFE), packed bed composed of ZnO/SiO_2 particles (PB) and packed bed of commercial sorbents (PBC).

Component	Wt.%			Vol.%		
	MFE	PB	PBC	MFE	PB	PBC
ZnO	13	17	100*	N.A.$^+$	N.A.	60
SiO_2	66	84	N.A.	22$^+$	60	N.A.
Fiber	22	N.A.	N.A	3	N.A.	N.A
Void	N.A.	N.A.	0	75	40	40

* The commercial sorbent contains 90 wt.% ZnO and 10 wt.% Al_2O_3 as binder

+ ZnO was loaded in the pores of SiO_2 particles

V.4.2. Model Evaluation
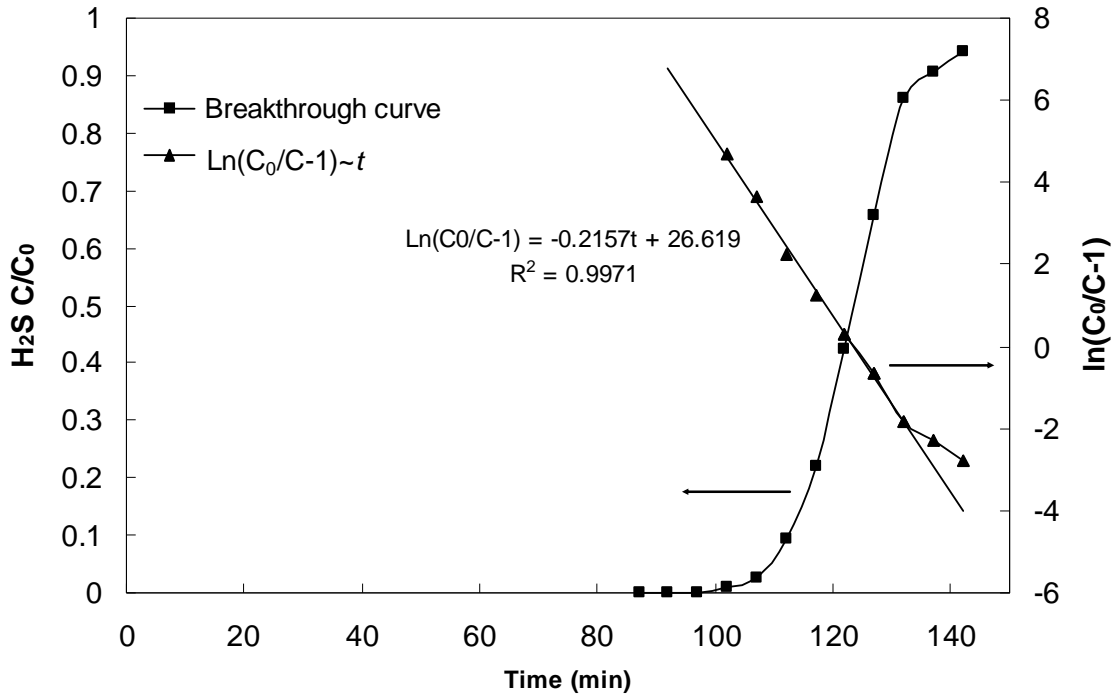
Figure V-3. Evaluation of service time equation.

Equation V-11 was evaluated in this section for kinetics study. The commercial sorbent was crushed and sifted into 60-80 mesh, and 1 g of the crushed sorbent particles was loaded into the reactor. It was tested with challenge gas concentration of 2 vol.% H_2S in H_2 and flow rate of 100 ml/min STP, at 400 °C. In the low concentration region, $\ln(\frac{C_{A0}}{C_A}-1)$ demonstrates a good linear relationship with onsite time t, as predicted by equations V-10 and 11, shown in **Figure V-3**. From the straight line of $\ln(\frac{C_{A0}}{C_A}-1) \sim t$, K and τ were calculated from linear regression, and the values obtained were 0.216 min^{-1}

(0.0036 s^{-1}) and 123.6 min respectively. Because of the symmetry of most breakthrough curves, τ is equal to the $t_{1/2}$ when the outlet H_2S concentration reaches 50% of inlet concentration C_{A0}. For example, τ and $t_{1/2}$ of the breakthrough in **Figure V-3** are 123.6 min and 123.8 min respectively. Therefore, $t_{1/2}$ was used to calculate the saturation capacities in this work. The amount of ZnO in packed bed and the flow conditions determine τ value, which in turn determines the position of the breakthrough curve, since it passes through the point of ($0.5, \tau$) in the $(\dfrac{C_{A0}}{C_A} - 1) \sim t$ plane. These results suggest

equation V-11 can be applied to analyze the heterogeneous reaction between ZnO and H_2S. As suggested by equation V-11, the lumped K determines the shape of a breakthrough curve. The larger value of K is, the sharper the breakthrough curve becomes. The $\ln(\dfrac{C_{A0}}{C_A} - 1) \sim t$ plot will not always be linear. In **Figure V-3**, after t is

increased past τ, the slope of $\ln(\dfrac{C_{A0}}{C_A} - 1) \sim t$ curve decreases gradually, indicating a new reaction control mechanism is dominating the process. In this case, the intra-particle mass transfer rate becomes the dominant factor as the reaction progresses.

V.4.3. Particle Size Effects

In this section, the commercial ZnO sorbent extrudates were crushed and sieved into desired particle sizes. The comparison between the performance of ZnO/SiO_2 and ZnO

particles is shown in **Figure V-4**. In each experiment, reactor temperature and face

velocity were maintained at 400° C and 1.2 cm/s respectively, and the packed bed

contained 0.18 g of ZnO. The only factor changed was the particle size. Breakthrough

curve of GFES tested at equivalent conditions is also shown **in Figure V-4** for

comparison. For convenience, the breakthrough was defined at the point that the outlet

concentration reached 1% inlet concentration (C_0).
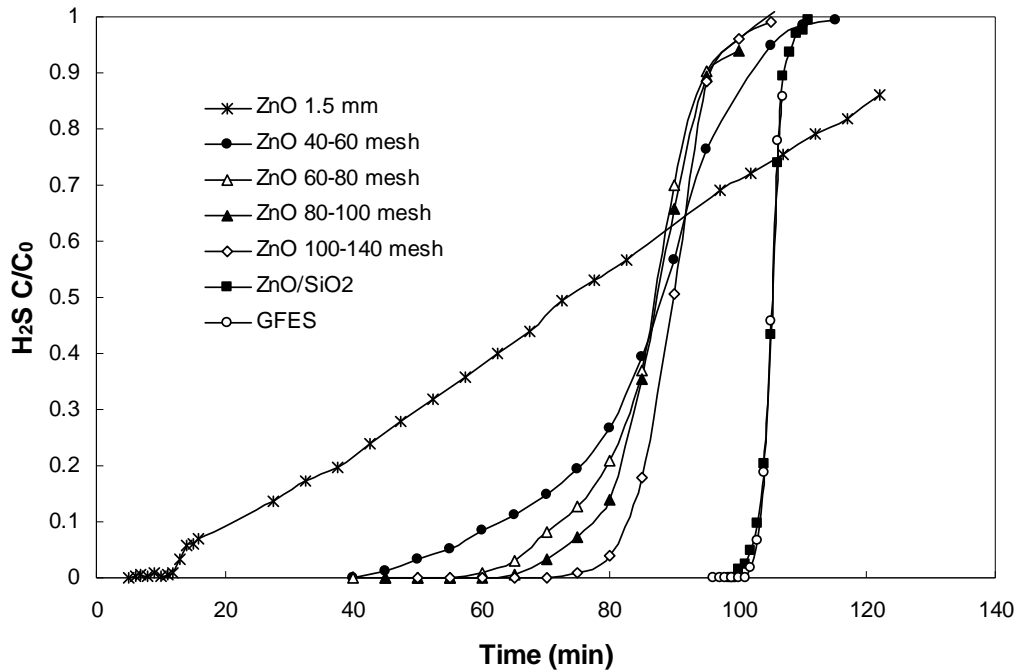
Figure V-4. Breakthrough curves of the commercial ZnO sorbent particles with different particle sizes, and breakthrough curve of ZnO/SiO_2 sorbent and glass fiber entrapped sorbent (GFES).

The results show the breakthrough curves shift to the right with the decrease in

particle size. This demonstrates an improvement in sorbent capacity by reducing

sorbent particle size. For example, a simple calculation suggests the ZnO particles of 1

mm average size demonstrated a saturation capacity of 0.28 g H_2S/g sorbent and a breakthrough capacity of 0.042 g H_2S/g sorbent; the particles of 100~140 mesh (105~149 μm) , 0.31 and 0.26 g H_2S/g sorbent respectively.   It is well known that using small particles can reduce pore diffusion resistance and increase the external surface area, making more ZnO accessible during the desulfurization.   Therefore, for the same type of sorbent, the saturation capacity increases with the reduction in particle size.   Similarly, small grain size can reduce the resistance of grain diffusion.   Grain diffusion is very slow especially at low temperatures.   For instance, at room temperature, H_2S can only access the ZnO on the outside layer with a 0.6 monolayer thickness (Baird *et al*., 1992). If the sorbent particles are small enough and the inside ZnO grains can be controlled at several nanometers, then theoretically all ZnO could be consumed by H_2S, and the breakthrough curve would appear as a step function at the theoretical saturation time. Although the nanosized ZnO particulates cannot be applied directly in the packed bed, the particulates could be supported on other particles of a reasonable size.   This concept is used in this paper to reduce the intra-particle mass transfer resistance that occurs in pellets of solid adsorbents used in packed beds.   Actually, through the impregnation process, nano-sized ZnO was dispersed on the silica particles to form ZnO/SiO_2 sorbent particles (Lu *et al*., 2005).

Particle size also affects the shape of breakthrough curves because the external surface area, α, and apparent rate constant, k_a, increase with the decrease in particle size

at an order of 1.39, as indicated by equations V-16, 17 and 20. As shown in **Figure V-4**, when the particle size decreases from 1 mm to 100-140 mesh (105~149 μm), the breakthrough curves become sharper, and the calculated lumped K value increases from 0.0003 s^{-1} to 0.0054 s^{-1}. By using nanosized ZnO grains impregnated on small SiO_2 support particulates, ZnO/SiO_2 and GFES significantly reduce the external mass transfer resistance, pore diffusion resistance and lattice diffusion resistance. Therefore, the breakthrough curves for the ZnO/SiO_2 and GFES shifted to the farthermost right side and demonstrated the sharpest breakthrough curve (K=0.0167 and 0.0215 s^{-1} respectively) and highest breakthrough capacity (0.35 g H_2S/g sorbent), which is 1.5 times higher than the commercial ZnO particles with similar size (80-100 mesh). **Figure V-4** also suggests that ZnO on the ZnO/SiO_2 and GFES demonstrated a utilization of ZnO (x) at 1% C_0 breakthrough above 93%.

Particle size (d_p) is also essential to the critical bed depth (z_c). Equation V-22 reveals that critical bed depth decreases with particle size at an order of 1.39. It is obvious that small particles will have less critical bed depth, and higher ZnO utilization (equation V-14). For example, if the particle size is reduced to 1/10 of original size, the critical bed depth will drop to 4 % of the original depth. In these experiments, the particle size was reduced from 40-60 mesh (250-400 μm) to 100-140 mesh (105-149 μm), and the calculated critical bed depth drops from 1.1 mm to 0.38 mm at 1% C_0 breakthrough. In logistic fuel processing units, the critical depth is usually much higher

than the values determined in this paper because of the presence of CO, CO_2 and water, large sorbent particle sizes, high face velocity, low breakthrough concentration, and severe channeling.

Small particle size can enhance the mass transfer rate and reduce the critical bed depth. However, small particles, like the 100-140 mesh particles, may be too small to be applied directly to packed bed reactors due to the high pressure drop and attrition; thus extrudates of larger sizes are widely used in most traditional approaches. A unique feature of microfibrous entrapped sorbent is the ability to utilize small particles. In microfibrous materials, particles between 30~300 μm can be entrapped in the sinter-locked microfibrous media . In this study, all the particles used were ZnO/SiO_2 sorbent particles (100-200 mm), which were also used in microfibrous entrapped sorbents as shown in **Figure V-2b**. The microfibrous technology offers the opportunity to utilize high efficiency catalyst/sorbent particles of small sizes without introducing penalties that would be present in conventional approaches.

V.4.4. Face Velocity Effects

In this study, all the ZnO/SiO_2 sorbents were tested at 400 ℃ with challenge gas of 2 vol.% H_2S-H_2. In the experiment "m:v", 0.1 g of prepared ZnO/SiO_2 sorbent was loaded in the reactor with a bed thickness of 2.2 mm, at a gas face velocity of 1.2 cm/s. In the following experiments, the amount of sorbent and face velocity were doubled at the same

time until the sorbent loading reached 0.8 g and face velocity reached 9.9 cm/s.   All of the packed beds in this set of tests had the same theoretical saturation time τ (or $t_{1/2}$) of 12 minutes, and the same residence time of 0.075 s.   The breakthrough curves are shown in **Figure V-5**.   Glass fiber entrapped sorbent containing 0.1 g of ZnO/SiO_2 sorbent was also tested at the velocity of 1.2 cm/s.   The sulfur capacities at 1 % breakthrough for all experiments are shown in **Figure V-6**.
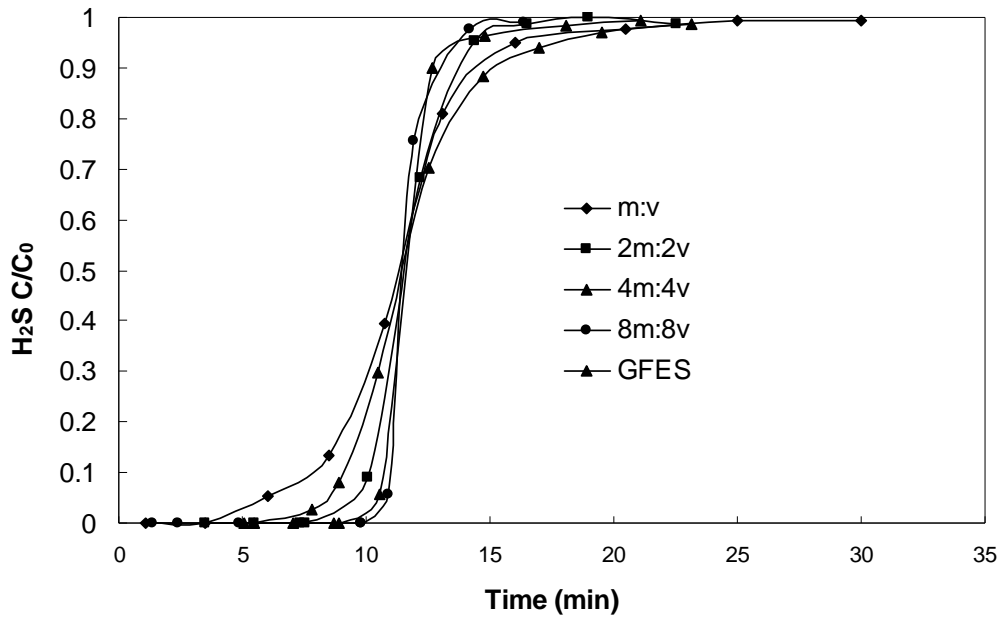
Figure V-5. Breakthrough curves of ZnO/SiO_2 at different face velocities.

All the breakthrough curves pass around the same point, which supports the consistency of the theoretical capacity.   Clearly, the breakthrough curves become sharper as the face velocity of challenge gas is increased.   For convenience, the breakthrough point was defined at 1% of inlet concentration C_0.   As shown in **Figure V-6**, the capacity at breakthrough increases significantly in the low face velocity range.

After the face velocity reaches 5 cm/s, the capacity slowly approached 0.36 g H_2S/g ZnO, about 90% of the theoretical capacity, which suggests that the unutilized ZnO before breakthrough was less than 10% and a further increase in challenge gas face velocity is not necessary for these thin bed tests.   The average reaction rate followed the same trend as capacity.   This could be explained using equations V-14 and 22.   Equation V-22 suggests that the critical bed depth increases with the increase in face velocity at an order of 0.39.   The experimental data confirmed this.   In **Figure V-5**, the critical bed depth for ZnO/SiO_2 sorbent particles at U=1.2 cm/s was calculated to be 0.14 cm; the one for same practices after U increased 8 times was 0.27 cm.   These results indicate the ZnO utilization (X) will decrease with the increase in face velocity if the bed depth z_t is maintained constant.   This phenomenon was observed by Novochinskii *et al*. (2004). However, in this paper, z_t was set to be proportional to U therefore unutilized ZnO of the accessible part (1-X) at breakthrough is proportional to $U^{-0.61}$ as predicated by equation V-22.   As a result, the breakthrough capacity increases with face velocity in the tests.

The breakthrough curve of glass fiber entrapped sorbents shows the capacity at breakthrough increases about 50 % compared with the experiment "m:V", though in both cases, the same type of sorbent (ZnO/SiO_2) with the same amount of ZnO was loaded. The only explanations for this improvement could be the enhancement of the glass fiber media.
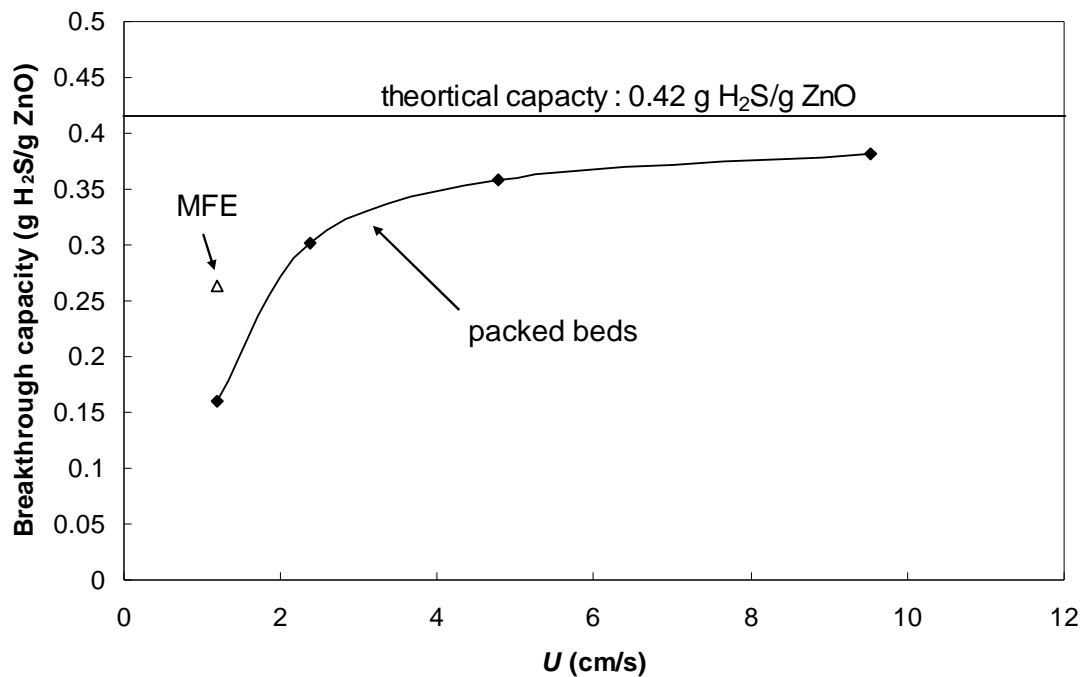
Figure V-6. Breakthrough capacities of ZnO/SiO_2 sorbent at different face velocities. Tested at 400 °C with the challenge gas of 2 vol.% H_2S in H_2.
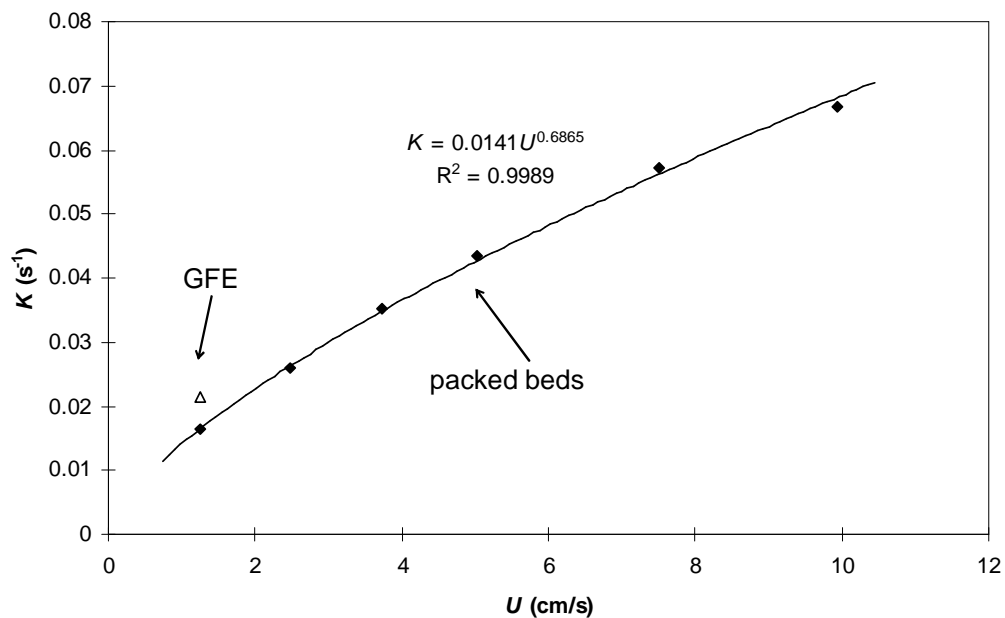
Figure V-7. Relationship between lumped K and face velocity. Tested at 400°C with challenge gas of 2 vol.% H_2S in H_2.

Lumped K values at different face velocities were obtained from breakthrough curves and are shown in **Figure V-7**. A linear regression suggests that lumped K increases with U at an order of about two thirds. MFES tested with the face velocity of 1.2 cm/s at 400 °C is also shown in **Figure V-7** for comparison. Compared with its packed bed counterpart at the same test conditions, microfibrous entrapped sorbents (GFES) demonstrated a sharper breakthrough curve with $K=0.022$ s^{-1}. The test result is 32 % higher than the K in packed bed of ZnO/SiO$_2$. Apparent rate constants (k_a) calculated from differential reactor analysis are listed in **Table V-2**. The relationship between lumped K and apparent rate constant k_a for packed beds is shown in **Figure V-8**. The linear relationship between K and k_a provides further support for equation V-12. The slope of $K \sim k_a$ curve is around 1.17×10^{-4}, and the calculated value of $\left(\phi \dfrac{C_{A0}}{\rho_c} \right)$ is 1.18×10^{-4}. These two values show exceptional agreement. Because of this relationship, it is safe to conclude that k_a also increases with face velocity U at an order around two-thirds. This result is close to the predication by equation V-20. According to classic mass transfer theory, the reactions in all the experiments in this section were controlled by the external mass transfer rate.

Table V-2. Apparent rate constants at different face velocities.

U	K	k_a
(cm/s)	(s^{-1})	(s^{-1})
1.2	0.016	135
2.5	0.026	217
3.7	0.035	296
5.0	0.043	370
7.5	0.057	488
9.9	0.067	562
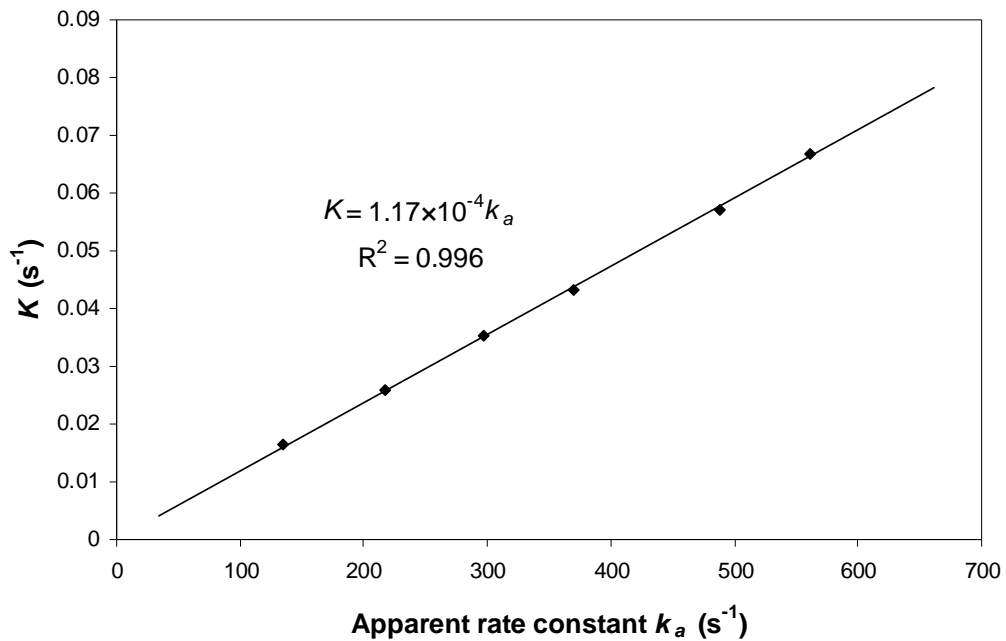
Figure V-8. Relationship between apparent rate constant k_a and lumped K. Tested at 400°C.

V.4.5. Dilution Effects

A series of experiments (series A) was carried out to investigate the effects of capacity density (ρ_c). In these experiments, sorbents were prepared with $Zn(NO_3)_2$ solutions of different concentrations. For example, for the experiment "2M", the

sorbent was prepared by impregnation of SiO_2 (100~200μm) in 2 mol/L $Zn(NO_3)_2$ solution. After impregnation, ZnO was calcined to produce a uniform dispersion on every particle in the packed beds. The details of these sorbents are listed in **Table V-3**. The packed beds in this series had different capacity densities (ρ_c), but they contained the same amount of ZnO (0.034 g). Every packed bed was tested with 2vol.% H_2S-H_2 at a face velocity of 1.2 cm/s at 400 °C. The breakthrough curves of the experiments are shown in **Figure V-9** and the K~$1/\rho_c$ plot is shown in **Figure V-11**, line A. The breakthrough curves in this series have different shapes; the one with less capacity density has a sharper breakthrough curve. K~$1/\rho_c$ plot suggests that lumped K is inversely proportional to the capacity density of a sorbent bed. The lower the capacity density, the larger K is. As the ρ_c approaches zero, K tends to infinity and the breakthrough curve becomes a step, which is exactly as expected. The good linear relationship between K~$1/\rho_c$ confirms the validity of equation V-12. The slope of K~$1/\rho_c$ curve is 2.01×10^{-5} and the calculated slope ($\phi k_a C_{A0}$) in equation 12 is 1.95×10^{-5} (in this calculation, k_a value of 135 s^{-1} was used-the apparent rate constant at face velocity of 1.2 cm/s in **Table V-2**). These two values are very close and this suggests the validity of equations V-11 and 12. Equations V-12 and 13 suggest that z_c remains constant at various capacity densities if the ZnO is uniformly dispersed on SiO_2 support particles and tested at the same conditions, as it was during this series of tests. However, z_t increases after dilution. As a result, the ZnO utilization increases after the uniform dilution.

Table V-3. Several sorbents prepared at different $Zn(NO_3)_2$ concentrations.

Test	$[Zn^{2+}]$ (mol/L)	ZnO wt.%	ρ_b (g/cm^3)	ρ_c (mol/cm^3)
2M	2	17.0	0.58	0.00123
1.5M	1.5	13.3	0.57	0.000931
1M	1	9.28	0.55	0.000626
0.5M	0.5	4.87	0.52	0.000315
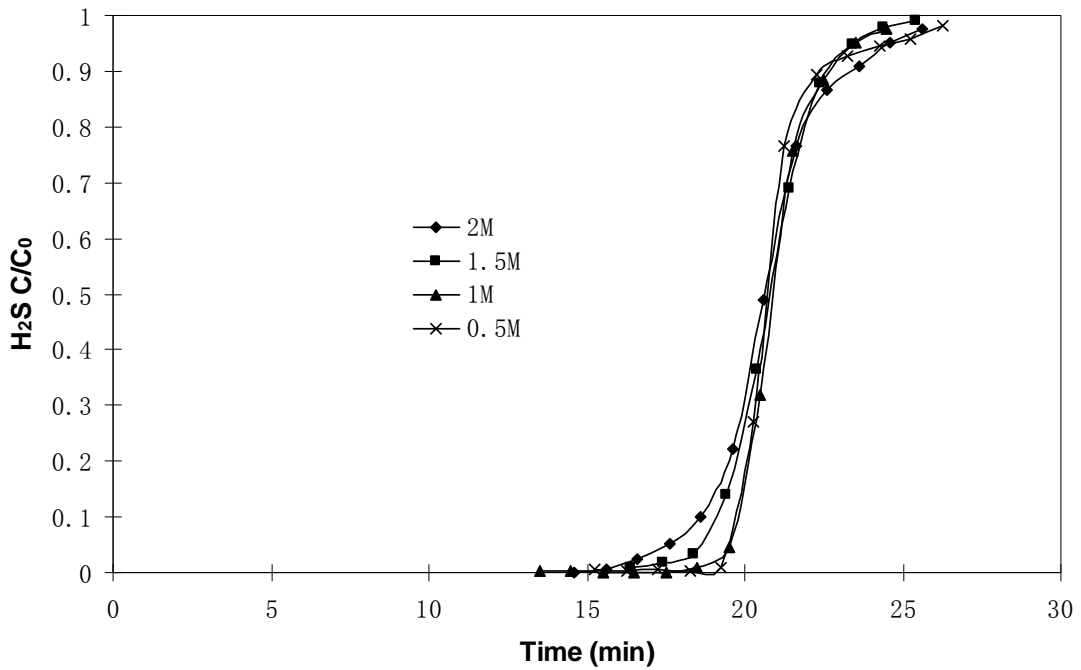
Figure V-9. Breakthrough curves of ZnO/SiO$_2$ sorbents (100-200 µm) at various ZnO loadings. Tested with 2 vol.% H$_2$S-H$_2$ at a face velocity of 1.2 cm/s at 400°C.
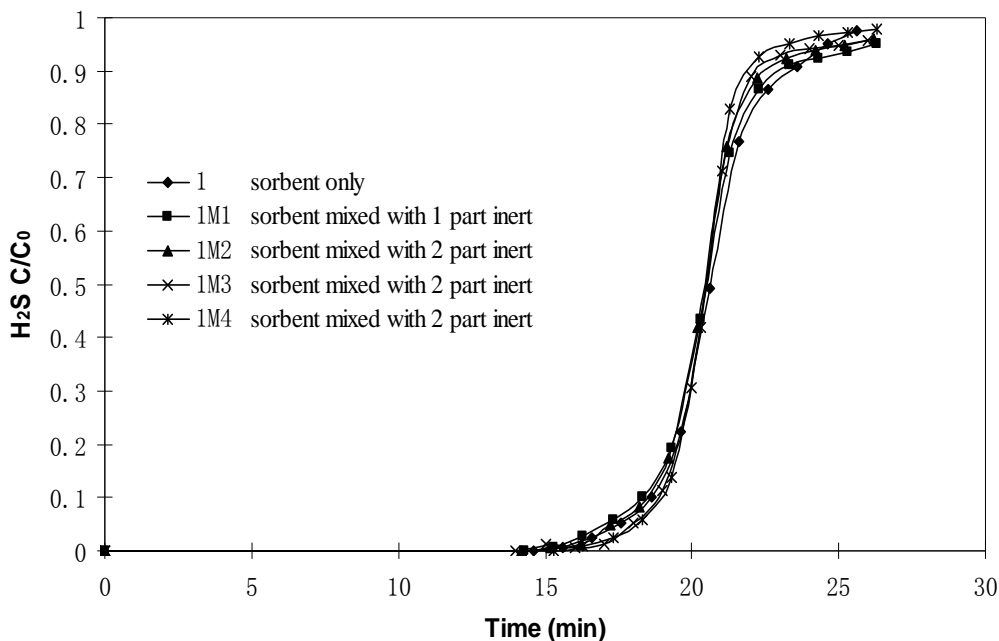
Figure V-10. Breakthrough curves of beds made of ZnO/SiO_2 sorbents (100-200 μm) and diluted by inert SiO_2 particles of the same size.Tested with 2 vol.% H_2S-H_2 at a face velocity of 1.2 cm/s at 400°C.
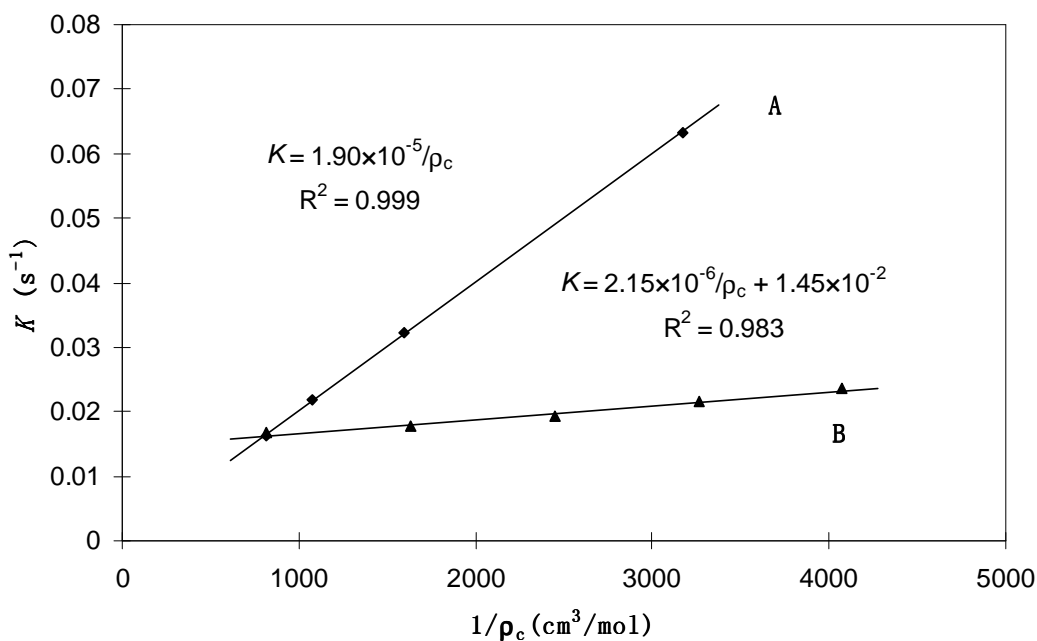
Figure V-11. Relationship between lumped K and molar capacity density of (A) packed beds of ZnO/SiO_2 sorbents (100-200 μm) with various ZnO loadings and (B) diluted packed beds of the ZnO/SiO_2 sorbents.

Another series of experiments (series B) has been conducted to discuss the effect of dilution by inert particles at same face velocity and temperature as in series A. The experiments in this series demonstrate that reduction of axial dispersion effects on the fixed bed adsorbent performance. In the following 5 experiments, every packed bed contained 0.2 g ZnO/SiO$_2$ (with 0.034 g ZnO) sorbent, which is exactly the sorbent used in the earlier experiment named "2M". The ZnO was nano-dispersed on the SiO$_2$ particles (dia. 100-200 μm). In the first experiment "1", the packed bed contained only the sorbent particle; for the rest of the experiments, the sorbent particles were well mixed with inert particles (SiO$_2$, dia. 100-200 μm). For example, 1M3 contained 1 volume part of sorbent particles and 3 volume parts of inert particles. In this series of experiments, ZnO/SiO$_2$ particles were well mixed with SiO$_2$. The breakthrough curves of all the experiments are shown in **Figure V-10** and the $K \sim 1/\rho_c$ curve is shown in **Figure V-11**. **Figures V-10** and **11** clearly indicate that all the breakthrough curves have similar shapes and lumped K values, which means the addition of inert particles, and corresponding increase in the bed Peclet number and reduction of axial dispersion, did not significantly change the performance of the packed bed. The effects of dilution by inert particles could be explained using equation V-12. After dilution the k_a (actually α and $k_a = k_c \alpha$) and ρ_c dropped by a factor of n, and the K value should remain unchanged. However, a slow incensement in the K value in the experiments was observed. It may result from the non-ideality of mixing and inertness of SiO$_2$ particles. SiO$_2$ particles

with high surface area employed in the study may not be ideally inert, especially since a large amount of SiO_2 was utilized in the diluted packed beds. These experiments demonstrate that a diluted packed bed has the same shape breakthrough curve as that of a SiO_2 packed bed, showing that dispersion effects are not responsible for the improved K values.

V.4.6. Concentration Effects

In this section, the effects of inlet H_2S concentration (C_0) are discussed. Breakthrough tests were conducted on a packed bed of 0.8 g ZnO/SiO_2 (17.0 wt.% ZnO) at inlet challenge concentration C_0 of 20000, 9800, and 4950 ppmv respectively. For a low concentration test at 321 ppm, 0.24 g of ZnO/SiO_2 was loaded and tested at the same experiment conditions. In this test, H_2S was analyzed by the Varian 3800GC equipped with a pulse flame photometric detector with a sulfur filter (PFPD-S). All breakthrough curves, except the one tested at 321 ppmv are shown in **Figure V-12.**

In **Figure V-12**, the breakthrough curves become sharper at higher challenge concentrations, while the saturation time becomes shorter. K values were calculated for all the tests and the relationship between lumped K and inlet challenge gas concentration C_{A0} is demonstrated in **Figure V-13**. The linear relationship indicates K is proportional to the challenge gas concentration C_{A0}, which is predicted by the model presented earlier.

The slope of $K \sim C_{A0}$ curve is 118843 and the calculated slope ($\phi \cdot k_a / \rho_c$) in equation V-12 is 120766 (In this calculation k_a value of 370 s^{-1} was used-the apparent rate constant at face velocity of 5.0 cm/s in **Table V-2**). These two values are very close and this suggests the validity of equations V-11 and 12. Equation V-12 suggests that lumped K decreases when C_{A0} decreases. Lower capacity density is required to maintain the sharpness of a breakthrough curve at low challenge concentrations.
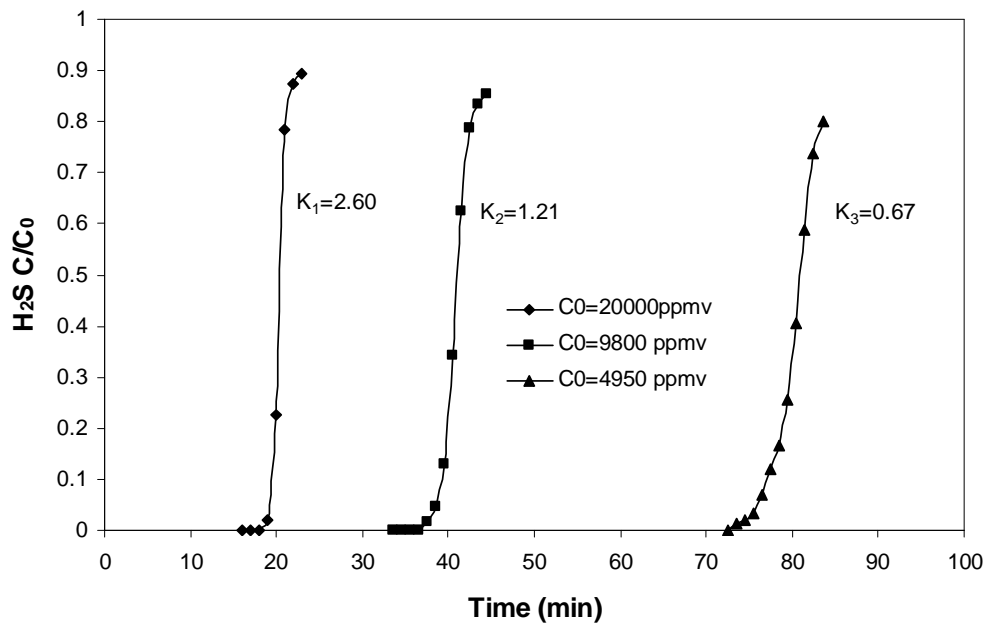
Figure V-12. Breakthrough curves of packed beds tested at different inlet H$_2$S concentrations. Each bed contained 0.8 g ZnO/SiO$_2$ sorbent (100-200 µm) and was tested at a face velocity of 5.0 cm/s at 400 °C.
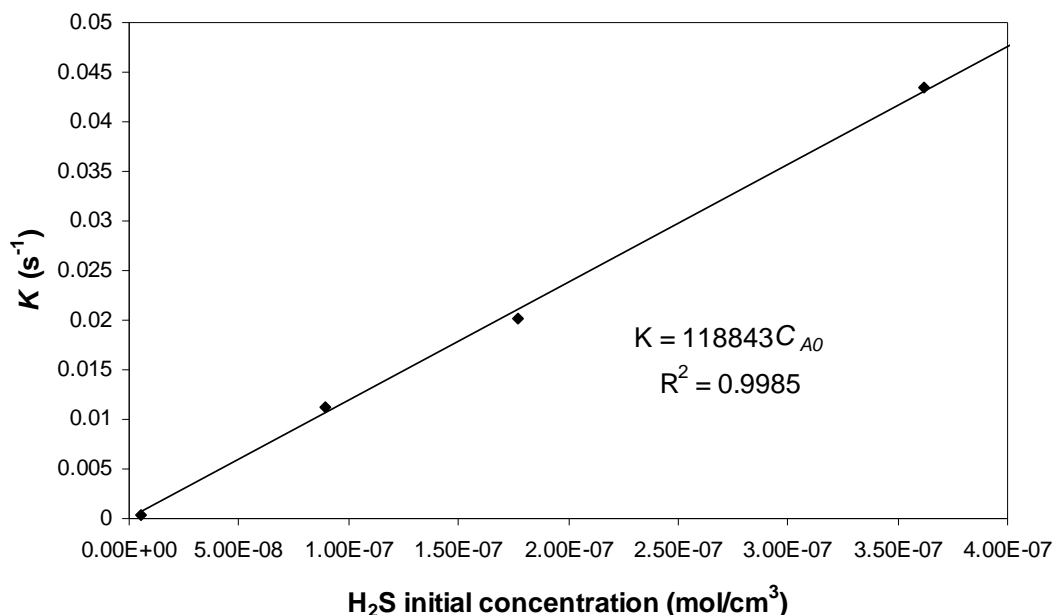
Figure V-13. The relationship between lumped *K* and challenging gas concentration. In each experiment, 0.8 g ZnO/SiO$_2$ was tested at a face velocity of 5.0 cm/s at 400°C.

V.4.7. Void Fraction and Microfibrous Media Effects

In the earlier discussion, equations V-11 and 12 have been verified experimentally. Using equation V-12, most phenomena associated with microfibrous media can be explained clearly. Microfibrous entrapped sorbent has two unique features: micro-sized fibers and high void fraction. The desulfurization performance of microfibrous entrapped sorbent will be discussed in detail based on these two features.

Equations V-23-28 are applied to discuss the effects of void and microfibrous media. A comparison between a packed bed of ZnO/SiO$_2$ sorbents, a void diluted packed bed of ZnO/SiO$_2$ sorbents and glass fiber entrapped sorbent is shown in **Table V-4**.

179

Table V-4. Influence of void fraction ϕ and microfibrous media.

	Packed bed	Packed bed (void diluted)	Microfibrous entrapped sorbents
ϕ	0.4	0.75	0.75
ρ_c (mol/cm^3)	0.0012	0.00042	0.00042
d_p (μm)	150	150	150
$\overline{d}_s$ (μm)	150	150	63
k_c/k_{cp}	1	0.30	0.42
k_a/k_{ap}	1	0.16	0.22
K/K_p	1	0.81	1.13
K/K_p (experimental)	1	-	1.32

If influence of micro-fibers is ignored, microfibrous entrapped sorbent could be treated as a packed bed with high voidage. Since the packed bed and the void-diluted packed bed are made of the same sorbent particles, the comparison between these two will reveal the effect of void fraction. Equation V-20 suggests the apparent rate constant k_a drops with the increase of ϕ. **Table V-4** reveals that the k_a in the void-diluted packed bed (ϕ=0.75) is only 16 % of that of the packed bed (ϕ=0.4). However, due to the low capacity density ρ_c in the diluted bed, the lumped K value reaches 81% of that of the packed bed.

Since the ϕ and ρ_c are the same in the void-diluted packed bed and microfibrous entrapped sorbents, the comparison between these two reveals the effects of microfibrous media. In microfibrous entrapped sorbents, a_f and a_p are 0.12 and 0.88 respectively. Therefore, the $\overline{d}_s$ is 63 μm for microfibrous entrapped sorbents. The

comparative results in **Table V-4** suggest k_a and K of microfibrous entrapped sorbents is 40% higher than for the void-diluted packed bed, which indicates the microfibrous media improved mass transfer rate due to the reduced dimensionality. However, **Table V-4** also shows that its k_a is still lower than that of the packed bed, due to the high void fraction in it. The lumped K is 1.13 times larger than that of the packed bed because of the low capacity density ρ_c in the microfibrous entrapped sorbent. This value is less than the experimental value of 1.32 for K_m/K_p. Another influence of the microfibers is to promote plug flow through the MFES. The fibers reduce the dimensionality in the bulk of the bed resulting in decreased axial dispersion in MFES compared to packed beds containing particles of the same size. However, this influence has not been included in this simple model. The discussion above may be used to explain improvement of microfibrous media. However, the functions of microfibrous media are not fully revealed yet; other research efforts are being made to understand microfibrous media from different points of view (Duggirala *et al*., 2006; Kalluri *et al*., 2006).

V.4.8. Composite Bed and Multi-stage Reactor Design

One application of the microfibrous entrapped sorbent is to use it as a polishing layer to extend the service time of a packed bed with reduced reactor size. In this section, a thin polishing layer of microfibrous entrapped sorbents was put at the downstream end of a thick packed bed made of extrudates to form a composite bed. The reactor was a

quartz tube with a diameter of 2.1 cm. Detailed information of the polishing layer, packed bed and composite bed is listed in **Table V-5**, and the breakthrough curves are shown in **Figure V-14**.

Table V-5. Configuration and performance of the polishing layer, packed bed and composite bed at different breakthrough concentrations.

Test	Bed thickness (cm)	Sorbent Weight (g)	ZnO (g)	Breakthrough Time (min.)		Breakthrough capacity (g S/ g sorbent)	
				@ 1 ppm	@ 1%C_0	@ 1 ppm	@ 1% C_0
Polishing layer	0.4	1	0.2	~9.5	11	0.046	0.054
Packed bed	2.2	10.6	9.5	94	156	0.043	0.071
Composite bed	2.6	11.6	9.7	299	305	0.125	0.128
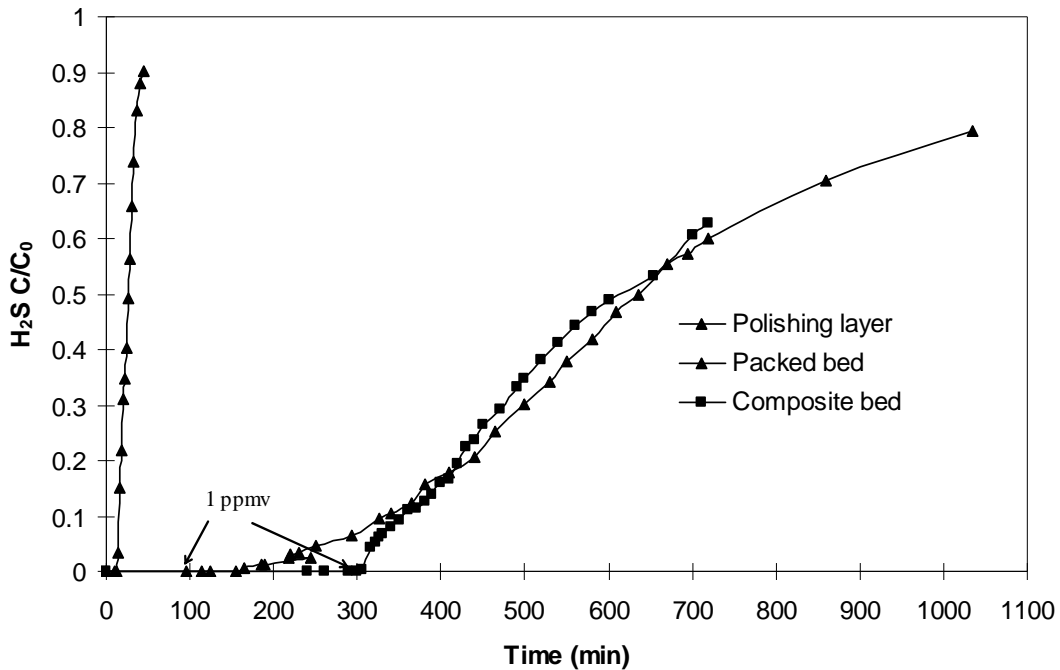
Figure V-14. Breakthrough curves of the polishing layer, packed bed and composite bed, tested at 400 °C with a challenge gas of 4815 ppmv H_2S-H_2 at a face velocity of 8.1 cm/s.

As expected, the polishing layer had a very sharp breakthrough curve, while the packed bed had a shorter breakthrough time than the composite bed. It was also observed that the breakthrough curve of the composite bed initially was almost as sharp as that of the polishing layer. The calculated apparent rate constants also confirmed this, see **Table V-6**. The lumped K values of packed bed and polishing layer are $4.08{\times}10^{-4}$ and $1.39{\times}10^{-2}$ s^{-1}, respectively. The microfibrous entrapped ZnO demonstrated 34 times higher K value than the packed bed made of ZnO extrudates, while the initial lumped K of composite bed is $4.02{\times}10^{-3}$ s^{-1} which is comparable to that of polishing layer and is 10 times larger than that of the packed bed. As the reaction took place, ZnO in the polishing layer was exhausted and the breakthrough curve of the composite bed began to take the shape of the packed bed. The critical bed depth (z_c) for each breakthrough curve was calculated and is shown in **Table V-6**. The comparison of z_c shows that the polishing layer made of MFES had the smallest z_c as expected, and composite bed design significantly reduced z_c especially at low breakthrough concentrations. For example, the critical bed depths for the packed bed and the composite bed at 0.1 ppm breakthrough are 4.03 cm and 2.17 cm receptively. Therefore, using MFES as polishing layer can improve the ZnO sorbent utilization especially for reactors with small size (small reactor length z_t) according to equation V-14.

Table V-6. Calculated values of lumped K and τ for the polishing layer, packed bed and composite bed.

Test	K (s^{-1})		τ (min.)		z_c (cm)	
	initial	final	initial	final	(1 ppmv)	(0.1 ppmv)*
Polishing layer	1.33×10^{-2}	-	18.3	-	0.149	0.189
Packed bed	4.08×10^{-4}	1.10×10^{-4}	370	630	1.84	4.03
Composite bed	4.03×10^{-3}	1.15×10^{-4}	327	595	1.36	2.17

* predicated by extrapolating the breakthrough curves using equation V-10.

The composite bed is functionally an integrated two-stage reactor. The first stage is usually a packed bed of extrudates which is able to reduce bulk H_2S to a low concentration. The packed bed may not meet the requirements of fuel cell applications, but it functions as a sulfur reservoir. The second stage is the polishing layer, which usually applies to specialized sorbents. The earlier discussion suggests that the second stage in a composite bed, made of highly efficient sorbent, determines overall kinetic behavior of the bed before breakthrough. The sorbents in this stage are not required to have a very high capacity; however, it should have high efficiency to remove H_2S from the gas stream from the first stage to a lower concentration to meet the fuel cell requirements. Because microfibrous entrapped sorbents have extremely high efficiency (large K value) and low capacity, they are the promising candidates employed in the second stage to miniaturize the desulfurization units as well as other fuel clean-up units in logistic fuel cell system.

V.5. Conclusions

The modified Amundson model was successfully used to characterize the shape of breakthrough curves at various desulfurization conditions. This model suggests that the shape of a breakthrough curve can be characterized in terms of lumped K. Lumped K in turn is determined by the characteristics of the packed bed (such as void fraction and capacity density), process dynamics such as apparent rate constant and initial H_2S concentration. Lumped K is an index of the contacting efficiency and desulfurization performance of sorbents. A large K value means a sharp breakthrough curve, a small critical bed depth and a high ZnO utilization at the same test conditions. Fast mass transfer rates and low sorbent loadings are critical to reduce the H_2S concentration to ppm or sub-ppm levels. Because of the severe intra-particle mass transfer resistance and high capacity density, packed beds made of traditional extrudates usually require large reactor sizes to achieve sub-ppm level breakthrough. In MEFS, the microfibers dominate the flow field reducing the mass transfer film thickness, and enhance the external mass transfer rate. The high void fraction ϕ in MEFS results in a lower apparent transfer rate k_a, and yields a low capacity density (ρ_c). These characteristics improve the lumped K value and make the overall performance of MFES much better than extrudates for low concentration H_2S removal. Besides low concentration applications, microfibrous entrapped sorbents can also be applied as polishing layers in composite beds or other two-stage reactor designs. For applications requiring low breakthrough thresholds, the addition of MFES polishing

layers can significantly improve the overall contacting efficiency and service time of the packed bed.

Notation

a	solid volumetric percentage	
A	cross section area	cm^2
C_1	dimensionless constant	
C_2	dimensionless constant	
C_0	initial H_2S concentration	ppmv
C_A	H_2S concentration in challenge gas	mol/cm^3

C_{A0} initial challenge H$_2$S molar concentration   mol/cm^3

C_b breakthrough concentration   ppmv

d_f fiber diameter   μm

d_p particle size   μm

$\overline{d}_s$ average characteristic size   μm

D_{AB} diffusivity   cm^2/s

J_d Colburn J mass transfer factor

k_2 second order reaction rate constant   cm^3/mol s

k_a apparent reaction rate (void volume based)   s^{-1}

k_c external mass transfer rate   cm/s

K lumped shape factor of breakthrough curve   s^{-1}

m_0 total mole of accessible ZnO in packed bed   mol

Mz molecular weight of ZnO   g/mol

n dilution factor

Re particle Reynolds number $\mathrm{Re} = \dfrac{d_p \rho_a U}{\mu}$

$Re"$ particle Reynolds number (surface area based) $\mathrm{Re}" = 6\dfrac{\rho_a U}{Sa\mu}$ and $\mathrm{Re}" = \dfrac{\mathrm{Re}}{(1-\phi)}$

for spherical particles

Sa	specific interfacial area of entire bed		cm^2/cm^3
Sc	Schmidt number	$Sc = \left(\dfrac{\mu}{\rho_a D_{AB}} \right)$	
Sh	Sherwood number	$Sh = \dfrac{k_c \cdot d_p}{D_{AB}}$	
t	onsite time		min
U	face velocity		cm/s
U_i	interstitial gas phase velocity		cm/s
x	overall ZnO utilization		
X	ZnO utilization of the accessible ZnO		
y	ZnO loading of the sorbent		
z	distance into the bed		cm
z_c	critical bed depth		cm
z_t	bed depth		cm
z_i	depth of inactive layer		cm

Greek letters

α	specific surface area of sorbent particles per unit bed volume	cm^2/cm^3
ϕ	void fraction	

φ	shape factor	
μ	gas viscosity	g/cm min
ρ_a	gas density	g/ cm^3
ρ_b	packing density of packed bed	g/ cm^3
ρ_c	molar capacity density	mol of H_2S/cm^3 packed bed
τ	saturation time	min

Subscript for a, K, k_a, ϕ, φ, γ and ρ_c

m   microfibrous entrapped sorbent

p   packed bed

CHAPTER VI.

CHARACTERIZATION OF THE REACTIONS BETWEEN ZINC OXIDE AND REFORMATES USING HIGH CONTACTING EFFICIENCY SORBENTS

Abstract

A novel ZnO based sorbent with minimized mass transfer resistance was applied to investigate the intrinsic behavior of the reactions between ZnO and reformates. The influences of gases such as CO, CO_2, and H_2O on H_2S removal and COS formation were examined. Both CO and CO_2 react with H_2S to form carbonyl sulfide (COS). The mechanisms of COS formation via two different pathways are discussed. CO reacted with H_2S to form COS homogeneously while CO_2 reacted with H_2S heterogeneously on the surface of ZnS. The COS formation by CO and CO_2 was suppressed by the presence of H_2 and water. Water also severely hindered the reaction between ZnO and H_2S, and H_2S breakthrough time was significantly decreased. At a low water concentration, the homogeneous COS formation determines the total sulfur breakthrough time. At high water concentrations, total sulfur breakthrough time was controlled by H_2S breakthrough. Capacity loss due to COS formation and adsorption of water was

observed.   Novel sorbents designs and process designs are required to improve the effectiveness of the desulfurization processes.

Keyword: H_2S, ZnO, COS, reformates, desulfurization, breakthrough

VI.1. Introduction

Logistic fuel cell power systems receive increasing attention due to their high energy efficiency.   A potential drawback to the systems is the use of precious metals as electrodes and catalysts, which are easy to be poisoned.   Thus, it is necessary to develop high efficiency fuel clean-up technologies to remove sulfur compounds from liquid or gas fuel streams.   Current technologies can successfully remove sulfur compounds from several thousand ppm to sub-ppm levels (Lu *et al*., 2005; Novochinskii *et al*., 2004; Slimane and Abbasian, 2000a; Westmoreland and Harrison, 1976; Tamhankar *et al*., 1986; Sasaoka, 1994b) using metal oxide based sorbents.   Due to the high sulfur capacity and favorable sulfidation thermodynamics at moderate temperatures, zinc oxide (ZnO) based sorbents are widely applied in gas phase desulfurization to remove sulfur species such as H_2S from gas streams.   ZnO can also be stabilized by addition of Fe_2O_3 (Gangwal *et al*., 1989; Gupta *et al*., 1992) or TiO_2 (Lew *et al*., 1989; Woods *et al*., 1990) for the applications at elevated temperatures.

The gas streams (reformates) from reformers usually contain H_2, CO, CO_2, water, low molecular weigh hydrocarbons, and sulfur species such as H_2S and COS.   The

191

reactions between ZnO and reformates has complications such as the reaction between ZnO and H_2S, water gas shift reaction (WGS), COS formation in the presence of CO and CO_2, and ZnO reduction. The reactions between ZnO and H_2S in the H_2S-H_2-CO-H_2O–CO_2-N_2 system were characterized by Sasaoka *et al*. in 1994. The sorbents utilized in their study were ZnO pellets around 1 mm with a surface area of 3.2 m^2/g. The gas face velocity through the reactor was 5.3 cm/s at 500 °C. Under these test conditions, the reaction process may be dominated by external and/or intra-particles mass transfer resistance; therefore, their experimental results may not reveal the intrinsic behavior of these reactions. They found that COS was not as active as H_2S to react with ZnO (Sasaoka *et al*., 1996). They also observed that ZnS had catalytic activity to convert COS to H_2S according to the following reaction (Sasaoka *et al*., 1995):

$$2COS+H_2+H_2O= 2H_2S+CO+ CO_2 \qquad\qquad (1)$$

The Center for Microfibrous Material Manufacturing (CM^3) at Auburn University has developed supported ZnO sorbent (ZnO/SiO_2) for PEM fuel cell applications. These sorbents containing supported nano-sized ZnO grains in the pores of SiO_2 support particulates (100-200 μm) have high BET surface areas and high porosities. These characteristics of the sorbent literally eliminate the intra-particle mass transfer resistance including pore diffusion and lattice diffusion. As a result, the sorbents are able to achieve multi-log sulfur removal within a thin, fixed bed of several millimeters thickness while achieving an overall ZnO utilization above 90% (Lu *et al*., 2005). In this study,

the intrinsic behavior of the reactions taking place in the desulfurization for reformates (H_2S-H_2-H_2O-CO-CO_2 system) was investigated by analyzing the breakthrough curves of packed beds of ZnO/SiO_2 sorbents at 400 °C.

VI.2. Experimental

Chemicals: If not otherwise stated, all gases in this work were purchased from Airgas Inc.   The sources of H_2S were 2 vol.% H_2S-H_2 and pure H_2S.   Other challenge gases at various H_2S concentrations, i.e., 4000 ppmv and 1.3 vol.%, were diluted from these two H_2S sources by adding other gases such as CO (>99.0 vol.%, Sigma-Aldrich), CO_2, H_2, and He.   Reformates containing H_2 (~40 vol.%), CO_2 (~20 vol.%), CO (10 vol.%) and water (~30 vol.%) was prepared by mixing single gas compounds together.

ZnO/SiO_2 sorbent preparation: ZnO/SiO_2 contains 17 wt.% of ZnO supported on SiO_2 (100-200 µm) fine particles.   The sorbent was prepared by incipient wetness impregnation at room temperature using $Zn(NO_3)_2$ (Fisher Scientific, Reagent grade purity >98%) solution (2 mol/L) as precursor followed by natural drying and calcination at 450 °C.   The ZnO loading was quantified by both mass balance and ICP analysis. Detailed sorbents preparation procedures were described elsewhere (Lu *et al.*, 2005).

Experimental setup and procedure: The experiment setup is shown **Figure VI-1**. All gas flows were controlled by mass flow controllers. H_2S source gas was introduced to reactor by 1/8" Teflon tubing.   Other gases were introduced to the reactor in stainless

steel tubing.   Water was introduced to the gas flow by passing He, H_2, or CO through a

vaporizer with temperature controller, and was carried in a 1/8" stainless steel tubing

wrapped with a heating tape.   The water in the vaporizer was pre-distilled and was

heated to 100 °C to remove oxygen.
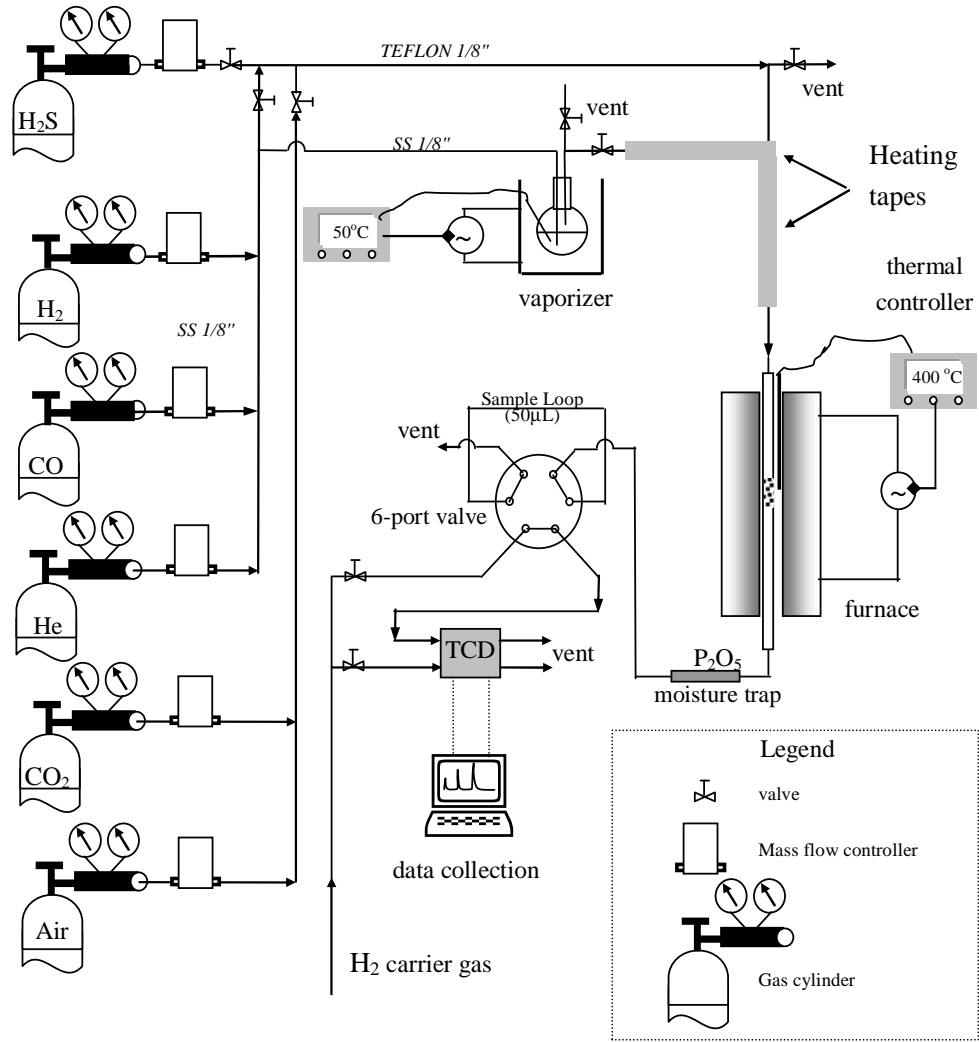
Figure VI-1. Experimental setup.

The reactor employed was a quartz tube (0.99 cm I.D.).   After loading the sorbents,

air (100 ml/min) was passed through the reactor before the temperature reached the set

point of 400 °C.   Next, helium (100 ml/min) flowed through the reactor for ten minutes

to eliminate oxygen in the reactor, which may introduce side reactions such as sulfide

oxidation.   Then, H_2 passed through the reactor for another 10 minutes to stabilize the

temperature profile along the reactor.   Finally, a challenge of various H_2S concentration

passed through the reactor at the same flow rate as H_2.   The outlet H_2S concentrations

were analyzed by a Varian GC-3800 with a TCD detector (H_2 as carrier gas).   The gas

chromatograph (GC) was able to measure the H_2S concentration down to 200 ppmv

precisely; COS, 20 ppmv.   Gas samples were injected into the GC every 3 minutes by a

programmed 6-port-valve with a sampling loop of 50 μL after commencing the

experiment.   In this paper, breakthrough concentration was defined at 40 ppmv, which

corresponds to 1 % of initial challenge gas concentration.   The breakthrough times were

read from the breakthrough curves.

In this study, each individual compounds in reformates were investigated first,

followed by multi-compound systems. C_1-C_3 hydrocarbons were considered inert and

thus not investigated.   Unless otherwise stated, each experiment challenged 0.5 g

ZnO/SiO$_2$ with 4000 ppmv H_2S at 9.9 cm/s (GHSV=13900 h^{-1}) at 400 °C.   The

stoichiometric saturation time of the packed beds was calculated to be 31.6 minutes.

The equilibrium constants of reversible reactions were calculated using HSC 3 software.

VI.3. Results and Discussion

The sharpness of breakthrough curves can be used as an index of the apparent reaction rate (Amundson, 1948; Klotz, 1946; Yoon and Nelson, 1984) given constant challenge gas concentration tested with the same sorbent at the same amount. For the sorbents containing the same amount of ZnO/SiO_2 sorbent tested in different challenge gases , it is easy to reach a conclusion that the one with shaper breakthrough curve and longer breakthrough time should have a faster reaction kinetic, or vice-versa. For example, if the addition of a gas compound significantly broadens H_2S breakthrough curve, then it must decelerate the reaction between ZnO and H_2S.

VI.3.1. H_2S-H_2 system

Hydrogen is the main component in reformates, usually in the range of 40~60 vol.%. According to Sasaoka (1994b), H_2 may inhibit the reaction between ZnO and H_2S at low temperatures and accelerate it at high temperatures. In this study, desulfurization performances of ZnO/SiO_2 at various H_2 concentrations are shown in **Figure VI-2**. The experimental results are different from the observations of Sasaoka. **Figure VI-2** suggests that H_2 at low concentrations has little effects on the desulfurization performance of ZnO/SiO_2. All breakthrough curves at H_2 concentrations in the range of 20~60 vol.% are overlapped with each other. The primary desulfurization reaction, the reaction between ZnO and H_2S, takes place according to reaction 2.

ZnO+H$_2$S=ZnS+H$_2$O   (2)

However, the sorbent demonstrates a sharper breakthrough curve and less capacity at 80 vol.% H$_2$ than at low H$_2$ concentrations, which means H$_2$ accelerates the reaction 2. The first possible reason is the ZnO reduction at high H$_2$ concentrations. According to Sasaoka (1994a, 1994b), zinc especially zinc vapor generated in ZnO reduction accelerates desulfurization reaction (reaction 3).

Zn+H$_2$S=ZnS+H$_2$ (3)

Sasaoka (1994b) observed the similar phenomenon at 500 °C in the tests on bulk ZnO sorbents. In ZnO/SiO$_2$ sorbent, the grain size of ZnO is around 5 nm. At this size, the ZnO was easy to be reduced and vaporized than zinc in bulk form; therefore, the desulfurization reaction was accelerated. The zinc vapor may introduce Zn loss under the test conditions. However, no zinc metal deposition was observed in this study.

Another possible reason for capacity lose is that high concentration H$_2$ tends to prevent H$_2$S from decomposing. In the other tests at low H$_2$ concentrations, yellowish rings of sulfur deposited on the walls of quartz tube were observed. This phenomenon was not observed at 80 vol.% H$_2$. As a result, the breakthrough curves at low H$_2$ concentrations demonstrated larger capacities than that at 80 vol.% H$_2$ due to element sulfur formation.

As shown in **Figure VI-2**, the H$_2$S breakthrough time in the test of 4000 ppmv H$_2$S-20 vol.% H$_2$-He was 28 min; the saturation time based on the t$_{1/2}$ concept (the time to

197

reaches the 50% of the inlet concentration) was 31.5 min. These results suggest the ZnO in ZnO/SiO_2 was completely accessible and ZnO utilization was 90% at breakthrough. Further increase in face velocity will have little effects on the shape of breakthrough curves. Thus, the breakthrough behaviors described in this study could be considered as close approximations to intrinsic reaction characteristics.
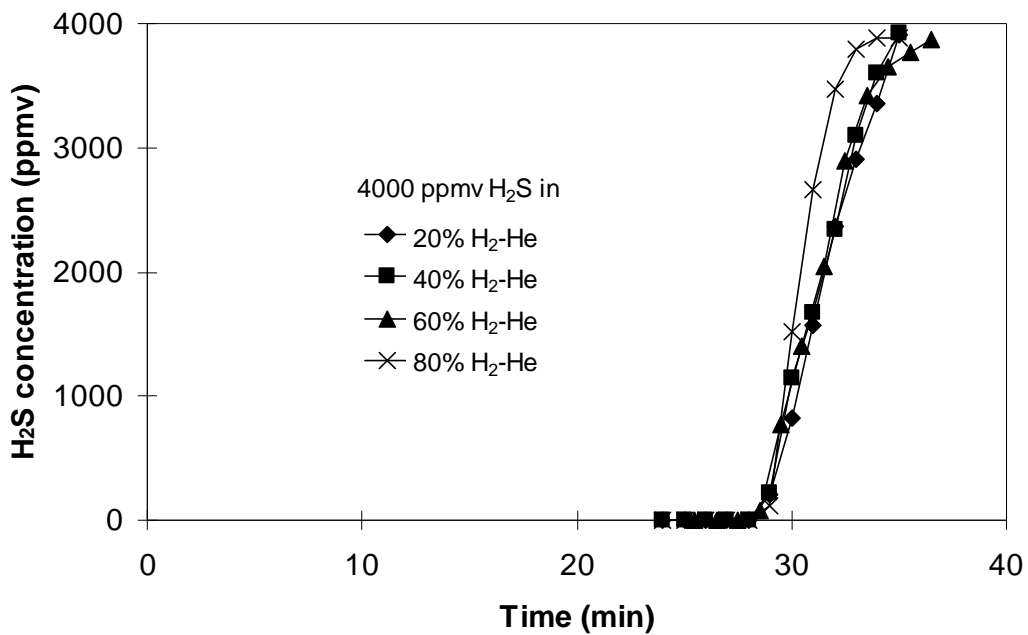
Figure VI-2. Effects of H_2 on H_2S breakthrough curves.

VI.3.2. H_2S-CO-H_2 system

CO has strong influences on the reaction between ZnO and H_2S according to Sasaoka (1994b). It also reacts with H_2S to form COS according to reaction 4.

$$CO + H_2S = COS + H_2 \tag{4}$$

Considering the similarity between sulfur and oxygen atoms, reaction 4 is analogous to the well-known water gas shift reaction (WGS) outlined in reaction 5.

$$CO+H_2O=CO_2+H_2 \tag{5}$$

Reaction 4 is a reversible reaction with an equilibrium constant of 0.0363 at 400 °C. Although this equilibrium constant is much lower than that of WGS (12.4), it is still critical for sulfur species requirements for fuel cell applications such as PEM fuel cells.

COS can also be captured by ZnO according to reaction 6.

$$COS+ZnO=ZnS+CO \tag{6}$$

Reaction 6 is the secondary desulfurization reaction in this study. According to Sasaoka *et al*. (1996), it is a slow reaction.
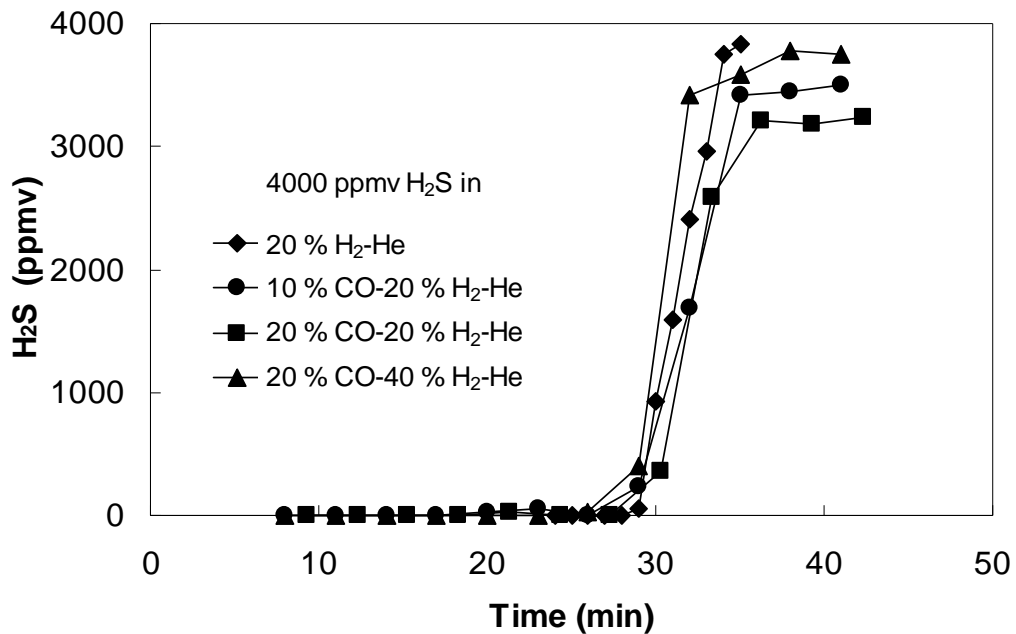
Figure VI-3. Effects of CO on H_2S breakthrough curves in the presence of H_2.
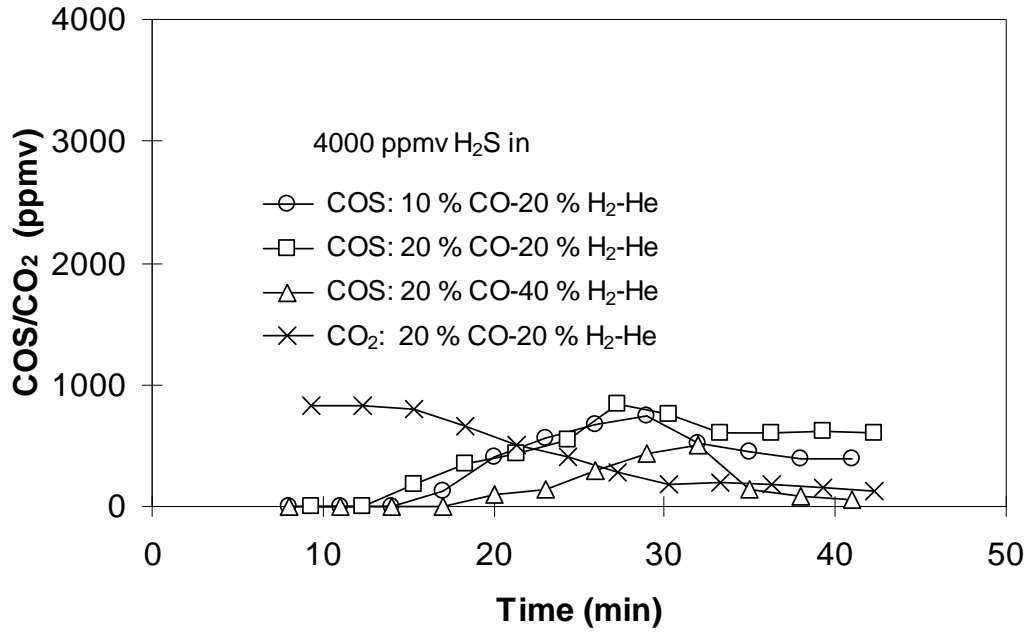
Figure VI-4. Effects of CO on COS formation in the presence of H_2.
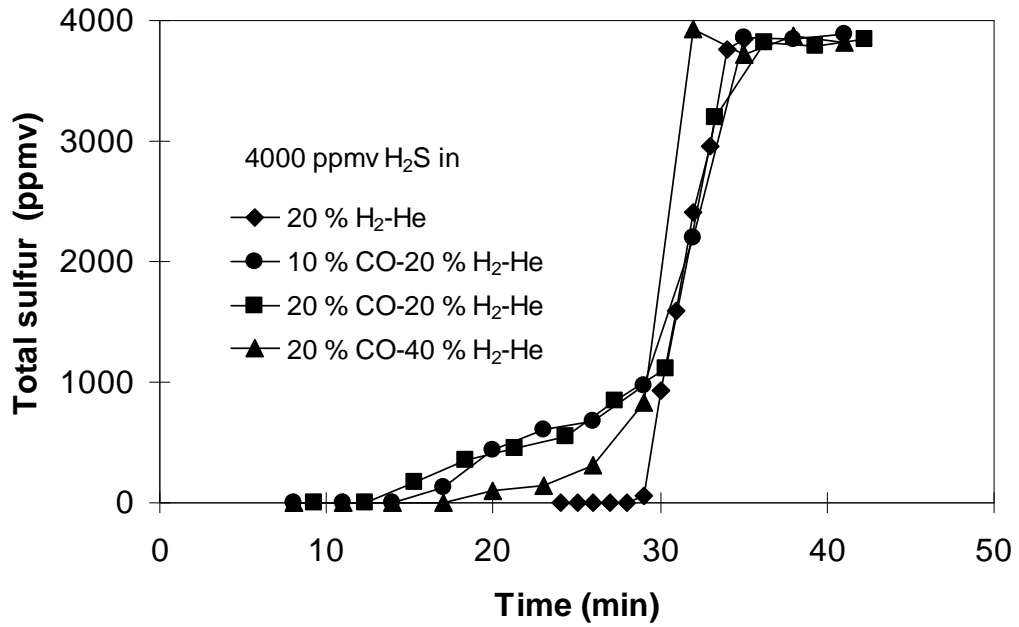
Figure VI-5. Effects of CO on total sulfur breakthrough in the presence of H_2.

200

Figure VI-3 shows that the addition of CO to H_2S-H_2-He system did not significantly change the shape of H_2S breakthrough curves. The result therefore suggests CO has little effects on reaction 2 at 400 °C. The addition of CO also shifted the H_2S breakthrough curves to the right side and made the saturation H_2S concentration of the breakthrough curves (plateau concentration) lower than the initial concentration (4000 ppmv). Unlike H_2 case, the shift of breakthrough curves to the right side does not mean an increase in sulfur capacity of sorbents due to the COS formation in the case of CO. This can be seen in **Figure VI-4**. The total sulfur breakthrough curves (as shown in **Figure VI-5**) also confirmed this.

Figures VI-3 and **4** suggest the breakthrough of COS took place earlier than that of H_2S in presence of CO. With 10% CO, COS broke at 14 min and reached a peak concentration of 1000 ppmv. In terms of H_2S saturation time, the sulfur capacity was 31.5 min under test conditions. This result implies that around 50% of ZnO was unutilized at COS breakthrough, however, this amount of ZnO was able to successfully remove H_2S but not COS from the gas stream. The difference between the breakthrough of H_2S and COS implies that COS may be generated homogeneously, and/or it is be hardly captured by the ZnO sorbent bed (Sasaoka *et al*., 1996).

Figure VI-4 also suggests that COS concentration increased with the increase in CO concentration as predicted by reaction 4. The outlet COS concentrations were higher than the calculated equilibrium values of 142 and 71 ppmv in the presence of 20 and 10

vol.% CO, respectively.   After reaching the highest values, the COS concentrations dropped gradually.   This phenomenon is contradictory to the result predicated by the homogeneous reaction hypothesis.   **Figure VI-4** also demonstrates that H_2 inhibited the formation of COS.   With the increase in H_2 concentration, the COS breakthrough was postponed and the plateau COS concentration decreased.   The breakthrough of COS in the presence of 40 vol.% H_2 started 5 minutes later and achieved a lower concentration plateau than that in the presence of 20 vol.% H_2.

Figure **VI-5** demonstrates the breakthrough curves for total sulfur concentration including both H_2S and COS.   The addition of CO dramatically broadened the total sulfur breakthrough curves, therefore it decelerated the reaction between ZnO and sulfur species, mainly due to the formation of COS and slow reaction between COS and ZnO (reaction 6).   **Figure VI-5** indicates that COS breakthrough time determined the total sulfur breakthrough time.   As shown in **Figure VI-5**, the total sulfur broke at 14 min in the presence of 20 vol.% CO and at 28 min without CO.   The sulfur capacity and bed utilization at total sulfur breakthrough dropped by 50% due to the presence of CO.

During the experiments, CO_2 was detected and its concentration decreased with time as shown in **Figure VI-4**. CO_2 concentration demonstrated a different profile from COS. Its initial concentration reached a peak concentration of 800 ppmv before dropping gradually.   In the experimental conditions, there are two possible pathways to form CO_2. The first one is CO oxidation by ZnO and the second is CO oxidation by H_2O generated

in the reaction between ZnO and H_2S. Considering the equilibrium constants of these two reactions (2.64×10^{-5} and 12.4 for the two reactions respectively) and the CO_2 concentration observed, the most possible pathway is the second one. The presence of CO_2 complicates the system because COS may also be generated by different pathways in the presence of CO_2 as shown by reactions 7 and 8:

$$CO_2 + H_2S = COS + H_2O \hspace{4cm} (7)$$

$$CO_2 + ZnS = COS + ZnO \hspace{4cm} (8)$$

VI.3.3. H_2S-CO_2-H_2 system

Like CO, CO_2 has influences on the reaction 2 and it can introduce COS formation according to reaction 7 homogeneously or heterogeneously. If heterogeneously, reaction 7 should be separated into two heterogeneous reactions 8 and 2. Reaction 7 is reversible with an equilibrium constant of 0.00293 at 400 °C.

H_2S breakthrough curves tested with 4000 ppmv H_2S-20 vol.% H_2-He challenge gases with various CO_2 concentrations are shown in **Figure VI-6**. Unlike the results of H_2S-CO-H_2 system, H_2 demonstrated little effects on desulfurization performance in the presence of CO_2. The shape of H_2S and total sulfur breakthrough curves and the COS concentration at various H_2 concentrations are almost the same. Like CO, CO_2 did not significantly change the shape of H_2S breakthrough curves, and it shifted the breakthrough curves right at low CO_2 concentration.
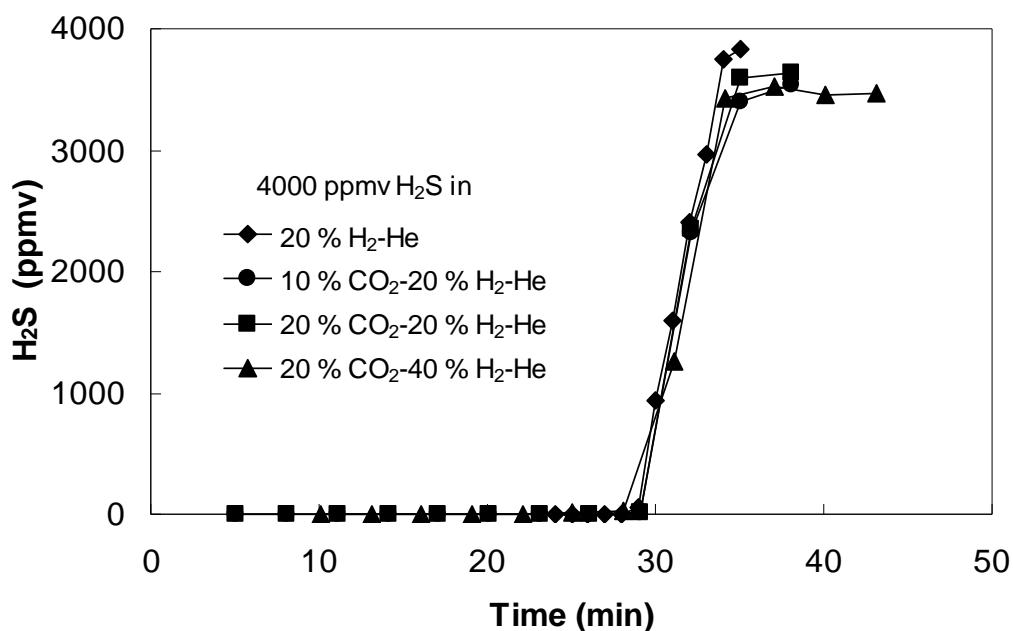
Figure VI-6. Effects of CO_2 on H_2S breakthrough curves in the presence of H_2.

COS was also detected and COS the breakthrough curves at various CO_2 concentrations are shown in **Figure VI-7**. In this figure, the COS breakthrough took place 7 minutes earlier than the H_2S breakthrough. The COS breakthrough times varied slightly with the change in concentration of CO_2 and H_2 in the challenge gas. Similar to CO, CO_2 inhibited the desulfurization kinetics as shown in **Figure VI-8**. With a higher CO_2 concentration, the total sulfur breakthrough time diminished slightly. However, CO_2 is not as active as CO in terms of COS formation. For instance, the total sulfur breakthrough took place at 22 minutes in the presence of 20 vol.% CO_2 and at 14 minutes in 20 vol.% CO. The plateau COS concentrations in the H_2S-CO_2-H_2 challenge gases was also lower than those observed in H_2S-CO-H_2 challenge gases.
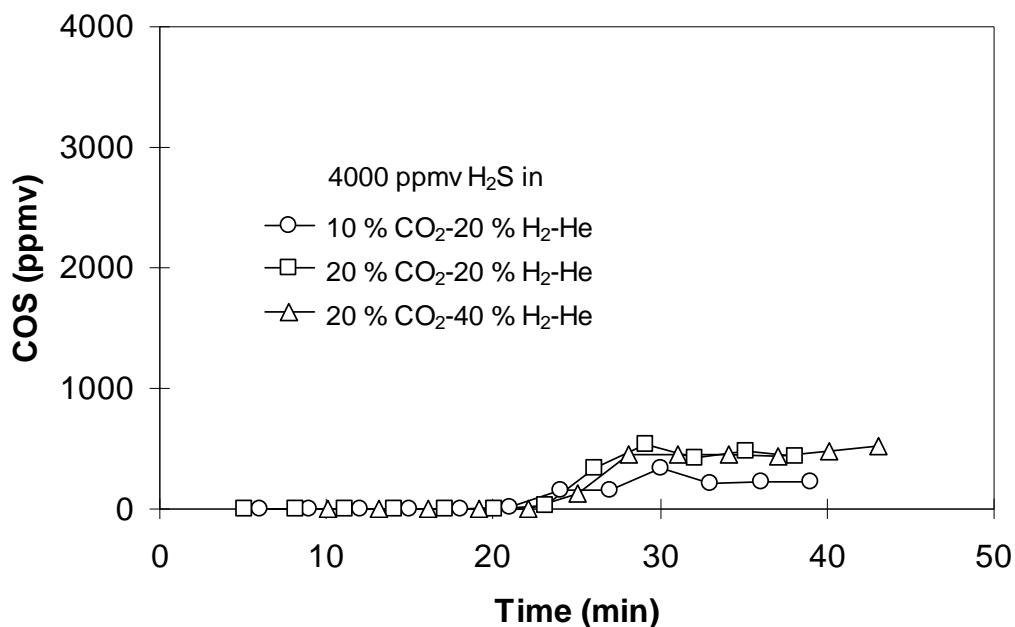
Figure VI-7. Effects of CO_2 on COS formation in the presence of H_2.

In the presence of CO_2 and H_2, the WGS reaction took place and CO was detected. COS was also detected and the concentration profiles at various CO_2 concentrations are shown in **Figure VI-7**. Therefore, there are two pathways for COS formation in the presence of CO_2. The first one is direct COS formation by reaction 7. The second is a two-step reaction where CO_2 is converted to a CO intermediate by WGS before forming COS by reaction 4. In **Figure VI-7**, COS plateau concentration was proportional to the CO_2 concentration present in challenge gas stream, and H_2 had no significant effect on COS plateau concentration. Moreover, H_2 is involved in reaction 4 but not in reactions 7. Therefore, these results hint that the direct COS formation via reaction 7 is dominant in the presence of CO_2 when the bed is close to saturation.

When the bed was close to saturation, CO was detected at 3500 ppmv in the presence of 20 vol.% H_2 due to the WGS reaction. This is far below the equilibrium CO concentration of WGS in the reaction conditions. The presence of CO also implies that an equal amount of H_2O (3500 ppmv) was generated due to WGS reaction. A further calculation for the challenge gas containing 20 vol.% CO_2, 20 vol.% H_2, 4000 ppmv H_2S, and 3500 ppmv H_2O indicated an equilibrium COS concentration of 502 ppm, close to the experimental value of 434 ppmv. This result suggests the COS formation via CO_2 (reaction 7) was a fast reaction, and the plateau COS concentration was controlled by the equilibrium of reaction 7 when the sorbent bed was close to saturation. This assumption can explain the linear relationship between the plateau COS concentration and CO_2 concentration observed in Figure VI-7.
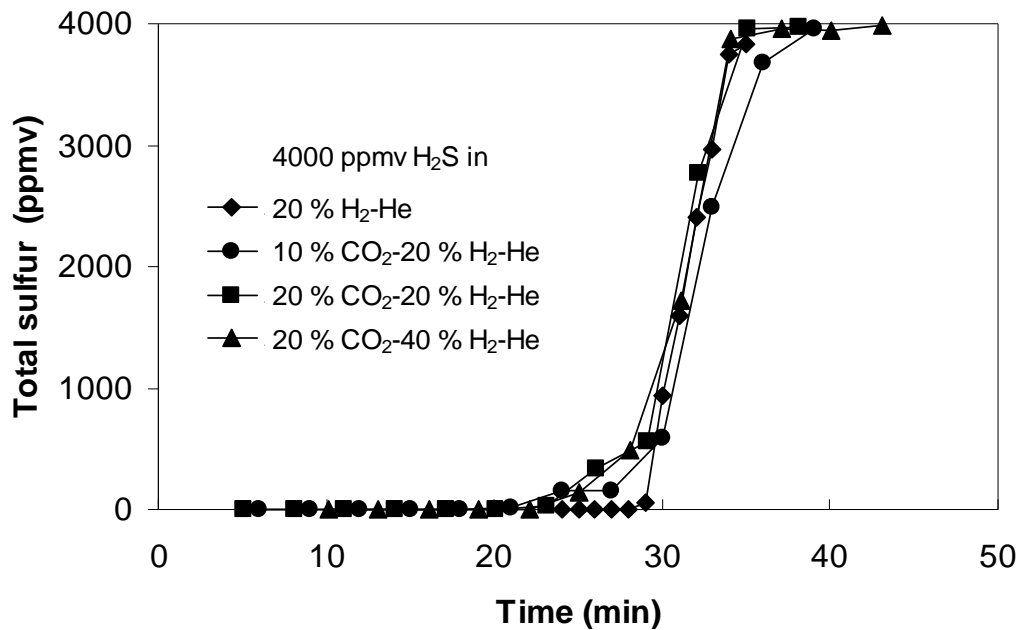
Figure VI-8. Effects of CO_2 on total sulfur breakthrough curves in the presence of H_2.

Hydrogen did not significantly inhibit the COS formation in the presence of CO_2, which is different from the results in the presence of CO. H_2 is a reactant in the reversible reaction 4. It directly affects COS formation by changing the equilibrium of reaction 4, and therefore significantly inhibits the COS formations and extend the breakthrough time of total sulfur concentration. In the presence CO_2, H_2 indirectly affects the COS formation via WGS reaction. In WGS, CO and water both are generated. CO is more active than CO_2, and accelerates the COS formation, while water inhabits COS formation by changing the equilibrium of reaction 7. As a result, the overall influence of H_2 on COS formation in the presence of CO_2 is negligible.

VI.3.4. H_2S-H_2O-H_2 system

Water is a key component in the desulfurization of reformates using ZnO based sorbents, because of its involvement in most reactions such as the reactions between ZnO and H_2S, CO_2 and H_2S, ZnO and H_2 (ZnO reduction), the WGS reaction. Addition of water will change the equilibrium concentrations of these reactions. The reactions in H_2S-H_2O-H_2 challenge gases are much simpler than in the presence of CO and/or CO_2, because there is no COS formation. The desulfurization performance of ZnO/SiO_2 sorbent beds were tested with 4000 ppmv H_2S-20 vol.% H_2-He challenge gases with various water contents. The breakthrough curves of H_2S are shown in **Figure VI-9**.

207
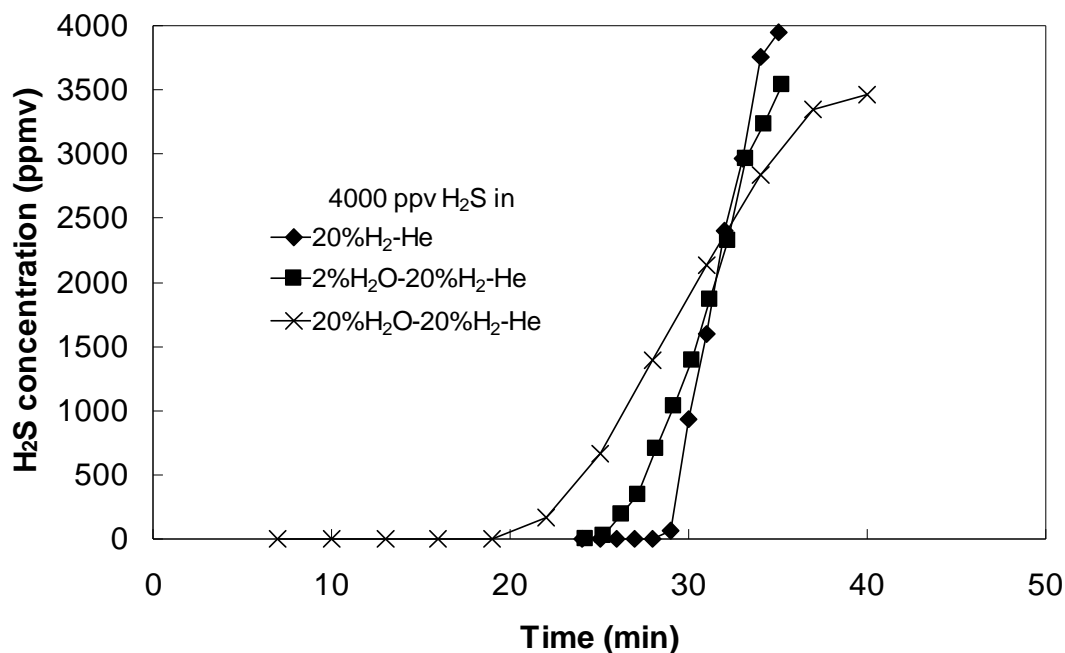
Figure VI-9. Effects of water on H_2S breakthrough curves.

Unlike CO and CO_2, water demonstrated very strong influence on the shape of H_2S breakthrough curves. Water of 2 vol.% significantly flattened the breakthrough curves. As water concentration increased the H_2S breakthrough took place sooner. In the presence of 20 vol.% water in gas stream, the breakthrough time was only 19 minutes (2/3 of that tested without water). All the results suggest water dramatically decelerates the reaction between H_2S and ZnO. A possible reason is that water was absorbed on ZnO and blocked the access of H_2S molecules to the ZnO grains.

Water also reduced the sulfur capacity of ZnO based sorbents. In the presence of 20 vol.% of water, the breakthrough curve was shift left by 1 minute, indicating 3 % of ZnO stoichiometric capacity loss in the presence of high water contents. Under the test

conditions, no zinc loss was observed, because of the presence of water, which tends to keep zinc at its oxide state, and the low desulfurization temperature. Moreover, the equilibrium H_2S concentration was 0.6 ppmv, a negligible amount compared with the initial H_2S concentration at 4000 ppmv. The equilibrium did not affect the sulfur capacity. The only explanation for lose in capacity under the experimental conditions is the adsorption of water on ZnO. In a word, water determines equilibrium of reactions 2, 5 and 7, significantly decelerates the reaction rate, and slight reduces the H_2S capacity due to water adsorption on the surface or ZnO sorbents.
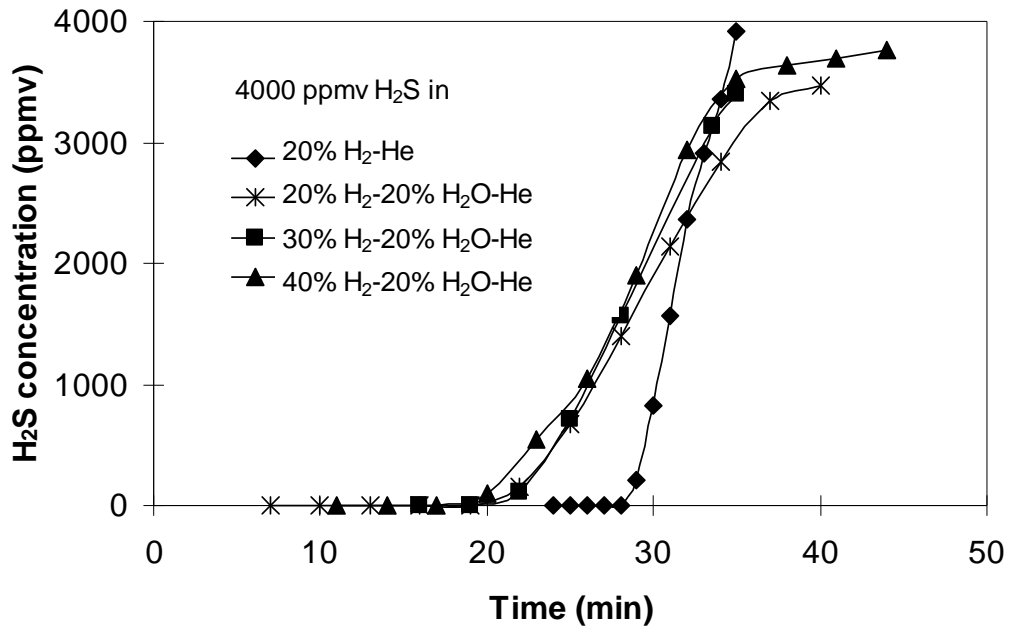
Figure VI-10. Effects of H_2 on H_2S breakthrough curves in the presence of water.

The addition of various concentrations of H_2 to the challenge gases containing 20 vol.% H_2O did not demonstrate significant effects on the shape of breakthrough curves,

as shown in **Figure VI-10**. The breakthrough curves at various H_2 concentrations in the presence of 20 vol.% H_2O are similar to each other. The same results were also observed in H_2 effect tests in the absence of additional water, as shown in **Figure VI-2**, in which the changes in H_2 concentration did not affect the shape of breakthrough curves significantly. These observations are different from the one observed at 500 °C by Sasaoka *et al.* The difference is the reaction of ZnO reduction (reaction 9). Under the tests conditions at 400 °C, reaction 9 can be written as:

$$ZnO(s)+H_2(g)=Zn(s)+H_2O(g) \tag{9'}$$

and at 500 °C, reaction 9 can be written as

$$ZnO(s)+H_2(g)=Zn(g)+H_2O(g) \tag{9''}$$

The equilibrium constant for reaction 9' was calculated to be 2.14×10^{-6} at 400 °C using HSC 3 software, which means water at a concentration above 2.14 ppm is able to convert Zn metal to ZnO. Even the nanosized nature of ZnO in ZnO/SiO_2 sorbent is helpful for ZnO reduction due to liquid Zn and zinc vapor formation, H_2 at low concentrations cannot easily reduce ZnO under the test conditions of a thousands ppm of water at 400 °C as it does at 500 °C. Thus, under the test conditions, H_2 demonstrates little effects on ZnO/SiO_2 performance. In a word, hydrogen of low concentrations does not have a strong effect on the reaction between ZnO and H_2S under the test conditions, especially in the presence of water.

VI.3.5. H_2S-CO-H_2-H_2O system

ZnO/SiO_2 sorbent (0.5 g) was tested with challenges containing 4000 ppmv H_2S with various CO and H_2O concentrations at 400 °C.   The test results and the results of the experiments in which CO or H_2O was absent were shown in **Figures VI-11, 12** and **13** for comparison.
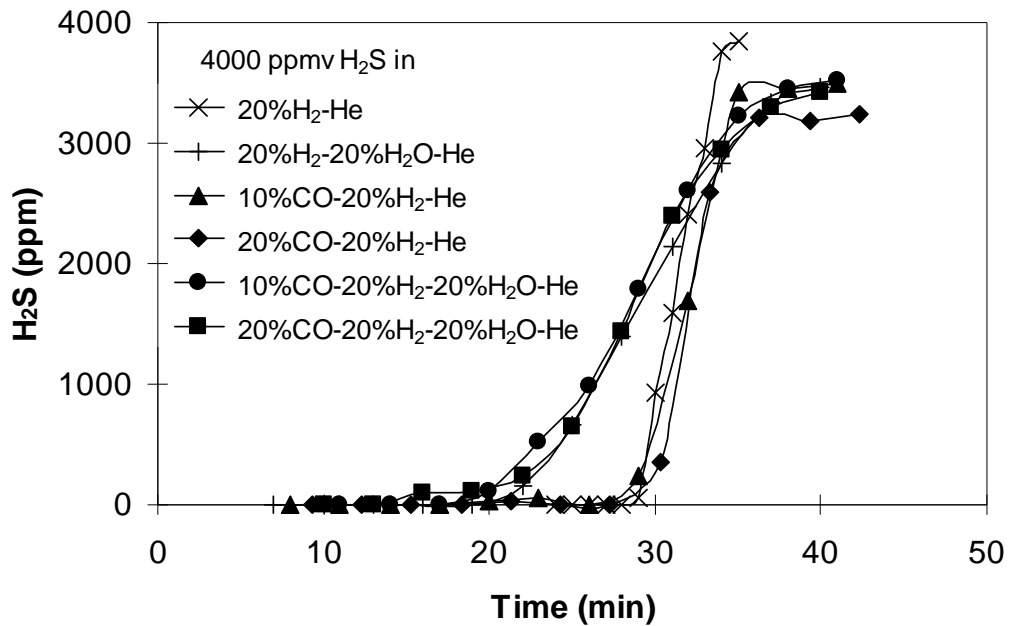
Figure VI-11. Effects of CO on H_2S breakthrough curves in the presence of water.

As indicated in these three figures, water has a dominant influence on the shape of the breakthrough curves.   In **Figure VI-11**, the H_2S breakthrough curves can be classified in two groups according to the water content.   All experiments performed in the absence of water posses a breakthrough curve located at the right side with a steep slope.   The tests involving 20 vol.% water have curves that are displaced to the left side

211

with lower capacities and broader breakthrough curves. This result suggests water

significantly hinders the reaction between H_2S and ZnO in the presence of CO. A

possible reason as mentioned earlier is the adsorption of water by ZnO. In **Figure**

VI-12, it should be noted that the addition of 20 vol.% water drastically reduced the

plateau COS concentrations from 400 to 600 ppmv in the absence of water to less than

100 ppm. Since water is not involved in the COS formation via reaction 5, a reasonable

explanation to this phenomenon is that COS concentration is primarily controlled by

reaction 7 in which both water and CO_2 are involved. The hypothesis is supported by

the detection of CO_2 generated by WGS during the experiments.
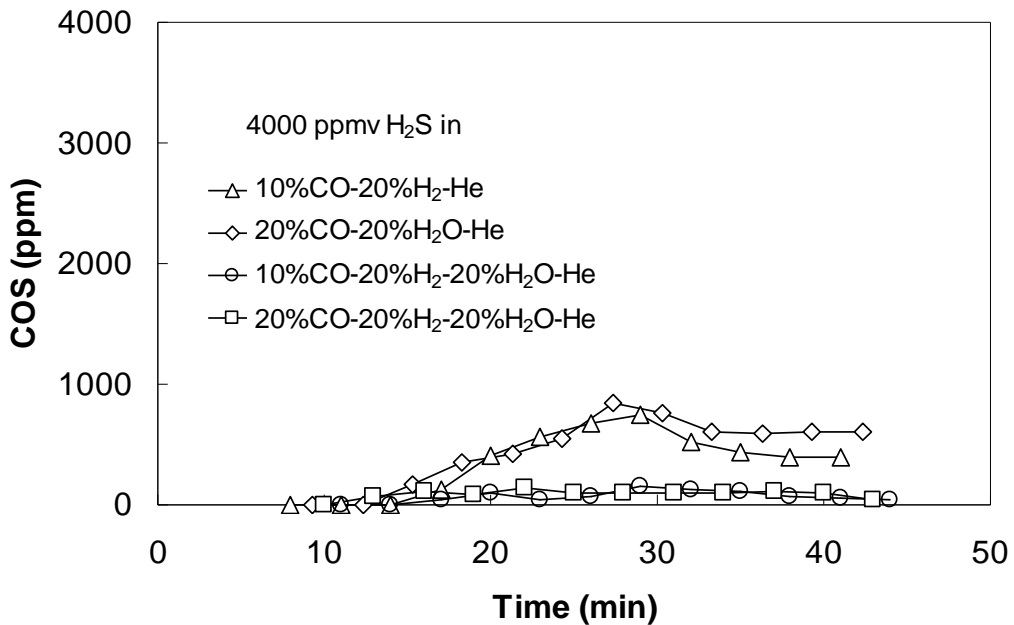
Figure VI-12. Effects of CO on COS formation in the presence of water.

CO has little effects on the reaction between H_2S and ZnO (reaction 2) in the

presence of 20 vol.% water (as shown in **Figure VI-11**). This is different from the

results of Sasaoka (1994b) at 500 °C.   However, CO changes the breakthrough time of

COS and total sulfur significantly.   The breakthrough times of H_2S and total sulfur

decreased with the increase in CO concentration as illustrated in **Figures VI-12 and 13**.

As for COS formation, it is obvious that a high CO concentration will generate more

COS, as shown in **Figure VI-12**.   The COS breakthrough time decreased slightly with

the increase in CO concentration, which is reasonable if the reaction between ZnO and

COS takes place very slowly.   The breakthrough time of H_2S also drastically decreased

with the increase in water content.   At high water content, ca. 20 vol.%, the

breakthrough time of H_2S was, though still larger than, very close to that of COS.   As a

result, the total sulfur breakthrough time was determined by COS breakthrough time in

the presence of 20% CO and 20% water, as shown in **Figure VI-13**.   At higher water

and lower CO concentrations, the H_2S breakthrough time will be less than that of COS.

In this case, the breakthrough time of total sulfur is equal to that of H_2S and, in turn, is

determined by water concentration.   Due to COS formation and hindering effects of

water, the bed utilization in the presence of 20% CO and 20% water was less than 40%.

It should be noted that the COS formation was controlled by different reactions

during reformates desulfurization.   Before breakthrough COS formation was determined

by the reaction between H_2S and CO (reaction 4), while plateau COS concentration was

significantly affected by water and CO_2 (reaction 7).   This transition in COS formation

is not clear yet.

213
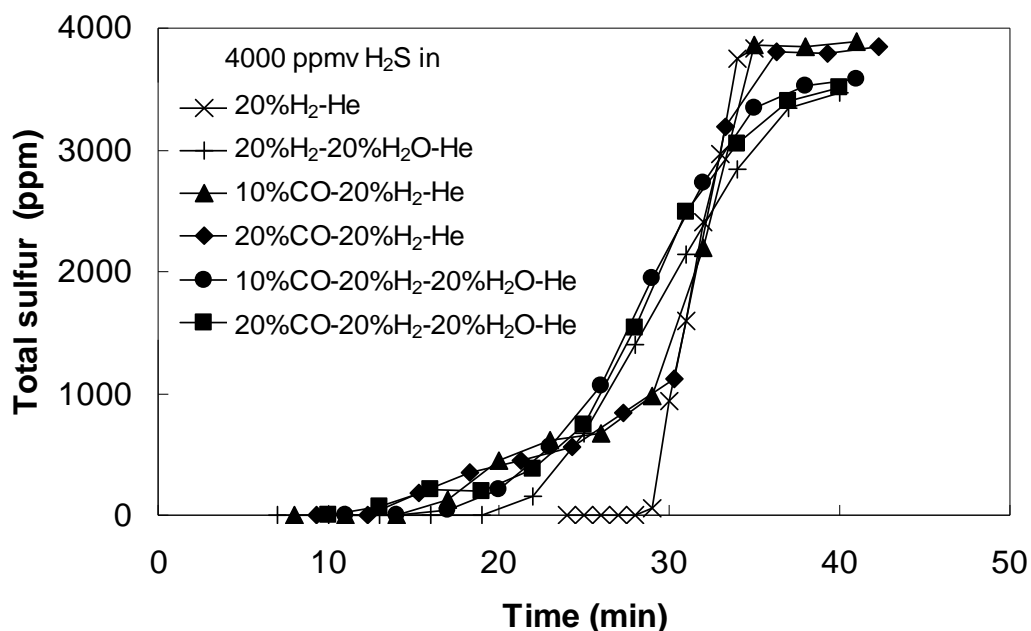
Figure VI-13. Effects of CO on total sulfur breakthrough curves in the presence of water.

VI.3.6. H_2S-CO_2-H_2-H_2O system

A series of similar experiments was performed for challenge gases containing 20 vol.% water and various concentrations of CO_2. Thus, the water generated by reaction 2 and WGS reaction was negligible. The test results are shown in **Figures VI-14, 15,** and **16**. Several experiments tested without water are also shown for comparison.

The H_2S, total sulfur, and the COS breakthrough curves are very similar to those discussed in the H_2S-CO-H_2O section. From the two sets of experiments, CO_2 and CO demonstrated similar influences on the desulfurization reactions and COS formation; however, the plateau COS concentrations in the H_2S-CO_2-H_2O tests were lower than these in H_2S-CO-H_2O tests.

214

As mentioned in the H_2S-CO-H_2O section, the plateau COS concentration was not controlled by the equilibrium of reaction 5, while CO_2 and water were involved in the controlling steps. The equilibrium concentration of COS for the challenge gas (4000 ppmv H_2S-20 vol.%CO_2-20 vol.% H_2-20 vol.% H_2O-He) at 400 °C was calculated to be 12 ppmv, which is very close to the experimental value ca. 20 ppmv. Moreover, the plateau COS concentration was proportional to the feeding CO_2 concentration, as shown in **Figure VI-15**. These results suggest the reaction between CO_2 and H_2S was fast and the COS concentration was determined by the equilibrium of reaction 7, which consistently supports the earlier discussions. **Figures VI-12** and **15** also implies that high water contents can be applied to reduce the plateau COS concentration.
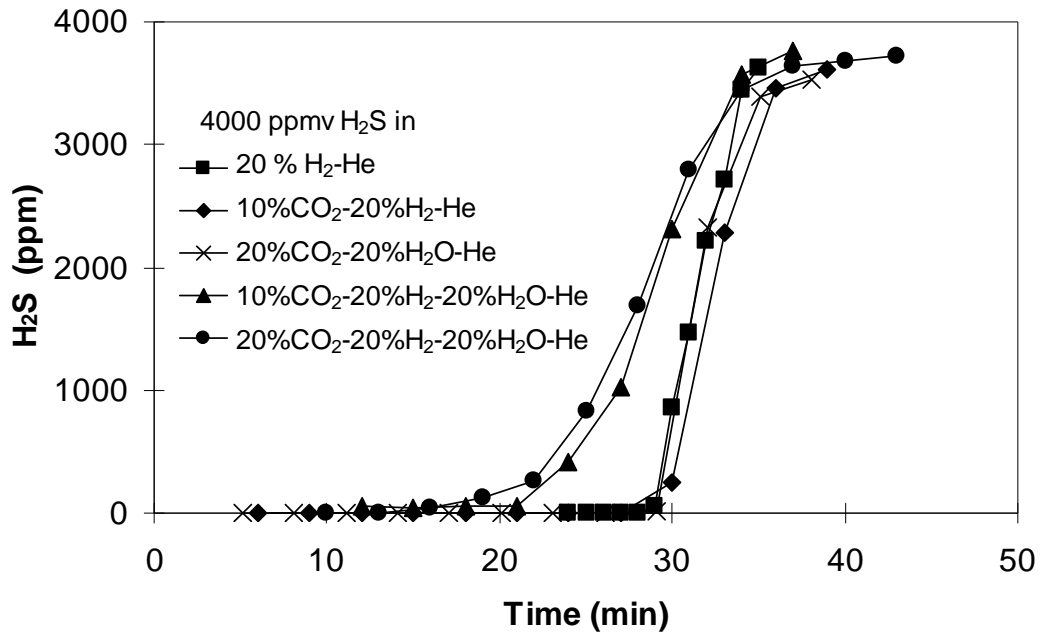
Figure VI-14. Effects of CO_2 on H_2S breakthrough curves in the presence of water.
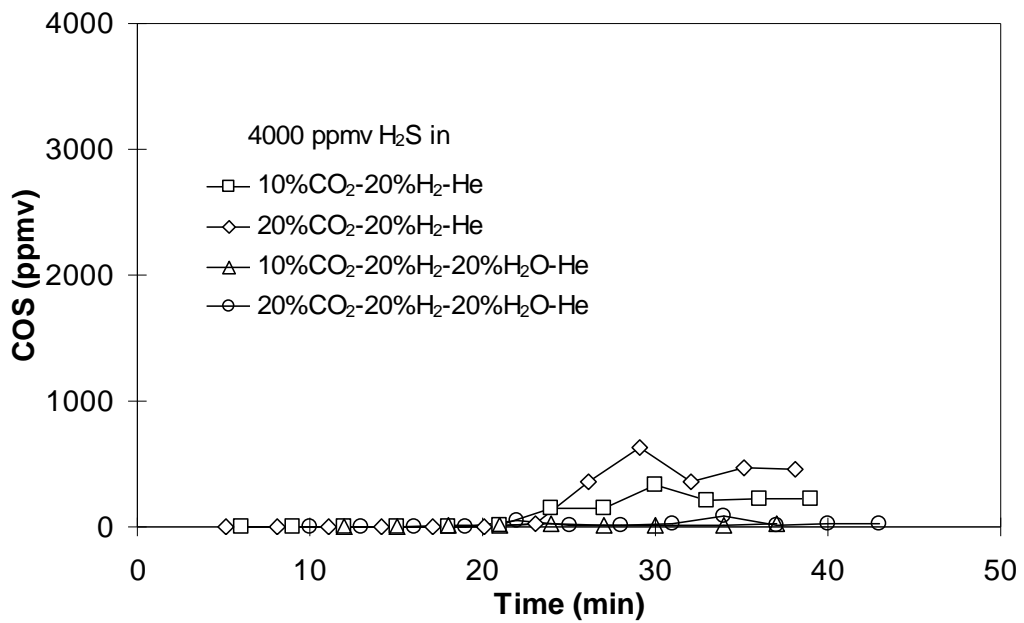
Figure VI-15. Effects of CO_2 on COS formation in the presence of water.
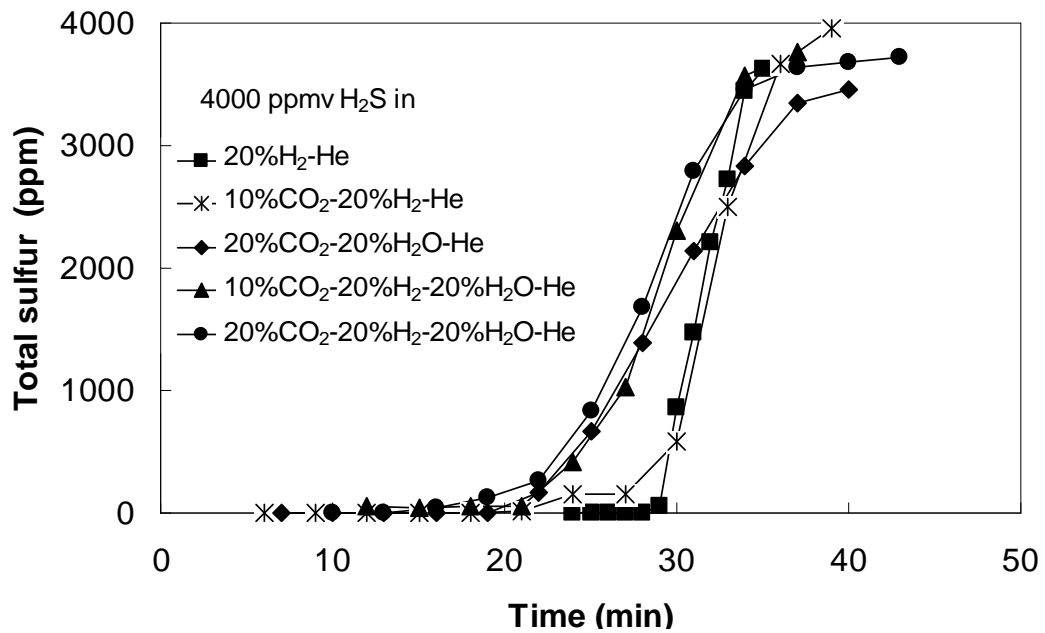
Figure VI-16. Effects of CO_2 on total sulfur breakthrough curves in the presence of water.

VI.3.7. H_2S-CO-CO_2 system

The ZnO/SiO$_2$ sorbent was tested with several challenge gases containing 4000 ppmv of H_2S and CO and CO_2 at various concentrations. The sorbent was tested at 400 °C and a face velocity of 9.9 cm/s. The results are shown in **Figures VI-17, 18**, and **19**. There is no significant difference between H_2S breakthrough curves at these various challenge gas systems, suggesting the CO and CO_2 gas mixture does not have significant influences on the reaction between ZnO and H_2S. However, the COS breakthrough curves and total sulfur breakthrough curves are quite different from each other. **Figures VI-18 and 19** suggest that CO concentration determined the breakthrough pattern of total sulfur. CO_2 did not demonstrate significant effect on the total sulfur breakthrough time and COS initial formation rate. This result implies that CO is more active than CO_2 in terms of COS formation before COS breakthrough, which is consistent with the earlier observances. Because the H_2S breakthrough times in these tests were larger than those of COS, and the total sulfur breakthrough time was determined by the COS breakthrough, which was in turn determined by CO concentration.

It is should be noticed that CO_2 is the dominant factor for the plateau COS concentration in the presence of CO and CO_2. The addition of 10 vol.% of CO to the 20 vol.% CO_2-20 vol.% H_2-He did not change the plateau COS concentration, because the COS formation when the packed bed was saturated was controlled by the reaction between CO_2 and H_2S.

A sulfur capacity loss in the presence of CO_2 and CO was also observed. As shown in **Figure VI-19**, the area above a total sulfur breakthrough curve is proportional to the saturation sulfur capacity of the packed bed. A simple manual integration suggests that the addition of 10 vol.% CO and 20 vol.% CO_2 reduced the saturation sulfur capacity of ZnO/SiO_2 by 7% of the stoichiometric capacity. This capacity loss is due to the formation of COS, which is hard be captured by ZnO/SiO_2 sorbent. Therefore, sulfur capacity can be improved by converting COS to H_2S that can be adsorbed by ZnO/SiO_2 sorbent at a high sulfur capacity, or by modifying the sorbent to make it more active to COS.
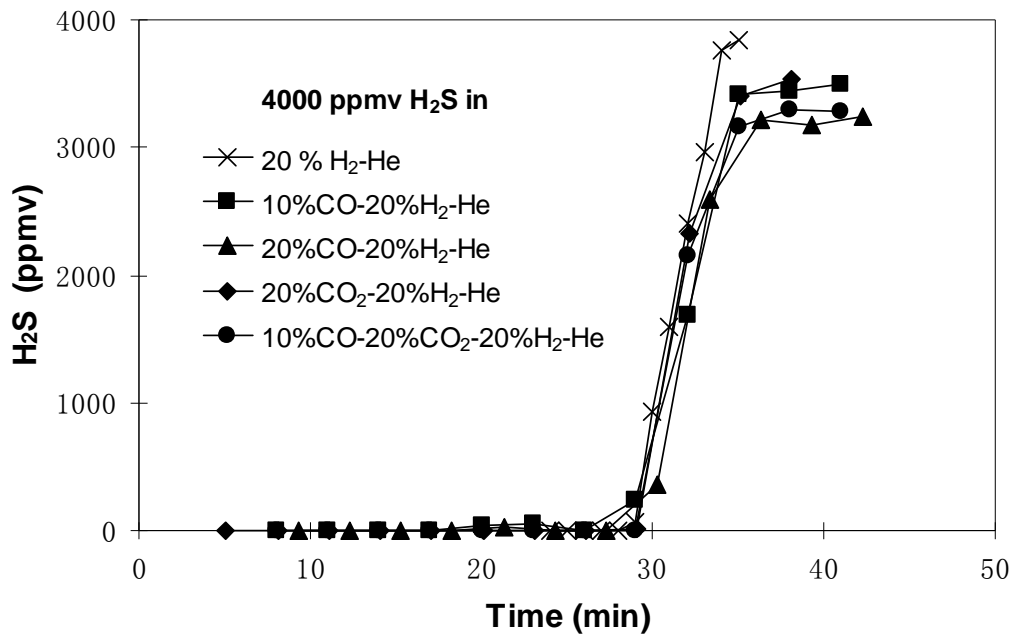
Figure VI-17. H_2S breakthrough curves in the presence of CO and CO_2.
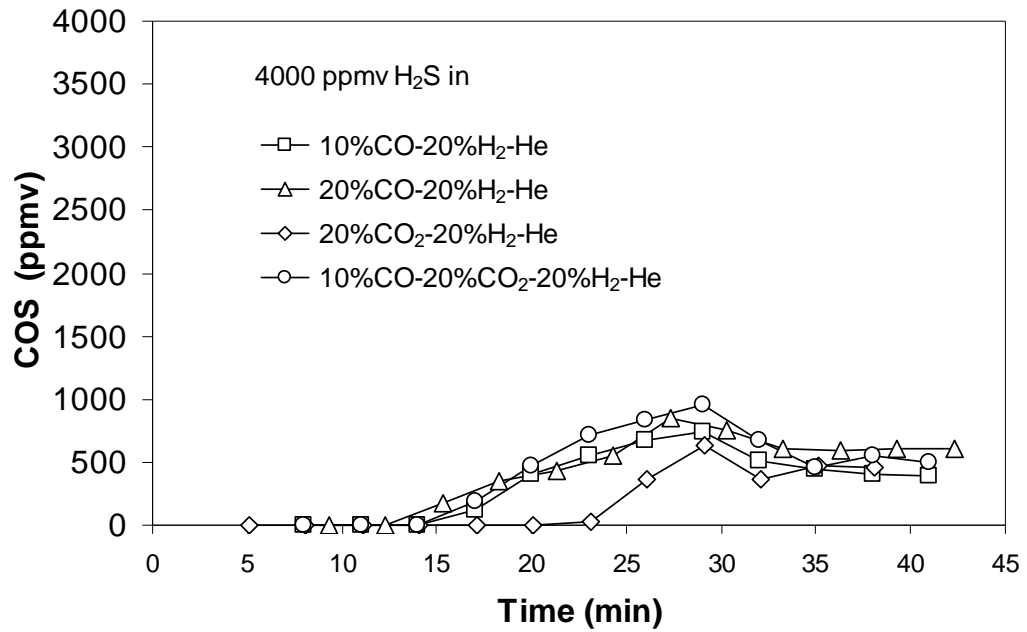
Figure VI-18. COS formation in the presence of CO and CO_2.
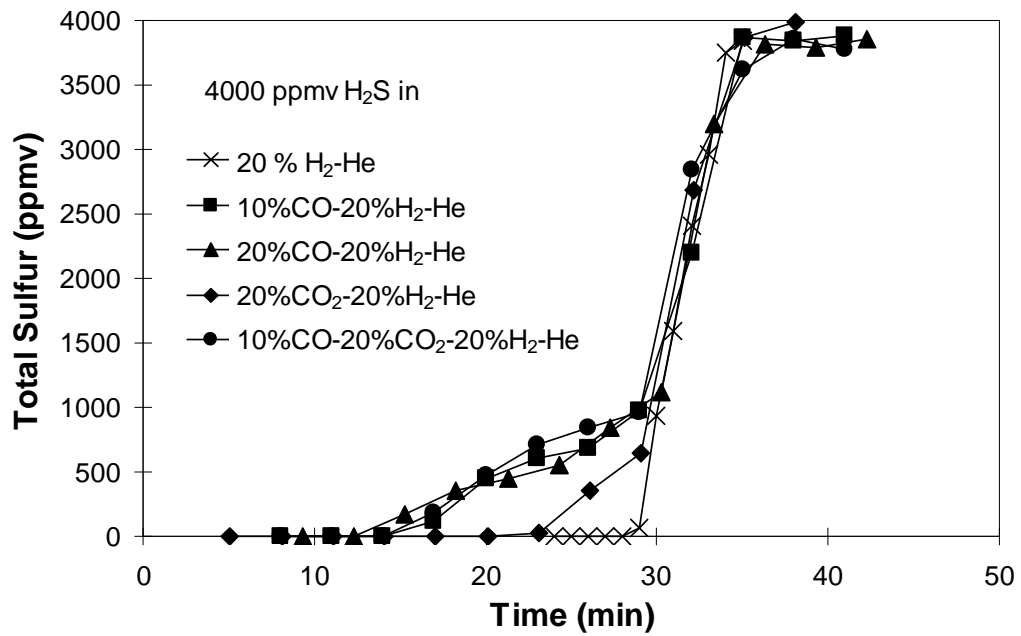
Figure VI-19. Total sulfur breakthrough curves in the presence of CO and CO_2.

219

The addition of H_2 to the challenge gas of 4000 ppmv H_2S-10 vol.% CO-20 vol.% CO_2-20 vol.% H_2-He significantly shifted the H_2S breakthrough curve left by 4 minutes and delayed the COS breakthrough by 4 minutes, as shown in **Figure VI-20**. As for the total sulfur breakthrough, H_2 demonstrated the same effect as it did in earlier discussions. It oppressed the COS formation (mainly via CO) and extended the total sulfur breakthrough time as shown in **Figure VI-21**.

Figure VI-20 also indicates that the addition of H_2 to the challenge gas containing CO and CO_2 did not change the plateau COS concentration when the packed bed was close to saturation. This phenomenon is different from the observations in H_2S-CO-H_2 section, and it is similar to these in H_2S-CO_2-H_2 section, where H_2 demonstrated little effects on plateau COS concentration. Based on the discussions earlier, this result hints that COS concentration was controlled by the equilibrium of reaction 7, though COS was also generated via reaction 4 under the desulfurization conditions.

The addition of H_2O to the challenge gases containing CO and CO_2 changed the H_2S breakthrough curves and COS formation as shown in **Figures VI-22** and **23**. The addition of 20 vol.% H_2O to the challenge gas of 4000 ppmv H_2S-10 vol.% CO-20 vol.% CO_2-20 vol.% H_2-He drastically broadened H_2S breakthrough curves and reduced the plateau COS concentration, as it was discussed in earlier sections. The addition of water also demonstrated a 3-minute increase in the COS breakthrough time and total sulfur breakthrough time. Both water and H_2 oppressed the COS formation and extended total

220

sulfur breakthrough time, but they functioned in different ways. H_2 affects the reaction

4 directly. The addition of H_2 will accelerate the reverse reaction rate of reaction 4 as

described in earlier discussion. Water affects equilibrium of the WGS and reaction 7.

The addition of H_2O to the challenge gas of 4000 ppmv H_2S-10 vol.% CO-20 vol.%

CO_2-20 vol.% H_2-He reduced the CO concentration which is more active than CO_2 in

COS formation before COS breakthrough. The addition of water also reduced the COS

formation via reaction 7. Therefore, the CO_2 is more stable in the presence of high

water concentrations. As a result, the addition of water will generate less COS and

therefore extend the COS breakthrough time and total sulfur breakthrough time as well.
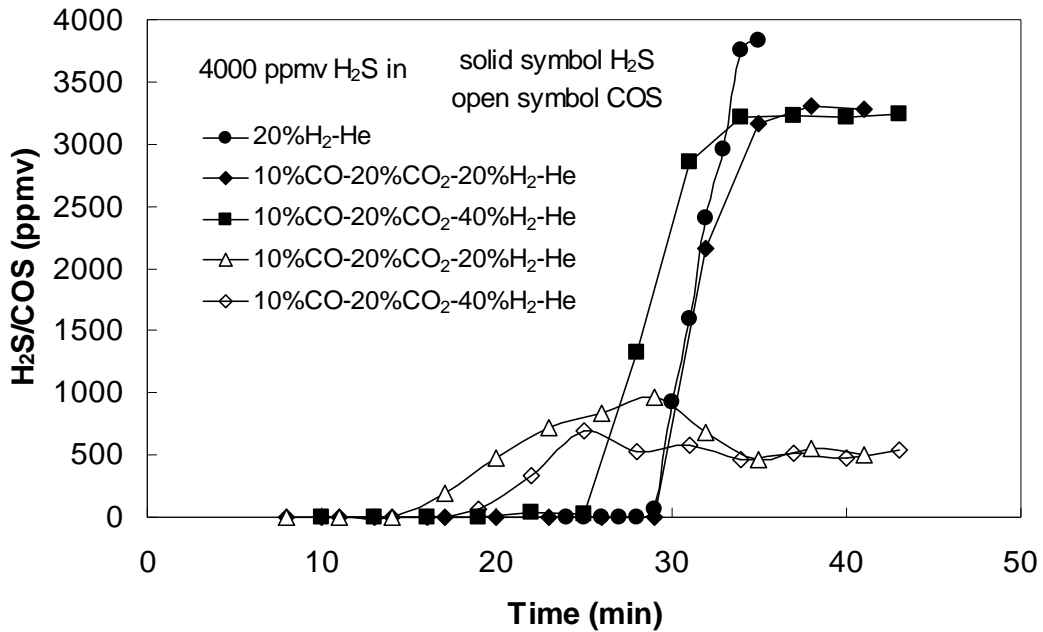
Figure VI-20. Effects of H_2 on H_2S and COS breakthrough curves in the presence of CO and CO_2.

221
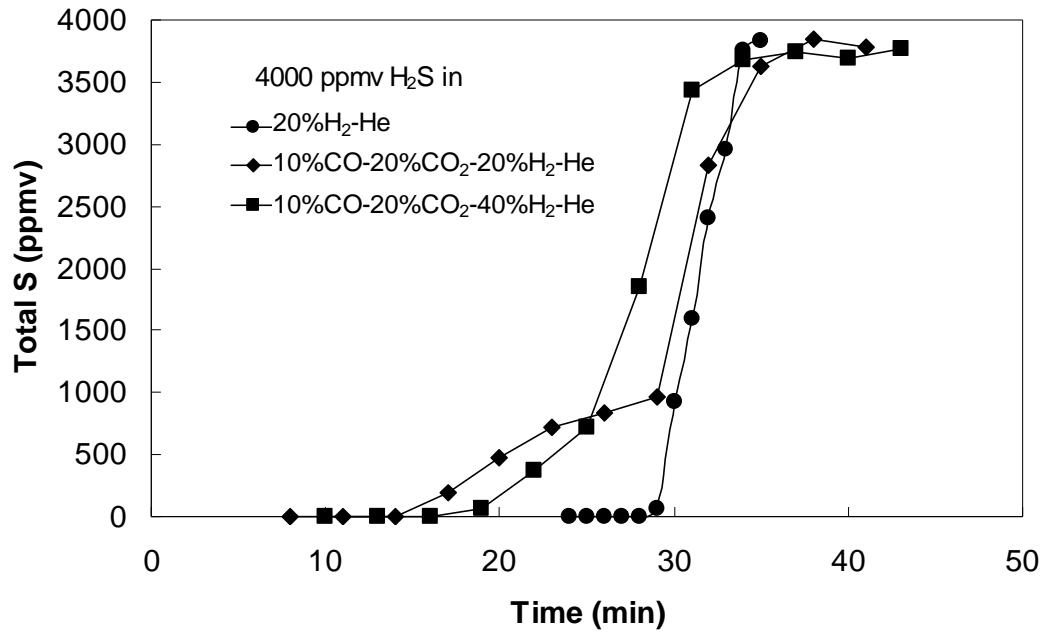
Figure VI-21. Effects of H_2 on total sulfur breakthrough curves in the presence of CO and CO_2.
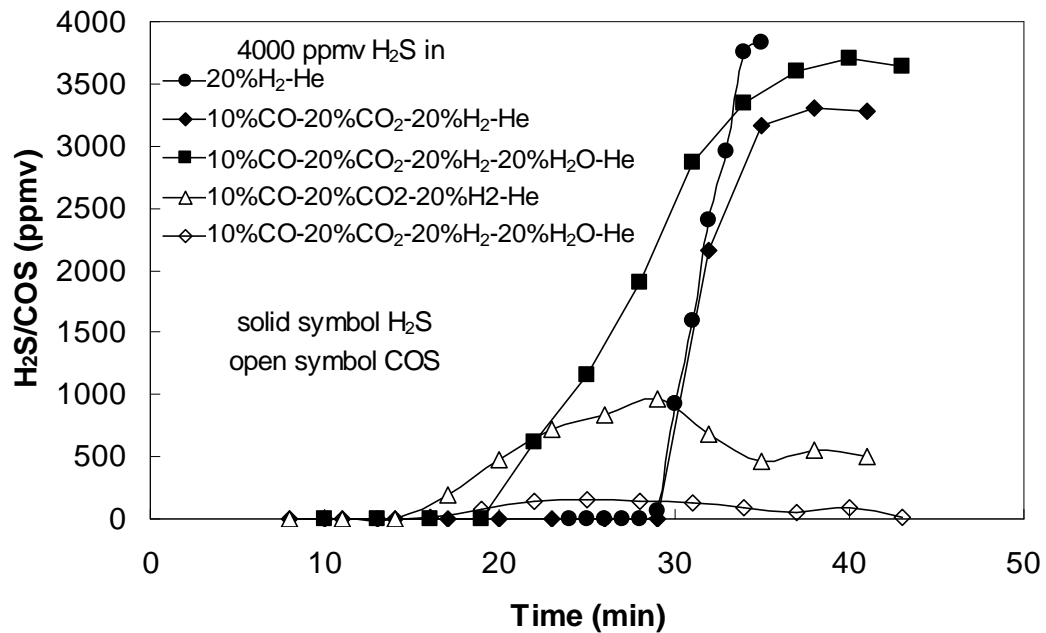
Figure VI-22. Effects of H_2O on H_2S and COS breakthrough curves in the presence of CO and CO_2.
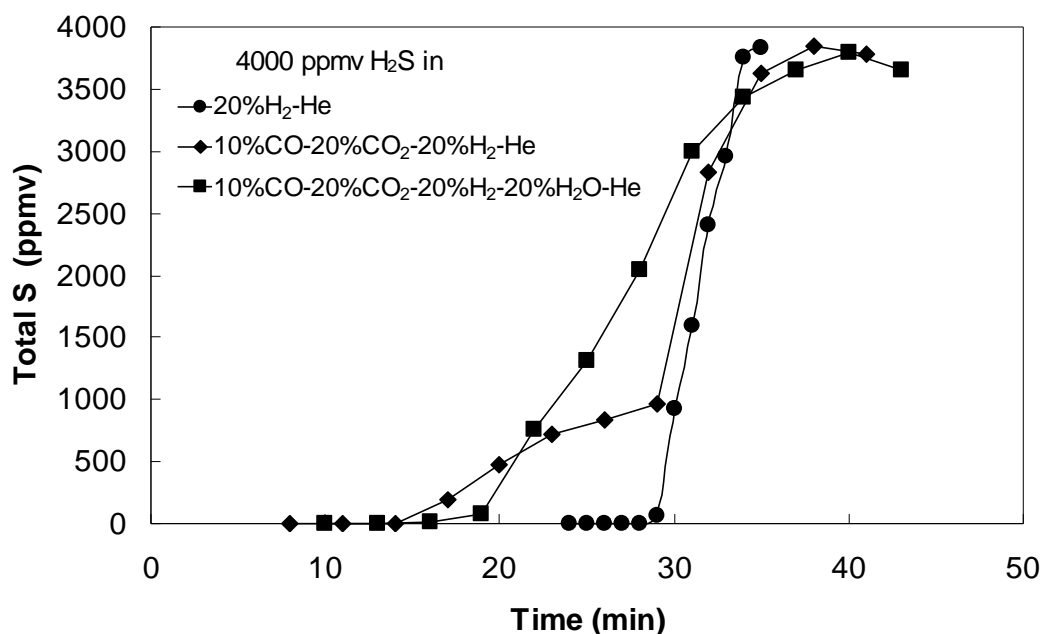
Figure VI-23. Effects of H_2O on total sulfur breakthrough curve in the presence of CO and CO_2.

VI.3.8. Desulfurization for Model Reformates

The following research focused on the desulfurization performance of ZnO/SiO_2 sorbents. In this section, water effect on desulfurization for reformates was discussed specially. A dry reformates containing 4000 ppmv H_2S-10 vol.% CO-20 vol.% CO_2-40 vol.% H_2-He and wet reformates containing 4000 ppmv H_2S-10 vol.% CO-20 vol.% CO_2-40 vol.% H_2-30 vol.% H_2 were tested with ZnO/SiO_2 sorbent (0.5 g) at 400 °C. The test results were shown in **Figures VI-24, 25** and **26** for comparison.
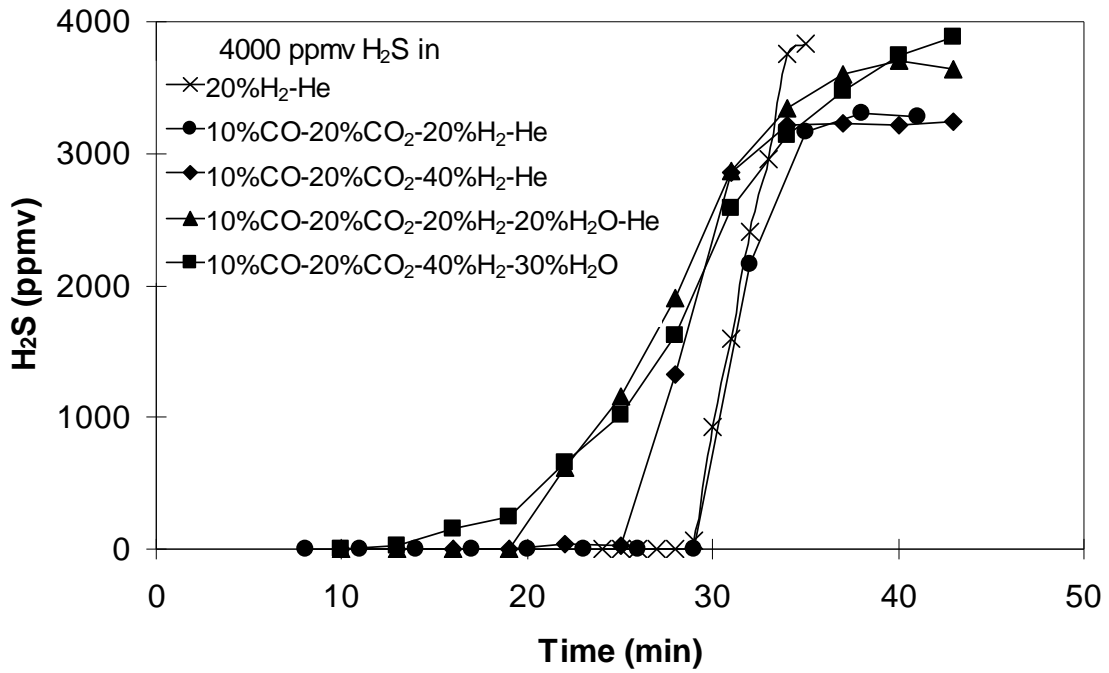
Figure VI-24. Effects of H_2O on H_2S breakthrough curves in the presence of reformates.
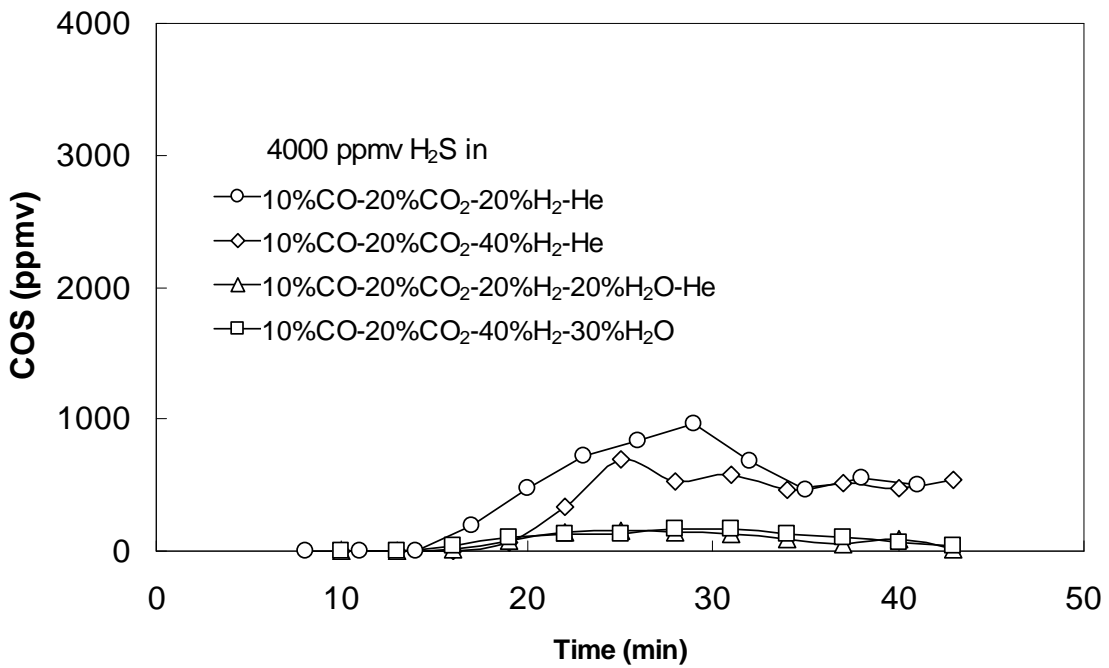
Figure VI-25. Effects of H_2O on H_2S breakthrough curves in the presence of reformates.
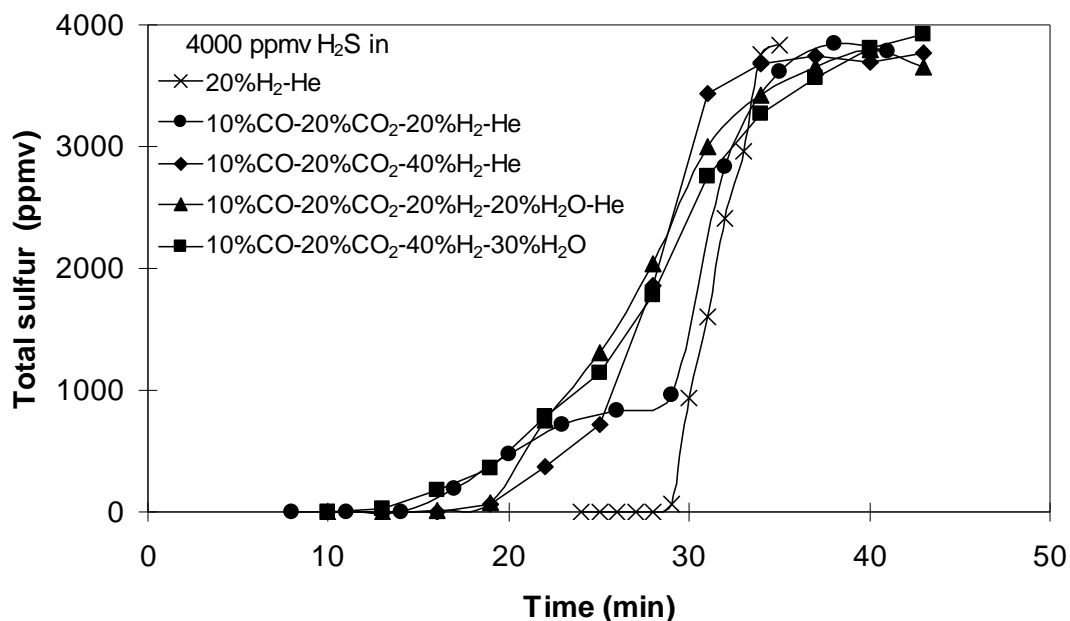
Figure VI-26. Effects of H_2O on total sulfur breakthrough curves in the presence of reformates.

Figure **VI-24** suggests water reduced the H_2S breakthrough time from 28 minutes (H_2S-H_2-He system) or 25 minutes (H_2S-CO-CO_2-H_2-He system) to only 13 minutes. It did not reduce the saturation time based on $t_{1/2}$ significantly. The wet reformates had a $t_{1/2}$ of 27 min., which is very close to with the $t_{1/2}$ of 28 minutes for dry reformates (H_2S-CO-CO_2-H_2-He). **Figures VI-24** and **26** suggest H_2S breakthrough determines the total sulfur breakthrough at high water content, ca. 30 vol.%.

Figure **VI-25** indicates the reduction of COS concentration in the presence of water. The COS concentration was reduced from 700 ppmv (H_2S-CO-CO_2-H_2-He system) to below 200 ppmv. The total sulfur breakthrough curve in **Figure VI-26** suggests the addition of water to reformates decelerated the sulfur removal rate. The lumped *K*

225

(shape factor in Yoon's model) in the presence of water is only 0.24 min^{-1}. It is only half of the dry reformates test (0.44 min^{-1}), and one third of that of the H_2S-H_2-He system (0.741 min^{-1}). **Figures VI 24** and **26** indicate the desulfurization of reformates in the presence of water is usually running at low efficiency. The efficiency of traditional sorbents with severe mass transfer resistance will suffer more. **Figure VI-26** demonstrated a sulfur capacity loss around 10% of saturation capacity in the test with this challenge gas. The adsorption of water accounted for 3% capacity loss and the COS formation accounted for the remaining 7%. By converting COS to H_2S, the sulfur capacity can be increased. **Figure VI-26** also suggests a low ZnO utilization at 30% during the desulfurization for reformates.

Since the experimental results reveal the intrinsic behavior of the reactions between ZnO and reformates, further changes in the face velocity will not significantly affect the performance at this gas composition. Novel process designs to change water content and/or CO content are favored to improve the capacity of ZnO based sorbents and reduce the reactor sizes at a high water content ($\geq$ 30 vol.%). At a low water content (< 30 vol.%) where the total sulfur breakthrough time is determined by COS formation via reaction 5, sorbents that have high COS capacity may overcome this intrinsic ineffectiveness. For the sorbents with severe mass transfer resistance, the performance will be much worse than the one described above.

VI.3.9. Mechanism of COS Formation

The COS is generated when CO and/or CO_2 are present in the gas phase desulfurization process; however, the mechanism of COS formation is not clear yet. The results in earlier discussion suggest CO was more active than CO_2 in terms of COS formation, and CO and H_2 had strong influences on the breakthrough of COS and initial COS formation. When the packed bed was saturated, however, CO_2 and H_2O became the controlling factors for the COS concentration. The controlling mechanism changed during the desulfurization process; therefore, several experiments were designed to reveal the possible pathways of COS formation.

VI.3.9.1. Homogeneous Tests

Two experiments were conducted in a clean, quartz reactor filled with ultra-high purity He and without any sorbent particles or packing materials. In the first experiment, the challenge gas containing 13000 ppmv H_2S, 25 vol.% CO and He passed through the reactor and the COS (around 200~300 ppmv) were recorded as seen in **Figure VI-27**. This result suggests that the reaction between CO and H_2S took place homogeneously in the tube reactor. **Figure VI-27** shows COS generated at a concentration much lower than the equilibrium concentration. This indicates that the homogeneous reaction was slow. Since COS formation via the homogeneous reaction does not require the ZnS, COS breakthrough in the presence of CO can be much earlier than the one without CO.

227

The equivalent COS concentration for the test containing 4000 ppmv H_2S was estimated to be 70~100 ppmv. This value is very close to the plateau COS concentration tested at high water content, where COS formation via CO_2 was literarily negligible.
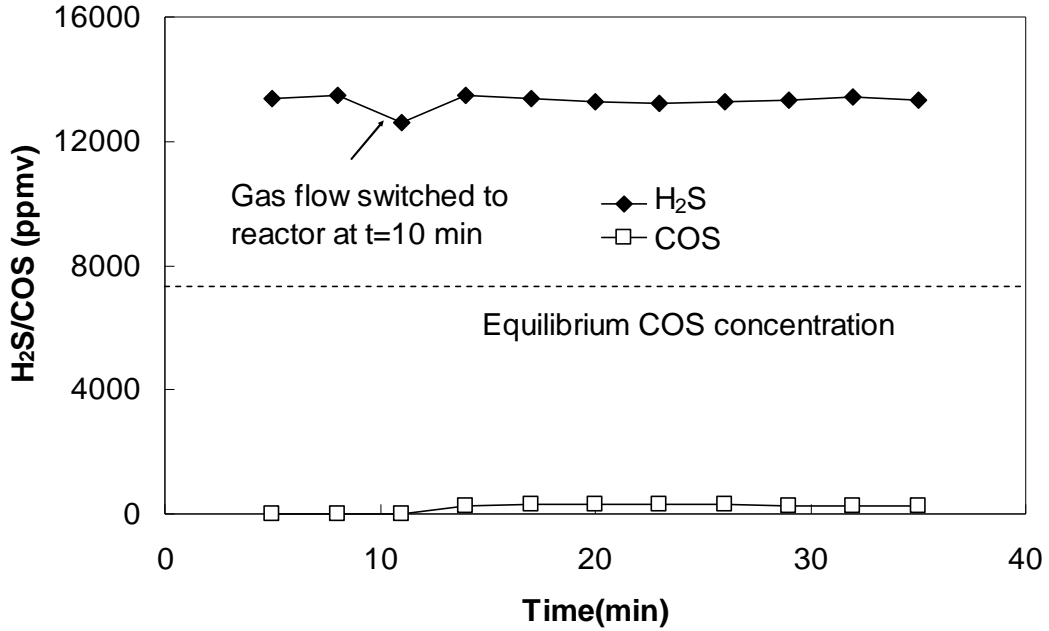
Figure VI-27. Homogeneous COS formation by the reaction between CO and H_2S at 400 °C. Tested with 13000 ppmv H_2S-25 vol.% CO-He challenge gas at a face velocity of 9.9 cm/s.

The second experiment was conducted using the challenge gas of CO_2-H_2S-He, which was switched to pass through the empty tube reactor at t=12 min, and the H_2S and COS concentrations were recorded as shown in **Figure VI-28**. The result is quite different from that of CO case. No COS was detected during the test, although the equilibrium concentration was 3000 ppmv at the test conditions. These results suggest COS formation via homogeneous reaction between CO_2 and H_2S was negligible at the test conditions.
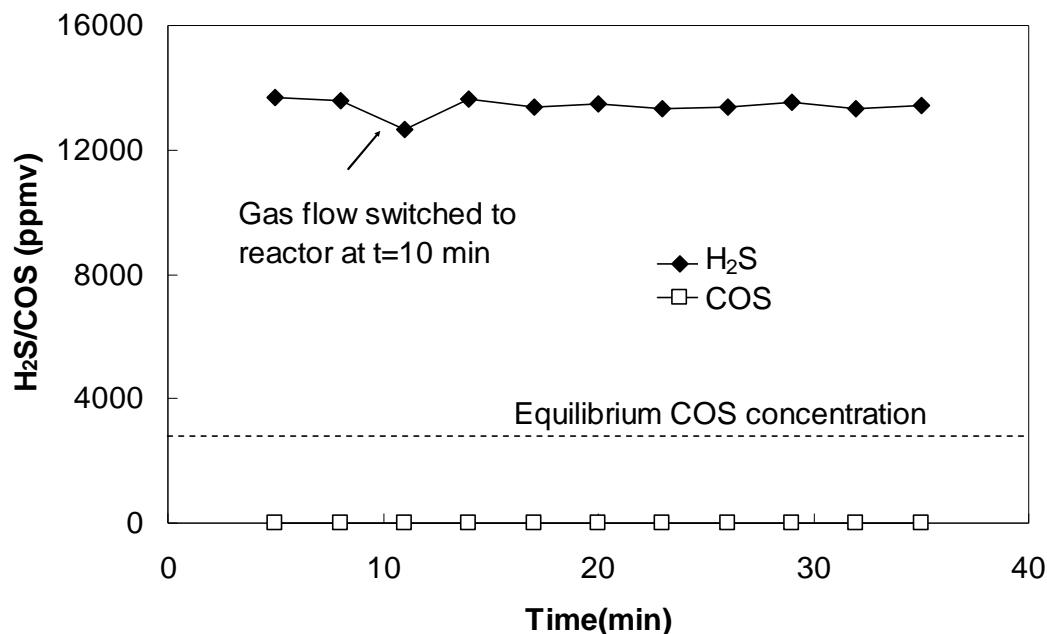
Figure VI-28. Homogeneous COS formation by the reaction between CO_2 and H_2S at 400 °C. Tested with 13000 ppmv H_2S-25 vol.% CO_2-He challenge gas at a face velocity of 9.9 cm/s

VI.3.9.2.Heterogeneous Tests

Since COS was detected in the packed bed in the presence of CO_2 and COS was not generated by the homogeneous reaction between CO_2 and H_2S, they must react heterogeneously. Besides the homogeneous reaction, CO may also react with H_2S heterogeneously in the presence of sorbents. In this section, heterogeneous reaction pathways were verified experimentally using packed beds of spent sorbent (ZnS/SiO_2).

In the spent sorbent tests, a bed of ZnO/SiO_2 sorbent particles (0.5g) were pre-saturated by 13000 ppmv H_2S-He challenge gas at a face velocity of 9.9 cm/s at 400 °C for 30 minutes. The theoretical saturation time of the bed is 7 minutes. Then the

H$_2$S-He was substituted by the challenge gas of 13000 ppmv H$_2$S-25 vol.% CO-He, and

the experimental record commenced as shown in **Figure VI-29**.   The spent sorbent bed

yielded a stable COS concentration, ca. 190 ppmv, which closely resembled the COS

concentration generated via homogeneous reaction.   At t=46 min, the H$_2$S was removed

from gas flow and only CO-He was fed to the reactor.   As shown in **Figure VI-29**, the

COS concentration dropped drastically to below the detection limit.   These phenomena

suggest that COS formation via reaction 10 is very slow or negligible.   Therefore, it is

safe to draw the conclusion that COS formation via the reaction between CO and H$_2$S is

unlikely heterogeneous, and the homogeneous reaction between CO and H$_2$S is the

dominant reaction between CO and H$_2$S.

$$ZnS+CO=Zn+COS \tag{10}$$
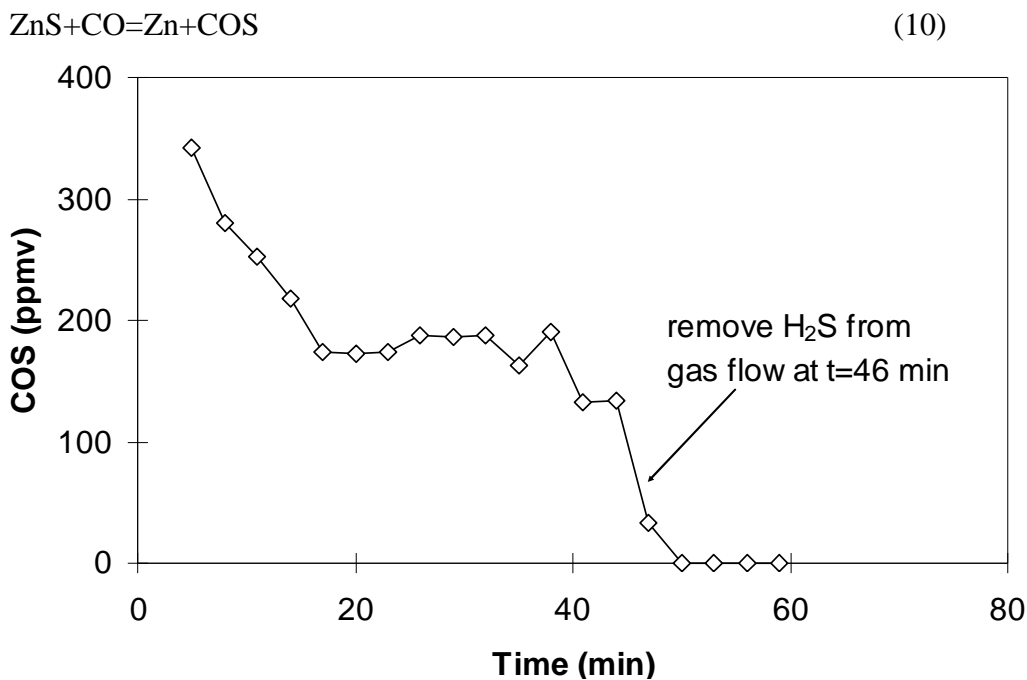
Figure VI-29. COS formation in the spent sorbent bed. Tested with 13000 ppm H$_2$S-25 vol.% CO-He challenge gas at 400 °C

230
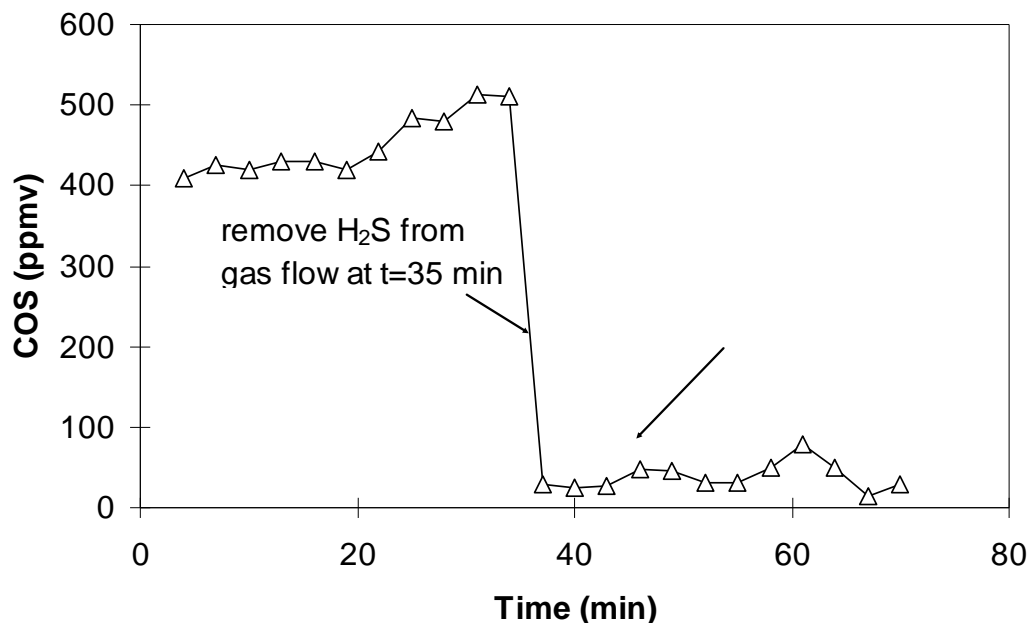
Figure VI-30. COS formation in the spent sorbent bed. Tested with 13000 ppm H_2S-25 vol.% CO_2-He challenge gas at 400 °C

A similar spent sorbent experiment was conducted in the presence of CO_2, as shown in **Figure VI-30**. The results were different from those observed in the presence of CO. In this spent sorbent test, COS concentration maintained above 400 ppmv, which was twice of the CO test. After H_2S was removed from gas flow, the COS concentration dropped as it did in CO test; however, the COS concentration remained at 30~80 ppmv. Under this test conditions, the only sulfur source was ZnS; therefore the presence of COS suggests that the reaction between ZnS and CO_2 took place heterogeneously according to reaction 8. The test results also indicate that ZnS behaves as a catalyst in COS formation via the heterogeneous reaction between H_2S and CO_2. The reaction 7 actually consists of two heterogeneous reactions:

231

$$ZnO+H_2S(g)=ZnS+H_2O(g) \hspace{4cm} (2)$$

$$ZnS+CO_2(g)=ZnO+COS(g) \hspace{4cm} (8)$$

Sasaoka et al. (1995) also observed the catalytic activity of ZnS. However, they included the homogeneous reaction between CO and H_2S in their reaction expression for COS formation. Although their result may also be true for the plateau COS concentration, because the homogeneous COS formation via CO and H_2S may be controlled by its equilibrium at a higher temperature, ca. 500 °C, their result cannot explain the COS breakthrough behaviors.

These two different reaction pathways for COS formation explain most COS related phenomena observed earlier. For example, the homogeneous reaction between CO and H_2S does not require ZnS, therefore, at very early stage COS formation is depended on CO and H_2 concentrations in the reformates. Therefore the breakthrough of COS takes much earlier than H_2S and the homogeneous COS formation is barely affected by water contents. As the reactions take place, more ZnS is generated and the heterogeneous reaction between CO_2 and H_2S gradually becomes the major contribution for COS formation in the absence of high water content. The COS concentration increases and becomes controlled by CO_2 and H_2O concentrations. If CO_2 is absent in challenge gas, e.g., H_2S-H_2-CO-He, the water gas shift reaction takes place and CO_2 is generated. As ZnO is consumed, less water and CO_2 is generated, and in turn COS concentration will drop gradually to and approach the level that the homogeneous

reaction between CO and H_2S can support.   In the presence of CO_2 and CO, the high

water content will virtually eliminate the heterogeneous COS formation allowing the

homogeneous COS formation to dominate.

Although the COS generation via the homogeneous reaction between H_2S and CO

significantly reduces the total sulfur breakthrough time, its homogeneous characteristic

can be utilized to mitigate the homogeneous COS formation by employing low reaction

temperatures because homogeneous reactions usually have high activation energies and

they are more sensitive to temperature changes than the heterogeneous reactions.

VI.4. Conclusions

The reactions involved in the desulfurization procedure of reformates are

complicated.   Desulfurization, water gas shift, ZnO reduction, and COS formation are

all involved in the reaction systems.   The reaction characteristics of each compound

were investigated by using high efficiency ZnO sorbents tested at a high face velocity.

The experimental results suggest the sulfur removal efficiency for reformates was

much worse than that for H_2S-H_2 or H_2S-He challenge gases.   This inefficiency is

intrinsic because of the presence of water, CO, and CO_2.   They impair the

desulfurization performances of ZnO sorbents in different ways.   CO and CO_2 do not

affect the reaction between ZnO and H_2S at 400 °C, but they produce COS, which is hard

to be captured by ZnO, and therefore reduce the desulfurization efficiency.   Although

233

water does not produce COS, it significantly decelerates the reaction between ZnO and H$_2$S and reduces the H$_2$S breakthrough time.

The total sulfur breakthrough time is determined by the smaller one of the H$_2$S breakthrough time and COS breakthrough time. In the absence of high concentration of water, the total sulfur breakthrough is determined by the homogeneous COS formation. After the ZnO in the bed is converted to ZnS, the COS formation in the packed bed is controlled by the heterogeneous COS formation. In the presence of high water concentration such as those encountered in reformates, the COS formation in the packed bed is determined by homogeneous COS formation. The reaction between H$_2$S and ZnO is hindered significantly and yields shortened H$_2$S breakthrough time. The total sulfur breakthrough time in the presence of reformates containing 30% water is determined by H$_2$S breakthrough. The desulfurization performance is substantially impaired due to the influences of CO, CO$_2$ and H$_2$O. In the reformates test, breakthrough sulfur capacity is below 30% of the stoichiometric value, a 7% loss of stoichiometric capacity due to COS formation was observed.

This study outlined the intrinsic characteristics of desulfurization using ZnO based sorbent. In practice, the desulfurization performance is usually worse than these described in this study and huge reactor sizes are usually required. In order to improve the intrinsic reaction characteristics, novel sorbent designs and process designs are highly favored. For example, the use of sorbents that are active to COS, such as rare earth

234

metal oxide based sorbents, CuO and Ag_2O based sorbents, will increase the total sulfur capacity and reduce the reactor size. The low temperature processes may be another choice to reduced the homogeneous COS formation, because homogeneous reactions usually have high active energies and are sensitive to temperature. In addition, the reduction of CO, CO_2 and H_2O concentrations in reformates before the desulfurization is a viable alternative.

Acknowledgements

CHAPTER VII.

NOVEL TRANSITION METAL DOPED ZINC OXIDE SORBENTS FOR REGENERABLE DESULFURIZATION APPLICATIONS AT LOW TEMPATURES

Abstract

Zinc oxide (ZnO) is a widely used sorbent for H_2S removal at moderate temperatures. In this study, nine different transition metal doped ZnO sorbents were prepared and supported on SiO_2 particles (100-200 μm) by incipient wetness impregnation. The results of desulfurization tests on these sorbents at room temperature indicate that a copper doped ZnO/SiO_2 sorbent ($Cu-ZnO/SiO_2$) has the highest saturation sulfur capacity of 0.213 g sulfur/g ZnO (54% of the theoretical capacity) which is twice that of ZnO/SiO_2 sorbent. Compared with ZnO/SiO_2, copper doped sorbent was more sensitive to temperature changes at low temperatures, ca. >100°C. A comparative study suggests that $Cu-ZnO/SiO_2$ is highly regenerable even at a low regeneration temperature, ca., 300 °C, which is 300 °C lower than the typical regeneration temperature of commercial ZnO sorbents. After ten cycles of regeneration/sulfidation, the sorbent maintained its sulfur capacity. Experimental results at 200 °C suggest that $Cu-ZnO/SiO_2$ had a higher

236

capacity than ZnO/SiO_2 sorbent and there was no carbonyl sulfide (COS) formation. In the tests at 400°C, the $Cu-ZnO/SiO_2$ demonstrated lower capacity than ZnO/SiO_2 sorbent due to the severe COS formation. The spent $Cu-ZnO/SiO_2$ catalyzed the reaction between CO_2 and H_2S, and this reaction kinetics fell into the equilibrium control regime.

Key word: Doped ZnO, Low temperature desulfurization, Reformates, Fuel cell.

VII.1. Introduction

Precious metals are widely used as catalysts to produce high purity hydrogen in fuel processing systems via such processes as: catalytic reforming, water gas shift (WGS), and preferential oxidation of carbon monoxide (PrOx). They are also used as electrode materials in fuel cells. These metals have low sulfur tolerance, e.g., 0.1 ppmv sulfur for PEMFC and 10 ppmv for SOFC. Typical sulfur concentrations in logistic fuels may be as high as 3000 ppmw. Metal oxide based sorbents, such as zinc oxide (ZnO), iron oxide (F_2O_3), and copper oxide (CuO), have been developed to remove sulfur species, mainly H_2S, from gaseous fuels and reformates (Slimane and Abbasian, 2000a). ZnO is widely used to remove H_2S from gas streams at low temperatures (<500 °C) because of its high equilibrium constant and high sulfur capacity. However, ZnO cannot remove H_2S below 0.6 ppmv at 400°C in the presence of 30 vol.% water, due to equilibrium limitations. Additional desulfurization units operated at lower temperatures (room temperature to 100 °C) is required to remove sulfur down to 0.1 ppmv to meet the sulfur

237

requirements of some PEM fuel cells. Moreover, during cold startup of a fuel cell system, the fuel processing units experience a temperature transient from room temperature to several hundred Celsius. Therefore, a protective sorbent bed may be necessary to remove H_2S residuals from the primary desulfurization unit before it reaches steady state. However, the reaction between H_2S and a metal oxide sorbent at fuel cell stack temperatures are confined to the outer layer of the solid sorbent particles (e.g., ZnO). Therefore the sulfur removal capacity at lower temperatures is limited by solid state diffusion and it is much lower than that at higher temperatures (Baird *et al*., 1992). The desulfurization performance of metal oxide based sorbents at low temperatures must be enhanced in order to protect fuel cells against permanent deactivation.

In order to improve desulfurization performance, sorbent with high porosity and small grain sizes are preferred. Therefore, mixed metal oxide sorbents, such as supported sorbents, sorbents mixed with inert, active sorbent mixtures, are widely used. In the supported sorbents, active sorbent substances are supported on secondary oxides to form high surface area and high porosity sorbent particles/extrudates. These secondary compounds are mainly inert to sulfur, such as Al_2O_3 particulates (Gasper-Galvin *et al*., 1998; Wang, and Lin, 1998; Ko *et al*., 2005; Wakker *et al*., 1993; Zhang *et al*., 2003; Flytani-Stephanopoulos *et al*., 1998), monolith (Bakker *et al*., 2003), SiO_2 (Kyotani *et al*., 1989; Ko *et al*., 2005), TiO_2 (Ko *et al*., 2005), zeolite (Kyotani *et al*. 1989; Atimatay *et al*., 1993; Gasper-Galvin *et al*., 1998), etc. In other instances, the above noted materials

238

may be used as high surface area supports to enhance the structural stability for the active sorbent (Wang and Lin, 1998; Atimatay *et al.*,1993) and to adhere/hold the ZnO crystallites within the micropores of the support in the absence of grain size growth and particle agglomeration (Wang and Lin,1998; Li and Flyzani-Stephanopoulos,1997; Goyette and Keenan, 1997; Klabunde *et al.*, 2004). Supports also serve to stabilize the active components against chemical reduction and vaporization (Flytani-Stephanopoulos *et al.*, 1998). The supported sorbent design also facilitates the incorporation of the sorbent into process system hardware, such as monoliths (Ruettinger and Farrauto, 2002). Due to the above noted advantages provided by supported sorbents, the supported sorbents provide stable performance with extended service lives (Kyotani *et al.*, 1989).

Another mixed oxide scheme is to dilute active sorbent compounds by secondary metal oxides, such as Al_2O_3 (Kamhankar *et al.*, 1986; Flytani-Stephanopoulos *et al.*, 1998; Schubert, 1993), CeO_2 (Akyurtlu and Akyurtlu, 1999; Li and Flyzani-Stephanopoulos, 1997), Cr_2O_3 (Li and Flyzani-Stephanopoulos, 1997), Fe_2O_3 (Kamhankar *et al.*, 1986; Woods *et al.*, 1991; Grindley *et al.*, 1981; Gangwal *et al.*, 1989; Gupta *et al.*, 1992), SiO_2 (Kyotani *et al.*, 1989; Schubert, 1991; Khare *et al.*, 2002), SnO_2 (Babich and Moulijn, 2003), TiO_2 (Lew *et al.* 1989, 1992; Ko *et al.*, 2005; Woods *et al.*, 1990; Harrison and Jothimurugesan, 1990; Faha and Gardner, 1982; Hatori *et al.*, 2001; Jothimurugesan and Gangwal, 1998; Sasaoka *et al.*, 1999; Pineda *et al.*, 2000; Mojtahedi, 1995; Jun *et al.*, 2002), in which Al_2O_3, Ce and Cr_2O_3 are usually used to stabilize CuO

from reduction, to disperse and reduce CuO grain size; Fe_2O_3 and TiO_2 are widely employed to stabilize ZnO from reductions. The solid state reactions between the active components and secondary metal oxides usually take place during the sorbent preparations.

Besides mixing with inert metal oxides, the active sorbents can also be mixed with other active metal oxides, e.g. ZnO-CuO. ZnO and CuO are the two most favored sorbents. ZnO has higher sulfur capacity than CuO in reducing environments, while CuO has an extremely high equilibrium sulfidation constant. CuO can thus yield extremely low equilibrium H_2S concentrations even at high steam contents and at high temperatures. The mixed metal oxides of Zn and Cu have been studied extensively as mentioned earlier. Simanek *et al*. (1976) found Cu mixed with ZnO could minimize the formation of SO_2 and S in the presence of oxygen. Dantsig *et al*. (1988) studied the Cu-ZnO mixed oxide sorbent, and found that Cu significantly enhanced the decomposition of H_2S before chemisorption. Gangwal *et al*. (1988) doped zinc titanate with Cu to achieve extremely low outlet H_2S concentrations (<1 ppm) in the presence of water at 600 °C. Baird *et al*. (1992) found that Cu and Co dopants reduced the ZnO grain size and enhanced the surface area, thus improve the sulfur capacity at room temperature. Pineda *et al*. (2000) performed cyclic sulfidation/regeneration tests on Cu doped ZnO and found the degradation in desulfurization performance due to severe loss in porosity. Chen *et al*. (2002) studied Cu-Zn oxide mixtures, and found that Cu

additives suppressed the cracking of hydrocarbons. Xue *et al*. (2003) found that ZnO

mixed with Cu, Mn and Co demonstrated significant improvements in reactivity. The

discussion above suggests that Cu-ZnO is a strong sorbent candidate for gas

desulfurization, even at low temperatures. It may have limitations such as oxide

reduction, H_2S oxidation and loss in porosity. Some of these limitations such as

porosity loss can be solved by using a supported sorbent design as noted above.

In some cases, addition of transition metals can significantly change desulfurization

performance. The function of these transition metal dopants are to: (i) increase the

surface area (Baird *et al*., 1992) and reduce the grain size (Davidson *et al*., 1995); (ii)

catalyze the desulfurization reaction by functioning as sulfur atom transporter (Sughrue,

2004; Gupta *et al*., 1993; Babich and Moulijn, 2003); (iii) generate more crystal defects

such as oxygen vacancies in the e.g., ZnO host crystallites. ZnO itself is a transition

metal oxide, and oxygen vacancies are the major defects in the ZnO crystallite (Barsoum,

2002). Oxygen vacancies are acceptors for oxygen and sulfur, and the active centers for

chemical reactions, such as hydrogenation and methanation (Borchert *et al*., 1992; Cheng

and Kung 1981). These defects/vacancies increase the mobility of oxygen and sulfur

atoms. At room temperature, a higher concentration of oxygen vacancy on the surface

of ZnO grain will accelerate the sulfidation reaction. Based on the above noted

rationale, this study demonstrates that transition metal oxides can be fortuitously used to

introduce high levels of oxygen vacancies into ZnO thereby providing desirable

desulfurization performance.   Since Zn is at an oxide state of +2 in ZnO, metal atoms with similar size to Zn atoms may replace Zn atoms in ZnO lattice.   Atoms have higher oxide state than Zn will generate Zn vacancies and atoms have lower oxides state will generate oxygen vacancies.   Therefore, the metals in Group IB, such as copper and silver, should be the right candidates to generate oxygen vacancies to facilitate the desulfurization reaction.   The simplified mechanism is shown in **Figure VII-1**.

$$
\begin{array}{cccccccc}
\text{Ag} & \text{Ag} & \boxed{\text{V}} & \text{O} & \text{Ag} & \text{Ag} & \boxed{\text{V}} & \text{O} \\
\Updownarrow & \Updownarrow & & \Updownarrow & \Updownarrow & \Updownarrow & & \Updownarrow \\
\text{Zn} & \text{Zn} & \text{O} & \text{O} & \text{Zn} & \text{Zn} & \text{O} & \text{O} \\
& & & & & & & \\
\text{Zn} & \text{Zn} & \text{O} & \text{O} & \text{Zn} & \text{Zn} & \text{O} & \text{O} \\
& & & & & & & \\
\text{Zn} & \text{Zn} & \text{O} & \text{O} & \text{Zn} & \text{Zn} & \text{O} & \text{O}
\end{array}
$$
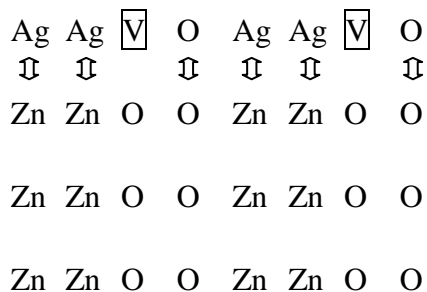
Figure VII-1. Addition of Ag_2O in ZnO creates oxygen vacancies on the anion sublattice. $\boxed{\text{V}}$ is the oxygen vacancy.

The Center for Microfibrous Materials Manufacturing (CM^3) at Auburn University has developed several microfibrous entrapped ZnO based sorbents for gas phase desulfurization at various temperatures.   Among them, Ni fiber entrapped ZnO/ACP prepared by incipient wetness impregnation demonstrated 3-fold longer breakthrough times during H_2S removal compared to packed beds of several carbon-based sorbents obtained from MSA, 3M, Willson and Scott with doubled bed thickness.   However, the Ni microfibrous entrapped ZnO/ACP was not regenerable because activated carbon particles were used as the support (Lu *et al*., 2005).   In this study, nine transition metal

doped ZnO based sorbents were evaluated for H_2S removal in the presence of CO, CO_2 and water at room temperature, low temperature (200 °C) and moderate temperature (400 °C). The supported sorbent design was employed to avoid the loss in surface area and porosity and therefore maintain fast mass transfer rate for regenerable applications. Moreover, microfibrous entrapped doped sorbents were also tested at room temperature.

VII.2. Experimental

ZnO and dopants were supported on SiO_2 particulates (100-200 μm) by incipient wetness impregnation. The dopants were copper, silver, cerium, copper and lanthanum mixture, lanthanum, magnesium, nickel, cobalt. All metal oxide precursors were metal nitrates (ACS certified) purchased from Fisher Scientific. The molar ratio of dopant metal to ZnO was fixed at 1:19. The impregnated SiO_2 particles were calcined in open air at 500 °C for 1 hour. The sorbents can be described using a general formula of $M_{0.05}Zn_{0.95}O/SiO_2$. The total metal oxide loading on the SiO_2 was 1.98 mmol/g sorbent, and the saturation sulfur capacity based on pure ZnO was 63 mg sulfur/g sorbent. The sulfur source gas was 2 vol.% H_2S-H_2 (Airgas). In the capacity analysis, the challenge gas employed was the H_2S source gas without any dilution. Other challenge gases at low H_2S concentrations were prepared by adding H_2, CO and CO_2 at various concentrations to the H_2S source gas. All the flow rates of H_2, H_2S-H_2, CO_2 and CO were well controlled by mass flow controllers.

All tests were carried out in a quartz tube reactor (0.99 cm in diameter). After loading the sorbents, air (100 ml/min) passed through the reactor until the temperature reached the set point i.e. 400 °C. Then helium (100 ml/min) flowed through the reactor for ten minutes to eliminate oxygen from the reactor, which may introduces side reactions such as sulfide oxidation. Then H_2 passed through the reactor for another 10 minutes to stabilize the temperature profile along the reactor. Finally, a challenge gas passed through the reactor at the same flow rate as H_2.

The outlet H_2S concentrations were measured by a Varian 3800 GC equipped with a thermal conductivity detector (TCD). The samples were injected in the GC every one (three minutes for challenge gas containing CO_2) by a programmed automatic 6-port-valve after experimental recording commenced.

VII.3. Results and Discussion

VII.3.1. Desulfurization Evaluation at Room Temperature

Nine transition metal doped ZnO/SiO_2 sorbents (doped metal(s): Zn=1:19) with a general formula of $M_{0.05}Zn_{0.95}O$ and ZnO/SiO_2 were tested at room temperature, i.e., 20°C. In each test, the packed bed contained 1 g of sorbent. The breakthrough curves and calculated capacities are shown in **Figure VII-2** and **Table VII-1**, respectively.
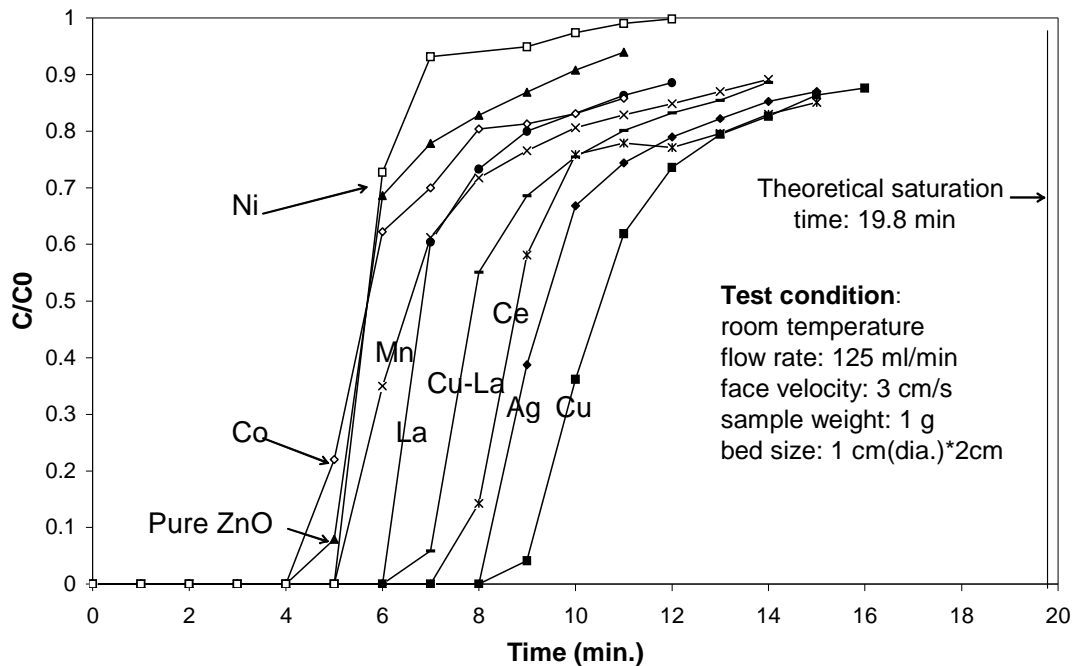
Figure VII-2. The breakthrough curves of transition metal doped ZnO sorbent tested with 2 vol.% H_2S-H_2 at room temperature.

Compared with ZnO/SiO$_2$, most doped ZnO sorbents demonstrated improvements in both saturation capacity and breakthrough capacity. Among all the doped sorbents, copper doped ZnO/SiO$_2$ sorbents (Cu-ZnO/SiO$_2$) showed highest saturation capacity and breakthrough capacity of 0.213 g sulfur/g ZnO and 0.163 g sulfur/g ZnO respectively, which were twice those of neat ZnO/SiO$_2$ at 0.113 g sulfur/g ZnO and 0.081 g sulfur/g ZnO respectively. The saturation capacity of silver doped ZnO/SiO$_2$ (Ag-ZnO/SiO$_2$) was 0.189 g sulfur/g ZnO, and ranked second at room temperature. Other metal dopants, such as Ni, Co, and Mn, which have oxide states of +2, did not demonstrate significant improvement in sulfur capacity.

245

Table VII-1. Sulfur capacities of several doped ZnO/SiO_2 sorbents.

Dopant	Saturation Capacity [1]		Breakthrough Capacity* (g S/g ZnO)
	(g S/g ZnO)	% of theor. [2]	
Cu_xO (1<x<2)	0.213	54	0.163
Ag_2O	0.189	48	0.163
Ce	0.177	45	0.142
$CuO-La_2O_3$	0.161	41	0.122
La_2O_3	0.140	35	0.122
MnO_x (1<x<1.5)	0.132	33	0.102
NiO	0.113	29	0.102
CoOx (1<x<1.5)	0.113	29	0.081
ZnO	0.113	29	0.081

1. Sulfur capacity calculated base on $t_{1/2}$ concept. Assume the sorbents are pure ZnO;
2. % of theoretical saturation capacity=capacity/theoretical saturation capacity $\times 100\%$
Note: adiabatic temperature rise at the test condition is 38 °C.

The addition of Fe^{3+} (Davidson *et al*., 1995) did not demonstrate positive effects on the sulfur capacity and reaction rate. The addition of Al^{3+} (Xue *et al*., 2003) even showed a negative effect on sulfur capacity. Moreover, copper dopants actually did not show significant decrease in the ZnO grain size (Baird *et al*., 1992), and the addition of copper may even increase it (Xue *et al*., 2003). Therefore, the above noted results confirmed the proposed oxygen vacancy theory that the addition of copper or silver may introduce more oxygen vacancies and therefore enhanced the oxygen mobility. The addition of copper yields a smaller crystal size of ZnO and exposes more ZnO to the challenge gases than the addition of silver, because silver atoms are much larger than copper atoms. Therefore, $Cu-Zn/SiO_2$ demonstrated better performance than Ag-ZnO. The effect of cerium doped ZnO demonstrated the third highest capacity. The function

of cerium may be different from Ag and Cu. Cerium may reduce the particle size and makes ZnO well dispersed on the support, as it does for CuO based sorbents (Li and Flyzani-Stephanopoulos, 1997). Reduced ceria (Ce^{3+}) may also introduce oxygen vacancies in the oxide matrix.

VII.3.2. Effects of Water, CO and CO_2 at Room Temperature

Water, CO and CO_2 have strong effects on the desulfurization performance at low temperatures. In this section, the effects of water, CO and CO_2 at room temperature (20 °C) are investigated. In the test of water, 3 vol.% water was introduced to the packed bed by passing H_2 (60 ml/min) through a vaporizer at 30 °C. In the tests for CO and CO_2, 30 vol.% CO/CO_2 (30 ml/min STP) was added to the flow consisting of 40 vol.% H_2S-H_2 (40 ml/min STP) and 30 vol.% H_2 (30 ml/min STP). In each the test, the total gas flow rate was maintained at 100 cm^3/min STP (dry basis) and the H_2S concentration was maintained at 8000 ppmv. The breakthrough curves are shown in **Figure VII-3**. The breakthrough curve tested with H_2S-H_2 is shown for comparison. The outlet H_2S concentrations in all the tests broke at almost the same time. This suggests that water, CO and CO_2 had no significant effects on the breakthrough time and desulfurization performance at room temperature. No COS formation was detected in the presence of CO and CO_2. Water did not show any hindering effect on desulfurization performance.
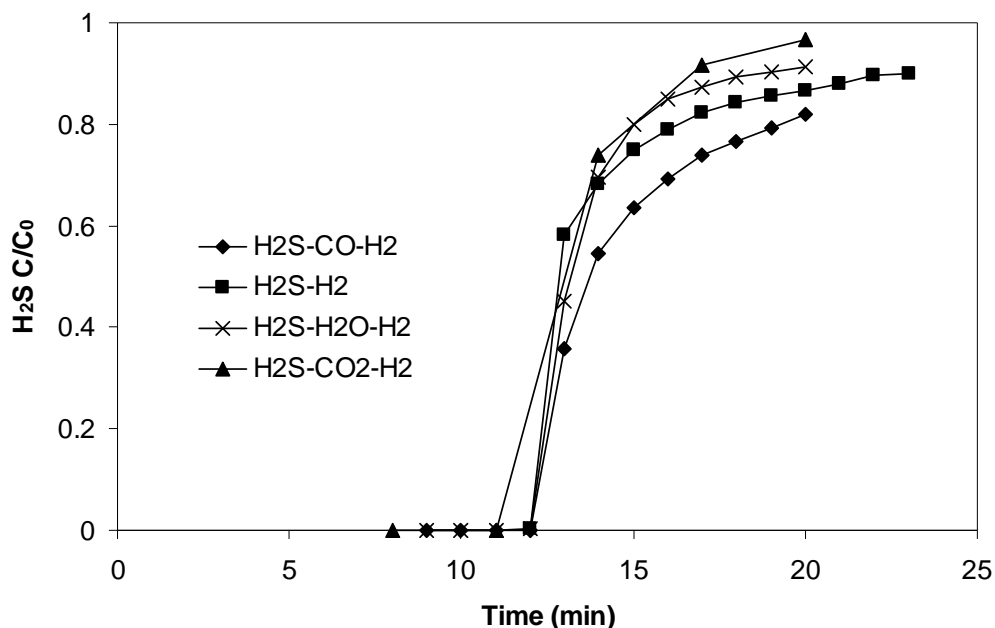
Figure VII-3. Breakthrough curves of Cu-ZnO/SiO$_2$ tested at room temperature in the presence of water, CO or CO$_2$. In each experiment, 0.5 g of Cu-ZnO/SiO$_2$ was loaded and tested with 8000 ppmv H$_2$S at a face velocity of 2.3 cm/s.

VII.3.3. Temperature Effects

The breakthrough curves of Cu-ZnO/SiO$_2$ and ZnO/SiO$_2$ at different temperatures are shown in **Figures VII-4** and **5**, and the breakthrough capacities at various temperatures are shown in **Figure VII-6.**

Figures VII-4 and **6** suggest the breakthrough sulfur capacity (time) of Cu-ZnO/SiO$_2$ at temperatures below 100 °C was stable, increased above 100 °C and became stable again at temperatures above 300 °C.   The breakthrough time/saturation time *vs.* temperature (t_b/t_s~T plot) of two sorbents shared some characteristics in common.   At low temperatures, a decrease in capacity was observed for both sorbents as the

temperature increased at low temperatures (T<150 °C). The increase in temperature reduced the absorption of H_2S on the sorbent, but it did not significantly change the apparent reaction rate at low temperatures, therefore the breakthrough capacity dropped. The increase in breakthrough capacity (time) with temperature is shown in **Figure VII-6**. Compared with the ZnO/SiO_2, at the same desulfurization temperature, $Cu-ZnO/SiO_2$ demonstrated larger breakthrough capacity (time). At lower temperatures, the difference between these two was more significant. For example, the breakthrough time (capacity) of $Cu-ZnO/SiO_2$ was twice that of ZnO/SiO_2 at a temperature below 150 °C. The t_b/t_s~T plot shows that ZnO capacity started to response the temperature change at a temperature around 200 °C, which is higher than that of $Cu-ZnO/SiO_2$, ca. 150 °C. This is reasonable, because ZnO needs a higher temperature to achieve enough oxygen mobility to continue the sulfidation reaction. However, at higher temperatures i.e. 300-400 °C, the oxygen mobility is fast enough even in the undoped ZnO, therefore the difference in the desulfurization performance of the two sorbents became less distinct.

Another phenomena noted in the shape of breakthrough curves is the step curb, this shape was not observed in all ZnO/SiO_2 tests nor in the $Cu-ZnO/SiO_2$ tests at temperatures above 300 °C. Those suggest new reaction mechanisms such as CuO reduction and grain cracking, were involved in the desulfurization reaction at low temperatures.
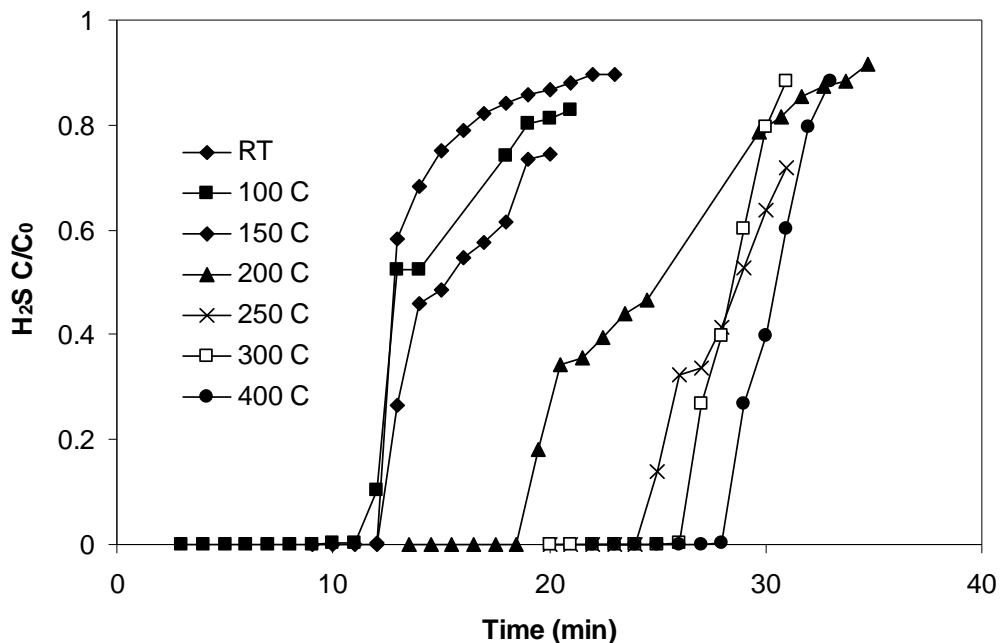
Figure VII-4. Breakthrough curves of Cu-ZnO at various desulfurization temperatures. In each experiment, 0.5 g of Cu-ZnO/SiO$_2$ was tested with 8000 ppmv H$_2$S at a flow rate of 100 cm^3/min STP.
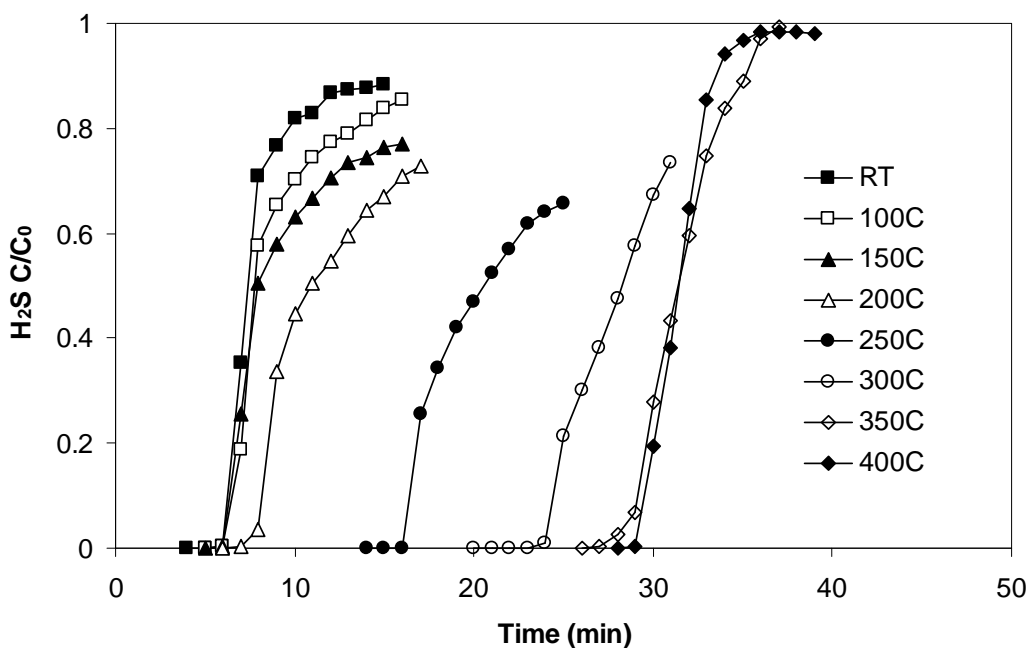
Figure VII-5. Breakthrough curves of ZnO/SiO$_2$ at various desulfurization temperatures. In each experiment, 0.5 g of ZnO/SiO$_2$ was tested with 8000 ppmv H$_2$S at a flow rate of 100 cm^3/min STP.
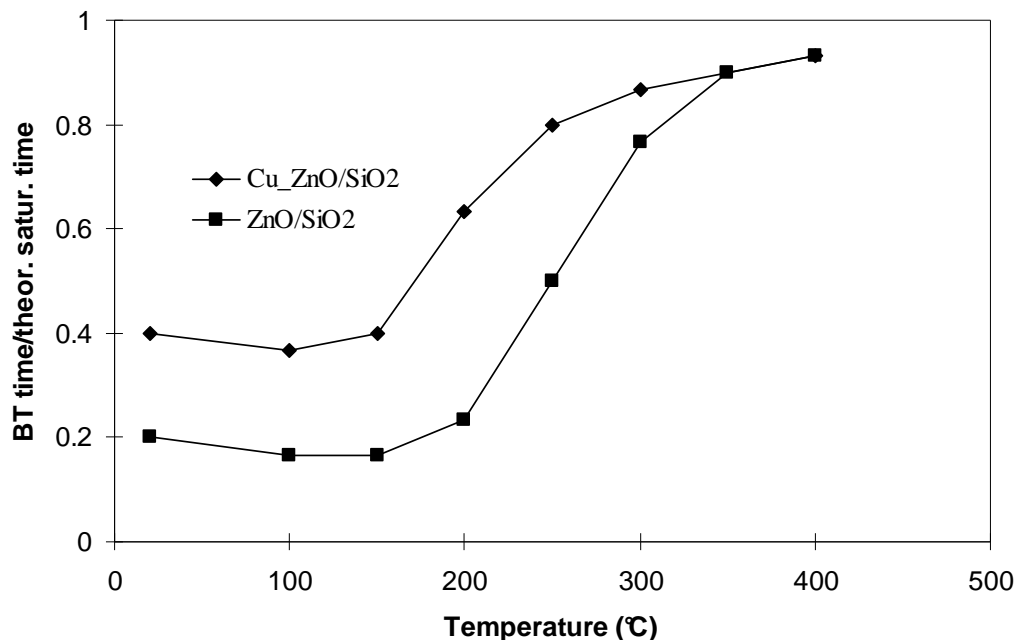
Figure VII-6. Breakthrough time/theoretical saturation time of ZnO/SiO$_2$ and Cu-ZnO/SiO$_2$ at various desulfurization temperatures.

VII.3.4. Regeneration Test

VII.3.4.1. Single Cycle Test

Sud-Chemie ZnO, ZnO/SiO$_2$ sorbents were tested for regenerable applications, and the breakthrough curves are shown in **Figures VII-7**, **8**, and **9** respectively. **Figure VII-7** suggests that ZnO particle (0.5 g) prepared by crushing ZnO extrudate was a good sorbent at room temperature, which yielded a breakthrough time of 14 min, higher than that of Cu-ZnO/SiO$_2$ sorbent. However, it was barely regenerated after 3-hour regeneration at 550 °C. Therefore, Sud-Chemie sorbent was considered a non-regenerable sorbent for the desulfurization application at room temperature.

251
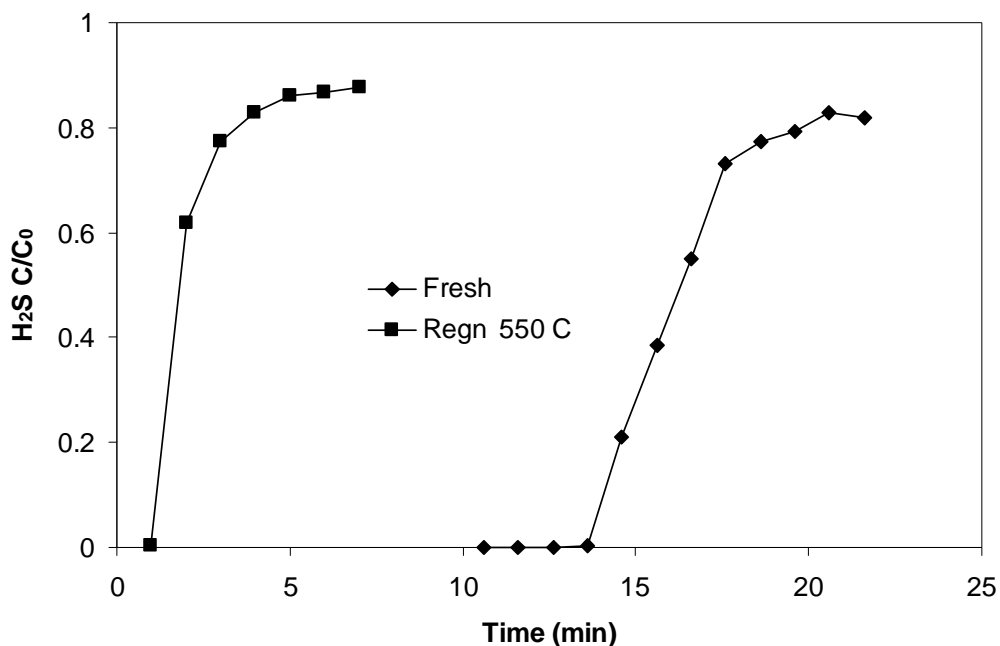
Figure VII-7. Breakthrough curves of fresh and regenerated Sud-Chemie ZnO particles (0.5 g, 105-250 μm, 25 m^2/g). Tested at room temperature with 8000 ppmv H$_2$S-H$_2$ at a face velocity of 2.3 cm/s.

Compared with Sud-Chemie, ZnO/SiO$_2$ sorbent demonstrated good regenerability as shown in **Figure VII-8**. The sulfur capacity can be recovered using a regeneration temperature above 550 °C for 1 hour. At low temperature, it cannot be fully recovered, but it retained longer breakthrough time (capacity) than Sud-Chemie as described above. Similar results were also observed in the regeneration of Cu-ZnO/SiO$_2$ sorbent as shown in **Figure VII-9**. The regeneration characteristic patterns of two supported sorbents are shown in **Figure VII-10**. In **Figure VII-10**, the recovery rate was defined as the ratio of a breakthrough time of a sorbent after regeneration to that of the breakthrough time of the sorbent when it was fresh.

252
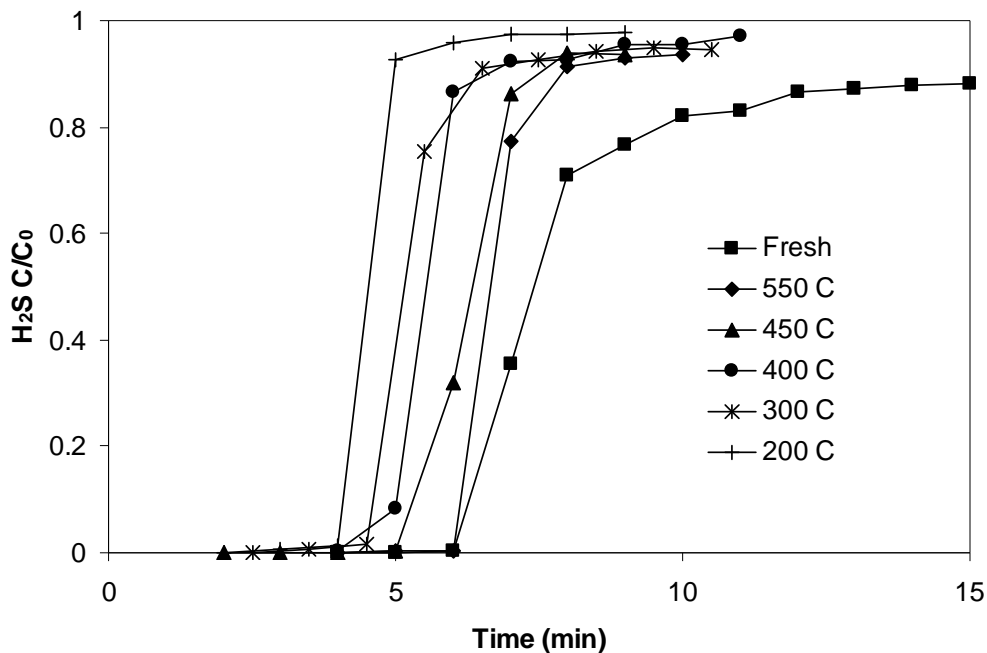
Figure VII-8. Breakthrough curves of regenerated ZnO/SiO_2 (0.5 g) at various regeneration temperatures for 1 hour. Sorbent tested at room temperature with 8000 ppmv H_2S at a face velocity of 2.3 cm/s.
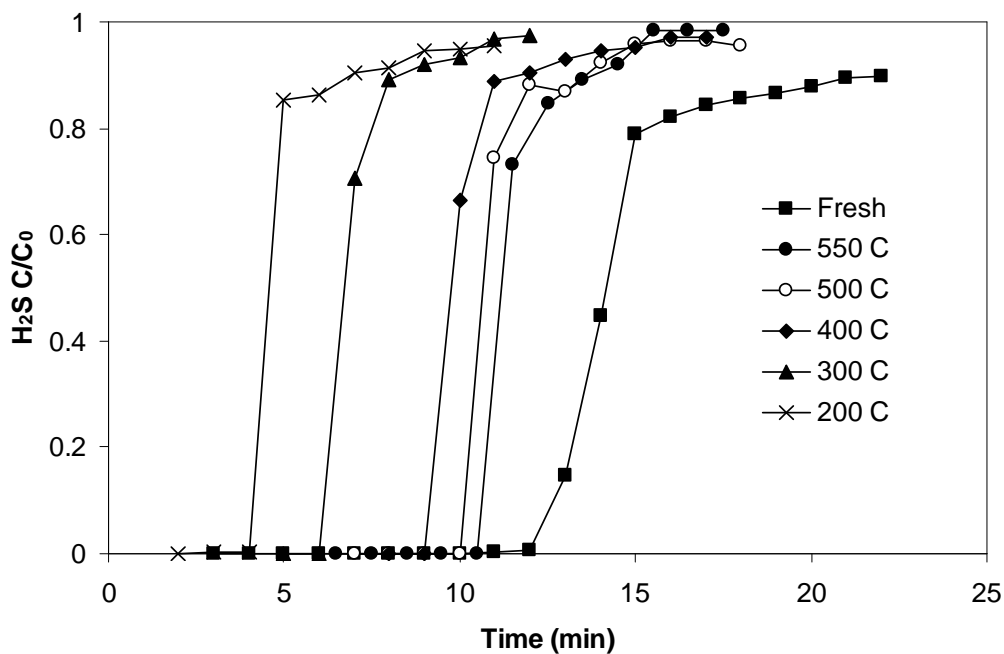
Figure VII-9. Breakthrough curves of regenerated $Cu\text{-}ZnO/SiO_2$ (0.5 g) at various regeneration temperatures for 1 hour. Sorbent tested at room temperature with 8000 ppmv H_2S at a face velocity of 2.3 cm/s.
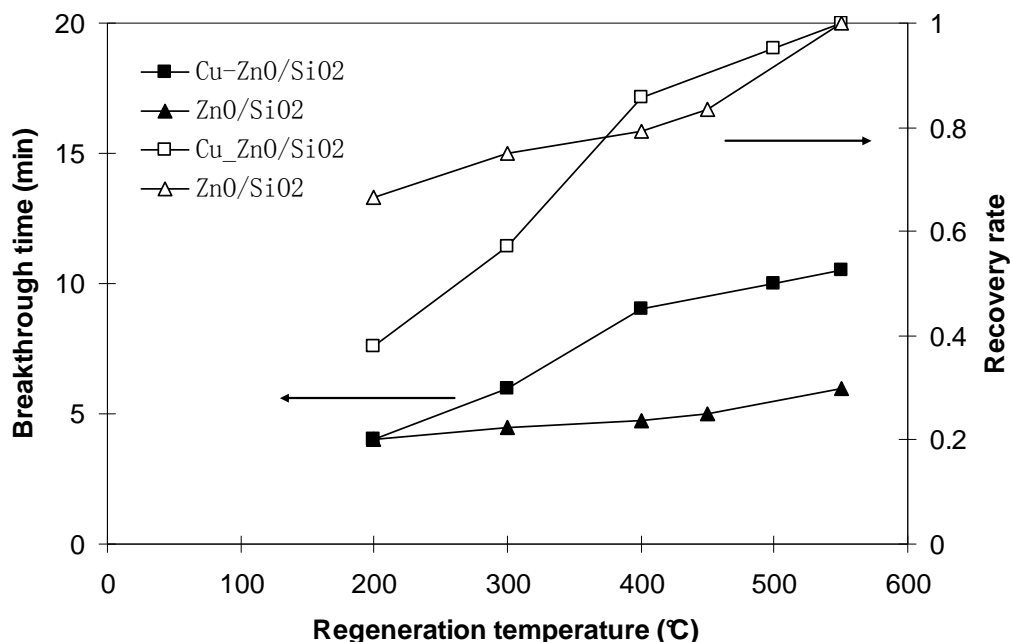
Figure VII-10. Regeneration characteristics of ZnO/SiO_2 and $Cu-ZnO/SiO_2$ sorbents. Sorbents were tested at room temperature. The recovery rate is defined as the breakthrough time of regenerated sorbent/breakthrough time of the fresh sorbent.

As shown in **Figure VII-10**, the two regenerated sorbents yielded the same breakthrough time at a regeneration temperature of 200 °C. The breakthrough times of both regenerated sorbents increased as the regeneration temperature increased. $Cu-ZnO/SiO_2$ was more sensitive to regeneration temperature than ZnO/SiO_2 sorbents in a low temperature range, ca., 200~400 °C, similar to the desulfurization tests. Since anionic vacancies accelerate the desulfurization reaction (sulfur ions substitute oxygen ions), they should accelerate the regeneration reaction (oxygen ions substitute sulfur ions) as well. Comparison shown in **Figures VII-6** and **VII-10** confirms this. As shown in these figures, the capacity of regenerated $Cu-ZnO/SiO_2$ was sensitive to the regeneration temperature, and it was also sensitive to the desulfurization temperature.

254

A comparison between ZnO/SiO_2 and $Cu-ZnO/SiO_2$ with ZnO extrudates, shown in **Table VII-2**, suggests that the dispersion of ZnO on inert supports with high surface area and high porosity is critical to maintain the desulfurization performance for multicycle applications, and the dopants can further improve the sulfur capacity.

Table VII-2. Saturation capacities of commercial ZnO sorbent, ZnO/SiO_2 and $Cu-ZnO/SiO_2$ after 1st regeneration at 550°C.

Sorbent	Saturation Capacity					
	(mg S/g ZnO)		(mg S/g sorbent)		(mg S/cm^3 bed)	
	Fresh	Regn.	Fresh	Regn.	Fresh	Regn.
ZnO	37.8	4.73	34.1	4.26	37.5	4.68
ZnO/SiO_2	113	93.1	19.2	14.9	11.5	8.94
$Cu-ZnO/SiO_2$	213	146	36.2	23.4	21.7	14.0

VII.3.4.2. Multiple Cycle Test on $Cu-ZnO/SiO_2$

The $Cu-ZnO/SiO_2$ sorbent is highly regenerable. $Cu-ZnO/SiO_2$ (1 g) was tested for H_2S removal and the breakthrough curves for multiple adsorption/desulfurization cycles are shown in **Figures VII-11** and **12**. All the desulfurization tests were carried out at the same conditions. In these multiple cycle tests, Regns 2 and 3 were regenerated at 400 °C for 1 hour, and Regn 4 at 400°C for 3 hour. All spent sorbents in the other tests were regenerated at 550°C for 1 hour. Breakthrough patterns of $Cu-ZnO/SiO_2$ after ten cycles and fresh $Cu-ZnO/SiO_2$ were almost the same. **Figure VII-11** also indicates that the $Cu-ZnO/SiO_2$ had high regenerability for multiple cycle applications, and the best regeneration condition for spent $Cu-ZnO/SiO_2$ is at 550 °C for 1 hour.
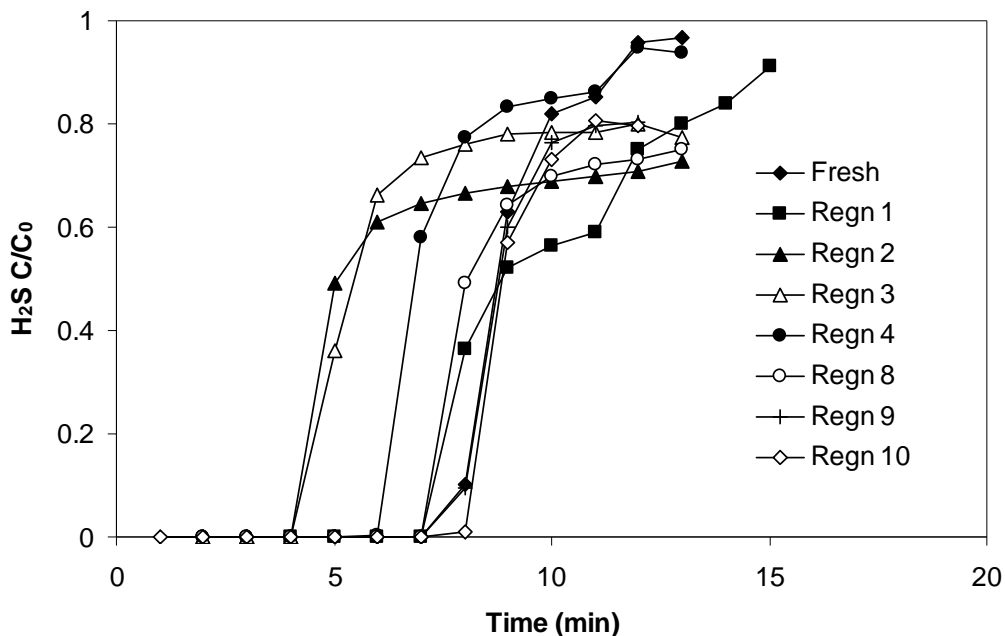
Figure VII-11. Breakthrough curves of multiple adsorption/desulfurization cyclic tests. Cu-ZnO/SiO$_2$ sorbent (1 g) was tested with 2 vol.% H$_2$S-H$_2$ at a face velocity of 3 cm/s at 20 °C.
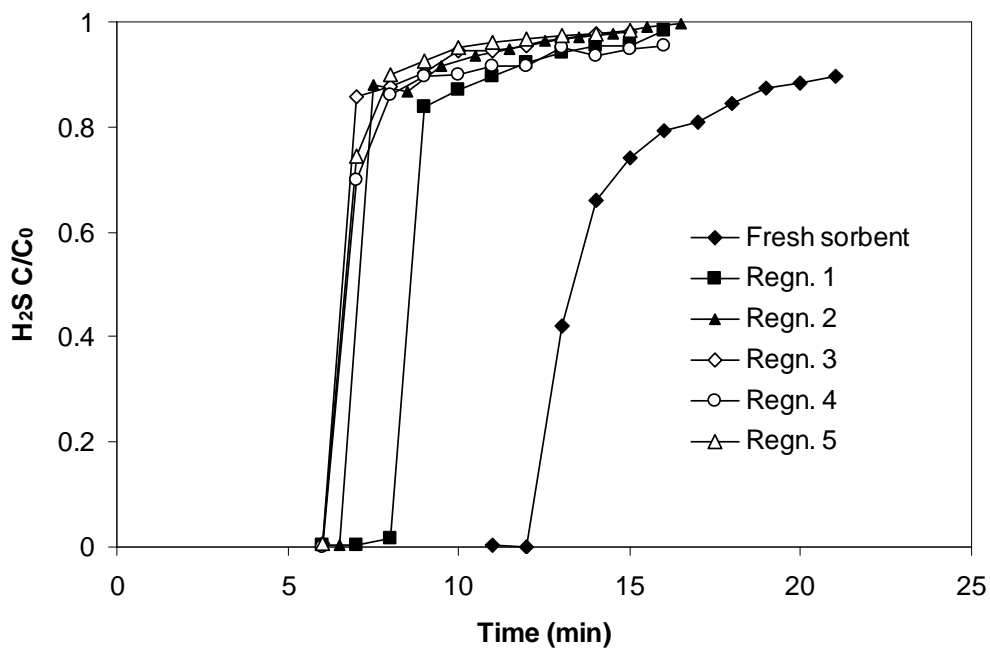
Figure VII-12. Breakthrough curves of multiple adsorption/desulfurization cyclic tests. Cu-ZnO/SiO$_2$ sorbent (0.5 g) was tested at 20°C with 8000 ppmv H$_2$S-H$_2$ at a face velocity of 2.3 cm/s. Sorbent was regenerated at 300 °C for 1 hour.

Due to the addition of copper, Cu-ZnO/SiO$_2$ sorbent can be regenerated at low temperatures. Further cyclic tests of Cu-ZnO/SiO$_2$ were carried out, in which the spent Cu-ZnO/SiO$_2$ were regenerated at 300 °C for 1 hour. The degradation in sorbent capacity was observed during the first few regeneration/adsorption cycles, and the breakthrough time (capacity) was finally stabilized around 6 minutes (79.8 mg S/g ZnO) , which is 20 % of theoretical saturation time (capacity), as shown in **Figure VII-12**.

VII.3.5. Aging Effects

The Cu-ZnO/SiO$_2$ sorbent employed in the earlier discussion was tested 1 days after calcination. The "fresh" sorbent, which here indicates the sorbent available right after sorbent preparation, demonstrated very high sulfur capacity and breakthrough time, as shown in **Figure VII-13**. The ZnO utilization of this "fresh" sorbent was about 90 %. The presence of H$_2$ slightly benefited the H$_2$S removal, while H$_2$O had slight negative effects. However, this outstanding sulfur capacity was not stable, even the sorbent particles were stored in sealed bottles. After regeneration, the sorbent just behaved like the aged sorbents as used in earlier discussion. The same tests were performed after aging the sorbents for 1 day and 7 days, as shown in **Figure VII-13**. The aging effects on the Cu-ZnO/SiO$_2$ show a consistent permanent loss of about 50% sorbent capacity. Further research efforts such as surface modification may maintain this high capacity.
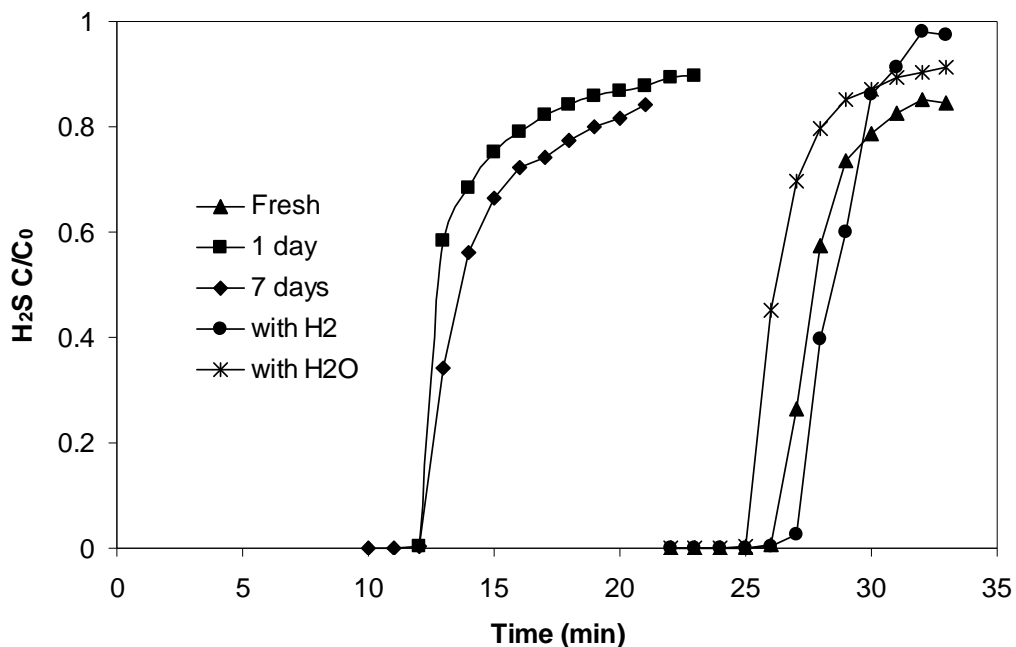
Figure VII-13. Aging effect of Cu-ZnO sorbent. Cu-ZnO/SiO$_2$ sorbent (0.5 g) was tested with 8000 ppmv H$_2$S-H$_2$ at a face velocity of 2.3 cm/s at room temperature.

VII.3.6. Desulfurization at 200 °C in the Presence of CO or CO$_2$

ZnO/SiO$_2$ and Cu-Zn/SiO$_2$ sorbents were tested at 200 °C in the two challenge gases of 1.4 vol.% H$_2$S-32 vol.% CO/CO$_2$-66.6 vol.% H$_2$. The COS equilibrium concentrations were calculated to be 330 ppmv for CO-H$_2$S-H$_2$, and 970 ppmv for CO$_2$-H$_2$S-H$_2$. The experimental results are shown in **Figures VII-14** and **15**. In the desulfurization test for CO-H$_2$S-H$_2$, COS was detected in the gas stream off the ZnO/SiO$_2$ sorbent bed. Its concentration decreased gradually to zero after reaching a peak value of 270 ppmv. During the test for Cu-Zn/SiO$_2$, no COS was detected. Possible reasons are (i) COS was converted to CO$_2$ by sulfide Cu-ZnO/SiO$_2$ sorbent (ii) Cu-ZnO/SiO$_2$ was more active and has a higher capacity to COS than ZnO/SiO$_2$. As shown in **Figure**

VII-14, the breakthrough curve of Cu-Zn/SiO$_2$ sorbent is sharper than that of ZnO/SiO$_2$

sorbent, which suggests faster apparent reaction kinetics in Cu-Zn/SiO$_2$ sorbents.

Moreover, the breakthrough time of Cu-ZnO/SiO$_2$ is also higher than that of ZnO/SiO$_2$.
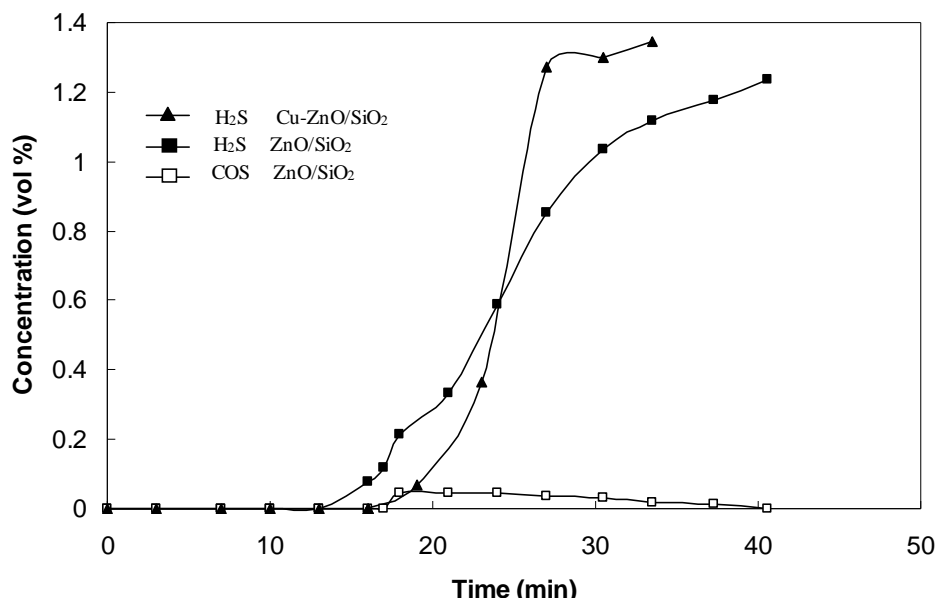
Figure VII-14. Outlet concentrations of COS and H$_2$S in the tests of ZnO/SiO$_2$ (1 g) and Cu-Zn/SiO$_2$ (1 g) at reactor temperature of 200 °C. Challenge gas was 1.4 vol.% H$_2$S-32 vol.% CO-66.6 vol.% H$_2$ at a face velocity of 4.6 cm/s.

In the experiments for CO$_2$-H$_2$S-H$_2$, no COS was detected for both ZnO/SiO$_2$ and

Cu-ZnO/SiO$_2$. It suggests that CO$_2$ was less active than CO in the formation of COS at

low temperatures. The breakthrough time of Cu-ZnO/SiO$_2$ was twice that of ZnO/SiO$_2$.

Figures VII-14 and **15** demonstrate breakthrough curves of different shapes. This

difference may result from the temperatures in the two series of experiments. It should

be noted that the reactions between CO and H$_2$S, CO and H$_2$O are an exothermic reaction,

while the reactions between CO$_2$ and H$_2$S, CO$_2$ and H$_2$ are endothermic. The actual

temperatures in the CO$_2$ experiments should be lower than those in CO experiments.

259
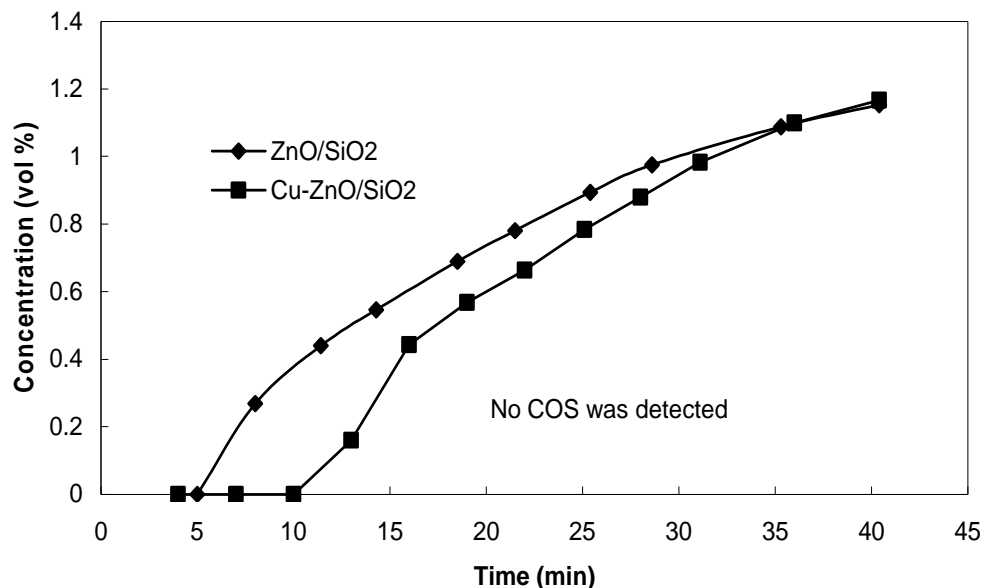
Figure VII-15. Outlet concentrations of COS and H_2S in the tests of ZnO/SiO_2 (1 g) and Cu-Zn/SiO_2 (1 g) at reactor temperature of 200 °C. Challenge gas was 1.4 vol.% H_2S-32 vol.% CO_2-66.6 vol.% H_2 at a face velocity of 4.6 cm/s.

VII.3.7. Desulfurization at 400 °C in the Presence of CO or CO_2

Similar experiments were conducted at 400 °C for both sorbents. The test results are shown in **Figures VII-16** and **17**. The experiment results on CO at 400°C are different from those tested at 200 °C. COS was detected in the both tests of Cu-ZnO/SiO_2 and ZnO/SiO_2 sorbents and the breakthrough curve of Cu-ZnO/SiO_2 was not as sharp as that of ZnO/SiO_2. Moreover, certain amount of CO_2 (<0.1 vol.%) with decreasing concentration was detected during the experiments on both sorbents. The CO_2 may be generated via the water gas shift reaction at 400 °C in the presence of water generated from the reaction between H_2S and Cu-ZnO. As Cu-ZnO converted to Cu-ZnS, less water was generated, therefore it yielded lower CO_2 concentrations.
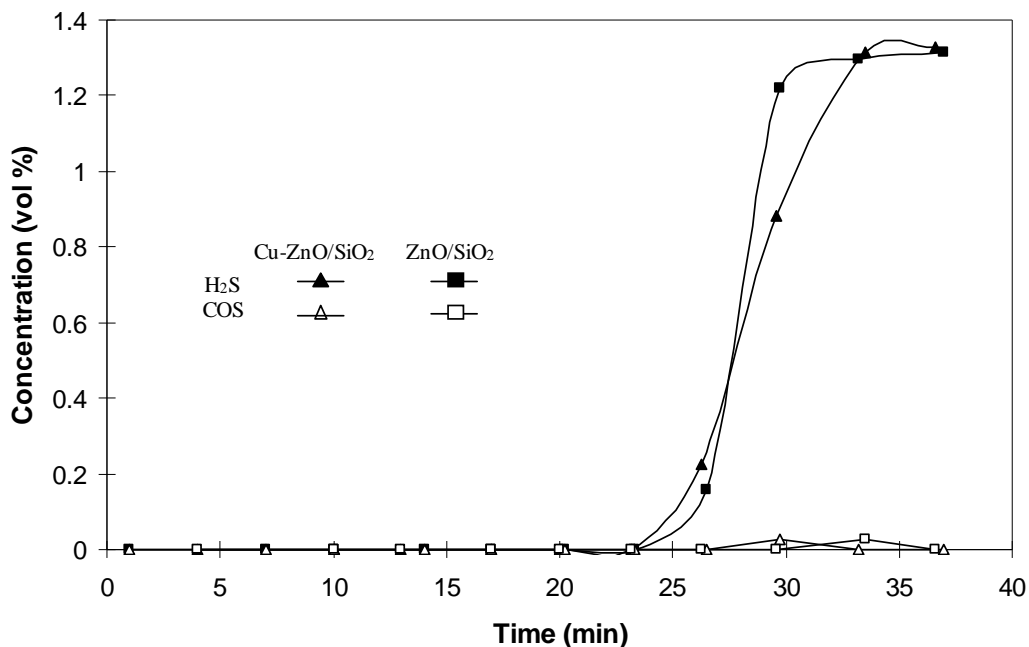
Figure VII-16. Outlet concentrations of COS and H_2S in the tests of ZnO/SiO_2 (1 g) and Cu-Zn/SiO_2 (1 g) at 400 °C. Challenge gas was 1.4 vol.% H_2S-32 vol.% CO-66.6 vol.% H_2 at a face velocity of 6.62 cm/s
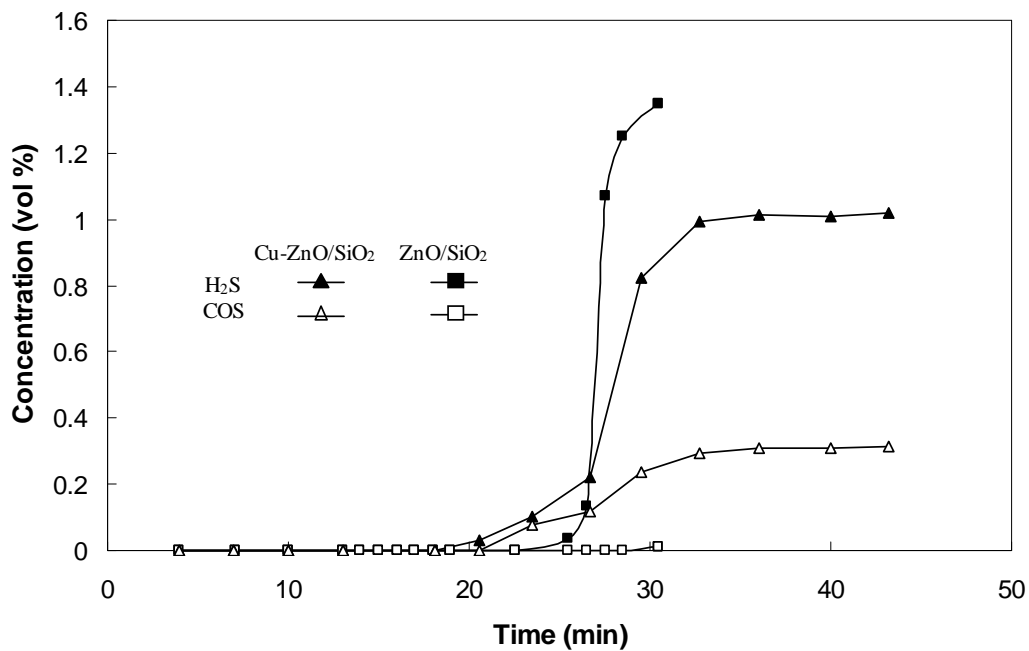
Figure VII-17. Outlet concentrations of COS and H_2S in the tests of ZnO/SiO_2 (1 g) and Cu-Zn/SiO_2 (1 g) at 400 °C. Challenge gas was 1.4 vol.% H_2S-32 vol.% CO_2-66.6 vol.% H_2 at a face velocity of 6.62 cm/s.

261

The experiments on CO_2-H_2S-H_2 challenge gas demonstrated different patterns. The H_2S breakthrough and COS formation occurred much earlier in the experiment of Cu-ZnO/SiO_2 sorbents than those in ZnO/SiO_2 sorbent. The outlet concentration of H_2S and COS maintained steady around their equilibrium values of 1 vol.% H_2S and 0.31 vol.% COS, as shown in **Figure VII-17**. The Cu-ZnO/SiO_2 behaved as a catalyst to accelerate the COS formation. The ZnO/SiO_2 sorbent demonstrated a very sharp breakthrough curve and generated trace amounts of COS, whose concentration was steadily increasing slowly throughout the test, as seen in **Figure VII-18**. This difference may result from the different water contents generated via WGS at high H_2 concentration in these two systems, and catalytic activity of two spent sorbents.
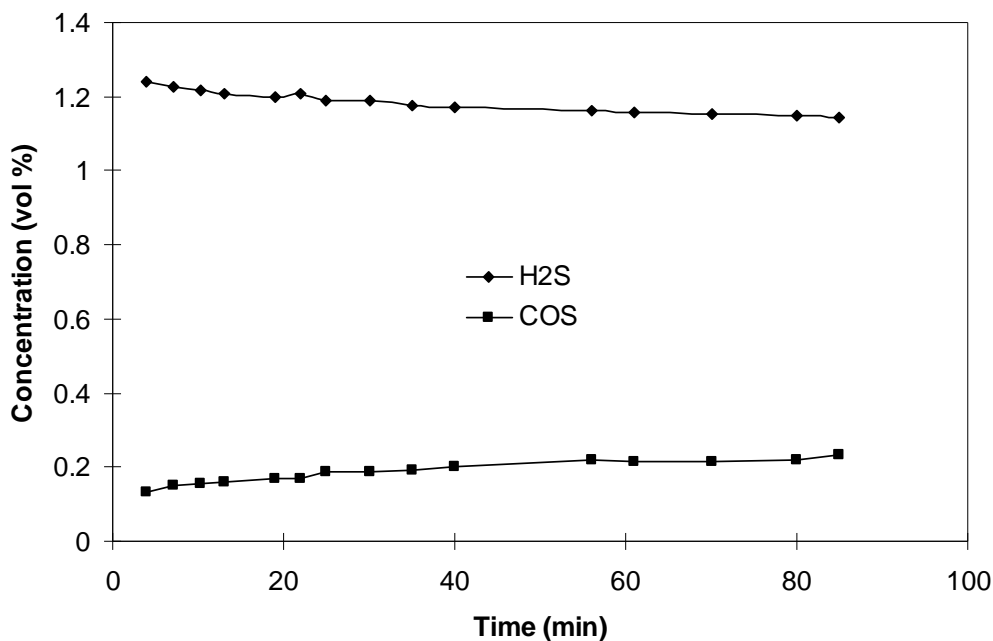
Figure VII-18. Outlet COS and H_2S concentrations in the test for spent ZnO/SiO_2 sorbent (1 g) at 400 °C. Tested with 1.4 vol.% H_2S-32 vol.% CO_2-66.6 vol.% H_2 at a face velocity of 6.62 cm/s.

VII.3.8. Microfibrous Entrapment

Microfibrous entrapped Cu-ZnO/SiO$_2$ was tested at room temperature.   A packed bed containing the same amount of Cu-ZnO/SiO$_2$ sorbent was also tested for comparison. The experimental results are shown in **Figure VII-19**.
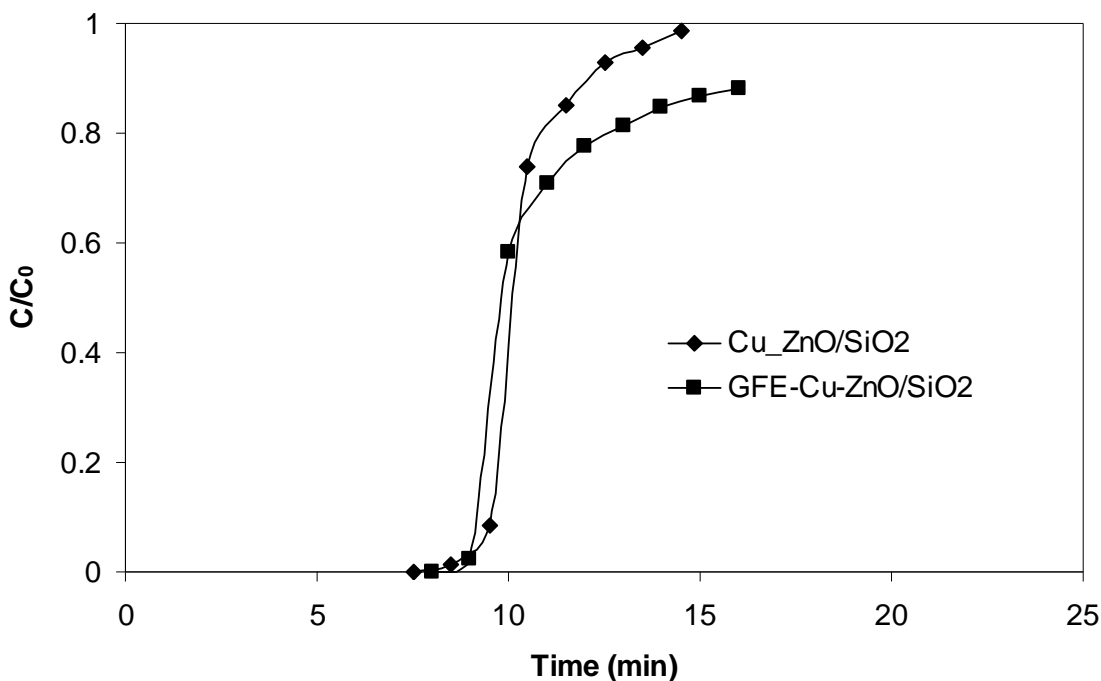
Figure VII-19. Comparison between E-glass fiber (8 μm dia.) entrapped Cu-ZnO/SiO$_2$ and Cu-ZnO/SiO$_2$ tested with 8000 ppmv H$_2$S-H$_2$ at a face velocity of 2.3 cm/s at room temperature.

In microfibrous entrapped sorbent test, three piece of E glass fiber (8 μm) entrapped Cu-ZnO/SiO$_2$ sorbent with a total weight of 0.466 g sorbent (containing 0.065 g Cu-ZnO, ZnO loading: 14 wt.%) was loaded in the quartz tube reactor.   In the packed bed, 0.38 g sorbent (containing 0.065g of Cu-ZnO) had a ZnO loading of 17 wt.%.   In **Figure**

VII-19, there is no significant difference in breakthrough capacity or the sharpness of the two breakthrough curves.

In order to understand the results above, a basic kinetic analysis was conducted, as shown in **Tables VII**-**3** and **4**. In **Table VII-3**, the intrinsic reaction rate (reaction rate for fresh sorbent) constant was calculated for Cu-ZnO/SiO$_2$ sorbent at room temperature. It suggests that the intrinsic reaction rate is larger than the external mass transfer rate. External mass transfer may be the rate-limiting step. However, the further investigation on two effectiveness factors for pore diffusion and grain diffusion are shown in **Table VII-4**. These two values suggest that pore diffusion resistance is negligible and grain diffusion resistance is severe. Therefore the microfibrous media did not show a significant improvement in breakthrough capacity at room temperature, compared the results at 400 °C.

Table VII-3. Kinetic parameters of the packed bed of Cu-ZnO/SiO$_2$.

z_t (cm)	z_a (cm)	U_i (cm/s)	t_r (s)	C_i (ppmv)	C_o (ppmv)	k_a^* (s^{-1})	$k_c\alpha^*$ (s^{-1})	K_i (s^{-1})
1.17	0.181	5.64	0.032	8000	43	65	118	409

* estimated based on the data in Chapter V.

Table VII-4. Effectiveness factor calculation.*

	K_i (s-1)	d (cm)	D_e cm^2/s	ϕ_1	η
Pore diffusion	409	0.015	0.108	0.6	0.97
Grain diffusion	409	5.0×10^{-7}	1.10×10^{-13}	16.9	0.16

*Calculation based on the data in Chapter IV.

VII.4. Conclusions

Several transition metal doped ZnO/SiO_2 sorbents ($M_{0.05}Zn_{0.95}O/SiO_2$) were prepared. The dopants of group IB metals, such as Cu and Ag, improved the desulfurization and regeneration performance of ZnO/SiO_2 significantly. The copper doped ZnO/SiO_2 ($Cu-ZnO/SiO_2$) demonstrated a high sulfur capacity of 14 mg sulfur/cm^3 bed, which is twice that of ZnO/SiO_2 and 3 times larger than the commercial ZnO sorbent at the same particle size. $Cu-ZnO/SiO_2$ requires a lower regeneration temperature than the commercial ZnO sorbents and ZnO/SiO_2 sorbent do. The sorbent can be well regenerated at a temperature above 300 °C for multi-cycle applications. Further reduction in regeneration temperature of $Cu-ZnO/SiO_2$ needs more research efforts. The mass transfer study suggests that the desulfurization process using $Cu-ZnO/SiO_2$ sorbents was controlled by grain diffusion at room temperature. A further reduction in ZnO grain size will yield an improved performance. The "fresh" $Cu-ZnO/SiO_2$ sorbent demonstrated even higher capacity than the aged one. The modification of the surface and structure properties may enhance the performance of this sorbents. Moreover, $Cu-ZnO/SiO_2$ did not introduce COS formation in the presence of CO and CO_2 at a temperature below 200 °C. At moderate temperatures, ca. 400 °C, copper significantly accelerated the reaction between CO_2 and H_2S, the COS formation was equilibrium controlled. Therefore, $Cu-ZnO/SiO_2$ is a strong choice for the reformate desulfurization at low temperatures (T<200 °C).

The desulfurization at room temperature was mainly controlled by lattice diffusion, future sorbent design should aim at reduction in grain size or improve the ionic mobility in the grain. However, due to the severe intra-particle mass transfer resistance, the microfibrous entrapment did not significantly improve the desulfurization performance, microfibrous entrapment makes the small sized $Cu-ZnO/SiO_2$ particulates applicable in logistic fuel procession units with reduced reactor size. For example, microfibrous entrapped $Cu-ZnO/SiO_2$ can be used as inline gas filters at stack temperature for fuel cells and protection filters during a fuel cell system startup.

Acknowledgement

Notation

C_i inlet H_2S concentration   ppmv

C_o outlet H_2S concentration   ppmv

d	characteristic size	cm
D_e	effective diffusivity	cm^2/s
k_a	apparent reaction rate	s^{-1}
k_c	mass transfer coefficient	cm/s
K_i	$K_i=k_s S_a \rho_b$ intrinsic reaction rate constant (reactor volume based)	s^{-1}
k_s	intrinsic reaction rate constant (surface area based)	cm/s
t_r	residence time	s
U_i	interstitial velocity	cm/s
z_t	the bed length	cm
z_a	the thickness of active layer	cm

Greek letters

α	external particle area per unit bed volume	cm^2/cm^3
ϕ_1	Thiele modulus	
η	effectiveness factor	

CHAPTER VIII.

CONCLUSIONS AND FUTURE WORK

For the desulfurization units in these logistic PEM fuel cell systems, the sorbents with high sulfur capacity, high regenerability and high sulfur removal efficiency, are extremely favored. Zinc oxide is a promising sorbent candidate for low temperature reformate desulfurization due to its high sulfur capacity (0.42 g H_2S /g ZnO), low regeneration temperature and high desulfurization reaction equilibrium constant (3.4×10^5 at 400 °C). In this work, the glass fiber entrapped ZnO/SiO_2 sorbent (GFES) has been developed to improve the desulfurization efficiency of ZnO sorbent with miniaturized reactors. Glass fibrous media solved the regeneration issues of Ni fiber entrapped ZnO/SiO_2 sorbent and maintained the same performance and functions of Ni fiber media. Glass fibrous media demonstrated excellent chemical stability in highly reducing and highly oxidative environments while maintaining the structural integrity after 50 cycles of regeneration/ desulfurization. The sorbent can be employed for low concentration sulfur removal; it can also be applied in a composite bed for high concentration sulfur removal.

The rest of this study focused on (i) understanding the relationship between the characteristics of GFES and its performance; (ii) testing the sorbent performance at

realistic conditions where CO, CO_2 and water are present; (iii) extending the application of the sorbent to lower temperatures.

The outstanding desulfurization performance of GFES benefited from the nano-sized ZnO grains, high porosity of SiO_2 support and the use of microfibrous media, which removes the lattice diffusion resistance, mitigates the pore diffusion resistance and improves external mass transfer rate, respectively. These results outlined the importance of using small support particles with big porosity and nanao-sized grains in sorbent design. The relationship between the apparent reaction rate (k_a) and the sharpness of a breakthrough curve (lumped K) has been established using modified Amundson equation. This relationship was employed to investigate the performance of microfibrous media. The microfibers enhanced the external mass transfer rate. The low ZnO loading in GFES improved the ZnO utilization and the sharpness of the breakthrough curves. Moreover, the high voidage reduced the pressure drop over the glass fibrous media. As a result, microfibrous entrapped ZnO/SiO_2 was able to achieve multi-log H_2S removal with few millimeter thickness and high ZnO utilization.

The negative influences of CO, CO_2, and H_2O on the H_2S removal rate and COS formation were observed. Both CO and CO_2 react with H_2S to form COS. The mechanisms of COS formation via two different pathways were revealed. CO reacted with H_2S to form COS homogeneously while CO_2 reacted with H_2S heterogeneously on the surface of ZnS. The COS formation by CO and CO_2 was suppressed by H_2 and

water.   Water severely hindered the reaction between ZnO and H_2S, and H_2S breakthrough time was significantly diminished.

Low temperatures may mitigate the COS formation and reduce the equilibrium H_2S concentration, however, they also decelerates the desulfurization kinetics and ZnO utilization.   Therefore, it is critical to maintain the sorbent activity at low temperatures. Chapter VII reported that Cu-ZnO/SiO$_2$ demonstrated highest saturation capacity at room temperature.   The addition of copper or silver dopant at 5 atomic% level doubled the sulfur capacity, compared with ZnO/SiO$_2$ sorbent.   The doped sorbents also demonstrated improved regenerability even at low temperatures, ca. 300 °C.   The microfibrous entrapped Cu-ZnO/SiO$_2$ is a good candidate to be used as an inline fuel filter working at stack temperatures.

Besides the success in the design of microfibrous entrapped ZnO based sorbents, some issues, such as COS formation and channeling on the reactor wall, have also been observed.   In order to solve the new issues, several suggestions on future research activities listed as follows.

(1) Novel sorbent or process design to mitigate COS issue

COS formation is a critical issue in the reformate desulfurization, especially in the presence of high concentration of H_2S.   The equilibrium COS concentrations in the presence of a typical model reformates containing 3000 ppmv H_2S are calculated at various temperatures, as shown in **Figure VIII-1**.   For instance, in the presence of 30

vol.% CO_2 and 20 vol.% water, the COS concentration is about 10 ppmv, much higher than the sulfur thresholds of most PEM fuel cells.   It is known that COS is hard to be captured by ZnO sorbent.   Therefore, if COS formation is oppressed and/or COS is removed efficiently, the service life of the packed bed can be extended consequentially.

$$H_2S+CO_2=H_2O+COS$$
3000 ppmv H_2S-30 % CO_2-H_2O-H_2 (balance)

$$H_2S+CO=H_2+COS$$
3000 ppmv H_2S-30% CO-H_2 (balance)
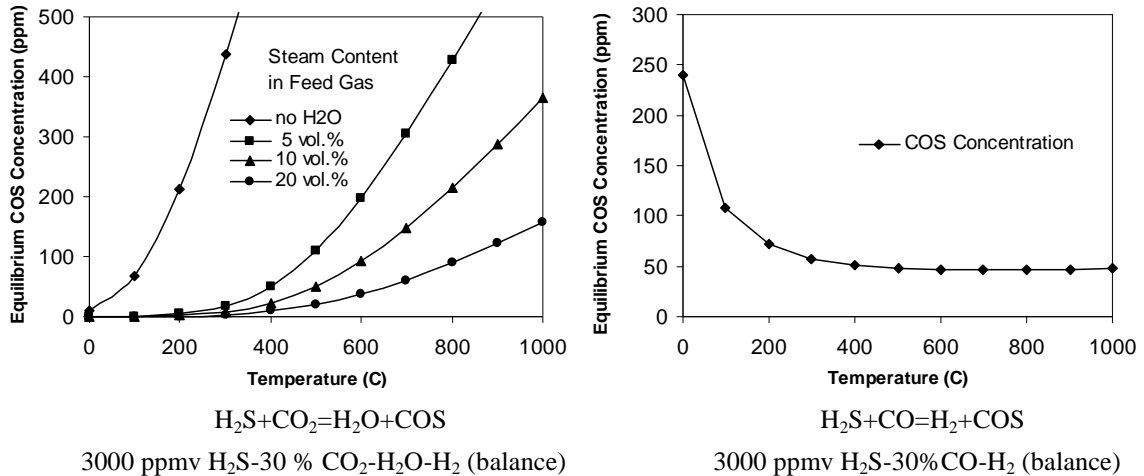
Figure VIII-1. COS equilibrium concentrations at various temperatures. Data generated by HSC software.

Due to homogeneous COS formation by CO and H_2S, and low COS capacity of typical sorbents, COS breakthrough typically takes place much earlier than H_2S, especially in the absence of high concentrations of water.   Water serves to lower the equilibrium concentration of COS as shown in **Figure VIII-1**.   At high temperatures, ca. 600 °C, the COS concentration (around 50 ppmv) is controlled by the homogeneous reaction between CO and H_2S.   At a lower temperatures ca. 400 °C, homogeneous COS formation is slow, and COS concentration (around 10 ppmv in the presence of 20 vol.% water) is controlled by the heterogeneous reaction between CO_2 and H_2S.

271

The heterogeneous COS formation in a bed can be reduced using high water content. However, the homogeneous COS formation cannot be completely removed. Novel sorbents with high COS capacities are strong choices for low temperature sulfur removal. Silver, copper and rear earth metal oxides based sorbents that have a stronger affinity to sulfur atom than ZnO does, may have good activities and capacities with respect to COS, as shown in **Figure VIII-2**. These oxides can be mixed with ZnO to form new sorbents or physically mixed with ZnO sorbent in a packed bed. The mixed sorbent or bed may eventually alleviate the COS issues. These oxides can also be placed at the downstream end of the reactors or in another reactor operated at lower temperatures.
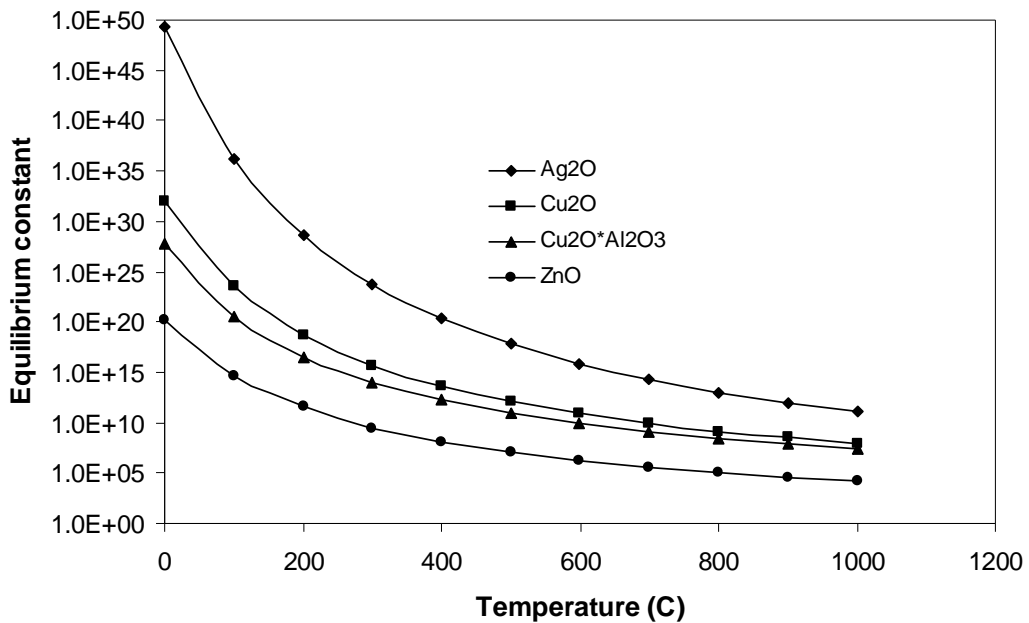
Figure VIII-2. Equilibrium constants for different COS sorbents. A generalized desulfurization reaction is described as: $COS + M_xO = CO_2 + M_xS$. Data were generated using HSC software.

If possible, even lower desulfurization temperatures (ca. 200 °C) are desirable to mitigate homogeneous COS formation and extend the service life of packed beds. The COS issues may also be solved using novel process designs. As shown in Chapter VII, the desulfurization at lower temperature ca. 200 °C yielded COS at negligible concentrations. The desulfurization temperature needs further optimization for the balance between sulfur capacity and the temperature requirement of the entire specified fuel cleanup process.

(2) Novel sorbent and process for low temperature desulfurization

Based on the results in this work, low temperature desulfurization is favored to reduce the equilibrium H_2S concentration and to mitigate the COS formation, especially the homogeneous COS formation desulfurization. Moreover, low temperature systems usually have fast cold-startup characteristics. Although low temperature fuel cleanup processes are attractive, there are several challenges in this direction.

The first challenge is the severe mass transfer resistance at low temperatures. The effective diffusivities through the pores and/or through the sorbent layer at low temperatures (i.e. <200 °C) are much smaller than those at high temperatures. (ca. > 400 °C) Therefore, the mass transfer rate is controlled by either by lattice diffusion and pore diffusion, at low process temperatures. Even in the desulfurization test using Cu-ZnO/SiO$_2$, the lattice diffusion was found to be the rate-limiting step, and the ZnO

utilization was only ~ 20% for ZnO/SiO$_2$ at room temperature, compared with the utilization of 80% of ZnO pellets at 400 °C.   The second challenge is the regeneration temperature of metal oxide sorbents.   Metal oxide sorbents can work at low temperatures, though at low efficiency.   They usually are regenerated at high temperature, ca. > 500 °C.   Therefore, the desulfurization and regeneration are operated at two temperatures with significant difference.   Extensive heating and cooling is necessary.   In a word, low temperature desulfurization using low conventional metal oxide sorbent is less efficient compared with its high temperature counterpart

These two challenges are closely related with the sorbent design.   Actually, the sulfur capacity and efficiency of sorbent at room temperature can be improved by novel sorbent design.   Due to the supported sorbent design, the ZnO/SiO$_2$ and glass fiber entrapped ZnO have improved mass transfer rate and high ZnO utilization compared with bulk ZnO sorbent.   Because of inert support and severe mass transfer resistance, these two sorbents have low saturation sulfur capacities.   Although dopants enhance ZnO utilization, the accessible ZnO is still confined to 1~2 monolayers.   Further increase in sorbent capacity at low temperatures may be realized in following directions: (i) to enhance the surface area of ZnO using SiO$_2$ or other similar supports with high surface areas and small pore, and improve the dispersion of ZnO on the surface on the support by modify the surface properties of supports.   The ZnO only covered a small amount of SiO$_2$ support, and grain growth during regeneration will further decrease the surface area.

274

Therefore, some high surface area supports with small micropores may hold ZnO grains and keep them from growth. (ii) to further optimize the sorbent composition. $Cu_{0.05}Zn_{0.95}O/SiO_2$ is only a preliminary example to demonstrate the effect of dopants. Its performance should be improved by carefully managing the Cu/ZnO and/or adding other promoters. Further research efforts under the direction of reasonable theories and assumptions are required to optimize the sorbent composition. (iii) to use active supports. The low capacities of supported sorbents are typically introduced by the using of inert supports. If the supports are active to sulfur, the sulfur capacity of supported sorbent will increase. For example, copper ion-exchanged Y type zeolite (Cu-Y) demonstrated good sulfur capacity to organic sulfur compounds in liquid fuels, as well as gaseous sulfur compounds. The hydrophobic nature of some zeolites may pose potential challenges in the presence of water.

The third challenge of using low temperature desulfurization is related to the systematic desulfurization unit design. Typically, the desulfurization temperature is between the reformer temperature and the WGS temperature in PEM systems or the cell temperature of SOFC, in order to avoid the use of heat exchangers. The conventional reforming, WGS and SOFC are usually operated at temperatures above 200 °C or even higher. The high operational temperatures make the low temperature post-reformer desulfurization become costly less effective. Due to these reasons, the current low temperature desulfurization sorbents are designed for the using as inline fuel filter to

protect PEM fuel cells, a secondary desulfurization unit. The application as primary

desulfurization unit is depended on the design of reformate cleanup process.

(3) Improvement of GFES

One direction is to optimize the void fraction of GFES. As discussed in Chapter V,

the high voidage has strong negative effects on the mass transfer coefficient and sulfur

capacity, though it may be necessary to reduce the pressure drop over the bed made of

fine particles. Therefore, the void fraction of the glass fibrous media should be

optimized for the balance between desulfurization performance and pressure drops.

The other direction is to modulize the glass fiber entrapped sorbents. GFES

successfully demonstrated excellent desulfurization performance and extremely high

structural stability during desulfurization and regeneration. However, the glass fiber

media is fragile and rigid especially after sintering. They may not match the tubing well

very well due to different shape and/or different thermal expansion, thus the channeling

may take place. GFES modules with special joints that can well connect with metal

tubing and strengthen the glass fiber media should be developed.

A proposed module structure is shown in **Figure VIII-3**. The thickness and diameter

of graphite O-ring are initially larger than those of GFES disk. When the Swagelok

fittings is tightened up, the graphite O-ring is then compressed and block the channels

between O-ring and screen, O-ring and wall. At the same time, the O-ring diameter

reduces, and it will be embedded slightly in the GFES. The design can also be used for

metal and polymer fibrous entrapped sorbents.   In these cases, the graphite O-ring and

screen may not be necessary.
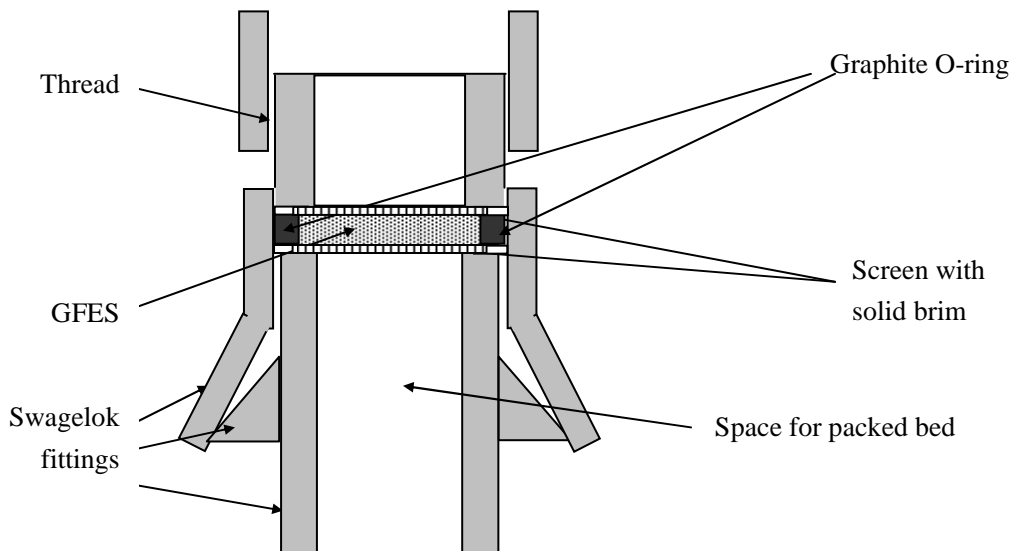
Figure VIII-3. Glass fibrous entrapped sorbents (GFES) module using modified
Swagelok fittings and graphite O-rings.

(4) Preferential oxidation of sulfur compounds

Similar to preferential oxidation of CO, sulfur compounds, such as H_2S, COS and

CS_2, may be converted to elemental sulfur or other sulfur compounds by air or oxygen.

In Claus process, the H_2S is oxidized by SO_2 and the elemental sulfur is produced.   The

oxidation of the possible sulfur containing compounds in reformates such as H_2S, COS

and CS_2 oxidation is thermodynamically favored, as shown in **Figure VIII-4**.

Theoretically, the addition of 1 vol.% O_2 to the reformates containing 30 vol.% H_2O and

20 vol.% CO_2 can reduce the H_2S concentration to 4.7×10^{-10} ppmv and COS

concentration to 3.1×10^{-13} ppmv, at 300 °C.
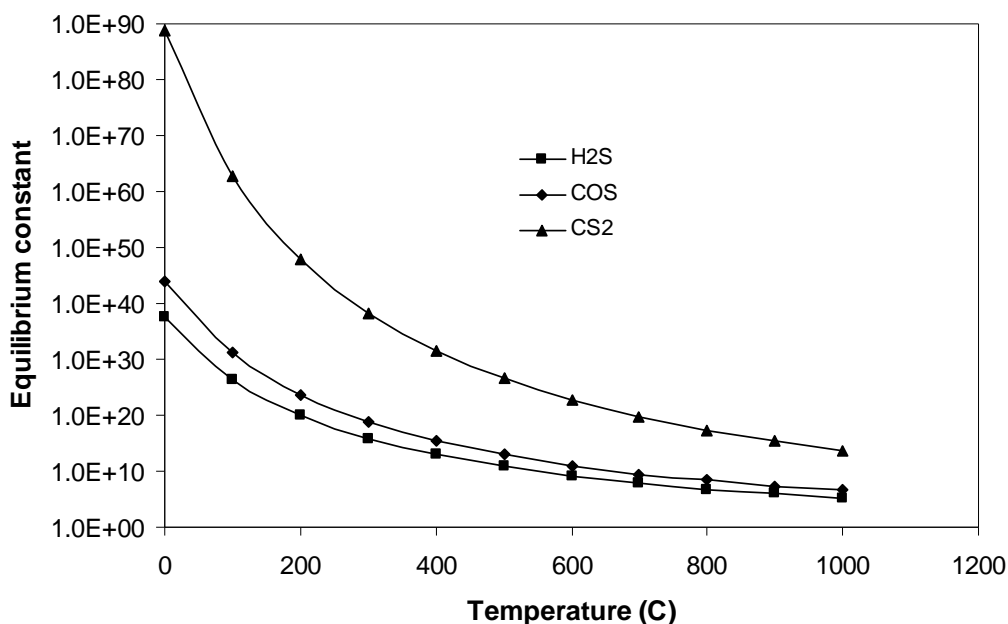
Figure VIII-4. Equilibrium constant for different desulfurization reactions of H_2S ($H_2S(g)+0.5O_2(g)=H_2O(g)+S(l)$), COS ($COS(g)+0.5O_2(g)=CO_2(g)+S(l)$) and CS_2 ($CS_2(g)+O_2(g)=CO_2(g)+2S(l)$). Data were generated using HSC software.

The kinetic data of preliminary results confirmed the feasibility of oxidation of sulfur containing compounds. In homogeneous reaction experiments, the H_2S challenge gas (2 vol.% H_2S) at 100 cc/min and household air at 10 cc/min were premixed before entering the clean quartz tube reactor without any packing materials at 300 °C. The hot zone was measured to be around 10 cm. The outlet sulfur concentration was found to be 0.5 vol.%. Another similar experiment was run at 350 °C and the outlet concentration was 0.3 vol.%. In these two experiments, yellow rings (elemental sulfur) on the cold quartz wall downstream were observed. However, H_2S was not reduced to the equilibrium concentrations. These results suggest that the H_2S oxidation was kinetically slow at

278

300~350 °C and the oxidation process was controlled by reaction kinetics. As a result, the sulfur removal by oxidation needs a large reactor to reduce the sulfur concentration to below the breakthrough concentration. For example, it was estimated that a reactor of 55 cm long (or residence time of 12 s) was able to reduce the sulfur concentration to less than 1 ppm at the experimental conditions, i.e. 300 °C and 100 cm^3/min. The same concentration can be reached easily using a packed bed of commercial ZnO sorbent with bed thickness of several centimeters. However, the sulfur "capacity" of oxidation can be considered as infinity, if elemental sulfur can be removed from the reactor continuously. Moreover, there are no regeneration issues with this process. Similar to the composite bed design, the oxidation reactor can be combined with a packed bed of sorbents (mainly copper oxide based sorbents that have high capacity to H_2S and SO_2) to achieve multi-log sulfur removal with high efficiency and high capacity.

The challenge in this direction is the O_2 management. Oxygen will introduce the formation of SO_2 and water especially in the presence of excess of O_2. Moreover, excess O_2 in anode side also has negative influences on the fuel cell performance. The addition of O_2 at sub-stoichiometric levels is preferred. If necessary, catalysts that can accelerate the preferential H_2S oxidation can also be applied to the process.

REFERENCES

Adănez, J., (1999). Utilization of Calcium Acetate and Calcium Magnesium Acetate for H$_2$S Removal in Coal Gas Cleaning at High Temperatures, *Energy & Fuels*, 13, 440-448.

Adănez J.; Garcia-Labiano, F.; de Diego, L. F.; Fierro, V., (1998). H$_2$S Removal in Entrained Flow Reactors by Injection of Ca Based Sorbents at High Temperatures, *Energy & Fuels*, 12, 726-733.

Ahmeda, M. A.; Alonsob, L.; Palaciosb, J. M.; Cillerueloc, C.; Abanadesc, J. C., (2000). Structural Changes in Zinc Ferrites as Regenerable Sorbents for Hot Coal Gas Desulfurization, *Solid State Ionics,* 138, 51–62.

Ahn, S.; Tatarchuk, B. J., (1997). Fibrous Metal–Carbon Composite Structures as Gas Diffusion Electrodes for Use in Alkaline Electrolyte, *Journal of applied electrochemistry*, 27, 9-17.

Akyurtlu, J. F.; Akyurtlu, A., (1999). Behavior of Ceria-copper Oxide Sorbents under Sulfation Conditions, *Chemical Engineering Science*, 54, 2991-2997.

Alonso, L.; Palacios, J. M.; Garcia, E.; Moliner, R., (2000). Characterization of Mn and Cu Oxides as Regnerable Sorbents for Hot Coal Gas Desulfurization, *Fuel Processing Technology*, 62, 31-44.

Amundson, N.R., (1948). A Note on the Mathematics of Adsorption in Beds. *Journal of Physical Colloid Chemistry*, 52, 1153-1157.

Alonso, L.; Palacios, J. M., (2002). Performance and Recovering of Zn-Doped Manganese Oxide as a Regenerable Sorbent for Hot Coal Gas Desulfurization, *Energy & Fuels*, *16*, 1550-1556.

Atimatay, A. T.; Gasper-Galvin, L. D.; Poston, J. A., (1993). Novel Supported Sorbents for Hot Gas Desulfurization, *Environmental Science & Technology*, 27, 1295-1303.

Ayala, R. E.; Marsh, D. W., (1991). Characterization and Long-range Reactivity of Zinc Ferrite in High-Temperature Desulfurization Processes, *Industrial & Engineering Chemistry Research*, 30, 55-60.

Ayala, R. E., (1993). Enhanced Durability of High Temperature Desulfurization Sorbents for Moving-Bed Applications Option 2 Program: Development and Testing of Zinc Titanate Sorbents, Topical Report, DOE/MC/25003-3495.

Babich, I. V.; Moulijn, J. A., (2003). Science and Technology of Novel Processes for Deep Desulfurization of oil Refinery Streams: a review, *Fuel*, 82, 607-631.

Barsoum, M.W., (2002). Fundamentals of Ceramics (Series in Materials Science and Engineering), 1st Ed., Taylor & Francis.

Baird, T.; Campbell, K.C.; Holliman, P. J.; Hoyle, R.; Stirling, D.; Williams, B. P., (1995). Mixed Co-Zn-Al Oxides as Absorbents for Low-temperature Gas Desulfurization, *Journal of the Chemical Society. Faraday Transactions*, 91(18), 3219-3230.

Baird, T; Campbell, K. C.; Holliman, P. J.; Hoyle, R. W.; Huxam, M.; Stirling, D.; Williams, B. P.; Morris, M., (1999). Cobalt–zinc oxide absorbents for low temperature gas desulfurization, *Journal of Materials Chemistry*, 9, 599–605.

Baird, T., Denny, P.J., Hoyle, R., McMonagle, F., Stirling, D., Tweedy, J., (1992). Modified Zinc Oxide Absorbents for Low-temperature Gas Desulfurization. *Journal of the Chemical Society. Faraday Transactions*, 88, 3375-3382.

Bakker, W. J.; Kapteijin, F.; Moulijin, J. A., (2003). a High Capacity Manganese-Based Sorbent for Regenerative High Temperature Desulfurization with Direct Sulfur production: Conceptual Process Application to Coal Gas Cleaning, *Chemical Engineering Journal,* 96, 223-235.

Barsoum, M.W., (2002). Fundamentals of Ceramics (Series in Materials Science and Engineering), 1st Ed.Taylor & Francis.

Ben-Slimane, R.; Hepworth, M. T., (1994a). Desulfurization of Hot Coal-Derived Fuel Gases with Manganese-Based Regenerable Sorbents. 1. Loading (Sulfidation) Test, *Energy & Fuels*, 8, 1175-1183.

Ben-Slimane, R.; Hepworth, M. T., (1994b). Desulfurization of Hot Coal-Derived Fuel Gases with Manganese-Based Regenerable Sorbents. 2. Regeneration and Multicycle Test, *Energy & Fuels*, 8, 1184-1191.

Biba, V.; Hrncir, J., (1979). Study of the Reaction of Calcium Oxide with Hydrogen Sulfide, *Chemicky Prumysl.*, 29, 205-209.

Bird, R., (2002). Transport phenomena, John Wiley & Sons, New York.

Borchert, H.; Zhang, Z. L.; Baerns, M., (1992). The effect of oxygen ion conductivity of catalysts for their performance in the oxidative coupling of methane. Preprints - American Chemical Society, Division of Petroleum Chemistry, 37, 111-16.

Cahela D. R.; Tatarchuk B. J., (2001). Permeability of Sintered Microfibrous Composites for Heterogeneous Catalysis and Other Chemical Processing Opportunities, *Catalysis Today*, 69, 33-39.

Cahela, D. R.; Chang, B. K.; Karanjikar, M.; Luna, E. A.; Tatarchuk, B.J., (2004). Microfibrous & micro-structured adsorbents and catalysts media: enhancement in effectiveness caused by static mixing, AIChE Annual Meeting, Conference Proceedings, Austin, TX, United States, Nov. 7-12, 2004.

Chang, B. K.; Lu, Y.; Tatarchuk, B. J., (2004). Materials Solutions Conference and Exposition, Columbus, Ohio, USA, Oct. 18-21.

Chang, B.-K., Lu, Y., Tatarchuk, B. J., (2006). Microfibrous Entrapment of Small Catalyst or Sorbent Particulates for High Contacting-Efficiency Removal of Trace Contaminants Including CO and H_2S from Practical Reformates for PEM H_2-O_2 Fuel Cells, *Chemical Engineering Journal (Amsterdam, Netherlands)*, 115, 195-202.

Chang, B. K.; Tatarchuk, B. J. (2003). *AIChE 2003 National meeting*, San Francisco, CA, November 16-21, 170a.

Chauk, S. S.; Agnihotri, R.; Jadhav, R. A.; Misro, S. K.; Fan, L.-S., (2000). Kinetics of High Pressure Removal of Hydrogen Sulfide Using Calcium Oxide Powder, *Separations*, 46, 1157-1167.

Chen, J.; Brown, L. D.; Baird, W. C. J.; McVicker, G. B.; Ellis, E.S.; Touvelle, M.S.; Klein, D.P.; Vaughan, D. E. W., (2002). PCT Int. Appl. WO:2002008160.

Cheng, W. H.; Kung, H. H., (1981). Chemical properties of anion vacancies on zinc oxide, *Surface Science*, 102, L21-L28.

Duggirala, R.K., Roy, C.J., Yang, H.-Y., Kalluri, R. R., Cahela, D. R., Tatarchuk, B. J., (2006). Simulation of Heterogeneous H_2S Removal in Micro-scale Gas Flows, Abstracts of Papers, 232nd ACS National Meeting, San Francisco, CA, United States, Sept. 10-14.

Dantsig, G. A.; Grechenko, A. N.; Grigorev, V. V.; Serova, L. P.; Yagodkina, G. N., (1988). Effect of the Method of Copper Oxide Addition on Chemisorption Properties of Zinc-containing Sulfur-purification Materials, *Zhurnal Prikladnoi Khimii (Sankt-Peterburg, Russian Federation)*, 61, 1240-1246.

Davidson, J. M.; Lawrie, C. H.; Sohail, K., (1995). Kinetics of the Absorption of Hydrogen Sulfide by High Purity and Doped High Surface Area Zinc Oxide, *Industrial & Engineering Chemistry Research*, 34, 2981-2989.

Desai, M; Brown, F.; Chamberland, B.; Jalan, V., (1990). Copper-Based Sorbents for Hot Gas Cleanup, *Preprints/American Chemical Society. Division of Fuel Chemistry*, 35, 87-94.

Desgrez, A.; Lescoeur, L.; Manjean, Mlle. S., (1926). Influence of pH on the Removal of Hydrogen Sulfide from Water by a Stream of Inert Gas, *Compt. Rend.,* 183, 1244-1247.

Delzer, G. A.; Kidd, D. R.; (1992). U.S. Patent 5,130,288.

Elseviers, W. F.; Verelst, H., (1999). Transition metal oxides for hot gas desulphurization, *Fuel*, 78, 601-612.

Farha, F. E.; Gardner, L. E., (1982). U.S. Patent 4,313,820.

Fenouil, L.A.; Lynn, S., (1994). Removal of H_2S from Coal Gas Using Limestone: Kinetic Consideration, *Industrial & Engineering Chemistry Research*, 33, 265-272.

Fenouil, L.A.; Lynn, S., (1995a). Study of Calcium-Based Sorbents for High-Temperature H_2S Removal. 1. Kinetics of H_2S Sorption by Uncalcined Limestone, *Industrial & Engineering Chemistry Research*, 34, 2324-2333.

Fenouil, L.A.; Lynn, S., (1995b). Study of Calcium-Based Sorbents for High-Temperature H_2S Removal. 2. Kinetics of H_2S Sorption by Calcined Limestone, *Industrial & Engineering Chemistry Research*, 34, 2334-2342.

Fenouil, L.A.; Lynn, S. (1995c). Study of Calcium-Based Sorbents for High-Temperature H_2S Removal. 3. Comparison of Calcium-Based Sorbents for Coal Gas Desulfurization, *Industrial & Engineering Chemistry Research*, 34, 2343-2348.

Flytzani-Stephanopoulos, M.; Wang, Z., (2004). Copper and Lanthanum Doped Cerium Oxide for Hot Reformate Gas Desulfurization, *Pre-print of AIChE*, [19e].

Flytzani-Stephanopoulos, M.; Gavalas, G. R.; Tamhankar, S. S., (1998). U.S. Patent: 4729889.

Focht, G. D., Ranade, P. V., Harrison, D. P., (1988). High-Temperature Desulfurization Using Zinc Ferrite: Reduction and Sulfidation Kinetics. *Chemical Engineering Science*, 43, 3005-3013.

Focht, G. D., Ranade, P. V., Harrison, D. P., (1989). High-Temperature Desulfurization using Zinc Ferrite: Regeneration Kinetics and Multicycle Testing. *Chemical Engineering Science*, 44, 2919-2926

Fogler H. S., (1992). Elements of Chemical Reaction Engineering, 2nd Edition, p543-659, Prentice-Hall, Englewood Cliffs, New Jersey.

Freund, H., (1981). Kinetics of Limestone/Dolomite with H_2S under Rich Combustion Conditions, *Combustion Science and Technology*, 26, 83-88.

Fukunaga, T.; Katsuno, H.; Matsumoto, H.; Takahashi, O.; Akai, Y., (2003). Development of kerosene fuel processing system for PEFC. *Catalysis Today*, 84, 197-203.

Gangwal, S. K.; Harkins, S. M.; Stogner, J. M.; Bossart, S. J., (1989). Testing of Novel Sorbents for H_2S Removal from Coal Gas, *Environmental Progress*, 8, 26-32.

Gangwal, S. K.; Harkins, S. M.; Stogner, J. M.; Woods, M. C.; Rogers, T. N., (1988). Bench-scale Testing of Novel High-temperature Desulfurization Sorbents: Final Report, Report, DOE/MC/23126-2662; Order No. DE89000935.

Gasper-Galvin, L. D.; Atimatay, A. T.; Gupta, R. P., (1998). Zeolite-Supported Metal Oxide Sorbents for Hot Gas Desulfurization, *Industrial & Engineering Chemistry Research*, 37, 4157-4166.

Gluud, W.; Schonfelder, R., (1927). The Removal of Hydrogen Sulfide from the Coke Gases, *Stahl und Eisen.,* 47, 453-456.

Goyette, W. J; Keenan; F. J., (1997). Method of removing hydrogen sulfide from hot gas mixtures, U.S. Patent: 5700439.

Garcia, E.; Cilleruelo, C.; Ibarra, J. V.; Pineda, M.; Palacios, J. M., (1997). Thermogravimetric Study of Regenerable Sulphur Sorbents for H_2S Retention at High Temperatures, *Thermochimica Acta*, 306, 23-30.

Gary, J. H.; Handwerk, G.E., (1984). Petroleum Refining Technology and Economics, 2nd Edition, Marcel Dekker, Inc..

Grindley, T.; Steinfeld, G, (1981). Development and Testing of Regenerable Hot Coal-Gas Desulfurization Sorbents, DOE/MC/16545-1125.

Gupta, R.; Gangwal, S. K.; Jain, S. C., (1992). Development of Zinc Ferrite Sorbents for Desulfurization of Hot Coal Gas in a Fluid-Bed Reactor, *Energy & Fuels*, 6, 21-27.

Gupta; R.P.; Gangwal; S.K.; Jain; S. C., (1993). United States Patent: 5254516.

Hamana, M.; Ikenaga, N.; Suzuki, T., (2004). Development of Calcium Ferrite Prepared from Oyster Shell for H_2S Adsorption*, Proceedings-Annual International Pittsburg Coal Conference*, 21st P2.2/1-P2.2/6.

Harris, D. K.; Cahela, D. R.; Tatarchuk, B. J., (2001). Wet layup and sintering of metal-containing microfibrous composites for chemical processing opportunities, *Composites, Part A: Applied Science and Manufacturing,* 32A(8), 1117-1126.

Harrison D. P.; Jothimurugesan, K., (1990). Reaction between H_2S and Zinc Oxide-Titanium Oxide Sorbents. 2. Single Pellet Sulfidaton Modeling, *Industrial & Engineering Chemistry Research*, 29, 1167-1172.

Hartman, D.R.; Greenwood, M.E.; Miller, D.M. (1994). High Strength Glass Fibers, Technical paper of Owens Corning.

Hatori, M.; Sasaoka, E.; Uddin, M. A., (2001). Role of TiO_2 on Oxidative Regeneration of Spent High-Temperature Desulfurization Sorbent $ZnO-TO_2$, *Industrial & Engineering Chemistry Research*, 40, 1884-1890.

285

Heinzel, J.; Nickens, A.; Hoffman, D.; Cervi, M., (2006). Advances in logistic flues desulfurization, *Preprints - American Chemical Society, Division of Petroleum Chemistry*, 51(2), 502.

Hernandez-Maldonado, A. J., Stamatis, S. D.; Yang, R. T.; He, A. Z.; Cannella, W., (2004). New Sorbents for Desulfurization of Diesel Fuels via π-Complexation: Layered Beds and Regeneration, *Industrial & Engineering Chemistry Research*, 43, 769-776.

Hernandez-Maldonado, A.J.; Yang, R.T.; Cannella, W., (2003). Desulfurization of Liquid Fuels by Adsorption via π Complexation with Cu(I)-Y and Ag-Y Zeolites, *Industrial & Engineering Chemistry Research*, 42, 123-129.

Hernandez-Maldonado, A. J., Yang, R. T., (2004a). Desulfurization of Commercial Jet Fuels by Adsorption via π-Complexation with Vapor Phase Ion Exchanged Cu(I)-Y Zeolites**,** *Industrial & Engineering Chemistry Research*, 43, 6142-6149.

Hernandez-Maldonado, A. J., Yang, R. T., (2004b). Desulfurization of Transportation Fuels by Adsorption, *Catalysis Reviews*, 46, 111-150.

Hernandez-Maldonado, A. J.; Yang, F. H.; Qi, G.; Yang, R. T., (2005). Desulfurization of Transportation Fuels by π-complexation Sorbents: Cu(I)-, Ni(II)-, and Zn(II)-zeolites, *Applied Catalysis. B, Environmental*, 56, 111–126.

Huff, W. J.; Logan, L., (1936). the Purification of Commercial Gases at Elevated Temperatures. II. The Simultaneous Removal of Hydrogen Sulfide and Organic Sulfur, *American Gas Association*, *Proceedings*, 18, 733-52,754-759.

Ikenaga, N.-O.; Ohgaito, Y.; Matsushima, H.; Suzuki, T., (2004). Preparation of Zinc Ferrite in the Presence of Carbon Material and Its Application to Hot-gas Cleaning, *Fuel*, 83, 661–669.

Jayaraman, A.; Yang, R. T.; Munson, C. L.; Chinn, D., (2001). Deactivation of π -Complexation Adsorbents by Hydrogen and Rejuvenation by Oxidation, *Industrial & Engineering Chemistry Research*, 40, 4370-4376.

Jonas, L. A., Rehrmann, J.A., (1973). Predictive Equations in Gas Adsorption Kinetics, *Carbon*, 11, 59-64.

Jothimurugesan, K.; Gangwal, S. K., (1998). Regeneration of Zinc Titanate H_2S Sorbents, *Industrial & Engineering Chemistry Research*, 37, 1929-1933.

Jun, H. K.; Lee, T. J.; Kim, J. C., (2002). a Study of Zn-Ti-Based H_2S Removal Sorbents Promoted with Cobalt Oxides, *Industrial & Engineering Chemistry Research*, 41, 3547-3556.

Kalluri, R.R., Cahela, D. R., Tatarchuk, B. J., (2006). Process Intensification Ssing Novel Micro-structured Heterogeneous Contacting Systems, Abstracts of Papers, 232nd ACS National Meeting, San Francisco, CA, United States, Sept. 10-14.

Kamhankar, S. S.; Bagajewicz, M.; Gavalas, G. R.; Sharma, P. K.; Flytzani-Stephanophoulos, M., (1986). Mixed-Oxide Sorbents for High-Temperature Removal of Hydrogen Sulfide, Industrial and Engineering Chemistry Process Design and Development, 25, 429-437.

Karanjikar, M. R.; (2005). Ph.D. thesis, Auburn University, Auburn, AL.

Karanjikar, M. R.; Lu, Yong; Chang, B. K.; Tatarchuk, B. J., (2004). Proceeding of the 41st Power Sources Conference, Philadelphia, Pennsylvania, United States, June 14-17, p.231-234

Kenaga, N.; Ohgaito, Y.; Suzuki, T., (2005). H_2S Absorption Behavior of Calcium Ferrite Prepared in the Presence of Coal. *Energy & Fuels*, 19, 170-179.

Khare, G. P., (1998). U.S. Patent: 5710089.

Khare, Gyanesh P.; Engelbert, Donald R., (2002). U.S. Patent: 6350422.

Klabunde, K; Sanford, B. R.; Jeevanandam, P., (2004). Method of sorbing sulfur compounds using nanocrystalline mesoporous metal oxides, U.S. Patent Application: 20040260139.

Klotz, I.M., (1946). the Adsorption Wave, *Chemical Reviews*, 39, 241-268.

Ko, T.-H.; Chu, H.; Chaung, L-.K., (2005). the Sorption of Hydrogen Sulfide from Hot Syngas by Metal Oxides over Supports, *Chemosphere*, 58, 467-474.

Kobayashi, M.; Flytzani-Stephanopoulos, M., (2002). Reduction and Sulfidation Kinetics of Cerium Oxide and Cu-Modified Cerium Oxide, *Industrial & Engineering Chemistry Research*, 41, 3115-3123.

Kobayashi, M.; Shirai, H.; Nunokawa, M., (2002). High-Temperature Sulfidation Behavior of Reduced Zinc Ferrite in Simulated Coal Gas Revealed by in Situ

X-ray Diffraction Analysis and Mossbauer Spectroscopy, *Energy & Fuel,* 16, 601-607.

Kobayashi, M.; Shirai, H.; Nunokawa, M., (2002). Estimation of Multiple-Cycle Desulfurization Performance for Extremely Low-Concentration Sulfur Removal with Sorbent Conating Zinc Ferrite-Silicon Dioxide Composite Powder, *Energy & Fuels*, 16, 1378-1386.

Kohler, D. A.; Zabasajja, J. N.; Krishnagopalan, A.; Tatarchuk, B. J., (1990). Metal-Carbon Composite Materials from Fiber Precursors , *Journal of the Electrochemical Society*, 137(1), 136-141.

Konttinen, J. T.; Zevenhoven, C. A. P.; Yrjas, K. P.; Hupa, M. M., (1997a). Modeling of Sulfide Zinc Titanate Regeneration in a Fluidized-Bed Reactor. 1. Determination of the Solid Conversion Rate Model Parameters *Industrial & Engineering Chemistry Research*, 36, 5432-5438.

Konttinen, J. T.; Zevenhoven, C. A. P.; Hupa, M. M., (1997b). Modeling of Sulfide Zinc Titanate Regeneration in a Fluidized-Bed Reactor. 2. Scale-Up of the Solid Conversion Model, *Industrial & Engineering Chemistry Research,* 36, 5439-5446.

Kundakovic L.; Flytzani-Stephanopoulos, M., (1998). Reduction Characteristics of Copper Oxide in Cerium and Zirconium Oxide Systems, *Applied. Catalysis A: General*, 171, 13-29.

Kyotani, T.; Kawashima, H.; Tomita, A., (1989). High_temperature Desulfurization Reaction with Cu-Containing Sorbents, *Environmental Science & Technology*, 23, 218-223.

Lew, S.; Jothimurugesan, K.; Flytzani-Stephanopoulos, M., (1989). High-Temperature H_2S Removal from Fuel Gases by Regenerable Zinc Oixde-Titanium Dioxide Sorbents, *Industrial & Engineering Chemistry Research*, 28, 535-541.

Lew, S.; Sarofim, A.; Flytzani-Stephanopoulos, M., (1992). Sulfidation of Zinc Titanate and Zinc Oxide Solids, *Industrial & Engineering Chemistry Research*, 31, 1890-1899.

Levenspiel, O., (1972). Chemical Reaction Engineering, John Willey & Sons, New York.

Fogler, H. S., (1999). Elements of Chemical Reaction Engineering (3rd Edition), Prentice Hall, New York.

Levenspiel, O., (2002). the Chemical Reactor Omnibook, OSU book store, Inc., Corvallis, Oregon.

Li, Z.-J.; Flyzani-Stephanopoulos, M., (1997). Cu-Cr-O and Cu-Ce-O Regenerable Oxide Sorbents for Hot Gas Desulfurization, *Industrial & Engineering Chemistry Research*, 36, 187-196.

Lu, Y., Sathitsuksanoh, N., Yang, H.Y., Chang, B. K., Queen, A. P., Tatarchuk, B. J., (2005). Microfibrous Entrapped ZnO-Supported Sorbent for High Contacting Efficiency H_2S Removal from Reformate Streams in PEMFC Applications, in: Wang, Y. & Holladay, J.D. (Eds), ACS Symposium Series, vol. 914. Microreactor Technology and Process Intensification, Washington DC, p. 406-422.

Lu, Y., Tatarchuk, B. J., (2003). Microfibrous Entrapped Supported-ZnO Sorbents with High Contacting Efficiency for Trace H_2S Removal in PEMFC Applications. Abstracts of Papers, 226th ACS National Meeting, New York, NY, United States, September 7-11.

Marrion, C. J.; Cahela, D. R.; Ahn, S.; Tatarchuk, B. J., (1994). Composite fiber structures for catalysts and electrodes, *J. Power Sources*, 47, 297-302.

McCreedy, T., (2000). Fabrication techniques and materials commonly used for the production of microreactors and micro total analytical systems, *Trend in Analytical Chemistry*, 19, 396-401.

Meffert; M. W., (1998). Ph.D. thesis, Auburn University, Auburn, AL.

Mojtahedi, M., (1995). H_2S Removal From Coal Gas at Elevated Temperature and Pressure in Fluidized Bed with Zinc Titanate Sorbents. 2. Sorbent Durability, *Energy & Fuels*, 9, 782-787.

Moran, M. J.; Shapiro, H. N., (1999). Fundamentals of Engineering Thermodynamics, 4th Ed. John Wiley & Sons, Inc., P804-805.

Nain, V. P. S. and Ferron, J. R., (1972). Prediction of Binary Diffusion Coefficients for Polar Gas Mixtures, *Industrial & Engineering Chemistry Fundamentals*, 11, 3, 420-421.

Newby, R. A.; Lippert, T. E.; Slimane, R. B.; Akpolat, O.M.; Pandya, K.; Lau, F.S.; Abbasian, J.; Williams, B.E.; Leppin, D., (2001). Novel Gas Cleaning /Conditioning for Integrated Gasification Combined Cycle, DOE Base Program Final Report, DOE Award Number: DE-AC26-99FT40674.

Nimmo, W., (1999). Removal of H_2S Spray-Calcined Calcium Acetate, *Industrial & Engineering Chemistry Research*, 38, 2954-2962.

Novochinskii, I.; Song, C.; Ma, X.; Liu, X.; Shore, L.; Lampert, J.; Farrauto, R. J., (2004). Low-Temperature H_2S Removal from Steam-Containing Gas Mixtures with ZnO for Fuel Cell Application. 1. ZnO Particles and Extrudates, *Energy & Fuels*, 18, 576-583.

O'Hayre, R.; Cha, S.-W.; Colella, W., Prinz, F. B., (2005). Fuel Cell Fundamentals, John Wiley and Sons, Inc., New Jersey.

Overbeek, R. A.; Khonsari, A. M.; Chang, Y.-F.; Murrell, L. L.; Tatarchuk, B. J.; Meffert, M. W., (2001). US Patent 6,231,792.

Ozdemir, S.; Bardakci, T., (1999). Hyrogen Sulfide Removal from Coal Gas by Zinc Titanate Sorbent, *Separation and Purification Technology*, 16, 225-234.

Patrick, V.; Gavalas, G.R.; Flytzani-Stephanophoulos, M.; Jothimurugesan, K., (1989). High-Temperature Sulfidation-Regeneration of $CuO-Al_2O_3$ Sorbents, *Industrial & Engineering Chemistry Research*, 28, 931-940.

Pineda, M.; Fierro, J. L. G.; Palacios, J. M.; Cilleruelo, C.; Garcla, E.; Ibarr, J. V., (1997). Characterization of Zinc Oxide and Zinc Ferrite Doped with Ti or Cu as Sorbents for Hot Gas Desulphurization, *Applied Surface Science*, 119, 1-10.

Pineda, M.; Palacios, J. M.; Alonso, L.; Garcia, E.; Moliner, R., (2000). Performance of Zinc Oxide Based Sorbents, for Hot Coal Gas Desulfurization in Multicycle Tests in a Fixed-Bed Reactor, *Fuel*, 79, 885-895.

Pham-Huu, C.; Crouzet, C.; Estournes, C.; Ledoux, M. J., (1998). High Temperature H_2S Removal over High Specific Surface Area-SiC Supported Iron Oxide Sorbent, *Journal of the Chemical Society. Faraday Transactions*, 94, 443-450.

Rajagopalan, V.; Amiridis, M. D., (1998). Hot Coal Gas Desulfurization by Perovskite-type Sorbents, *Fuel*, 78, 319-325.

Rosebaugh, T.W., (1938). Tripotassium Phosphate Process for Hydrogen Sulfide Removal, *National Petroleum News*, 30, R280-282.

Rosso, I.; Galletti, C.; Bizzi, M.; Saracco, G.; Specchia, V., (2003). Zinc Oxide Sorbents for the Removal of Hydrogen Sulfide from Syngas, *Industrial & Engineering Chemistry Research*, 42, 1688-1697.

Ruettinger, W.F.; Farrauto, R.J., (2002). U.S. Patent Application: 20020041842.

Sasaoka, E., (1994a) Stability of Zinc Oxide High-Temperature Desulfurization Sorbents for Reduction, *Energy & Fuels*, 8, 763-769.

Sasaoka, E., (1994b). Characterization of Reaction between Zinc Oxide and Hydrogen Sulfide, *Energy & Fuels*, 8, 1100-1105.

Sasaoka, E.; Hatori, M.; Sada, N.; Uddin, M. A., (2000). Role of H_2O in Oxidative Regeneration of ZnS Formed from High-Temperature Desulfurization ZnO Sorbent, *Industrial & Engineering Chemistry Research*, 39, 3844-3848.

Sasaoka, E.; Ichio, T.; Kasaoka, S., (1992). High-Temperature H_2S Removal from Coal-Derived Gas by Iron Ore, *Energy & Fuels*, 4, 603-608.

Sasaoka, E.; Sakamoto, M.; Ichio, T.; Kasaoka, S., (1993). Reactivity and Durability of Iron Ore Oxide High Temperature Desulfurization Sorbents, *Energy & Fuels*, 7,632-638.

Sasaoka, E.; Sada, N.; Manabe, A.; Uddin, M.A.; Sakata, Y., (1999). Modification of ZnO-TiO_2 High-Temperature Desulfurization Sorbent by ZrO_2 Addition, *Industrial & Engineering Chemistry Research*, 38, 958-963.

Sasaoka, E.; Taniguchi, K.; Hirano, S.; Uddin, M. A.; Kasaoka, S.; Sakata, Y., (1995). Catalytic Activity of ZnS Formed from Desulfurization Sorbent ZnO for Conversion of COS to H_2S, *Industrial & Engineering Chemistry Research*, 34(4), 1102-1106.

Sasaoka, E.; Taniguchi, K.; Uddin, M. A.; Hirano, S.; Kasaoka, S.; Sakata, Y., (1996). Characterization of Reaction between ZnO and COS, *Industrial & Engineering Chemistry Research*, 35(7), 2389-2394.

Schubert; P.F., (1991). Sulfur absorbents, U.S. Patent: 5077261.

Schubert; P.F., (1993). Sulfur absorbents, U.S. Patent: 5177050.

Simanek, J.; Pick, P.; Havlicek, J., (1976). Hydrogen sulfide removal by zinc oxide, *Sbornik Vysoke Skoly Chemicko-Technologicke v Praze, D: Technologie Paliv*, D31,437-483.

Slimane, R. B.; Abbasian, J. (2000a). Regenerable Mixed Metal Oxide Sorbents for Coal Gas Desulfurization at Moderate Temperature, *Advances in Environmental Research*, 4, 147-162.

Slimane, R. B.; Abbasian, J., (2000b). Copper-Based Sorbents for Coal Gas Desulfurization at Moderate Temperatures, *Industrial & Engineering Chemistry Research,* 39, 1338-1344.

Smith, F. Frank; Pryde, D. R., (1934). a Wet Process for the Removal of Hydrogen Sulfide from Coke-oven Gas, *Gas World*, 100, Coking Sect. 44-46.

Sohn, H. Y., (1978). the Law of Additive Reaction Times in Fluid-Solid Reactions, *Metallurgical Transactions*, 9B(3), 1978-1996.

Sotirchos, S. V.; Smith, A. R., (2004). Performance of Porous CaO Obtained from Decomposition of Calcium-Enriched Bio-Oil as Sorbent for SO_2 and H_2S Removal, *Industrial & Engineering Chemistry Research*, 43, 1340-1348.

Song, C., (2002). Fuel Processing for Low-temperature and High-temperature Fuel Cells: Challenges, and Opportunities for Sustainable Development in the 21st Century, *Catalysis Today*, 77(1-2), 17-49.

Song, C. S., (2003). An Overview of New Approaches to Deep Desulfurization for Ultra-clean Gasoline, Diesel Fuel and Jet Fuel, *Catalysis Today*, 86, 211–263.

Song, C.-S.; Ma, X.-L., (2004). Ultra-deep Desulfurization of Liquid Hydrocarbon Fuels: Chemistry and Process*, International Journal of Green Energy*, 1, 167-191.

Squires, A. M.; Graff, R.A.; Pell, M., (1971). Desulphurization of Fuel with Calcined Dolomite. I. Introduction and First Kinetic Result, *Chemical Engineering Progress symposium series*, 67, 23-34.

Yang, R. T.; Chen, J. M., (1979). Kinetics of Desulphurization of Hot Fuel Gases with Calcium Oxide Reaction bwteen Carbonul Sulfide and Calcium Oxide, *Environmental Science & Technology*, 13, 549-553.

Srinivasan, R.; Hsing, I.M.; Berger, P. E.; Jensen, K. F.; Firebaugh, S. L.; Schmit, M. A.; Harrold, M. P.; Lerou, J. J.; Ryley, J. F., (1997). Micromachined reactors for catalytic partial oxidation reactions, *AIChE Journal*, 43, 3059-3069.

Stavorinus, D., (1910). the Removal of Hydrogen Sulphide from Illuminating Gas by the Method of Walther Feld., *Amsterdam. J. Gasbel.*, 53, 705-706.

Sughrue, E. L.; Johnson, M. M.; Dodwell, G. W.; Reed, L. E.; Bares, J. E.; Gislason, Jason J.; Morton, Robert W.; (2004). United States Patent Application: 20040140244.

Tamhankar, S.S., Bagajewicz, M., Gavalas, G.R., Sharma, P.K., Flytzani-Stephanopoulos, M., (1986). Mixed-Oxide Sorbents for High-temperature Removal of Hydrogen Sulfide. *Industrial & Engineering Chemistry Process Design and Development*, 25, 429-437.

Takahashi, A.; Yang, F. H.; Yang, R. T., (2002). New Sorbents for Desulfurization by π -Complexation: Thiophene/Benzene Adsorption, *Industrial & Engineering Chemistry Research*, 41, 2487-2496.

Tatarchuk, B. J., (1992a). US Patent 5,096,663.

Tatarchuk, B. J., (1992b).US Patent 5,102,745.

Tatarchuk, B. J.; Rose, M. F.; Krishnagopalan, A.; Zabasajja, J.N.; Kohler, D., (1992). US Patent 5,080,963.

Tatarchuk, B. J.; Rose, M. F.; Krishnagopalan, A.; Zabasajja, J. N.; Kohler, D., (1994). US Patent 5,304,330.

Tewari, S. K.; Pandey, K. K., (1989). Reactions of Carbonyl Sulfide and Carbon Disulfide with Rhodium Complexes, *Synthesis and Reactivity in Inorganic and Metal-Organic Chemistry*, 19(6) pp545-556.

Trubac, R. E.; Dautzenberg, F. M.; Griffin, T. A.; Paikert, B.; Schmidt, V. R.; Overbeek, R. A., (2001). Micro-engineered Catalyst Systems: ABB's advancement in Structured Catalytic Packings, *Catalysis Today*, *69*, 17-24.

Turkdogan, E. T.; Olsson, R. G., (1978). Desulfurization of Hot Reducing Gases with Manganese Oxide Pellets, *Proceedings of the Third International Iron and Steel Congress, American Society for Metals*: Chicago, Illinois, April 16-20, 277-288.

Turton, R; Berry, D. A.; Gardner, T. H.; Miltz, A., (2004). Evaluation of Zinc Oxide Sorbents in a Pilot-Scale Transport Reactor: Sulfidation Kinetics and Reactor Modeling, *Industrial & Engineering Chemistry Research*, 43(5), 1235 -1243.

Twigg, M. V., (1989). Catalyst Handbook (2nd ed.); Wolfe: London, p.209.

Upadhyay, S. N., Tripathi, G., (1975). Mass Transfer in Fixed and Fluidized Beds, *Journal of Scientific & Industrial Research*, 34, 10-35.

Vargas-Tah, A. A.; García, R.C., Archila, L. F. P.; Solis, J. R.; López, A. J., (2005). A study on sulfur reduction in FCC gasoline using Zn–Mg–Al spinels, *Catalysis Today*, 107-108, 713–718.

Velu, S.; Ma, X.; Song, C. S., (2003). Selective Adsorption for Removing Sulfur from Jet Fuel over Zeolite-Based Adsorbents**,** *Industrial & Engineering Chemistry Research,* 42, 5293-5304.

Velu, S.; Ma, X.; Song, C. S., (2005). Desulfurization of JP-8 Jet Fuel by Selective Adsorption over a Ni-based Adsorbent for Micro Solid Oxide Fuel Cells**,** *Energy and Fuels*, 19, 1116-1125.

Wakker, J. P.; Gerritsen, A. W.; Moulijin, J. A., (1993). High Temperature H_2S and COS Removal with MnO and FeO on γ-Al_2O_3 Acceptors, *Industrial & Engineering Chemistry Research*, 32, 139-149.

Wang, Z.-M.; Lin, Y.-S., (1998). Sol-Gel Derived Alumina-Supported Copper Oxide Sorbent for Flue Gas Desulfurization, *Industrial & Engineering Chemistry Research*, 37, 4675-4681.

Watanabe, K.; Sakairi, M.; Takahashi, H.; Takahiro, K.; Nagata, S.; Hirai, S., (2001). Anodizing of Aluminum Coated with Silicon Oxide by a Sol-Gel Method, Journal of the Electrochemical Society, 148(11), B473-481.

Westmoreland, P. R.; Harrison, D. P., (1976). Evaluation of Candidate Solids for High-Temperature Desulfurization of Low-Btu Gases, *Environmental Science & Technology*, 10, 659-661.

Westmoreland, P. R.; Gibson, J. B.; Harrison, D. P., (1977). Comparative Kinetics of High-Temperature Reaction Between H_2S and Selected Metal Oxide, *Environmental Science & Technology,* 11, 488-491.

Wheeler, A., Robell, A.J., (1969). Performance of Fixed-bed Catalytic Reactors with Poison in the Feed, *Journal of Catalysis*, 13, 299-305.

White, J. D.; Groves JR., F.R.; Harrison, D. P., (1998). Elemental Sulfur Production during the Regeneration of Iron Oxide High-Temperature Desulfurization Sorbent, *Catalysis Today*, 40, 47-57.

Wilson, E.J. and Geankoplis, C.J., (1966). Liquid Mass Transfer at Very Low Reynolds Numbers in Packed Ceds, *I&EC Fundamentals*, 5, 9-14.

Woods, M. C.; Gangwal, S. K.; Jothimurugesan, K.; Harrison, D. P., (1990). Reaction between H_2S and Zinc Oxide-Titanium Oxide Sorbents. 1. Single–Pellet Kinetic Studies, *Industrial & Engineering Chemistry Research*, 9, 1160-1167.

Woods, M.C.; Gangwal, S. K.; Harrison, D. P.; Jothimurugesan, K., (1991). Kinetics of the Reactons of a Zinc Ferrite Sorbents in High-Temperature Coal Gas Desulfurization, *Industrial & Engineering Chemistry Research*, 30, 100-107.

Wood, W. R.; Storrs, B. D., (1938). The Girbotol Purification Process. *Proc. Am. Petroleum Inst.,* 19, 34-36.

Wu, X.; Weng, D.; Xu, L.; Li, H., (2001). Structure and Performance of γ-alumina Washcoat Deposited by Plasma Spraying, *Surface & Coating Technology*, 145, 226.

Xue, M.; Chitrakar, R.; Sakane, K.; Ooi, K., (2003). Screening of Adsorbents for Removal of H_2S at Room Temperature, *Green Chem.*,5, 529-534.

Yrjas, K. P.; Zevenhoven, C. A. P.; Hupa, M. M., (1996). Hydrogen Sulfide Capture by Limestone and Dolomite at Elevated Pressure. 1. Sorbent Performance, *Industrial & Engineering Chemistry Research*, 35, 176-183.

Yang, R. T.; Takahashi, A.; Yang, F. H., (2001). New Sorbents for Desulfurization of Liquid Fuels by π -Complexation, *Industrial & Engineering Chemistry Research*, 40, 6236-6239.

Yoon, Y. H.; Nelson, J. H., (1984). Application of Gas Adsorption Kinetics: I. "A Theoretical Model for Respirator Cartridge Service Life, *American Industrial Hygiene Association Journal*, 45, 509-516.

Zeng, Y.; Kaytakoglu S.; Harrison, D. P., (2000). Reduced Cerium Oxide as an Effecient and Durable High Temperature Desulfurization Sorbnet, *Chemical Engineering Science*, 55, 4893-4900.

Zeng, Y.; Zhang, S.; Grovess, F. R.; Harrison, D. P., (1999). High Temperature Gas Desulfurization with Elemental Sulfur Production, *Chemical Engineering Science*, 54, 3007-3017.

Zheng, J.; Strohm, J. J.; Hoehn, M.; Song, C., (2004). Pre-reforming of jet fuels on modified Rh/CeO_2-Al_2O_3 catalysts for micro solid oxide fuels cell. *Preprints/American Chemical Society. Division of Petroleum Chemistry*, *49*, 21-24.

Zhang, J.-C.; Wang, Y.-H.; Ma, R.-Y.; Wu, D.-Y., (2003). A study on Regeneration of Mn-Fe-Zn-O Supported upon γ-Al_2O_3 Sorbents for Hot Gas Desulfurization, *Fuel Processing Technology*, *84*, 217-227.

Appendix A. Pressure Drop of Reactor without Sorbent
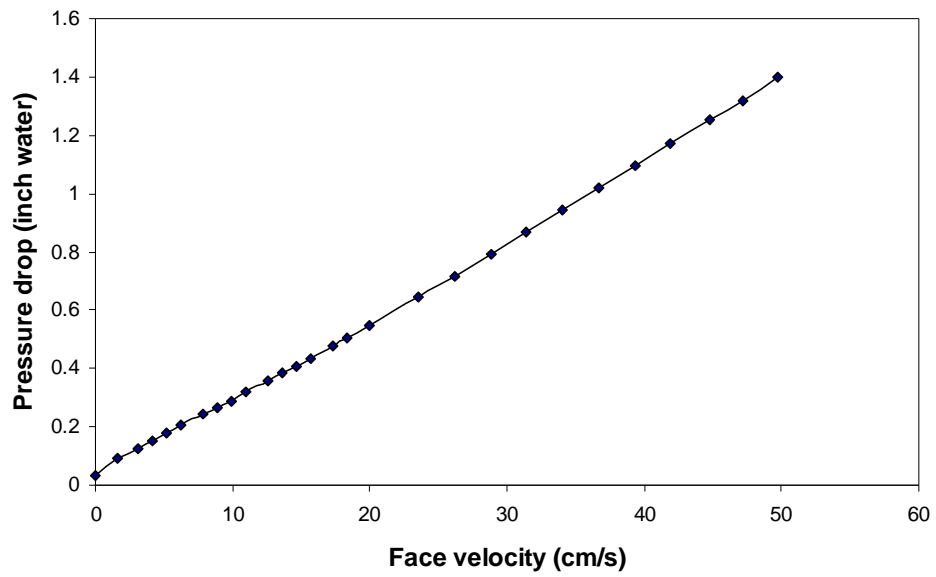
Figure A1. Pressure drop of reactor without sorbent loaded.

Appendix B. Calibration of Mass Flow Controllers
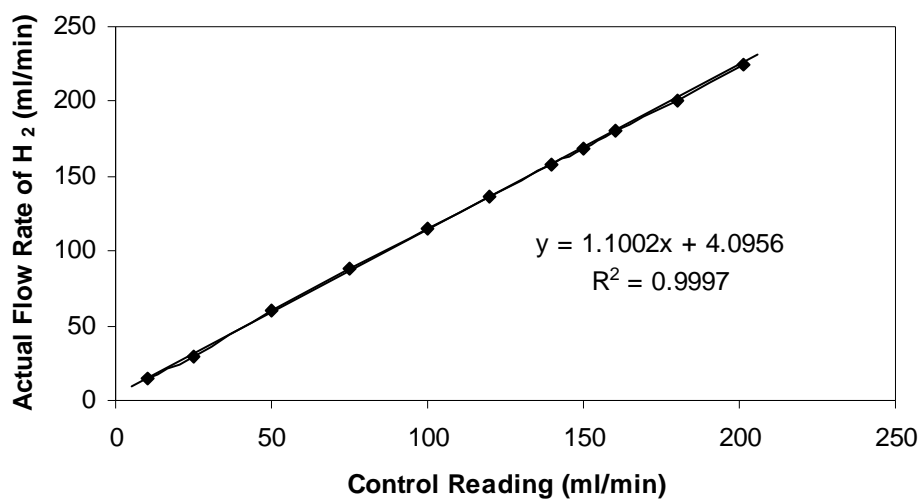
Figure A2. Calibration curve of H_2 mass flow controller
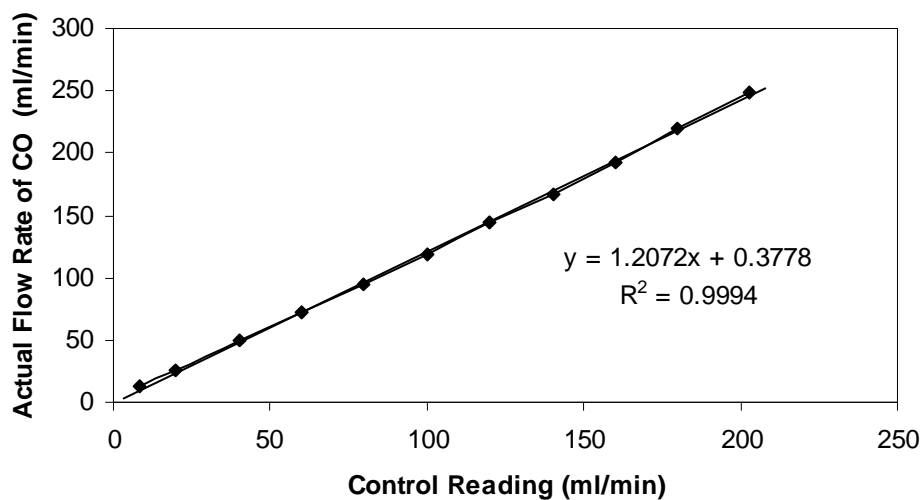
Figure A3. Calibration curve of CO mass flow controller
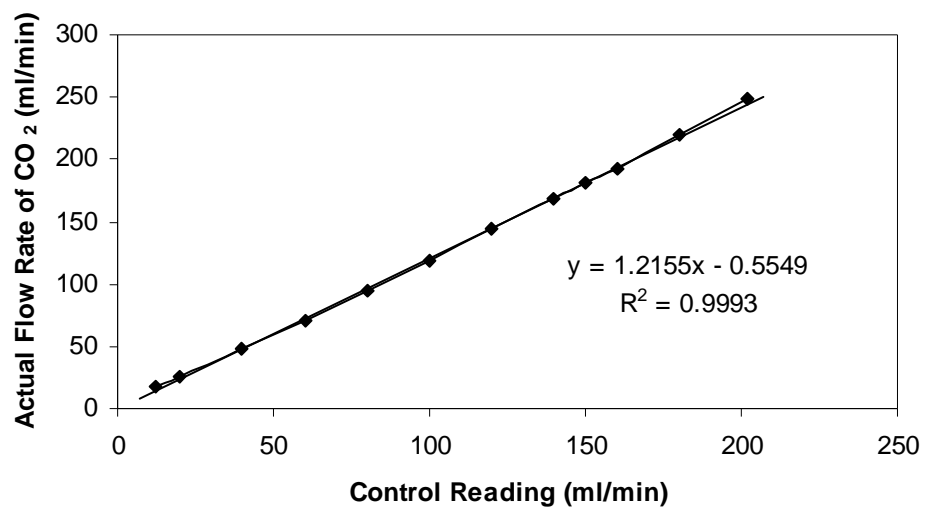
Figure A4. Calibration curve of CO_2 mass flow controller
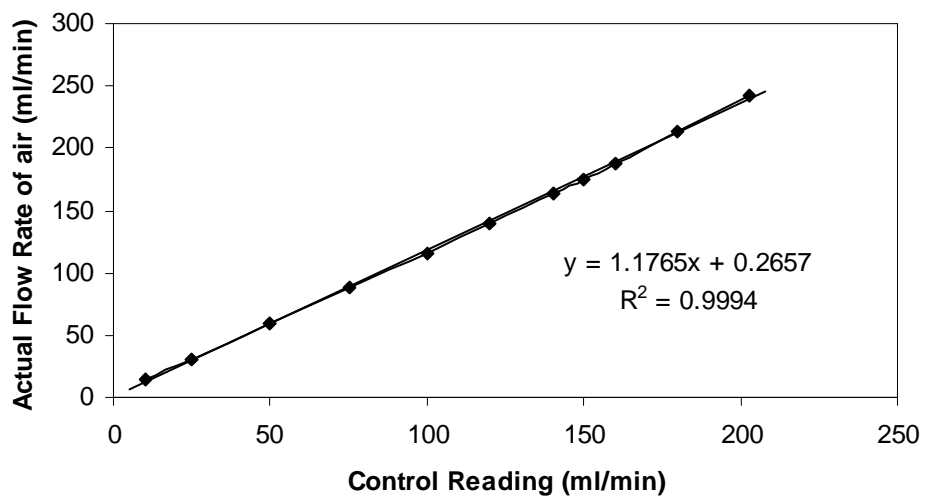
Figure A5. Calibration curve of the air mass flow controller
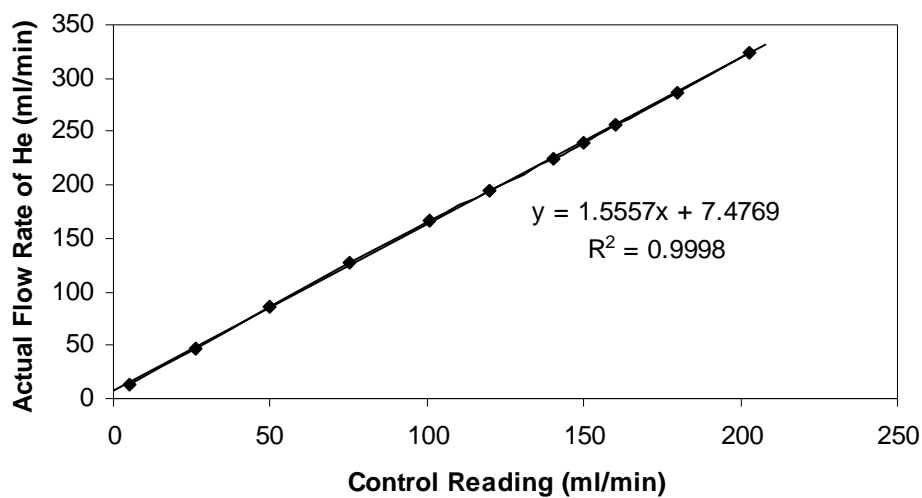
Figure A6. Calibration curve of the He mass flow controller
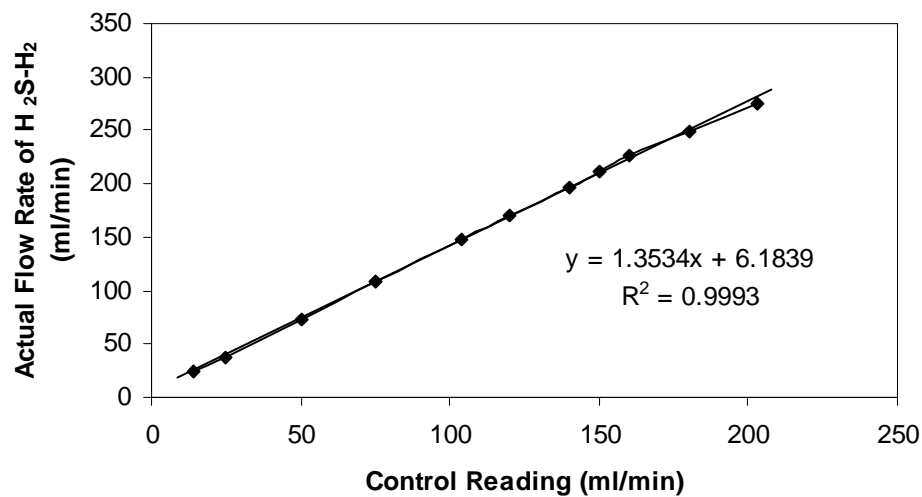
Figure A7. Calibration curve of the H$_2$S challenge gas flow rate on a mass flow

controller specified for H$_2$
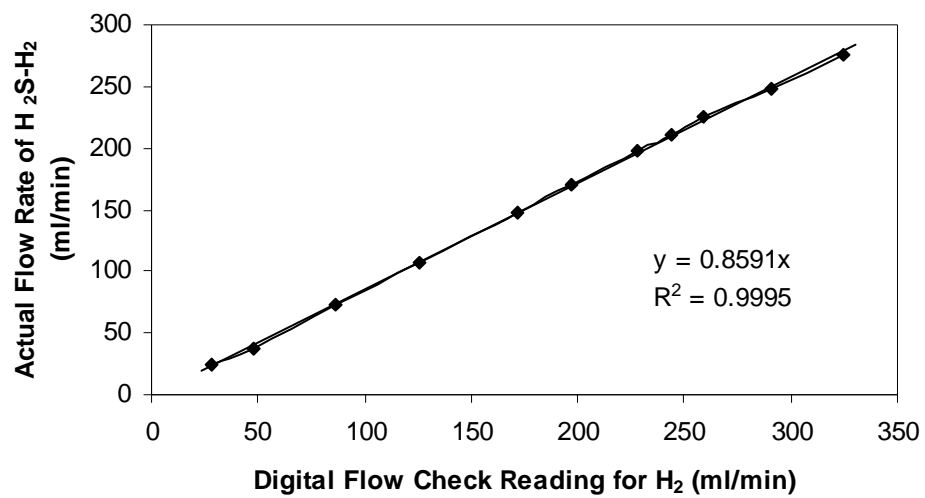
Figure A8. Calibration curve of the H₂S challenge gas flow rate read on the Alltech Digital Flow Check at pure H₂ mode.

Appendix C. Steam Table
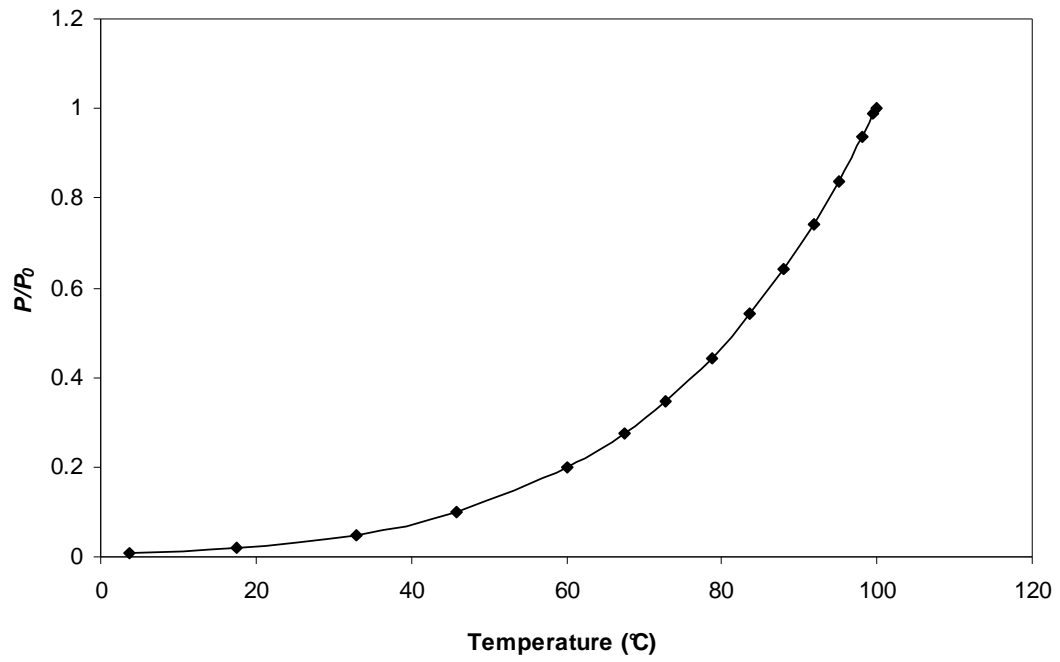
Figure A9. Saturation steam table (Moran and Shapiro, 1999).

Appendix D. Mesh Micron Conversion Chart*

Mesh	inches	microns	millimeters
4	0.187	4760	4.76
5	0.157	4000	4
6	0.132	3360	3.36
7	0.111	2830	2.83
8	0.0937	2380	2.38
10	0.0787	2000	2
12	0.0661	1680	1.68
14	0.0555	1410	1.41
16	0.0469	1190	1.19
18	0.0394	1000	1
20	0.0331	841	0.841
25	0.028	707	0.707
30	0.0232	595	0.595
35	0.0197	500	0.5
40	0.0165	400	0.4
45	0.0138	354	0.354
50	0.0117	297	0.297
60	0.0098	250	0.25
70	0.0083	210	0.21
80	0.007	177	0.177
100	0.0059	149	0.149
120	0.0049	125	0.125
140	0.0041	105	0.105
170	0.0035	88	0.088
200	0.0029	74	0.074
230	0.0024	63	0.063
270	0.0021	53	0.053
325	0.0017	44	0.044
400	0.0015	37	0.037

*http://www.fluideng.com/FE/meshmicron.html

Appendix E. Sorbent Characteristics

Table A1. Characteristics of SiO_2 gel

	Particle size (μm)	Pore size* (Å)	N$_2$-BET area (m^2/g)	
			Claimed	Measured
SiO_2	100-200	60	500-600	560

*provided by manufacture

Table A2. Void fraction of packed bed of ZnO

	bulk density (g/ml)	solid volume (ml/ml)	porosity* (g/ml)	pore volume (ml/ml)	void (ml/ml)
G-72E	1.18	0.244	0.232		
SiO_2	0.49	0.204	0.80	0.392	0.404

* provided by manufacture

Table A3. Porosity of ZnO/SiO_2 sorbent particles*

	bulk density	packed bed voidage	particle density	V of Solid	V void
	(g/ml)		(g/ml)	(ml/ml)	ml/ml
ZnO/SiO_2	0.59	0.4	0.96	0.37	0.64

* Assume the ZnO loading did not change the void fraction of packed bed

Table A4. Composition of Sud-Chemie (G-72E) (Newby *et al*., 2001).

	Al_2O_3	CaO	ZnO
Wt.%	7.9	1.6	90

Table A5. Characteristics of Sud-Chemie (G-72E) (Newby *et al.*, 2001).

Hg Particle Density (g/cm^3)	Hg Bulk Density (g/cm^3)	Skeletal He Density (g/cm^3)	Hg Pore Volume (cm^3/g)	Porosity (%)	Hg Surface Area (m^2/g)	BET N$_2$ Surface Area (m^2/g)	Median Pore Diam (Å)	Average Pore Diam (Å)
2.28	1.51	4.83	0.232	52.8	47.75	40.3	223	382

Appendix F. Surface Area Evaluation

Table A6. Surface area evaluation

grain size nm	weight g	Weight of ZnO g	Density of ZnO g/cm3	Surface area m^2/g sorbent
0.1	1	0.17	5.606	1819
0.2	1	0.17	5.606	910
0.3	1	0.17	5.606	606
0.4	1	0.17	5.606	455
0.5	1	0.17	5.606	364
0.6	1	0.17	5.606	303
0.7	1	0.17	5.606	260
0.8	1	0.17	5.606	227
0.9	1	0.17	5.606	202
1	1	0.17	5.606	182
2	1	0.17	5.606	91
3	1	0.17	5.606	61
4	1	0.17	5.606	45
5*	1	0.17	5.606	36
6	1	0.17	5.606	30

Assume ZnO grains are spheres.

*the grain size calculated by Debye-Sheer Equation

The ZnO grains have an average size less than 5 nm, and they contribute a surface area higher than 36 m^2/g sorbent

Appendix G. Gas Chromatography Analytic Methods

G.1. TCD Analysis Methods

- Column   HayeSep Q, 80/100 8'×1/8" SS

- Oven Temperature (°C)   80

- Injector Temperature (°C)   80

- Detector Temperature (°C)   175

- Bridge Current for Gow-mac GC (mA)   200

- Filament Temperature for Vaian GC(°C)   375

- Reference Gas Flow Rate (cm^3/min)   60

- Carrier gas H_2

- Carrier Gas Flow Rate (cm^3/min)   60

- 6-port valve is switched to "inject" mode at the very beginning of every minute and switched back to "fill" mode after 2 seconds after injection.

G.2. PFPD Analysis Method

- Gas Chromatographic Model   Varian 3800

- Column   Restek XTI-5 (30m×0.25mm×0.5 μm)

- Oven Temperature Program: keep at 60 °C for 1 minutes, ramp to 90°C at a rate

  of 20 °C/min, and stay at 90 °C for 3.5 minute. Total run time 6 minutes

- Injector Temperature (°C)   80

- Capillary Flow Rate (cm^3/min)   1.2

- Air 1 Flow Rate (cm^3/min)   17

- H_2 Flow Rate (cm^3/min)   13

- Air 2 Flow Rate (cm^3/min)   10

- Splite Ratio program: initial split ratio=200; at t>0.75 min split ratio=20

- Tube Voltage (V)   510

- Trigger Level (mA)   200

- Sample Delay (ms)   4

- Sample Width (ms)   10

- Gain Factor   2

- Syring size   250 μL